Thermodynamic modeling of complex systems

Liang, Xiaodong; Kontogeorgis, Georgios; Thomsen, Kaj; Yan, Wei

Publication date:
2014

Document Version
Publisher's PDF, also known as Version of record

Thermodynamic modeling of complex systems

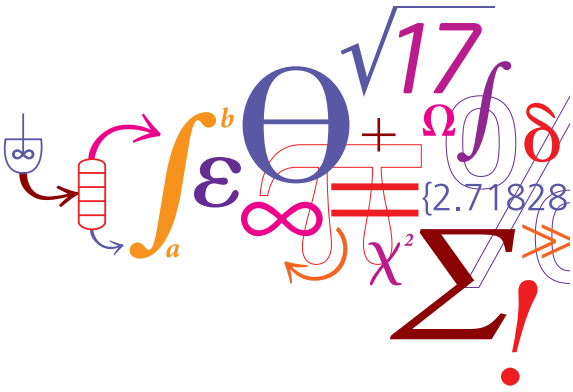

Xiaodong Liang
Ph.D. Thesis
August 2014

DTU Chemical Engineering
Department of Chemical and Biochemical Engineering

Thermodynamic modeling of complex systems

PhD Thesis

Xiaodong Liang

August 2014

Center for Energy Resources Engineering
Department of Chemical and Biochemical Engineering
Technical University of Denmark
DK-2800 Kgs. Lyngby, Denmark

DTU Chemical Engineering
Department of Chemical and Biochemical Engineering

Address: Center for Energy Resources Engineering
Department of Chemical and
Biochemical Engineering
Technical University of Denmark
Søltofts Plads, Building 229
DK-2800 Kgs. Lyngby
Denmark
Phone: +45 4525 2800
Fax: +45 4525 4588
Web: www.cere.dtu.dk

Print: J&R Frydenberg A/S
København
December 2014

ISBN: 978-87-93054-46-2

Preface

This thesis is submitted to fulfill the partial requirements for the Ph.D. degree at the Technical University of Denmark (DTU). The work has been carried out at the Department of Chemical and Biochemical Engineering and Center for Energy Resources Engineering (CERE), from August 2011 to August 2014, under the supervision of Professor Georgios M. Kontogeorgis, Associate Professor Kaj Thomsen, and Senior Scientist Wei Yan. The project was funded by the Danish National Advanced Technology Foundation (DNATF) and the Department of Chemical and Biochemical Engineering, Technical University of Denmark.

I would like to express my most sincere gratitude to my supervisors for their full support throughout the project. I would like to thank my main supervisor Professor Georgios M. Kontogeorgis, firstly for offering me such a dream project, secondly for inspiring me so many exciting ideas, thirdly for allowing me so much research freedom, fourthly for encouraging me all the time, fifthly for putting me in the CHIGP meetings/giving me many presentation opportunities/improving my language, and last but not least for your enthusiasm of thermodynamics. I would like to thank my supervisor Associate Professor Kaj Thomsen for many help on revising articles and understanding the electrolyte solution thermodynamics. I would like to thank my supervisor Senior Scientist Wei Yan for many fruitful discussions on both the technical level, especially on oil characterization methods, and the life side, especially for giving me so many help on different aspects.

I would like to thank all the colleagues, from top managements to secretaries to IT managers, and from professors to researchers to Ph.D. students. I thank Associate Professor Nicolas von Solms for the opportunity of teaching assistance of the course “Chemical Engineering Thermodynamics”, and many inspirations on the association theory. I appreciate many suggestions and critical opinions on various projects and general applied thermodynamics from Professor Michael L. Michelsen. Computational details are rarely mentioned in this thesis, but there is no doubt that they are the corner stone for most of the presented results. I thank my fellow colleagues in the CHIGP project, Ioannis, Bjørn, Michael and Martin, for coauthoring publications, co-participating international conferences, and for many fruitful discussions during the meetings. I thank Louise and Patricia for preparing various documents, booking flight tickets and hotels for travels, and organizing different events, etc. I thank Michael and Christine for improving the Danish Summary. I would also very much like to thank many people in the lunch and running clubs – I have been having a great time.

I would like to express my special thanks to my former officemate – Dr. Peter Jørgensen Herslund. It is a fate to meet some people in the life, and Peter is one of mine. Peter gave me tremendous help on many things – Danish letter translations from different organizations, delicious Danish food, fruitful discussions about family, about life, about work. Peter, I wish all best for you and your friendly family – Hélène, Marius and Iris.

I would like to thank many professionals around the world, some of whom I even did not meet, for their constructive suggestions, ideas and explanations, and sending me inaccessable experimental data, especially Dr. Ilya Polishuk from Ariel University, Israel.

I would like to thank my master supervisor Professor Honglai Liu at ECUST, China, for bringing me into this old but energetic field, for explaining/sharing me many concepts/theories in details, for such a long contribution to the molecular thermodynamics community – one of the most important concepts of PC-SAFT is actually from the works of Professor Honglai Liu and Professor Ying Hu. I would like to thank my former lead at HONEYWELL, Dr. Ensheng Zhao, for teaching me so many things – research and development skills of applied thermodynamics in such a large commercial process simulator, behaviors, languages, encouragements, managements, and very importantly for inspiring me how amazing applied thermodynamics is, which is the most important reason why I am at DTU.

We arrived in Copenhagen on August 11th, 2011. In the past three years, I mentally spent more than necessary time on the project. Without the accompanying of my family, it would have been a tough time, both mentally and physically.

"*It is only in the mysterious equations of love that any logic or reasons can be found.*"

Thank you for your love. I love you and our coming 'little princess' till "海枯石烂，天荒地老".

Dedicated to

Lijuan, Peishi and Anni

My parents and my brothers

Summary

Offshore reservoirs represent one of the major growth areas of the oil and gas industry, and environmental safety is one of the biggest challenges for the offshore exploration and production. The oil accidents in the Gulf of Mexico in 1979 and 2010 were two of the biggest disasters in history. Contrary to earlier theories, the oil is not only present on the surface, but also in great volumes both in the water column and on the seafloor, which indicates that we do not know enough about how oil behaves in water and interacts with it. Sonar detection is one of the most important and necessary technologies to reduce the environmental effects of offshore oil exploration. It could be used (1) to detect oil and gas leaks around the subsea well head enabling faster responses, especially in deep water and/or ice covered areas; (2) to detect and map the oil in the seawater column during cleanup process after an oil spill. Engineering thermodynamics could be applied in the state-of-the-art sonar products through advanced artificial technology, if the speed of sound, solubility and density of oil-seawater systems could be satisfactorily modelled.

The addition of methanol or glycols into unprocessed well streams during subsea pipelines is necessary to inhibit gas hydrate formation, and the offshore reservoirs often mean complicated temperature and pressure conditions. Accurate description of the phase behavior and thermal-physical properties of complex systems containing petroleum fluids and polar compounds are extremely important from viewpoints of the economical operation and environmental safety.

The classical thermodynamic models used by the oil industry are semi-empirical and not suitable for mixtures containing water and other polar chemicals. The complex nature of water, its anomalous properties due to hydrogen bonding and the hydrophobic interactions with hydrocarbons (oils), are not described well by such simple models. The perturbation theory based models have an explicit term to account for the hydrogen bonding, and these models are also believed to have better performance for derivative properties, e.g. speed of sound, and for density under extreme conditions.

This PhD thesis studies the capabilities and limitations of the Perturbed-Chain Statistical Association Fluid Theory (PC-SAFT) equation of state. It consists of three parts. In the first part, the PC-SAFT EOS is successfully applied to model the phase behaviour of water, chemical and hydrocarbon (oil) containing systems with newly developed pure component parameters for water and chemicals and characterization procedures for petroleum fluids. The performance of the PC-SAFT EOS on liquid-liquid equilibria of water with hydrocarbons has been under debate for some

years. An interactive step-wise procedure is proposed to fit the model parameters for small associating fluids by taking the liquid-liquid equilibrium data into account. It is still far away from a simple task to apply PC-SAFT in routine PVT simulations and phase behaviour of petroleum fluids. It has been extensively studied on how to develop general petroleum fluid characterization approaches for PC-SAFT. The performance of the newly developed parameters and characterization procedures for the description of the phase equilibria of well- and ill-defined binary and ternary systems containing water, chemicals and/or hydrocarbons (oils) is quite satisfactory, if compared to the models available in literature. The modeling of petroleum fluid-water-MEG systems provides further information to develop simpler and more robust characterization approaches.

In the second part, the speed of sound data and their correlations of various systems are reviewed. Two approaches are proposed to improve the speed of sound description within the PC-SAFT framework by putting speed of sound data into the parameter estimation and/or the universal constant regression. The first approach works only for short associating fluids, while the second approach significantly improves the speed of sound description for various systems both qualitatively and quantitatively. The possibility of simultaneous modeling of phase behavior and speed of sound, including the effects of parameter estimation approaches for 1-alcohol containing systems, are also investigated.

In the third part, the fundamentals of PC-SAFT are investigated based on the universal constant regression. The PC-SAFT EOS has been criticized for some numerical pitfalls during the recent years. A new variant of universal constants has been developed, which has avoided the numerical pitfalls of having more than three volume roots in the real application range. It has been shown that it is possible to directly use the original PC-SAFT parameters with the new universal constants for the systems considered in this thesis. Finally, the salt effects on the solubility of hydrocarbons, the speed of sound, and the static permittivity of aqueous solutions are briefly discussed. It is still an open question how to estimate the model parameters for associating fluids with pure component properties only. The possibility of using the static permittivity data in the parameter estimation is discussed by adopting a newly developed theory of static permittivity and association theory based EOS.

Resumé

Offshore reservoirer repræsenterer et af de store vækstområder i olie- og gasindustrien, og miljøsikkerhed er en af de største udfordringer for offshore efterforskning og produktion. Olie ulykkerne i Den Mexicanske Golf i 1979 og 2010 var to af de største katastrofer i historien. I modsætning til tidligere teorier findes olien ikke kun på overfladen, men også i store mængder både i vandsøjlen og på havbunden, hvilket indikerer, at vi ikke ved nok om, hvordan olien opfører sig i vand og interagerer med det. Sonarlyde er en af de vigtigste og mest nødvendige teknologier til at mindske miljøvirkningerne af offshore olieefterforskning . Det vil kunne bruges (1) til at detektere olie og gas lækager omkring den undersøiske brønd overbygning, hvilketmuliggøre hurtigere svar, især i dybt vand og / eller isdækkede områder; (2) til at registrere og kortlægge olie i havvandsøjlen under rensningen efter et olieudslip. Engineering termodynamik vil kunne anvendes i state-of-the-art sonar produkter gennem avanceret kunstig teknologi, hvis lydens hastighed, opløselighed og massefyldeaf olie-havvand-systemer kan blive modelleret tilfredsstillende.

Tilsætning af methanol eller glycoler i uforarbejdede brøndstrømme i undersøiske rørledninger er nødvendig for at hæmme gashydratdannelse, og offshore reservoirer betyder ofte ekstreme og komplicerede temperatur og trykforhold. For den økonomisk drift og den miljømæssige sikkerheds synsvinkel er det ekstremt vigtigt med en præcis beskrivelse af fase opførsel og termisk-fysiske egenskaber af komplekse systemer, der indeholder petroleumsvæsker og polære forbindelser. .

De klassiske termodynamiske modeller, som olieindustrien anvender, er semi-empiriske og ikke egnet til blandinger, der indeholder vand og andre polære kemiske stoffer. Den komplekse karakter af vand, dets unormale egenskaber på grund af hydrogenbinding og hydrofobe interaktioner med kulbrinter (olie), er ikke velbeskrevet af sådanne simple modeller. De perturbationsteori baserede modeller har et eksplicit ledtilat tage højde for hydrogenbinding, og disse modeller menes også at have bedre ydeevne for afledte egenskaber, fx lydens hastighed og for massefyldenunder ekstreme forhold.

Denne ph.d.-afhandling undersøger de begrænsninger og muligheder i den perturberede-kæde Statistical Association Fluid Teori (PC-SAFT) tilstandsligning. Den består af tre dele. I den første del er PC-SAFT EOS anvendt med succes til at modellere vands opførsel, kemikalier og kulbrinter (olier) der indeholder systemer mednyudviklede rene komponent parametre for vand og kemikalier, og karakteriserings procedurer for petroleumsvæsker. PC-SAFT EOS ydeevne på væske-væske

ligevægte af vand med kulbrinter har været under debat i nogle fåår. En interaktiv trinvis procedure er foreslået til at tilpasse modelparametrene for små associerende væsker ved at tage ligevægtsdataene for væske-væske i betragtning. Det er stadig langt fra en simpel opgave at anvende PC-SAFT i rutinemæssige PVT simuleringer og til petroleumsvæskers fase opførsel. Det er blevet undersøgt grundigt, hvordan man skal udvikle generelle petroleumsvæske karakteriserings tilgange til PC-SAFT. Ydeevnen af de nyudviklede parametre og karakteriserings procedurer til beskrivelsen af faseligevægte veldefineret og dårligt definerede binære og ternære systemer, der indeholder vand, kemikalier og / eller kulbrinter (olier), er ganske lovende, hvis der sammenlignes med tilgængelige litteratur parametre og / eller CPA EOS. Modelleringen af petrolium væske-vand-MEG-systemer giver yderligere information til at udvikle enklere og mere robuste karakteriserings tilgange.

I den anden del er lydhastighedsdata og deres korrelationer af forskellige systemer revideret. Der foreslås to tilgange til at forbedre beskrivelsen af lydens hastighedinden for PC-SAFT rammen ved at sætte lydhastighedsdata ind i parameterestimering og / eller den universelle konstant regression. Den første fremgangsmåde fungerer kun i korte associerende væsker, mens den anden strategi forbedrer beskrivelsen af lydens hastighed for forskellige systemer fra både kvalitative og kvantitative synspunkter. Muligheden for samtidig modellering af fase opførslenog lydens hastighed, herunder virkningerne af parameterestimerings tilgangene for systemer indeholdene 1-alkohol, er også undersøgt.

I tredje del er de grundlæggende elementer i PC-SAFT undersøgt baseret på universel konstant regression. PC-SAFT EOS er blevet kritiseret for nogle numeriske faldgruber i løbet af de seneste år. En ny variant af universelle konstanter er blevet udviklet, som har undgået de numeriske faldgruber ved at have mere end tre volumen rødder i den virkelige anvendelsesområde. Det er blevet påvist, at det er muligt direkte at anvende de oprindelige PC-SAFT parametre med de nye universelle konstanter for de systemer, der behandles i denne afhandling. Til sidst er salt indvirkningen på opløseligheden af carbonhydrider, lydens hastighed og den statiske permittivitet for vandige opløsninger kort diskuteret. Det er stadig et åbent spørgsmål, hvordan man kan estimere modelparametrene til inddragelse af væsker med kun rene egenskaber. Muligheden for at anvende de statiske permittivitet data i parameterestimering diskuteres ved at anvende en nyudviklet teori for statisk permittivitet og associations teori baseret på EOS.

Table of Contents

Chapter 1. Introduction

1.1 Background

As the offshore reservoirs represent one of the major growth areas of the oil and gas industry for decades, the complex phase behavior between petroleum fluids and polar compounds such as water, methanol or glycols has gained increasing attention. For instance, the addition of methanol or glycols into unprocessed well streams in subsea pipelines is necessary to inhibit gas hydrate formation. Since the mutual solubility of petroleum fluids and water will considerably increase when chemicals are involved, the phase behavior modeling of oil-water-chemicals is very important from the viewpoints of economical operation and environmental safety. The offshore reservoirs often mean extreme temperature and pressure conditions, accurate description of fluid properties at such conditions are far from a simple task.

Environmental safety is one of the biggest challenges for the offshore exploration and production. In 1979, an oil accident occurred in Mexico with a total of approximate three million barrels oil poured into the ocean. In more than 30 years, the marine life after the incident is still affected [Ixtoc I oil spill]. In 2010, the oil accident in the Gulf of Mexico was one of the biggest oil disasters in history [Deepwater Horizon oil spill]. More than 4.9 million barrels crude oil were leaked into the ocean and this could be an environmental disaster for many years. Contrary to earlier theories, the oil is not only present on the surface, but also in great volumes both in the water column and on the seafloor. This may in part be attributed to the use of dispersing agents, but a lot indicates that we do not know enough about how oil behaves in water and interacts with it, when the oil leak occurs at great depths as the case with Deepwater Horizon. In order to reduce the environmental impact of the offshore oil exploration and production, sonar detection is one of the most important and necessary technologies, which could be used to: (1) detect oil and gas leaks around the subsea well head enabling faster responses, especially in deep water and/or ice covered areas, (2) detect and map the oil in the seawater column during cleanup process after an oil spill. It would be possible to detect or even classify the presence of oil in the seawater column, by combining the knowledge from engineering thermodynamics, geophysical inversion and underwater acoustics into the design of an optimal detection/classification algorithm. It is sketched in Figure 1.1 how to apply

thermodynamic models in such an artificial intelligence technology system. The required properties are mainly acoustic properties, solubility and density of oil-seawater systems.

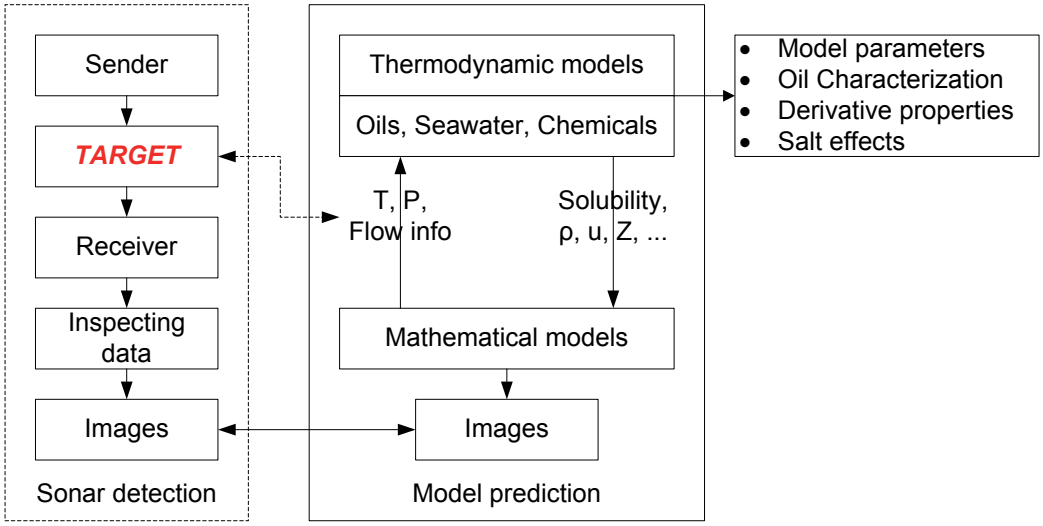

Figure 1.1 Applying thermodynamic models in sonar subsea detection

1.2 Thermodynamic models

The main purpose of this PhD project is to develop thermodynamic models capable of describing the phase behavior, density and speed of sound for complex systems, involved in the oil and gas industry, over a wide range of conditions (temperature, pressure, oil types and origins).

1.2.1 Phase behavior

The classical thermodynamic models used by the oil industry are semi-empirical and not suitable for mixtures containing water and other polar chemicals. The complex nature of water, its anomalous properties due to hydrogen bonding and the polar and hydrophobic interactions with hydrocarbons (oil) are not described well by such simple models.

In the early 1990's the theory of Wertheim emerged from statistical thermodynamics. It turned out to be a useful tool for describing chemical substances and their mixtures when hydrogen bonding is significant. This theory has been implemented into a new generation of engineering equations of state (EOS) such as SAFT and CPA [Kontogeorgis et al. (2010a)]. CPA stands for Cubic-Plus-Association and SAFT is the Statistical Association Fluid Theory. Both equations contain

essentially the same association term but different ways of accounting for the short range physical interactions. The CPA model uses a conventional cubic EOS for the physical interactions whereas SAFT uses theoretically-based terms for the repulsive and attractive contributions as well as a separate "chain" term to account for the macromolecular effects in large molecules. These models can be simply illustrated by the following equations, based on the reduced residual Helmholtz free energy:

$$a^r = a^{short} + a^{inter} + a^{long} \tag{1.1}$$

where short, inter and long indicate the energy contributions from short, intermediate or long range interactions.

Specifically, SAFT can be formulated as:

$$a^r = a^{seg} + a^{chain} + a^{disp} + a^{assoc} + a^{polar} + a^{elec} + \cdots \tag{1.2}$$

A thorough review of these models can be found in a recent monograph [Kontogeorgis et al. (2010a)]. CPA has been used with great success for the prediction of thermodynamic properties in mixtures of hydrocarbons (including oil), water and polar chemicals like the gas hydrate inhibitors methanol and glycols, over the last 15 years. CPA has already been widely accepted for applications in the petroleum and chemical industries, while the general and large scale applications of SAFT models in the oil and gas industry are on the way.

1.2.2 Physical properties

1.2.2.1 Density

In general, density is, due to its easy and reliable measurements, one of the most common properties that is used to estimate the model parameters. Density is a function of temperature and pressure, and an input/output property for EOS models, and it is predicted for given conditions (temperature, pressure and composition) in real applications when the model is ready, by solving the following equation:

$$P^{spec} = P^{calc} = P^{id} - RT\left(\frac{\partial a^r}{\partial V}\right)_T \tag{1.3}$$

Where the subscript *spec*, *calc* and *id* represent the specified, calculated and ideal contributions of pressure, respectively.

SAFT models are believed to have potentially better description for density at extreme conditions, e.g. high pressure, than traditional cubic EOS models, even with volume-translation, due to their more theoretical sound reference term.

1.2.2.2 Speed of sound

Speed of sound, by definition, equals to the distance that a sound wave propagates through an elastic medium in a unit of time. It is a thermo-physical property, which can be accurately determined in wide ranges of temperature and pressure. In classic mechanics, speed of sound can be calculated by the following equation:

$$u^2 = \left(\frac{\partial P}{\partial \rho}\right)_S \tag{1.4}$$

where u is the speed of sound, P is the pressure, ρ is the mass density, and subscript S denotes the derivative taken adiabatically. Since

$$\frac{C_P}{C_V} = \left(\frac{\partial P}{\partial \rho}\right)_S \Big/ \left(\frac{\partial P}{\partial \rho}\right)_T \tag{1.5}$$

where C_P and C_V are isobaric and isochoric heat capacities, respectively.

By inserting equation (1.5) into equation (1.4), we get:

$$u^2 = \frac{C_P}{C_V}\left(\frac{\partial P}{\partial \rho}\right)_T \tag{1.6}$$

If replacing ρ with the total volume V, speed of sound is given by [Michelsen and Mollerup (2007)]:

$$u^2 = -\frac{V^2}{Mw}\frac{C_P}{C_V}\left(\frac{\partial P}{\partial V}\right)_T \tag{1.7}$$

The C_P and C_V are calculated by the following equations:

$$C_P = C_P^{ig} + C_P^r = C_P^{ig} - R - T\left(\frac{\partial^2 a^r}{\partial T^2}\right)_{V,n} + T\left(\frac{\partial P}{\partial T}\right)_{V,n}\left(\frac{\partial V}{\partial T}\right)_{P,n} \tag{1.8}$$

$$C_V = C_V^{ig} + C_V^r = C_P^{ig} - R - T\left(\frac{\partial^2 a^r}{\partial T^2}\right)_{V,n} \tag{1.9}$$

The ideal gas heat capacity could be found from various databases, and the DIPPR database (2012) is used in this PhD thesis. SAFT models are also believed to have a better description for speed of sound than cubic EOS models, due to their more theoretical sound reference term. Speed of sound modeling may gain wide applications for petroleum fluids in geophysics for seismic interpretations.

1.3 Scope and outline

The Perturbed-Chain Statistical Associating Fluid Theory (PC-SAFT) equation of state is selected as the working model in this project, mainly for two reasons: (1) we have extensively used this model for various research projects in the past decade; (2) this model, as mentioned in the previous sections, is believed to have better performance for physical properties over wide ranges of temperature and pressure. Besides, our selection is also motivated by some challenges for PC-SAFT, including how to apply this model into the routine modeling and simulation in the oil and gas industry in a general manner, how to estimate the five PC-SAFT parameters for certain associating compouds like water, and whether it is possible to simultaneously model phase behaviour and speed of sound with only three parameters for non-associating fluids. In addition, PC-SAFT has been criticized for its numerical pitfalls in recent years, and we would like to see if they can be resolved.

This PhD project is going to address the above challenges, and the thesis is outlined as follows:

Chapter 2 discusses the parameter estimation of water, which in general has five parameters within the association theory based models, and proposes a general optimization procedure, by taking account of the liquid-liquid equilibrium data of water and non-aromatic hydrocarbons into the estimation process. The same procedure is also adopted for other chemicals like mono-ethylene glycol. This chapter presents the performance of these parameters on the properties of pure substances and the phase equilibria of binary and ternary systems containing water, hydrocarbons and chemicals, by comparing to the literature available parameters and/or the CPA EOS. This chapter also presents how to setup the binary interaction schemes and parameters, which provides solid foundation for applying PC-SAFT into oil-water-chemical systems.

Chapter 3 studies the influence of different options for developing general oil characterization methods with PC-SAFT. These options include the molar composition distribution function, the density correlation, the number of pseudo-components, the estimation method of PNA contents, the binary interaction parameters, the significance of fitting parameters and of the fitting strategy. Based on the performance of the characterization approaches for predicting saturation pressure and

density of various petroleum fluids, and the activity coefficients of pseudo-components, two of them are selected for further study.

Chapter 4 applies the newly developed parameters and interaction schemes from Chapter 2 and the two characterization approaches from Chapter 3 to model oil-water-chemical systems. The overall results are quite promising, when compared to the published results in the literature. It also provides more information to develop simpler and more robust characterization approaches.

Chapter 5 reviews and analyzes the speed of sound data of hydrocarbons, alcohols and their binary and multi-component mixtures, including petroleum fluids, and it reviews the correlations of the speed of sound in various systems, and develops the correlation coefficients for the speed of sound in pure hydrocarbons and 1-alcohols within one general framework.

Chapter 6 proposes two approaches to improve the speed of sound description with the PC-SAFT framework, after a brief comparison of SRK, CPA and PC-SAFT for normal hydrocarbons. The performance of these two approaches has been evaluated on predicting the speed of sound in wide range of mixtures – binary hydrocarbons, binary hydrocarbon + alcohol, binary alcohols, ternary hydrocarbons and petroleum fluids. The possibility of simultaneous phase behavior and speed of sound modeling has been investigated, including the effects of parameter estimation approaches for 1-alcohol containing systems.

Chapter 7 analyzes the temperature and volume dependence of the PC-SAFT EOS in a somewhat deterministic way, and develops a new variant of universal constants with focus on vapor pressure and density. It then evaluates the performance of the new variant on the properties of pure normal hydrocarbons, and on the behavior of isothermal curves and critical points, by comparing with the original universal constants. It finally investigates the possibility of using the original PC-SAFT parameters with the new universal constants.

Chapter 8 briefly discusses the salt effects on the solubility of hydrocarbons, the speed of sound, and the static permittivity of aqueous solutions. It also discusses the possibility to use the newly developed theory of calculating the static permittivity from the association theory based EOS to simplify the parameter estimation for associating fluids.

Chapter 9 presents the conclusions and future work.

Chapter 2. Phase behavior of well-defined systems

The Statistical Associating Fluid Theory (SAFT) and Cubic Plus Association (CPA) equations of state (EOS), with an association term based on the first-order thermodynamic perturbation theory, are two of the most successful and widely used model families. In the past three decades, numerous SAFT variants have been proposed, among which the perturbed-chain SAFT (PC-SAFT) has gained widespread acceptance with great successes in the fields of polymers, chemical, biochemical, pharmaceutical, and so on.

It is well-known that crude oils from petroleum reservoirs are made up of a large number of highly diversified chemical compounds, which in general are only partially miscible at normal temperature and pressure conditions. In order to develop thermodynamic models, which can describe the phase behavior and physical properties of these complex mixtures, model parameters and binary interaction parameters have to be setup for the relevant pure substances and binary mixtures. The relevant ternary or multicomponent mixtures are very helpful on validating the model and its predictive capabilities.

The purpose of this study is to develop new parameters for relevant associating fluids with the PC-SAFT EOS, and then to investigate the performance of these parameters, by comparing to PC-SAFT with the available parameters in the literature and/or the CPA EOS, on the properties of pure substances and the phase equilibria of binary and ternary systems containing water, hydrocarbons and chemicals, along which the binary interaction schemes and parameters will be setup.

2.1 Models

Over the past two decades, the popularity of SAFT EOS, based on a perturbation theory for associating fluids proposed by Wertheim (1984a, 1984b, 1986a, 1986b), has grown very fast. The model appeared in the form known today due to the work of Chapman et al. [Chapman et al. (1988, 1990); Jackson et al. (1988)] and of Huang and Radosz (1990, 1991) and for this reason both of these models are often referred to as 'original' SAFT. After this, many different versions of SAFT have followed, some of the successful ones being the SAFT-VR from 1997 by Gil-Villegas et al. [Gil-Villegas et al. (1997); Galindo et al. (1998)], the soft-SAFT from 1997 by Blas and Vega

(1997, 1998), and the PC-SAFT in both its original version from 2001 by Gross and Sadowski (2001, 2002) and the simplified version from 2003 by von Solms et al. (2003), the SAFT-VR Mie by Lafitte et al. (2006, 2007, 2013), and the SWCF-VR by Li et al. (2009, 2011)

In SAFT EOS, molecules are modeled as chains of covalently bonded spheres. The models are typically written as a sum of the contributions to the reduced residual Helmholtz free energy as in the form:

$$a^r = \frac{A^r}{NkT} = a^{seg} + a^{chain} + a^{assoc} \tag{2.1}$$

where $a^{seg}$is the part of the Helmholtz energy due to segment-segment interactions, $a^{chain}$is the term due to chain formation, and a^{assoc}represents the contribution due to association, i.e. hydrogen bonding, between different molecules. The biggest differences in the different SAFT variants are the dispersion term and the choice of reference fluid. Almost all of the different SAFT variants more or less use the same expressions for the chain formation and association terms, and include in most cases five pure component parameters with well-defined physical meanings (the number of segments, the segment size and energy, and the association volume and energy).

Nowadays this theoretical SAFT-type approach is very popular due to its versatility and the good results obtained for different applications [Kontogeorgis et al. (2010a)]. However, while SAFT's ability to describe the phase equilibria of chain and associating pure fluids and mixtures is well-established, its performance for the simultaneous description of phase equilibria and second-order derivative properties is still limited and not sufficiently explored [Lafitte et al. (2006)].

2.1.1 PC-SAFT EoS

The PC-SAFT EoS was developed by Gross and Sadowski (2001) by extending the perturbation theory of Barker and Henderson (1967) to a hard-chain reference. The reduced residual Helmholtz free energy for mixtures containing associating fluids in PC-SAFT can be formulated as:

$$a^r = \left(a^{hs} + a^{chain}\right) + a^{disp} + a^{assoc} \tag{2.2}$$

where a^{hs} and a^{chain} are the contributions from hard sphere segment-segment interaction and chain formation, of which the summation is the reference to build the dispersion force a^{disp}. The term a^{assoc} represents the contributions of association forces of sites.

Instead of accounting the dispersion force among hard spheres first and then forming chains in other SAFT variants, hard-sphere chain is formed first and then the dispersion force is accounted among chains in PC-SAFT. So it has the same hard sphere, hard chain terms and quite similar association term as those of other SAFT variants, and a fundamental difference on the dispersion term.

In this work, the simplified PC-SAFT version proposed by von Solms et al. (2003) will be used. It is not a new EOS, rather a simplified version in terms of mixing rules of the original PC-SAFT EOS, which aims to simplify and reduce the computational time of the PC-SAFT EOS. All details can be found in the original literature [Gross and Sadowski (2001, 2002), von Solms et al. (2003)] or the book of Kontogeorgis and Folas [Kontogeorgis et al. (2010a)]. The dispersion and association terms, however, will be extensively studied, so brief introductions are presented below.

2.1.1.1 Dispersion term

The reduced residual Helmholtz free energy for the dispersion term is given as the sum of a first-order and a second-order term:

$$a^{disp} = a_1^{disp} + a_2^{disp} \tag{2.3}$$

$$a_1^{disp} = -2\pi\rho m^2\sigma^3 \frac{\varepsilon}{kT}\left[\int_1^{\propto} \tilde{u}(x) g^{hc}(m;\eta)\, x^2 dx\right] \tag{2.4}$$

$$a_2^{disp} = -\pi\rho m\left(1 + Z^{hc} + \rho\frac{\partial Z^{hc}}{\partial\rho}\right)^{-1} m^2\sigma^3\left(\frac{\varepsilon}{kT}\right)^2 \frac{\partial}{\partial\rho}\left[\rho\int_1^{\propto} \tilde{u}^2(x) g^{hc}(m;\eta)\, x^2 dx\right] \tag{2.5}$$

Where,

$$\left(1 + Z^{hc} + \rho\frac{\partial Z^{hc}}{\partial\rho}\right) = \left(1 + m\frac{8\eta - 2\eta^2}{(1-\eta)^2} + (1-m)\frac{20\eta - 27\eta^2 + 12\eta^3 - 2\eta^4}{[(1-\eta)(2-\eta)]^2}\right) \tag{2.6}$$

Where x is the reduced radial distance around a segment ($x = r/\sigma$), $\tilde{u}(x) = u(x)/\varepsilon$ denotes the reduced potential function, and $g^{hc}(m;\eta)$ is the average segment-segment radial distribution function of the hard-chain fluid with temperature-dependent segment diameter $d(T)$.

The reduced density or packing fraction and temperature-dependent segment diameter are given as:

$$\eta = \frac{\pi}{6}\rho m d^3 \tag{2.7}$$

$$d = \sigma[1 - 0.12\, exp(-3\varepsilon/kT)] \tag{2.8}$$

A novel idea in PC-SAFT is to use polynomials to represent the two integrals, inspired by the work of Liu and Hu (1996), which are given by:

$$I_1(m,\eta) = \int_1^{\infty} \tilde{u}(x) g^{hc}(m;\eta)\, x^2 dx = \sum_{i=0}^{6} a_i \eta^i \tag{2.9}$$

$$I_2(m,\eta) = \frac{\partial}{\partial \rho}\left[\rho \int_1^{\infty} \tilde{u}^2(x) g^{hc}(m;\eta)\, x^2 dx\right] = \sum_{i=0}^{6} b_i \eta^i \tag{2.10}$$

With the power series in reduced density being given by the equations:

$$a_i = a_{0,i} + \frac{m-1}{m} a_{1,i} + \frac{m-1}{m}\frac{m-2}{m} a_{2,i} \tag{2.11}$$

$$b_i = b_{0,i} + \frac{m-1}{m} b_{1,i} + \frac{m-1}{m}\frac{m-2}{m} b_{2,i} \tag{2.12}$$

By applying the van der Waals one-fluid mixing rules to the perturbation terms, it gives:

$$a_1^{disp} = -2\pi\rho I_1(\eta,\bar{m}) \sum_i \sum_j x_i x_j m_i m_j \sigma_{ij}^3 \frac{\varepsilon_{ij}}{kT} \tag{2.13}$$

$$a_2^{disp} = -\pi\rho\bar{m}\left(1 + Z^{hc} + \rho\frac{\partial Z^{hc}}{\partial \rho}\right)^{-1} I_2(\eta,\bar{m}) \sum_i \sum_j x_i x_j m_i m_j \sigma_{ij}^3 \left(\frac{\varepsilon_{ij}}{kT}\right)^2 \tag{2.14}$$

The mixing rules for the parameters are needed:

$$\sigma_{ij} = \frac{1}{2}(\sigma_i + \sigma_j) \tag{2.15}$$

$$\varepsilon_{ij} = \sqrt{\varepsilon_i \varepsilon_j}(1 - k_{ij}) \tag{2.16}$$

2.1.1.2 Association term

The association term a^{assoc}, which represents the contributions of association forces of sites, is formulated as:

$$a^{assoc} = \sum_i x_i \left[\sum_{A_i} (ln X^{A_i} - X^{A_i}/2) + M_i/2\right] \tag{2.17}$$

where M_i is the association site number of molecule *i*, and X^{A_i} is the fraction of molecules *i* not bonded at site A, given by:

$$X^{A_i} = \left[1 + \sum_j \sum_{B_j} \rho_j X^{B_j} \Delta^{A_i B_j}\right]^{-1} \tag{2.18}$$

The original and the simplified PC-SAFT have the same pure component parameters, while a simple conversion is needed for the association volume parameter due to a slightly different expression for the association strength employed in the simplified PC-SAFT:

$$\Delta^{A_i B_j} = N_{av} \sigma_{ij}^3 g^{hs} \frac{\pi}{6} \kappa^{A_i B_j} \left[exp\left(\frac{\varepsilon^{A_i B_j}}{kT}\right) - 1\right] \tag{2.19}$$

In other words, the association volume $\kappa^{A_i B_j}$ from the original PC-SAFT should be divided $\pi/6$ when used into the simplified PC-SAFT.

In this project, the following combing rules are used for cross-associating mixtures:

$$\varepsilon^{A_i B_j} = \frac{1}{2}(\varepsilon^{A_i B_i} + \varepsilon^{A_j B_j}) \tag{2.20}$$

$$\kappa^{A_i B_j} = \sqrt{\kappa^{A_i B_i} \kappa^{A_j B_j}} \tag{2.21}$$

More details can be found in the literature [von Solms et al. (2003), Grenner et al. (2006), Kontogeorgis et al. (2010a)].

2.1.2 CPA EOS

The CPA EOS, proposed by Kontogeorgis et al. (1996), is a combination of the SRK (or other cubic) EOS, widely used in the petroleum industry (e.g. for mixtures with gases and hydrocarbons), and of the association term of the SAFT type models. The CPA model reduces to SRK in the absence of hydrogen bonding compounds (water, alcohols, acids, etc.), thus achieving a balance between accuracy and simplicity and gaining acceptance in the oil, gas and chemical industries.

The CPA EOS can be expressed for mixtures in terms of pressure P as:

$$P = \frac{RT}{V_m - b} - \frac{a(T)}{V_m(V_m + b)} - \frac{1}{2}\frac{RT}{V_m}\left(1 + \rho \frac{\partial lng}{\partial \rho}\right) \sum_i x_i \sum_{A_i} (1 - X^{A_i}) \tag{2.22}$$

Where ρ is the molar density ($\rho = 1/V_m$), and $g = 1/(1 - 0.475\ b\rho)$. More details of CPA can be found in the literature [Kontogeorgis et al. (1996, 2010a)].

For non-associating components, the main difference of CPA and SRK comes from the parameterization. The critical properties and acentric factor are used in the SRK, while the pure component parameters of CPA are regressed from vapor pressure and liquid density. Besides simplicity and accuracy, the numerical implementation of the association term ensures that the computation time is not much higher than that of SRK and other simple models [Michelsen et al. (2001, 2006)].

CPA is a useful EOS in modeling aqueous systems [Kontogeorgis et al. (2010a)]. It can predict satisfactorily multicomponent, multiphase equilibria for mixtures containing water, hydrocarbons and chemicals, e.g. alcohols or glycols [Kontogeorgis et al. (1996, 2006a, 2006b, 2010a, 2011)]. More specifically, the CPA EOS has been previously shown to perform very well in correlating with one adjustable parameter (per binary) LLE for water-alkanes [Yakoumis et al. (1998)] and with two adjustable parameters (as cross association is accounted for) LLE and VLE for water-aromatics [Folas et al. (2005)]. A characteristic application of the model that reveals its predictive capabilities is the LLE aqueous multicomponent systems with glycols and hydrocarbons [Kontogeorgis et al. (2011)]. The CPA EOS is a well established model for associating fluids containing mixtures, and it is used in many cases for comparing the results obtained with the PC-SAFT model in this project.

2.1.3 Deviations

The percentage (average) absolute deviation will be used to evaluate the quantitative performance in this work, defined as:

$$\%AAD(\Omega) = \frac{1}{N}\sum_{i=1}^{N}\left|\frac{\Omega_i^{calc}}{\Omega_{\mathrm{i}}^{\mathrm{exp}}} - 1\right| \times 100\% \tag{2.23}$$

$$\%AD(\Omega) = \left|\frac{\Omega_i^{calc}}{\Omega_{\mathrm{i}}^{\mathrm{exp}}} - 1\right| \times 100\% \tag{2.24}$$

where Ω is vapor pressure, liquid molar volume, speed of sound, residual isochoric and isobaric heat capacities, or composition in LLE.

The following equation is used for temperature:

$$\%\Delta T = \frac{1}{N}\sum_{i=1}^{N}\left|\mathrm{T}_i^{calc} - \mathrm{T}_{\mathrm{i}}^{\mathrm{exp}}\right| \tag{2.25}$$

And for vapor composition, it is:

$$\%\Delta y = \frac{1}{N}\sum_{i=1}^{N}\left|\mathrm{y}_i^{calc} - \mathrm{y}_\mathrm{i}^{\exp}\right| \times 100\% \tag{2.26}$$

The percentage (average) relative deviation is also used in certain cases, and it gives the information to show if the deviations are positive or negative, and if the modeling results qualitatively match the experimental data well. It is defined as:

$$\%ARD(\Omega) = \frac{1}{N}\sum_{i=1}^{N}\left(\frac{\Omega_i^{calc}}{\Omega_\mathrm{i}^{\exp}} - 1\right) \times 100\% \tag{2.27}$$

$$\%RD(\Omega) = \left(\frac{\Omega_i^{calc}}{\Omega_\mathrm{i}^{\exp}} - 1\right) \times 100\% \tag{2.28}$$

2.2 Water parameters

Modeling water is a vital part of this project, and it is also very important in research and industrial applications. Water is, in many respects, a unique molecule and it is a challenge for any EOS to simultaneously model the physical properties and phase equilibria of water containing systems with satisfactory accuracy [Kontogeorgis et al. (2010a)].

Hydrogen-bonding and the associated tetrahedral structure are considered to be the dominant factors for the unusual and complex behavior of water containing systems [Nezbeda et al. (1999)]. The association models, which explicitly account for hydrogen bonding interactions, show advantages over the classical ones, especially from a predictive point of view [Kontogeorgis et al. (2010a)].

2.2.1 Literature review

Water has been modeled as a two-site (2B), three-site (3B) or four-site (4C) molecule within the SAFT framework [Huang et al. (1990)]. Numerous water containing systems have been studied with PC-SAFT in the past decade, and more than 20 sets of pure component parameters have been published with emphasis on different applications. This is because, as clearly demonstrated by Clark et al. (2006), the five pure component parameters have a degeneracy when fitted solely to vapor pressure and saturated liquid density.

In the work of extending PC-SAFT to associating systems, Gross and Sadowski (2002) published a 2B parameter set for water along with other associating fluids, i.e. alcohols, amines and one acid. In order to have a better description of experimental data in a narrow temperature range, Cameretti et al. (2005) refitted the pure component parameters with the 2B scheme. Later, Cameretti et al. (2008) proposed to use a temperature dependent segment diameter to obtain an excellent description of the density of water. This new water parameter set has been recently applied for biological systems [Held et al. (2011, 2013, 2014)]. In order to find an appropriate association scheme for water, Kleiner (2008) fitted the pure component parameters using the 3B and 4C schemes as well, which were tested for the binary systems of water with different hydrocarbons along with the 2B parameters from Gross and Sadowski (2002). It was found that the mutual solubility of water and hydrocarbons could be described only with the 4C scheme.

In order to investigate the performance of PC-SAFT for describing spectroscopy data, seven 4C parameter sets with gradually fixed segment number (m=2.00-3.50) were proposed by von Solms et al. (2006b), where they are compared with the 2B parameters of Gross and Sadowski (2002). The 4C scheme was found to be more appropriate by using the spectroscopy data as a guide in finding suitable model parameters. Using physically justified values for the association energy and the dispersion energy, Grenner et al. (2006) proposed a 4C parameter set with a fixed segment number (m=1.5). They showed that in this way good results are obtained for the phase equilibria of water containing systems [Grenner et al. (2008), Tsivintzelis et al. (2008)]. To comment on parameter estimation of water, Grenner et al. (2007b) published a new 4C parameter set by fitting to vapor pressure, liquid density and enthalpy of vaporization data. They pointed out that the use of mixture data, especially LLE data for mixtures of associating and inert compounds, is possibly the ultimate test for obtaining optimum parameters. Kontogeorgis et al. (2010b) published three parameter sets for 2B, 3B and 4C directly using monomer fraction in the parameter estimation, and it was found that 4C scheme is the best choice for water. Meanwhile it is still an open question whether the phase behavior calculations could be improved by including monomer fraction data in the parameter estimation [Kontogeorgis et al. (2010b), Tsivintzelis et al. (2014)].

Aparicio-Martínez and Hall (2007) fitted the PC-SAFT parameters of water to vapor pressure and saturated liquid data with the consideration of hydrogen-bonding energy for the association schemes 2B, 3B and 4C. They found that the 3B scheme seems to be the most appropriate choice from the structural point of view. They also commented that the experimental spectroscopic data may be

helpful for selecting the most adequate association scheme. Then the 3B parameters were further rescaled to match the critical points with the association parameters retained, and with this new parameter set, promising results were shown for modeling aqueous mixtures with CO_2, N_2 and n-alkanes.

Diamantonis and Economou (2010) published a PC-SAFT 4C parameter set which shows overall satisfactory results for the physical properties of pure water, and has found applications in carbon capture and sequestration (CCS) related systems.

2.2.2 Comparison of literature parameters

Eight of the PC-SAFT parameter sets for pure water reviewed above will be compared in this work. The parameters are listed in Table 2.1, and the association volume parameter has been converted to those used in the simplified PC-SAFT EOS [von Solms et al. (2003), Grenner et al. (2006)]. It can be readily seen that the five pure component parameters cover wide ranges, e.g. the segment number from 1 to 3, the dispersion energy from 140K to 372K, and the association energy from 1259K to 2501K. These parameter sets are selected because, besides the wide ranges, they are reported from different groups, and are optimized from different criteria, e.g. best pure properties, including monomer fractions, and LLE of water containing binaries. Also, we can reproduce the published deviations for the vapor pressure and the liquid density.

Table 2.1 The water pure component parameters with the simplified PC-SAFT EOS

Set name*	m	σ (Å)	ε/k (K)	ε^{HB}/k (K)	κ^{HB}	scheme	T range(K)
GS	1.0656	3.0007	366.51	2501.00	0.06659	2B	273-647
W2B	1.3112	2.7613	372.37	2123.10	0.09356	2B	273-634
W3B	1.7960	2.4697	327.62	1558.40	0.1304	3B	273-634
W3B_C	2.3753	2.5609	275.81	1558.40	0.1304	3B	273-634
AG	1.5	2.6273	180.30	1804.22	0.1800	4C	324-583
DE	2.1945	2.2290	141.66	1804.17	0.3894	4C	275-640
NVS	3.0	2.0135	182.92	1259.00	0.8188	4C	275-640
W4C	1.5725	2.6270	291.13	1334.20	0.1420	4C	273-634
XL	2.0	2.3449	171.67	1704.06	0.3048	4C	280-620

* The names are based on the authors, GS, AG, DE, NVS and XL are parameters from Gross and Sadowski (2002), Grenner et al. (2006), Diamantonis and Economou (2010), von Solms et al. (2006b) and this work, respectively. While the names starting with the letter 'W' followed by the association schemes are from Aparicio-Marínez et al. (2007), since there are four parameter sets from the same work. The parameter set W3B_C represents the set with non-associating parameters matched to critical points with scheme 3B.

Table 2.2 %AADs for pure water properties using the parameters of Table 2.1

Sets	%AAD of different properties against NIST data in 280-620K [REFPROP (2010)]						
	Vap. Pres.	Density	Res. C_V	Res. C_P	Speed of sound	dP/dV	sum (%AAD)
GS	2.30	6.22	22.8	25.9	41.0	94.4	193
W2B	*0.82*	4.28	*19.8*	*14.5*	55.3	137	232
W3B	*0.71*	4.02	29.1	*14.2*	66.9	156	271
W3B_C	3.92	61.1	***18.4***	26.4	55.7	*29.0*	195
AG	1.85	3.50	20.1	29.7	*19.1*	61.1	135
DE	2.03	***0.86***	23.8	20.1	***7.20***	***16.9***	***70.9***
NVS	***0.30***	*1.41*	34.5	***9.33***	45.6	89.5	181
W4C	*0.70*	4.85	*18.9*	*13.8*	63.3	176	278
XL	1.46	2.14	21.8	20.6	21.1	49.7	*117*
CPA	*0.75*	*1.16*	***15.1***	*11.0*	*9.05*	*18.4*	***55.5***

Note: (1) The ***Bold and Italic*** values are the smallest %AAD; (2) The *Italic* values are slightly worse than the best ones, but they are quite satisfactory; (3) The Highlight (gray) values are the largest %AAD; (4) If the result of CPA is best, it is also marked; (5) The same marks are used in the following tables.

As found in Table 2.1, a name is given to each parameter set. In general, these names are based on the authors, for instance, GS, AG, DE and NVS are parameters from Gross and Sadowski (2002), Grenner et al. (2006), Diamantonis and Economou (2010) and von Solms et al. (2006b). The parameters from Aparicio-Marínez et al. (2007), however, are based on the association scheme, since there are four parameter sets from the same work. Their names start with the letter 'W' followed by the association schemes. The parameter set W3B_C represents the set with non-associating parameters matched to critical points with scheme 3B. In the following discussion, the association scheme will be attached in many cases as well for clearer explanation.

Firstly, the physical properties of pure water are calculated using these eight parameter sets with the simplified PC-SAFT EOS. The %AADs of the predictions against from the NIST data [REFPROP (2010)], in the temperature range of 280-620K, are listed in Table 2.2. Almost all parameter sets give quite reasonable and similar deviations for the vapor pressure, while they show different deviations for the saturated liquid density. The set W3B_C, as expected, presents worst deviations for these two properties, since the parameters are forced to match the critical properties. Most of the sets fail to represent the second-order derivative properties within 10%. It is shown in Figure 2.1 (a) that none of the parameter sets satisfactorily describes the residual isochoric heat capacity from

either the quantitative or the qualitative points of view. This property is directly related to the derivatives of Helmholtz free energy with respect to temperature as shown in equation (1.9). Table 2.2 also shows that the parameter set DE presents the smallest deviation for the speed of sound. As seen in Figure 2.1 (b), however, all sets fail to capture the curvature of speed of sound against temperature, especially the maximum around 350K. The results of residual isochoric heat capacity and speed of sound indicate that the temperature dependences of the model must be improved for water. The parameter sets with the 4C association scheme tend to provide an overall better description of pure water properties from a quantitative point of view, as seen in Table 2.2.

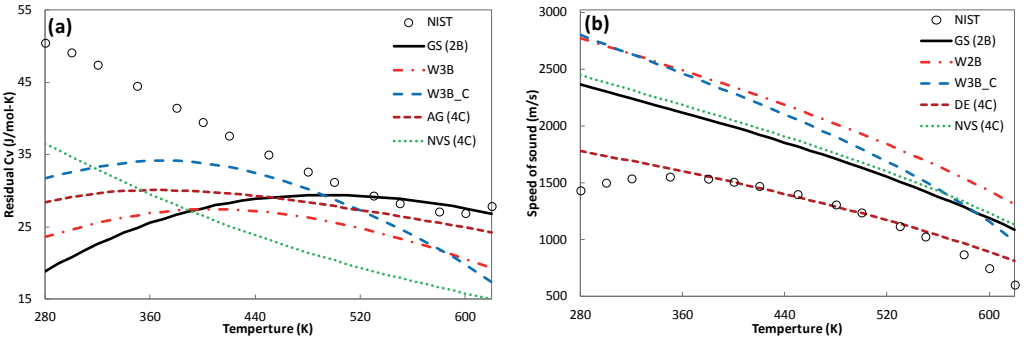

Figure 2.1 Experimental and calculated properties with PC-SAFT using different model parameters (a) residual isochoric heat capacity of saturated water and (b) speed of sound in saturated water. The experimental data are from NIST [REFPROP (2010)].

The calculated percentage monomer fractions using the eight parameter sets are plotted in Figures 2.2 (a). It can be seen that the predictions from the sets NVS (4C) and W4C are closest to the experimental data at the low and high temperature regions, respectively. The parameters with both 2B and 3B association schemes over-predict the monomer fractions. In the original article [Luck (1980)] and a later publication [Luck (1991)], as discussed and verified by von Solms et al. (2006b), Luck assumed four sites on water to calculate the monomer fractions. So it might be unfair to compare the monomer fractions predicted from 2B or 3B schemes to the 'experimental 4C data'. It is, however, possible to obtain the 'experimental' free site fraction from monomer fraction by applying the following equation, which was given by von Solms et al. (2006b):

$$X_1 = \prod_{A=1}^{A=S} X^A \tag{2.29}$$

where X_1 is the monomer fraction, X^A is the free site fraction, S is the total site number.

The free site fraction can be directly calculated from the association models using equation (2.18). This indicates that it is more straightforward to compare the free site fractions instead of monomer fractions if different association schemes are to be compared at the same conditions, so the free site fractions will be used hereafter in the following discussions. As shown in Figure 2.2 (b), the two 2B parameter sets under-predict the free site fractions.

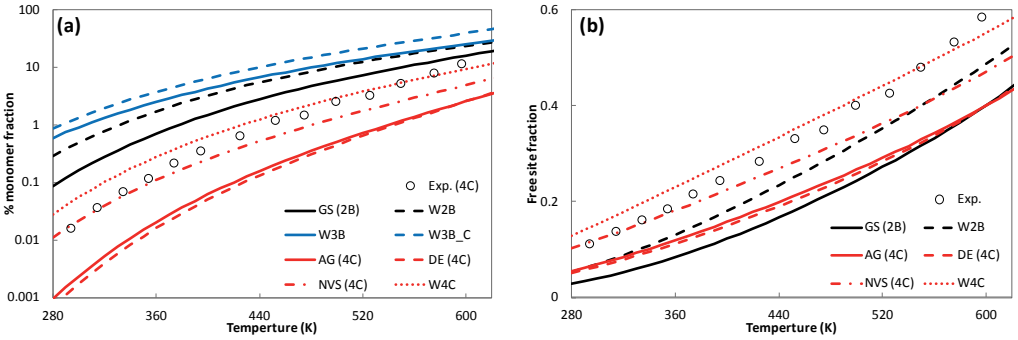

Figure 2.2 Calculated percentage (a) monomer fractions and (b) free site fractions of saturated water with PC-SAFT. In Figure 2.2 (a), the experimental monomer fractions were obtained assuming four sites on water (4C scheme), and the corresponding free site fractions in Figure 2.2 (b) are converted by applying equation (2.25). Data are taken from Luck (1980, 1991).

The investigations on properties of pure water discussed above show that the parameter sets with the 4C scheme present better performance, but none of them seems to be clearly superior to the others. The binary systems of water with non-aromatic hydrocarbons are perfect candidate systems to study the associating interactions of water, as the non-aromatic hydrocarbons are considered to be inert compounds. The solubility of water in the hydrocarbon rich phase is a few orders of magnitude higher than the solubility of hydrocarbon in the water rich phase, mainly due to the self-associating interactions of water.

The prediction and correlation of LLE of binary systems of water with n-hexane, n-octane or cyclo-hexane [Tsonopoulos et al. (1983, 1985)] are shown in Table 2.3, in which both %ARD and %AAD are reported for the mutual solubility of water and hydrocarbons. The pure component parameters of these hydrocarbons are taken from Gross and Sadowski (2001). The %ARD is helpful to distinguish a positive or negative deviation, and give an intuitive idea about how good or bad the results are. Typical prediction and correlation results of the binary system of water with n-hexane

are presented in Figures 2.3 (a) and (b), respectively. A temperature independent binary interaction parameter (k_{ij}) is fitted to the solubilities in both phases. The fitted k_{ij} values are sorted from smallest to largest, and plotted against the parameter sets in Figure 2.4. It can be concluded that:

(1) The behavior for the three binary systems is quite similar for all the parameter sets as shown by the %AAD in Table 2.3, and also indicated by the k_{ij} values in Figure 2.4;
(2) The correlations of the solubilities of hydrocarbons in the water rich phase show a weak dependence on the parameters within the same association scheme, i.e. different parameters with the same association scheme have quite similar results; the minimum in the solubilities of hydrocarbons in water are not captured by any set;
(3) The parameter sets with the 2B or 3B association schemes over-predict the solubility of water in the hydrocarbon rich phase;
(4) The two parameter sets AG (4C) and DE (4C) are the only ones able to simultaneously describe the solubilities in both phases, and AG (4C) gives the best results (at the slight cost of the density prediction shown in Table 2.2);
(5) The parameter set NVS (4C), which has the best representation of vapor pressure and quite accurate description of liquid density for pure water, shows difficulties in simultaneously capturing the solubility in both phases of the binary mixtures. This is mainly because it significantly under-predicts the solubility of hydrocarbon in the water rich phase.
(6) The parameter set W3B_C over-predicts the solubility of water in the hydrocarbon rich phase most.

As seen from Table 2.3 and Figure 2.3, the two solubility lines move in the same direction, and the sign of k_{ij} value is determined by the solubility of hydrocarbon in the water rich phase for the parameters discussed above. Figure 2.3 also shows that the solubility lines of hydrocarbons in the water rich phase have quite similar slopes for association schemes 2B and 3B, while they are significantly different from those of the scheme 4C. This leads to large differences on the deviations of the solubility of hydrocarbons in the water rich phase for the schemes 2B and 3B, as listed in Table 2.3. Based on this fact, it can also be anticipated that quite different results might be obtained when the data in different temperature ranges are used to fit the k_{ij} values.

Table 2.3 %AADs (%ARD)s for the mutual solubility of water and hydrocarbons with PC-SAFT and CPA*

Model	Prediction			Correlation	
	x(HC) in H_2O	x(H_2O) in HC	kij	x(HC) in H_2O	x(H_2O) in HC
	n-Hexane (Experimental data from Tsonopoulos et al. (1983) in 270-490K)				
GS	517 (+)	568 (+)	0.0349	86.6 (49.2)	385 (+)
W2B	***43.6 (-)***	671 (+)	-0.0239	104 (60.3)	864 (+)
W3B	94.6 (-)	678 (+)	-0.0732	89.0 (44.5)	1482 (+)
W3B_C	1513 (+)	1339 (+)	0.0590	110 (64.0)	609 (+)
AG	636 (+)	*14.2 (13.3)*	0.0488	*49.4* (16.5)	*13.2 (-11.0)*
DE	80.6 (65.4)	*31.5 (-)*	0.0088	*46.4* (16.5)	*34.6 (-)*
NVS	99.4 (-)	43.3 (+)	-0.1087	***42.3*** (6.39)	248 (+)
W4C	85.8 (-)	312 (+)	-0.0503	*58.8* (20.1)	505 (+)
XL	*52.3(24.5)*	***9.83 (+)***	0.0021	*46.2* (14.1)	***8.67 (+)***
CPA	*75.8 (54.9)*	*15.8 (11.5)*	0.0355	***35.6*** (-14.9)	*11.7(1.67)*
	n-Octane (Experimental data from Tsonopoulos et al. (1985) in 270-530K)				
GS	680 (+)	470 (+)	0.0319	101 (64.6)	325 (+)
W2B	*46.9 (-)*	568 (+)	-0.0255	130 (88.6)	753 (+)
W3B	96.3 (-)	572 (+)	-0.0739	110 (67.3)	1308 (+)
W3B_C	2592 (+)	1116 (+)	0.0560	152 (108)	509 (+)
AG	955 (+)	***5.74 (-2.88)***	0.0461	*49.5* (11.8)	*23.2 (-)*
DE	77.8 (54.2)	43.1 (-)	0.0067	*45.1* (9.72)	45.1 (-)
NVS	99.7 (-)	*22.8 (15.4)*	-0.1095	***38.6*** (2.53)	189 (+)
W4C	90.6 (-)	252 (+)	-0.0517	63.6 (25.7)	427 (+)
XL	***44.0 (8.93)***	*8.37(-)*	0.0001	*43.7* (8.34)	***8.42 (-)***
CPA	***30.8 (-13.0)***	*10.4 (-)*	-0.0165	*47.3* (18.3)	***6.40 (-)***
	Cyclohexane (Experimental data from Tsonopoulos et al. (1983) in 270-520K)				
GS	1236 (+)	984 (+)	0.0656	59.3 (22.4)	422 (+)
W2B	122 (92.7)	1091 (+)	0.0112	70.8 (26.7)	952 (+)
W3B	*71.6 (-)*	1041 (+)	-0.0349	58.0 (11.4)	1585 (+)
W3B_C	2789 (+)	2358 (+)	0.0869	84.8 (36.7)	583 (+)
AG	886 (+)	*31.6* (+)	0.0647	*25.3* (3.80)	*10.5 (-8.9)*
DE	198 (+)	*26.4* (-)	0.0279	*24.0* (5.85)	*37.6 (-)*
NVS	95.5 (-)	65.5 (+)	-0.0714	***17.9*** (-10.8)	221 (+)
W4C	***48.4 (-)***	450 (+)	-0.0170	34.4 (-2.17)	537 (+)
XL	152 (+)	***25.7*** (+)	0.0243	*21.2* (0.84)	***8.73 (7.19)***
CPA	230 (+)	*38.8* (+)	0.0510	59.6 (46.1)	*22.7(18.1)*

* The values in parentheses are %ARD. For simplicity and clarity, if $|\%ARD| > 0.95\%AAD$, using plus and minus to denote its sign only, i.e. positive or negative corresponding to %AAD.

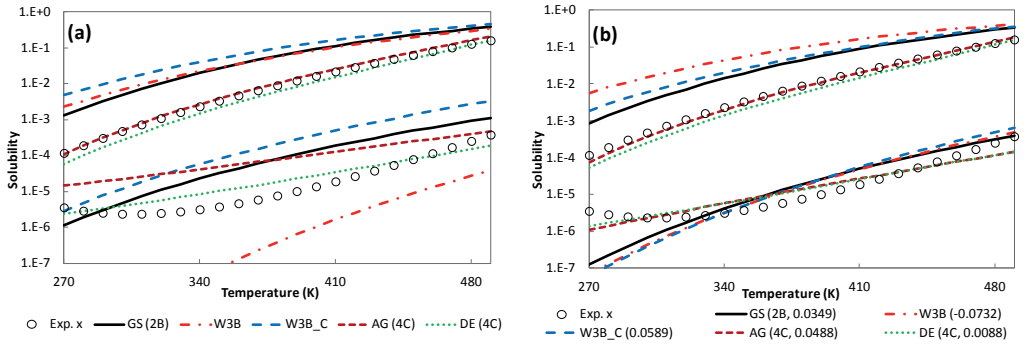

Figure 2.3 Experimental and calculated mutual solubilities of water and n-hexane with PC-SAFT, (a) model predictions, and (b) correlations with k_{ij} shown in the parentheses. The data are taken from Tsonopoulos et al (1983).

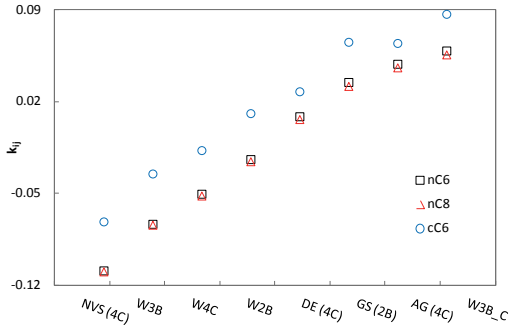

Figure 2.4 Water-HC binary interaction parameter k_{ij} for the considered parameter sets.

2.2.3 2B versus 4C

As shown in Table 2.1 and discussed above, the model parameters from different sources cover wide ranges, thus it is of interest to compare the association schemes in some systematic ways from both qualitative and quantitative viewpoints. We have decided to investigate the water parameters with fixed values of association energy. The assumed ranges 1000-2500K and 1000-2000K are, respectively, chosen for 2B and 4C for the association energy. The other four parameters are fitted to vapor pressure and saturated liquid density of water in the temperature range 280-620K based on the data from NIST [REFPROP (2010)] using the following objective function:

$$Obj(m,\sigma,\varepsilon,\kappa^{HB}) = \sum_{i}\left(\frac{\Omega_i^{Exp} - \Omega_i^{Calc}(m,\sigma,\varepsilon,\varepsilon^{HB},\kappa^{HB})}{\Omega_i^{Exp}}\right)^2 \tag{2.30}$$

where, Ω is vapor pressure or saturated liquid density.

The %AADs for vapor pressure and liquid density are plotted against association energy in Figure 2.5 (a). It can be seen that 2B and 4C have quite similar performance for vapor pressure from the qualitative point of view, but 2B gives smaller deviations in the range close to the experimental association energy value (~1800K). The parameters with 4C association scheme present smaller deviations for saturated liquid densities in the whole range. The %AADs for residual isochoric and isobaric heat capacities are presented against association energy in Figure 2.5 (b). It is revealed that the 4C scheme sets show smaller deviations for residual isochoric heat capacity, while the 2B scheme sets seem to give better description of the residual isobaric heat capacity, again in the region close to the experimental value of the association energy (~1800K). The %AADs for speed of sound and *dP/dV* are presented in Figure 2.5 (c), which clearly shows that the 4C scheme sets present smaller deviations for both properties. As discussed in some previous works [de Villiers et al. (2011, 2013), Liang et al. (2012)], the speed of sound is dominated by the derivative property *dP/dV* when density is described well.

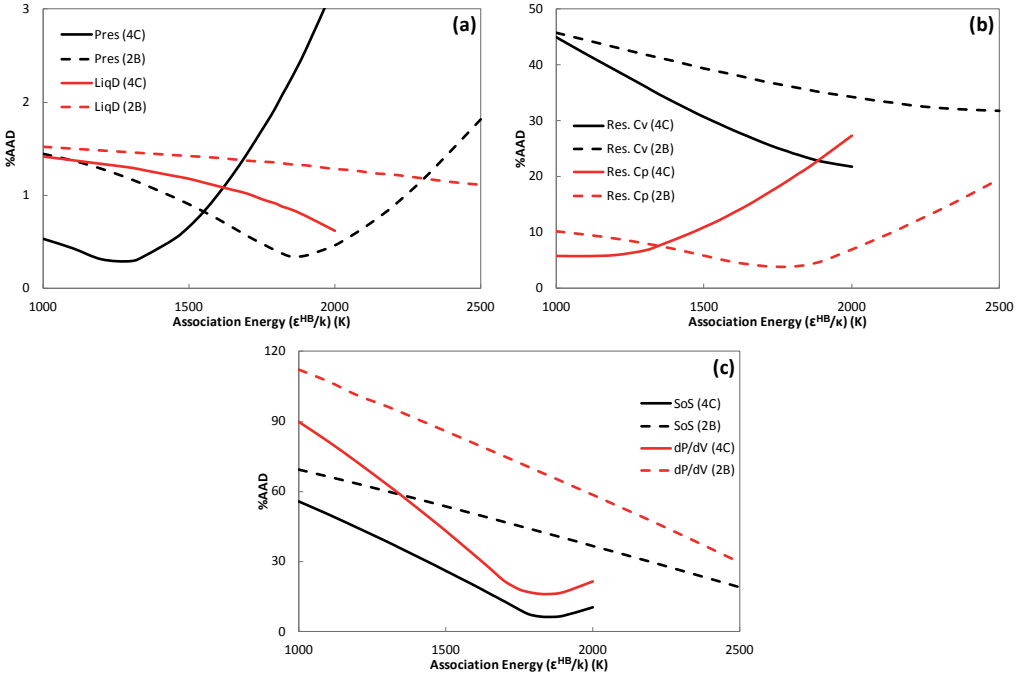

Figure 2.5 %AADs for vapor pressure (Pres), liquid density (LiqD), residual isochoric (Res. C_V) and isobaric (Res. C_P) heat capacities, speed of sound (SoS) and the derivative *dP/dV* (dP/dV) calculated with PC-SAFT using the 2B and 4C schemes.

In order to further study the relationship of water properties on association energy, five parameter sets are chosen for each association scheme. The selected parameter sets cover wide association energy ranges and have enough differences, e.g. larger than 200K, to distinguish each other. The ratios of the calculated and experimental vapor pressure of water are presented in Figures 2.6 (a) and (b) for these two association schemes. Though the best representation of vapor pressure locates at different association energy regions, it can be readily seen that the relationships of this property against association energy are quite similar for these two schemes. The calculated and experimental speed of sound in saturated water are plotted in Figures 2.7 (a) and (b). Figure 2.7 shows that the slope of the calculated speed of sound curve can be slightly changed for both association schemes by changing the parameters, but none of the sets can capture the curvature of speed of sound against temperature. This fact suggests that it is not feasible to put speed of sound directly in parameter estimation as the curvature change occurs in a wide temperature range.

The free site fractions that are predicted using these five parameter sets are presented in Figures 2.8 (a) and (b) for both association schemes. It can be seen that these two association schemes perform quite similarly for this property as well. The same trends, as seen here for vapor pressure, speed of sound and free site fractions against association energy, are also observed for other properties, e.g. liquid density, residual heat capacities. This observation reveals that it is hard to determine which association scheme is superior to the others, in terms of describing the properties of pure water.

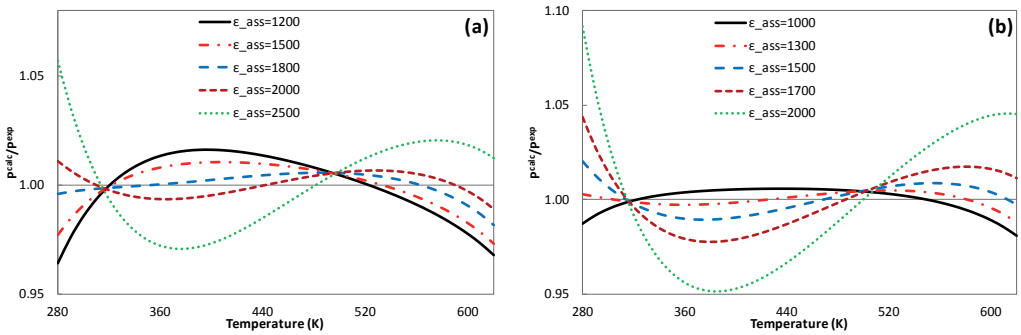

Figure 2.6 Ratio of correlated and experimental vapor pressure values against temperature, (a) 2B and (b) 4C. The label $\varepsilon\_ass = 2000$ denotes the parameters with fixed association energy equal to 2000K. The experimental data is from NIST [REFPROP (2010)].

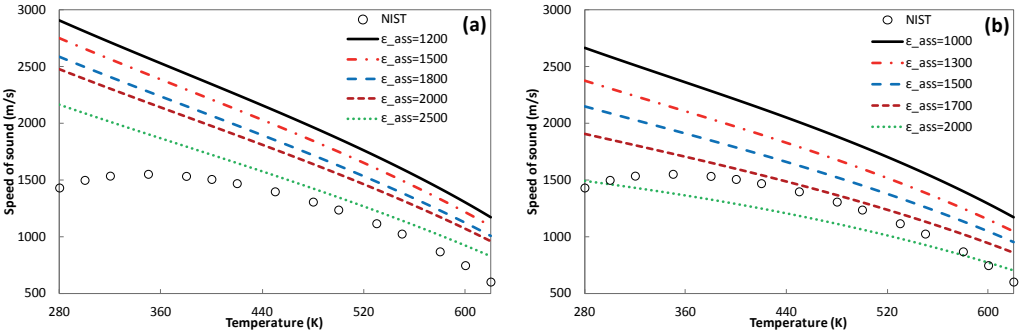

Figure 2.7 Speed of sound prediction with PC-SAFT, (a) 2B and (b) 4C. The label $\varepsilon\_ass = 2000$ denotes the parameters with fixed association energy equal to 2000K. The experimental data is from NIST [REFPROP (2010)].

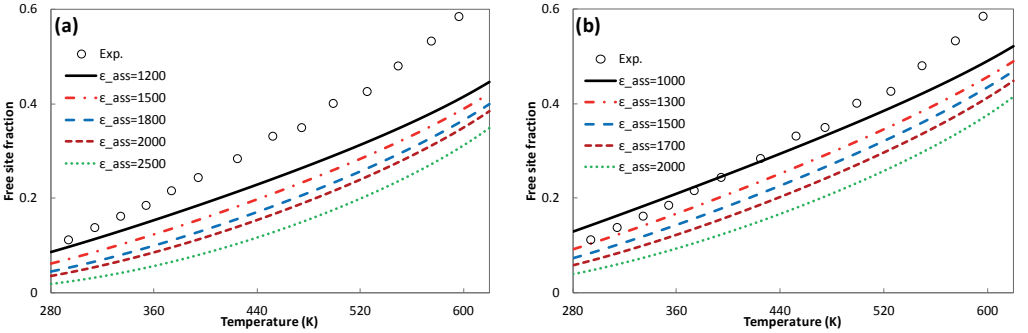

Figure 2.8 Free site fractions predicted with PC-SAFT, (a) 2B and (b) 4C. The label $\varepsilon\_ass = 2000$ denotes the parameters with fixed association energy equal to 2000K. The experimental data are taken from Luck (1980, 1991).

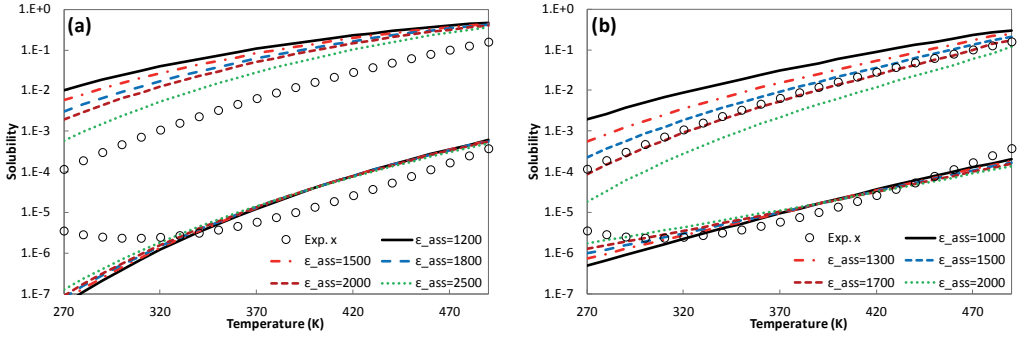

Figure 2.9 Mutual solubilities of water and n-hexane. Calculations with PC-SAFT using the (a) 2B and (b) 4C schemes. The label $\varepsilon\_ass = 2000$ denotes the parameters with fixed association energy equal to 2000K. The data are taken from Tsonopoulos et al. (1983).

The correlated LLE for water with n-hexane is shown in Figure 2.9 for these five parameter sets, for both 2B and 4C. It confirms that it is relatively easy to tune the solubility of hydrocarbons in the water rich phase for both association schemes, while with the 2B scheme some difficulties in describing the solubility of water in the hydrocarbon rich phase are observed without strongly deteriorating the description of the other phase.

If we consider the liquid-liquid equilibria of associating and inert compound mixtures to be the ultimate test for obtaining optimum parameters,

There is no doubt that the 4C scheme is a better choice.

2.2.4 New water pure component parameters

The two parameter sets AG (4C) and DE (4C) have almost the same association energy, but the other four parameters are quite different. They show comparable performance for the phase behaviors of binary systems investigated in this work. Inspired by this fact, following the analysis of association scheme above, we propose a procedure to take the LLE of water and hydrocarbons into account for the estimation of water pure component parameters with the PC-SAFT EOS. This procedure may also be suitable for other SAFT variants.

According to the works of Gupta et al. (1994) and Pfohl et al. (2001), the association energy can be approximately connected to the hydrogen bonding energy:

$$E^{HB} = N_A \varepsilon^{HB} = R\, \varepsilon^{HB}/k \tag{2.31}$$

where E^{HB} is the hydrogen bonding energy, while ε^{HB} is the association energy in perturbation theory based models.

The experimental hydrogen bonding energy is reported as 3.7 kcal/mol from IR measurements [Luck (1980, 1991)], while Luck reported 3.4±0.1 kcal/mol from the two-state theory [Luck (1980)]. If taking the hydrogen bonding energy range 3.3-3.7 kcal/mol, the corresponding association energy range will be 1660-1860K by applying equation (2.31). Therefore the parameters with association energy in the range 1660-1860K will be investigated in this work.

The five pure component parameters are obtained with the following objective function:

$$Obj(\sigma, x_1, x_2) = \sum_i \left(\frac{\Omega_i^{Exp} - \Omega_i^{Calc}(m, \sigma, \varepsilon, \varepsilon^{HB}, \kappa^{HB})}{\Omega_i^{Exp}} \right)^2 \quad (2.32)$$

where Ω is vapor pressure or saturated liquid density.

The estimation procedure is as follows: with a given fixed association energy and another fixed parameter, the other three parameters are fitted to vapor pressure and liquid density. The segment diameter (σ) is adjustable in all cases, while the three parameters segment number (m), dispersion energy (ϵ) and association volume (κ^{HB}) are fixed sequentially, which means that the fitting parameters x_1 and x_2 could be the combinations $\{\epsilon, \kappa^{HB}\}$ if m is fixed, $\{m, \kappa^{HB}\}$ if ϵ is fixed, or $\{m, \epsilon\}$ if κ^{HB} is fixed. The association energy is taken gradually from 1660K to 1860K with an interval 20K, while the ranges for the other three parameters are, respectively, m=[1.5, 3.5], ε=[120, 190], and κ^{HB}=[0.1, 0.6]. A quite similar procedure was adopted in the work of Clark et al. (2006), in which the association energy and the dispersion energy were fixed in wide ranges. This approach makes the optimization procedure be more or less of global character in a rather manual way.

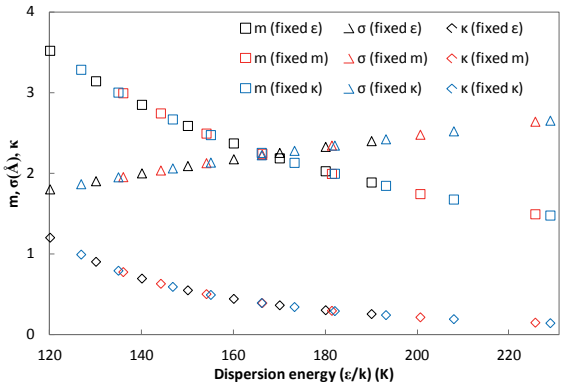

Figure 2.10 The comparison of obtained PC-SAFT parameters using three combinations of fixing two of them. The parameters being fixed are shown in the parentheses.

The parameters from these three different combinations are presented in Figure 2.10. It can be seen that the parameters are consistent with each other. This indicates that a unique solution can be obtained for the three parameters to match the two properties, i.e. vapor pressure and saturated liquid density, when the other two model parameters are fixed. The scenario that both the association energy and association volume are fixed is preferable according to our experience. So

the parameters are refitted with this scenario in the range of association energy from 1660K to 1860K with an interval 10K, and association volume from 0.1 to 0.6 with an interval 0.01.

The final parameters are manually chosen for each given association energy based on the deviations of the solubilities of water in the hydrocarbon rich phase. The main criteria are:

(1) If it is possible to keep the deviations of the solubility of water in all three systems less than 10%, the parameter set is chosen with the smallest sum of the deviations of water with n-octane and with cyclohexane;

(2) Otherwise, the parameter set with smaller sum of the deviations in either the systems of water with n-hexane and with cyclohexane, or the systems of water with n-octane and cyclohexane is chosen, but the later one is given a higher priority. This is because n-hexane and cyclohexane both have six carbon numbers, and quite similar results are obtained for the systems of water with n-hexane and with n-octane, while the correlated 'experimental' data of the system with n-octane is more reliable according to Mączyński et al. (2004).

The %AADs for vapor pressure and saturated liquid density of pure water, and the %AAD for the solubilities of water in the n-hexane, n-octane and cyclohexane rich phases are presented in Figure 2.11. With this parameter estimation strategy, the %AADs for vapor pressure and saturated liquid density increase linearly with the association energy, while the changes of the %AAD for vapor pressure are smoother. It is also readily seen that the solubility of water in all three systems can be correlated with quite good accuracy, i.e. less than 15%, using either small or large k_{ij} values, in the investigated association energy range.

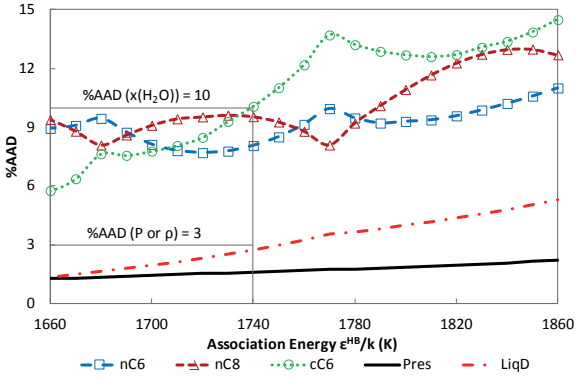

Figure 2.11 %AADs for the solubility of water in hydrocarbon rich phases, vapor pressure and liquid density against the association energy for parameters obtained using the procedure developed in this work for PC-SAFT.

It is noticed that the parameters with association energy below 1740K can present the %AAD for water solubility in the hydrocarbon rich phases less than 10% and the %AADs for vapor pressure and saturated liquid density less than 2% and 3%, respectively. The k_{ij} values are relatively small for the parameters with association energy in the range of 1660-1740K, as presented in Figure 2.12 (a). These k_{ij} values increase linearly with the association energy. Moreover, very good linear correlations can be obtained between the other four parameters and association energy in this range, as shown in Figure 2.12 (b).

All these results indicate that it is hard to determine a unique parameter set if only based on the information available here. Even if the prediction of the mutual solubility of water and hydrocarbons is used as an extra constraint, it is still a difficult decision to make, since mixtures with different hydrocarbons (n-hexane, n-octane or cyclohexane) are described better with different parameter sets. As shown in Figure 2.12 (a), the sets giving better predictions for mixtures of water with n-octane or n-hexane have much higher association energy (around 1700K) than the sets which present better predictions for water with cyclohexane (less than 1660K).

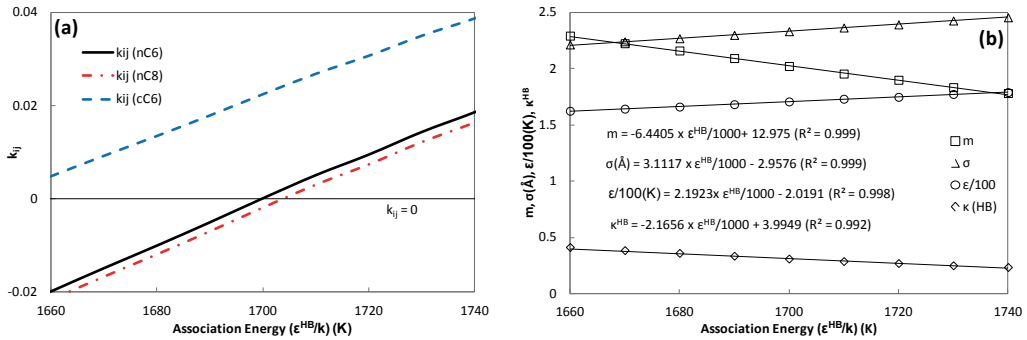

Figure 2.12 (a) The binary interaction parameters of water-hydrocarbons using the water parameters obtained by the procedure developed for PC-SAFT. (b) Linear correlations for the PC-SAFT parameter trends against the association energy in the range of 1660-1740K.

As shown in Figure 2.12 (a), the parameter sets with association energy around 1700K give best predictions for the LLE of water with n-hexane and n-octane, while the corresponding segment number is around 2. So without loss of generality, we have decided to assume the segment number *m* to be equal to 2, instead of assuming association energy to be equal to 1700K. The association energy can be reversely calculated by the correlation of *m*, and then the other parameters can be calculated sequentially using the correlations shown in Figure 2.12 (b). The pure component

parameters (*m=2, σ=2.3449Å, ε=171.67K, ε^{HB}=1704.06K, κ^{HB}=0.3048*) will be used hereafter in this work. Again, here the association volume κ^{HB} is based on the simplified PC-SAFT EOS, and it should be multiplied by π/6 (thus κ=0.1596) if it is used with the original PC-SAFT EOS. It needs to be pointed out that it would not be surprising that equally good LLE correlation results could be obtained using the parameter sets with association energy 1690K, 1700K or 1710K. The calculated deviations of the properties of water from this new water parameter set are also given in Table 2.2.

As seen from Table 2.2, with the new water parameters, the PC-SAFT EOS gives 1.45% and 2.12% deviations for vapor pressure and saturated liquid density, respectively, against from the NIST data [REFPROP (2010)], in the temperature range of 280-620K, which are satisfactory compared to those from the literature available parameters. The deviations of CPA EOS predictions for the properties of water are also reported in Table 2, which are calculated with the water parameters from Kontogeorgis et al. (1999). It is worth noticing that the CPA EOS gives smallest deviations for description of pure water properties.

The calculated and experimental residual isochoric and isobaric heat capacities are compared in Figures 2.13 (a) and (b). Even though CPA gives much smaller %AAD values, we cannot conclude that CPA performs better than PC-SAFT for these two properties, apparently from the qualitative point of view.

The calculated and experimental speed of sound in liquid water at saturated, isobaric and isothermal conditions are presented in Figures 2.14 (a), (b) and (c), respectively. It is shown, on one hand, that both models have apparent difficulties in describing the temperature dependence of speed of sound, even though CPA gives much smaller quantitative deviations. On the other hand, PC-SAFT describes the pressure dependence of speed of sound at constant temperature quite well from a qualitative point of view, which can be demonstrated using a simple translation strategy, as shown in Figure 2.14 (c). The whole calculated line could successfully match the experimental data if a multiplying factor was used. The factor, in this case, equals to the ratio of the experimental and the calculated speed of sound at atmospheric pressure, i.e. the starting point of the line.

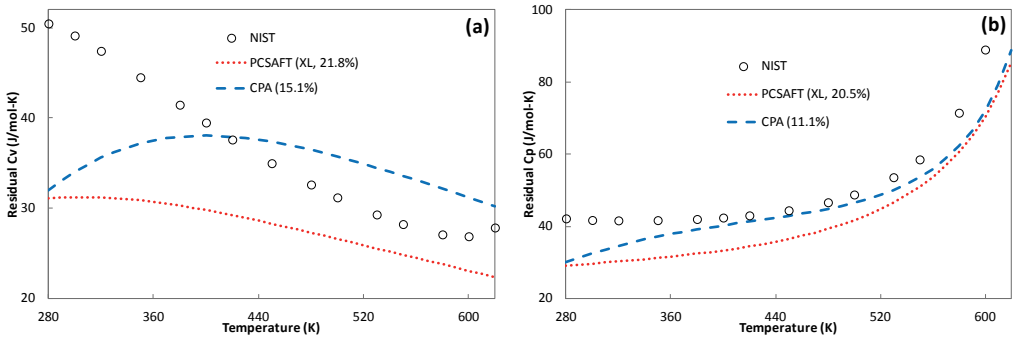

Figure 2.13 Modeling results of PC-SAFT with the new proposed water parameters and CPA for the (a) residual isochoric heat capacity and (b) the residual isobaric heat capacity. The experimental data are taken from NIST [REFPROP (2010)].

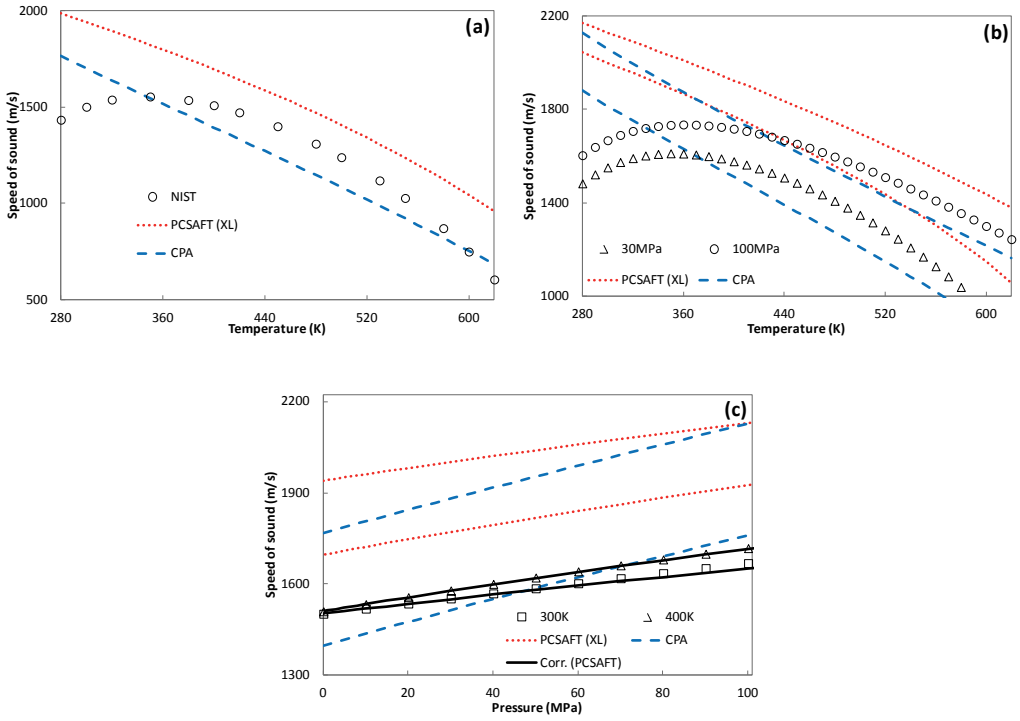

Figure 2.14 Experimental and calculated speed of sound in pure water with PC-SAFT using the new proposed water parameters and CPA at (a) saturated, (b) isobaric and (c) isothermal conditions. The solids lines are correlations obtained if the PC-SAFT results (red-dot lines) are multipled by the ratio of the experimental and the caculated speed of sound from PC-SAFT at the starting points. The experimental data are taken from NIST [REFPROP (2010)].

The prediction and correlation LLE results for water-hydrocarbon systems from the simplified PC-SAFT with the new parameters and CPA are also reported in Table 2.3. The results obtained with the new parameters proposed in this work are denoted as XL. Typical correlation results are shown in Figures 2.15 (a) and (b) for the binary systems of water with n-octane and with cyclohexane, respectively. The two models apparently show quite satisfactory deviations for both phases for these systems. They give similar results for the systems of water with n-hexane and with n-octane, while PC-SAFT seems to have a better description of mutual solubility of water and cyclohexane. The two models also show slightly different slopes of the solubility of hydrocarbons in the water rich phase. Compared to the results in Figure 2.3 (b), this indicates that the association term plays a more important role than the physical (non-association) terms in describing the solubility of hydrocarbons in the water rich phase.

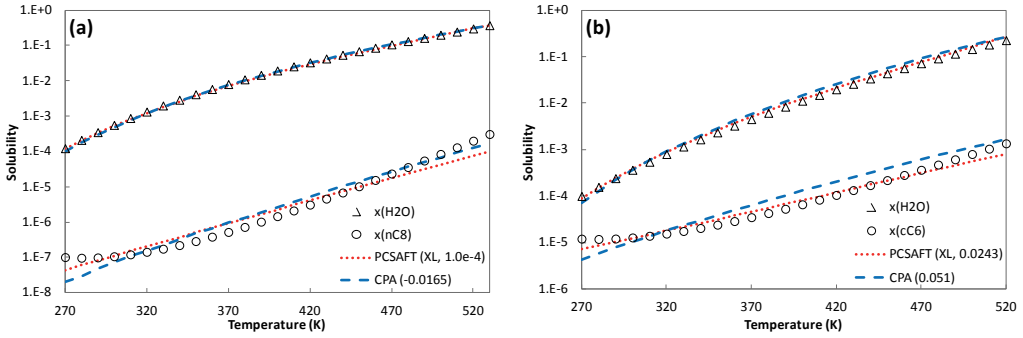

Figure 2.15 Mutual solubilities of water with (a) n-octane and (b) cyclohexane. Experimental data [Tsonopoulos et al. (1983, 1985)], PC-SAFT (with the new proposed water parameters) and CPA.

2.2.5 Comments on free site (monomer) fraction

The calculated and experimental monomer fractions are presented in Figure 2.16 for CPA and PC-SAFT with the new parameters. Similar results are obtained, while predictions from both models show large deviations from the experimental data. However, the predicted results, multiplied by a factor (K_f) 1.3 and 1.4 respectively for CPA and PC-SAFT, match the experimental data quite well, as shown in Figure 2.16.

Comparing Figures 2.8 and 2.9, it can be seen that all five 2B parameter sets under- and over-predict the free site fractions and the solubility of water in the n-hexane rich phase, respectively. However, the watershed happens around association energy 1700K for the 4C parameter sets, from

where the parameter sets under-predict both the free site fraction and the solubility of water. The same behavior is also observed in the binary system of water with n-octane.

The results presented above suggest, on one hand, that either the experimental free site fraction could be much smaller than what are currently being used, or the current association framework prevents them from a simultaneous satisfactory description of the free site fractions and LLE of water-hydrocarbon systems. On the other hand, reinterpretation of the connection between the association models and the experimental free site or monomer fractions may be needed, as we show above, i.e. with multiplying factors.

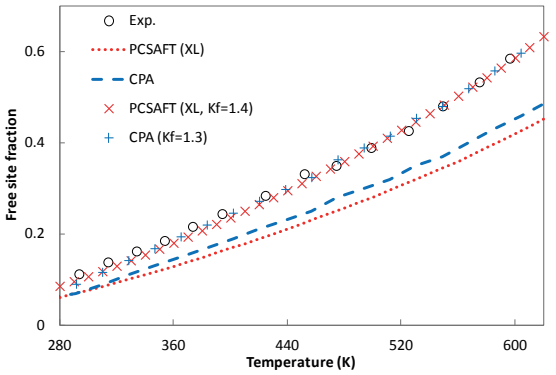

Figure 2.16 Free site fractions of saturated water with PC-SAFT (using the new proposed water parameters) and CPA. Correlations obtained if the PC-SAFT predictions (red dot line) are multiplied by a factor equal to 1.4 (X), and if the CPA predictions (blue dash line) are multiplied by a factor equal to 1.3 (+) are also shown. The experimental data (o) is taken from Luck (1980, 1991).

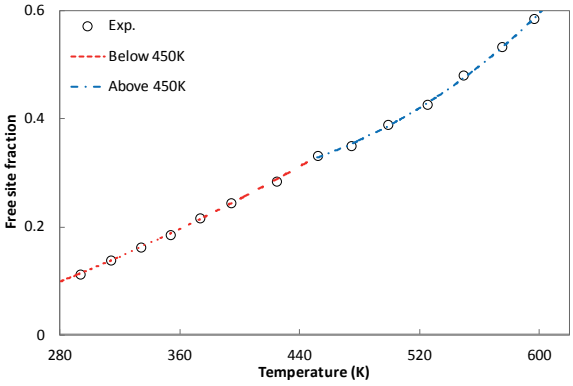

Figure 2.17 Different trends of free site fraction of pure saturated water below and above 450K. The experimental data is taken from Luck (1980, 1991).

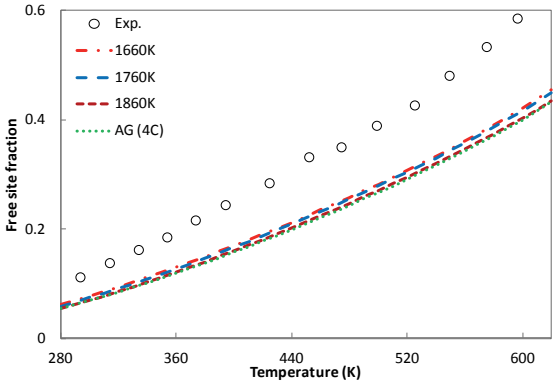

Figure 2.18 Water free site fractions with PC-SAFT using different parameters. The experimental data were converted by applying equation (13) from the monomer fraction data of Luck (1980, 1991). The parameter sets 1660K, 1760K and 1860K were obtained in this work with when considering LLE of water with hydrocarbons, and the parameter set W4C_1 is taken from Grenner et al. (2006).

It is also interesting to note that the trends of the experimental free site fractions are slightly different from below and above 450K, as shown in Figure 2.17, based on the experimental data of Luck (1980, 1991). This indicates that, to some extent, the water may not be stabilized in one structure over a wide range of temperature.

The free site fractions calculated from the three parameter sets with association energies of 1660K, 1760K, 1860K and the set AG (4C) are presented in Figure 2.18. It can be seen that these four parameter sets perform quite similarly from both the quantitative and qualitative points of view. This reveals that the predicted values for the free site fractions or monomer fractions are insensitive to the pure component parameters, when they are estimated under the same constraints, e.g. equally good description of the mutual solubility of water and non-aromatic hydrocarbons in this work. Therefore it may not be surprising that free site fractions or monomer fractions could not provide much help to find a unique parameter set for associating fluids, especially when the experimental uncertainties are not reported.

More systematically experimental investigations are needed based on these discussions, especially due to the fact the LLE of water and hydrocarbons have been measured and critically evaluated by several groups [Tsonopoulos et al. (1983, 1985), Mączyński et al. (2004)]. Tsivintzelis et al. (2014) also suggested that the data for the monomer fractions of methanol and ethanol from the same study of Luck (1980) have to be validated from other groups.

2.2.6 Summary

In this section, the performance of eight parameter sets from the literature is investigated on properties of pure water and LLE of water with non-aromatic hydrocarbons. Then in order to investigate which association scheme is a better choice for water, the pure component parameters are obtained for the 2B and 4C association schemes by fitting to vapor pressure and saturated liquid density with fixed association energies in a wide range. These parameters are subsequently studied for the properties of pure water and the LLE of water with n-hexane from both qualitative and quantitative aspects. The results show that it is hard to determine which scheme (2B or 4C) performs better if we compare them based only on the properties of pure water. This is because 2B tends to have smaller deviations for vapor pressure and residual isobaric heat capacity in the 'experimentally' reasonable association energy ranges, while 4C shows smaller deviations of liquid density, residual isochoric heat capacity and speed of sound. The most important finding is that the two association schemes perform quite similarly from the qualitative point of view for all the properties investigated in this work. For neither scheme do we get parameters able to yield acceptable deviations for the residual isochoric heat capacity, nor could they capture the maximum of speed of sound in water against temperature.

It is shown, however, that the association scheme 4C presents definitely better performance than 2B on phase equilibria of water with non-aromatic hydrocarbons. These binary systems represent a good way to investigate the effect of the self-association interactions of water. An interactive optimization procedure is proposed to take LLE of water with non-aromatic hydrocarbons into account when estimating the water pure component parameters with the simplified PC-SAFT EOS. It is found that numerous parameter sets could give comparably good results in wide parameter ranges. A new parameter set is obtained with the segment number being fixed to 2, which coincidentally presents k_{ij} values close to 0.0 for the systems of water with n-hexane and with n-octane. The new parameter set gives 1.45% and 2.12% deviations for vapor pressure and saturated liquid density, respectively, from NIST data [REFPROP (2010)] in the temperature range of 280-620K, and it represents the description for the mutual solubility of water and hydrocarbons with very high accuracy, which is superior to the other parameter sets available in literature. Finally, the investigations of the free site fractions of water reveal that more systematically experimental and theoretical studies are needed for measuring and explaining the free site fractions or monomer fractions of water, and their relationships with the hydrogen-bonding structure of liquid water.

2.3 Parameters for 1-alcohols and MEG

Chemicals are extensively used in the oil and gas industry [Kontogeorgis et al. (2010a)]. In order to model these compounds, and to compare the water and chemical parameters in a more complete sense, it is crucial to investigate the phase equilibria of binary or ternary mixtures of water, chemicals and hydrocarbons. In this work, methanol, ethanol, 1-propanol, 1-butanol, 1-pentanol and mono-ethylene glycol (MEG) are chosen, because of, besides their industrial importance, the wide variations of molecular interaction strength and the variety of phase equilibrium types. In these systems, VLE, LLE and VLLE types of phase equilibria are observed, and azeotropic behavior also appears in some cases.

Table 2.4 PC-SAFT model parameters of 1-alcohols and MEG and %AADs for vapor pressure and liquid density

Comp.	m	σ (Å)	ε/k (K)	ε^{HB}/k (K)	κ^{HB}	Name*	%AAD	
							Pres.	Dens.
Methanol	1.5255	3.2300	188.90	2899.50	0.06718	GS	1.89	0.52
	1.8824	3.0020	181.77	2738.03	0.1044	XL	1.42	0.23
	2.0	2.9392	180.28	2721.93	0.1071	XL2	2.23	0.32
Ethanol	2.3827	3.1771	198.24	2653.40	0.06185	GS	1.02	0.55
	2.6351	3.0577	191.90	2574.01	0.07885	XL	0.37	0.13
1-propanol	2.9997	3.2522	233.40	2276.80	0.02916	GS	1.06	1.21
	3.2802	3.1234	214.45	2230.20	0.06260	AG	0.37	0.14
1-butanol	2.7515	3.6139	259.50	2544.60	0.01278	GS	0.99	0.79
	2.8317	3.5574	252.15	2504.00	0.01845	IK	1.22	0.81
1-pentanol	3.6260	3.4508	247.28	2252.10	0.01971	GS	0.74	0.36
	2.6048	3.9001	282.31	2811.02	0.006303	AG	3.20	0.34
MEG	1.9088	3.5914	325.23	2080.03	0.04491	AG	1.06	2.27
	2.4064	3.2913	277.13	2000.00	0.09100	XL	1.74	1.73

* The explanations of the names are seen from the content just above the table.

The pure component parameters of these associating fluids are listed in Table 2.4. The parameter sets of all primary alcohols (methanol to 1-pentanol), named as GS, are taken from Gross and Sadowski (2002). The parameter sets of methanol and ethanol, named as XL, are from Liang et al. (2012, 2013), for which the speed of sound were used in the parameter estimation, The parameter sets of 1-propanol and 1-pentanol, named as AG, are from Grenner et al. (2007a), but the 'optimized' set is used for 1-propanol, while the 'generalized' set is used for 1-pentanol. The parameter set of 1-butanol, named as IK, is from Kouskoumvekaki et al. (2004), where they successfully applied the simplified PC-SAFT for complex polymer systems. The parameter set of

MEG, also named as AG, is from Tsivintzelis et al. (2008). Finally the parameter sets XL2 of methanol and XL of MEG are obtained by using the same procedure developed for water in this work. Association schemes 2B and 4C are assumed for 1-alcohols and MEG, respectively. The %AADs for the vapor pressure and liquid density against from DIPPR database (2012) in the reduced temperature range Tr=[0.5, 0.9] are also given, which show they have noticeable deviations.

2.4 Phase behavior

2.4.1 Associating + Inert binary mixtures

2.4.1.1 Vapor-liquid equilibria (solubility)

The VLE correlations of water with methane and with ethane are presented in Figures 2.19-2.22. It can be seen that the correlations from the parameters with the 4C scheme (AG and XL) are better than those of the parameters with the 2B scheme (GS), especially for the water composition in the vapor phase. The two 4C scheme parameter sets AG and XL have similar performance in describing the both phases. It is also clearly shown that a temperature dependent k_{ij} is necessary for describing the solubility of methane or ethane in water, while k_{ij} has very limited impacts on the correlation of water fraction in the vapor phase, i.e. the composition of water is mainly determined by its parameters. As shown in Figures 2.20 (c) and 2.22 (c), the k_{ij} is not a simple function of temperature, e.g. linear with temperature or reciprocal temperature.

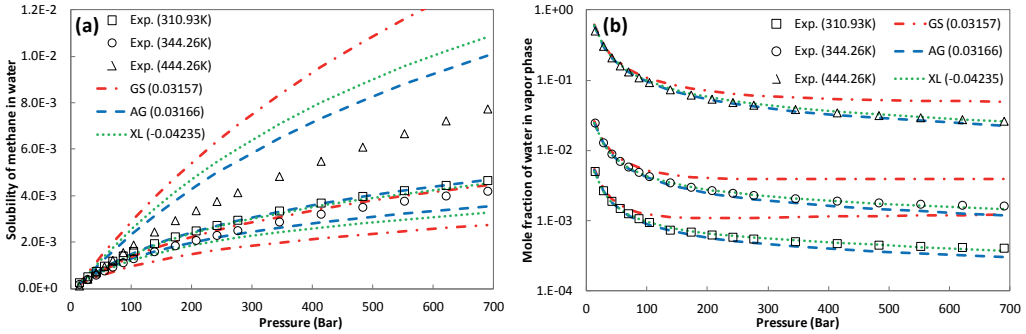

Figure 2.19 Correlations of water + methane with a temperature independent (constant) k_{ij}. The experimental data are from Olds et al. (1942), Culberson et al. (1951), Lekvam (1997), Wang et al. (2003), Chapoy et al. (2004, 2005a, 2005b), Mohammadi et al. (2004), and Frost et al. (2014). GS, AG and XL denote the PC-SAFT parameters of water are from Gross and Sadowski (2002), Grenner et al. (2006) and this work, respectively.

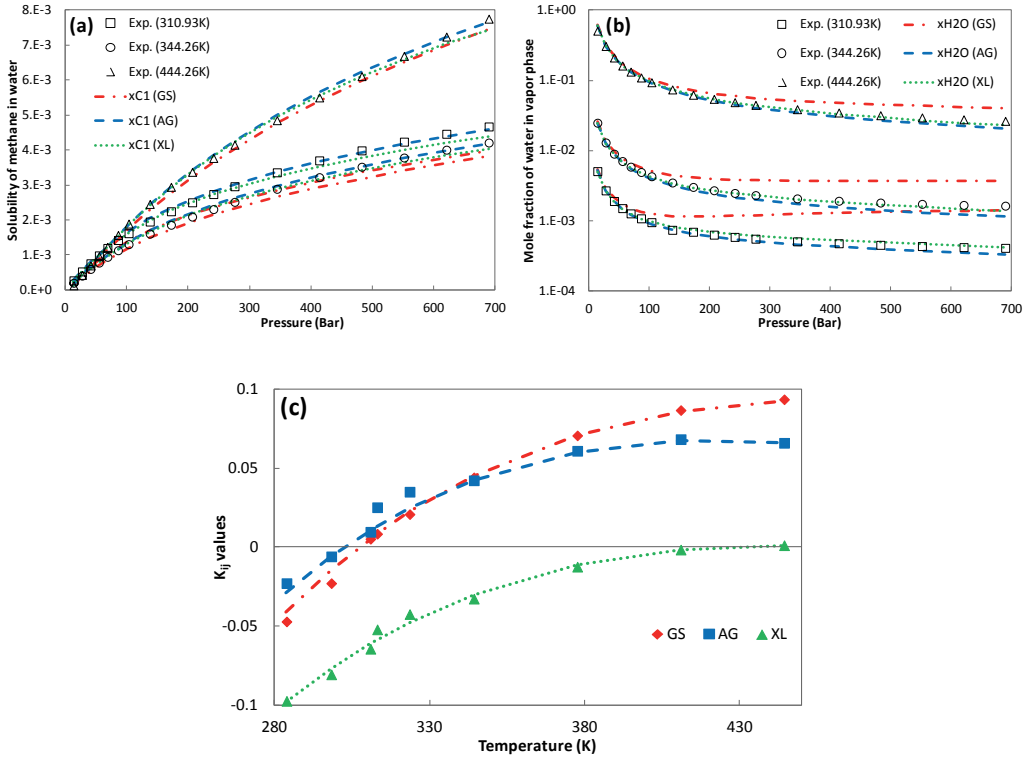

Figure 2.20 Correlations of water + methane with a temperature dependent k_{ij}. The experimental data are from Olds et al. (1942), Culberson et al. (1951), Lekvam (1997), Wang et al. (2003), Chapoy et al. (2004, 2005a, 2005b), Mohammadi et al. (2004), and Frost et al. (2014).

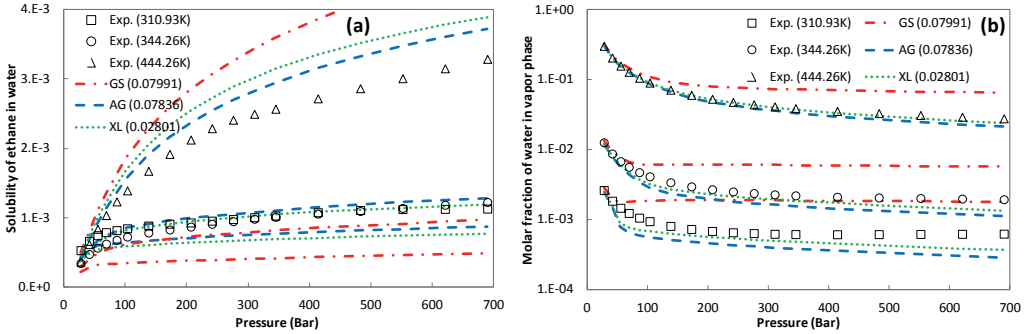

Figure 2.21 Correlations of water + ethane with a temperature independent (constant) k_{ij}. The experimental data are from Culberson et al. (1950), Coan et al. (1971), and Dhima et al. (1998). GS, AG and XL denote the PC-SAFT parameters of water are from Gross and Sadowski (2002), Grenner et al. (2006) and this work, respectively.

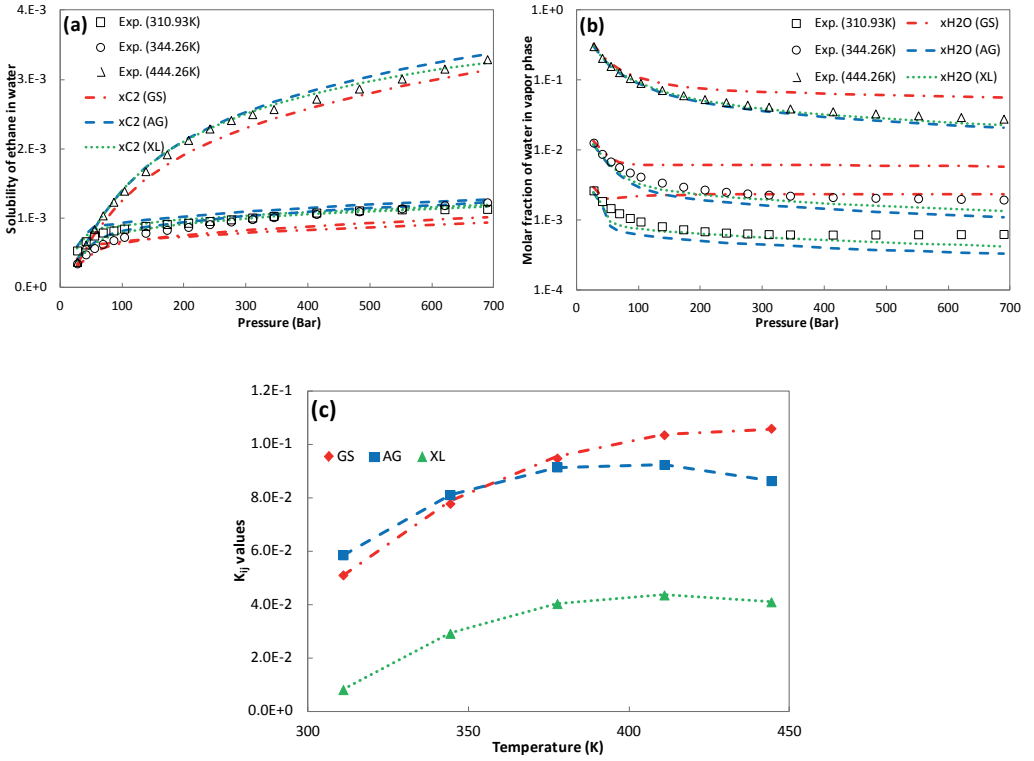

Figure 2.22 Correlations of water + ethane with a temperature dependent k_{ij}. The experimental data are from Culberson et al. (1950), Coan et al. (1971), and Dhima et al. (1998).

The correlations of VLE of methanol with methane are presented in Figures 2.23 and 2.24. The results show that the three parameter sets give similar correlations for the solubility of methane in the polar phase, and the methanol composition in the vapor phase under 20MPa, from which all parameter sets start to present significant deviations, which indicate that the interactions of this system at high pressure are not described satisfactorily with the model, for instance, the 2B scheme may not be appropriate anymore. As for the binary mixture of water with methane, a temperature dependent k_{ij} has significant and limited impacts on the solubility of methane in the polar phase and the methanol composition in the vapor phase, respectively. In this case, a simple correlation of k_{ij} against reciprocal temperature could be found as shown in Figure 2.24 (c). From a quantitative point of view, however, the temperature dependent k_{ij} gives comparable results to those from a constant k_{ij}. As shown in Figures 2.23 (a) and 2.24 (a), the experimental data seems to show some uncertainties, so the constant k_{ij} values will be used in this work.

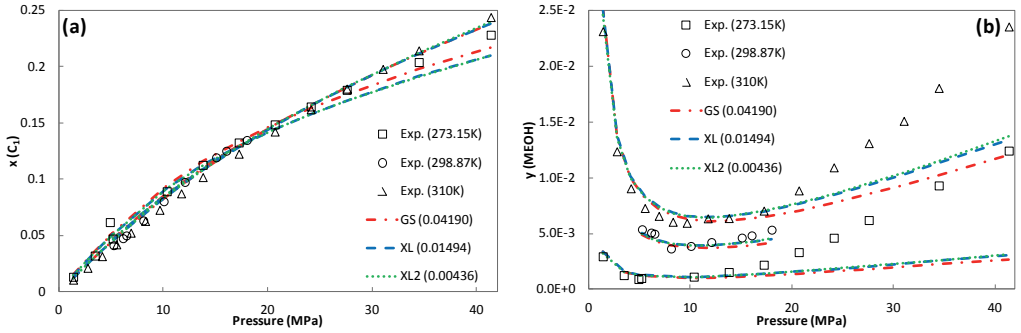

Figure 2.23 Correlations of methanol + methane with a temperature independent (constant) k_{ij}. The experimental data are from Hong et al. (1987), Wang et al. (2003) and Frost et al. (2014). GS, XL and XL2 denote the PC-SAFT parameters of water are from Gross and Sadowski (2002), Liang et al. (2012) and this work, respectively.

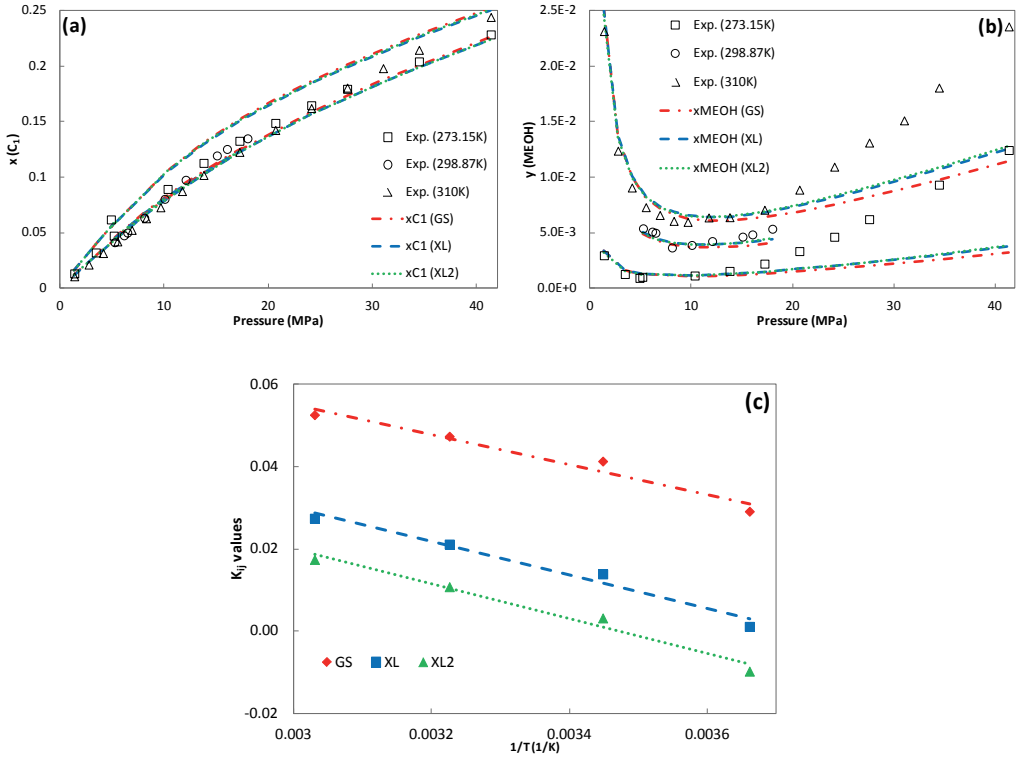

Figure 2.24 Correlations of water + methane with a temperature dependent k_{ij}. The k_{ij} values are plotted in (c). The experimental data are from Hong et al. (1987), Wang et al. (2003) and Frost et al. (2014).

The correlations of the VLE of methanol and propane with a constant k_{ij} are presented in Figure 2.25, which reveals that almost the same results are obtained for the three parameter sets. The correlations of the VLE of MEG and methane with the AG and XL parameter sets using constant k_{ij} values are presented in Figure 2.26. They are reasonably good, and the two sets give similar results.

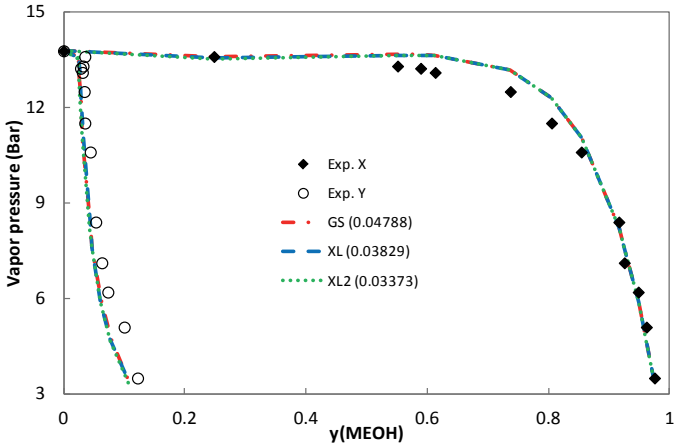

Figure 2.25 Correlations of methanol + propane with the parameters from Gross and Sadowski (2002), and Liang et al. (2012). The parameter set XL2 is from this work. The experimental data are from Galivel-Solastiouk et al. (1986) and Lev et al. (1992).

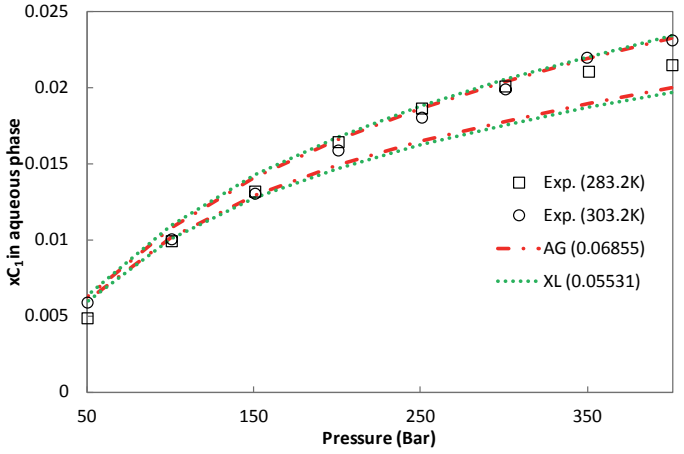

Figure 2.26 The correlations of the MEG + methane with the MEG parameters from Tsivintzelis and Grenner (2008) and this work. The experimental data are from Wang et al. (2003) and Folas et al. (2007).

2.4.1.2 Liquid-liquid equilibria

The predictions and correlations of the mutual solubilities of water with normal hydrocarbons are presented in Figures 2.27-2.28. The predictions of the solubility of water from the two parameter sets present quite high accuracy, and the predictions of the solubility of normal hydrocarbons with the new proposed parameters are quite satisfactory. A simply linear k_{ij} correlation against carbon number (or molecular weight) could make the AG parameters give almost the same accuracy of the solubility of normal alkanes in water with a noticeable deterioration of the solubility of water in hydrocarbons, especially at the low to medium temperature range.

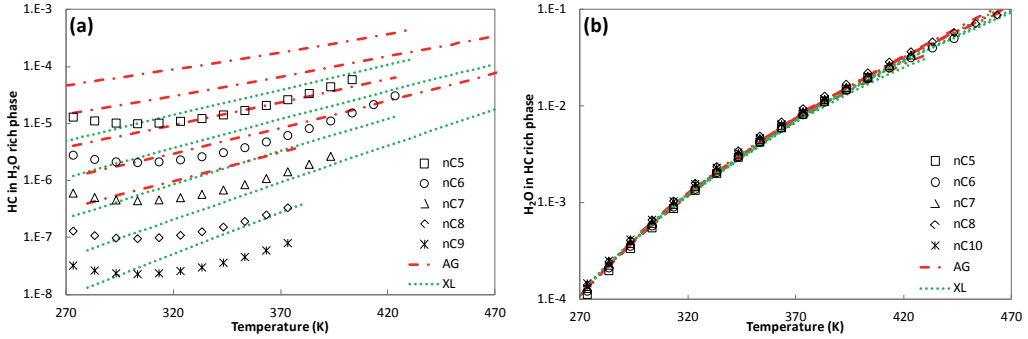

Figure 2.27 The prediction of the mutual solubility of water and n-alkanes. The water parameters AG and XL are respectively from the parameters of Grenner et al. (2006) and Liang et al. (2014). The experimental data are from Mączyński et al. (2004).

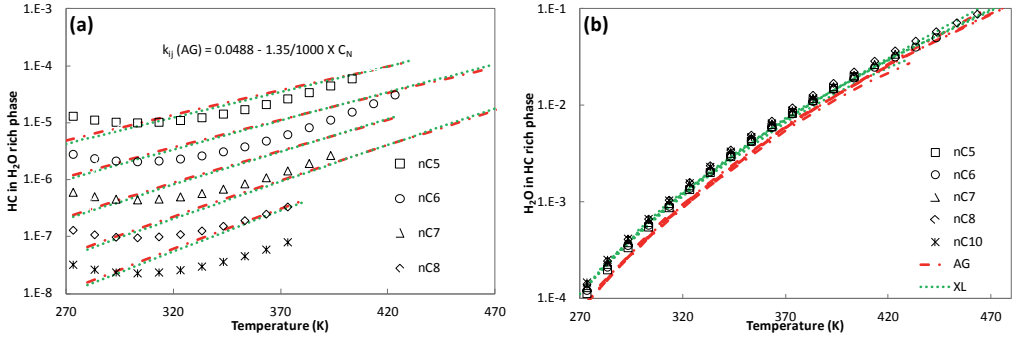

Figure 2.28 The mutual solubility of water and n-alkanes, correlations and predictions from the water parameters AG of Grenner et al. (2006) and XL of Liang et al. (2014), respectively. The experimental data are from Mączyński et al. (2004).

The correlations of LLE of methanol + nC6, nC8 and nC10 are presented in Figure 2.29. It is shown that the XL and XL2 parameters perform better than GS on correlating the hydrocarbon rich branch. As shown in Figure 2.30, a constant k_{ij} could be used for the binary mixtures of methanol and normal hydrocarbons heavier than n-butane, which will be very useful for modeling oil and methanol containing systems.

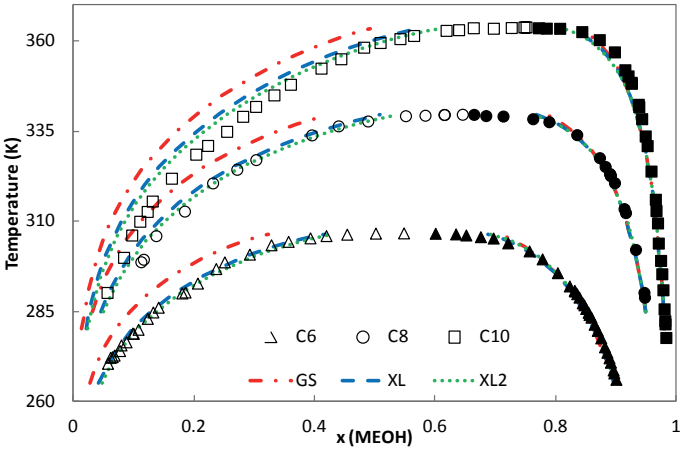

Figure 2.29 Correlations of the methanol + nC6, nC8 and nC10 with the parameters from Gross and Sadowski (2002), and Liang et al. (2012). The parameter set XL2 is from this work. The experimental data are from Matsuda et al. (2002, 2004), Kurihara et al. (2002).

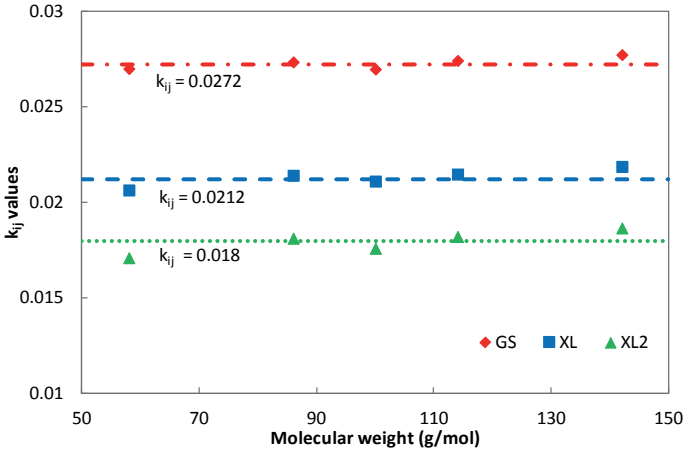

Figure 2.30 The k_{ij} values for the correlations of the methanol + n-alkanes with the parameters from Gross and Sadowski (2002), and Liang et al. (2012). The parameter set XL2 is from this work.

The correlations of the LLE of water with nC_6 and with nC_7 are presented in Figures 2.31, which show that the parameter set XL performs better than the parameter set AG on describing the mutual solubility. Similar results have been seen for the binary mixture of water and nC_9. As shown in Figure 2.32, a simple linear correlation of the k_{ij} values against molecular weight could be found for both parameter sets, which is very useful in modeling oil/MEG containing systems.

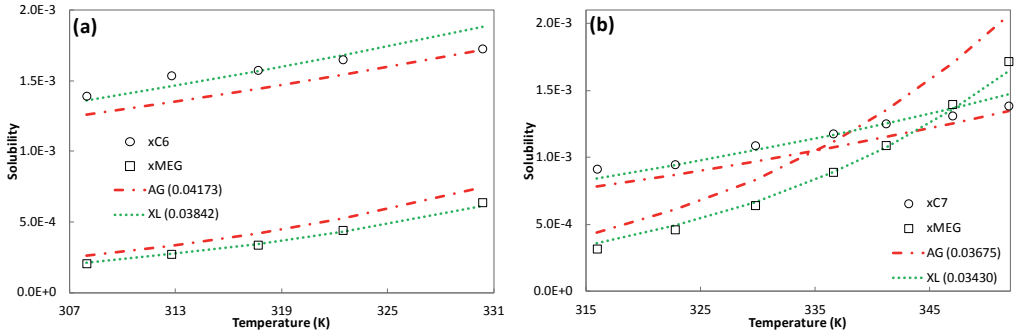

Figure 2.31 The correlations of the (a) MEG + nC6 and (b) MEG + nC7. The MEG parameters AG and XL are respectively from Tsivintzelis and Grenner (2008) and this work. The experimental data are from Derawi et al. (2002).

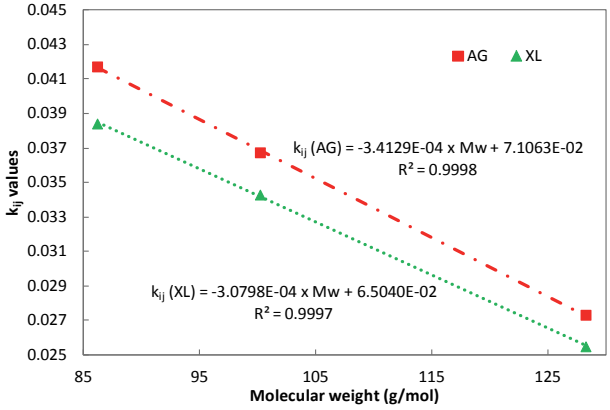

Figure 2.32 Linear correlations of the k_{ij} values against molecular weight for the systems of MEG + n-alkanes with the MEG parameters of AG from Tsivintzelis and Grenner (2008) and XL from this work.

2.4.1.3 Summary

A temperature dependent k_{ij} is crucial for correlating the solubility of light hydrocarbons (methane and ethane) in water, while a constant k_{ij} could be used for the binary mixtures of methane with methanol or with MEG.

The predictions of water and normal hydrocarbon series from the new water parameters are quite satisfactory, so k_{ij} is not needed for these binaries. A simply linear k_{ij} correlation against carbon number (or molecular weight) has been introduced for the water parameter set AG to improve the description of the solubility of normal alkanes in the water rich phase.

The model parameters of methanol having speed of sound data and LLE data of methanol with normal hydrocarbons considered in the parameter estimations, i.e. XL and XL2, give almost the same performance for the systems investigated in this study. So the parameter set XL, which has been published [Liang et al. (2012)], will be used hereafter. It has been found that constant k_{ij} values could be used to model the LLE of methanol with hydrocarbons heavier than butane, and simple linear correlations of the k_{ij} values against molecular weight have been developed for both MEG parameter sets (AG and XL). These findings are very useful in modeling oil/chemical containing systems.

2.4.2 Associating + Associating binary mixtures

2.4.2.1 Impacts of water parameters

In order to investigate the water parameters in a more complete way, the phase equilibria of binary mixtures of water and primary alcohols are extensively studied with the alcohol parameters from the same group, i.e. Gross and Sadowski (2002).

The prediction and correlation of VLE or VLLE of water and 1-alcohols are reported in Tables 2.5 and 2.6. Quite large deviations from the predictions are seen for some cases, for which incorrect phase behavior is predicted. These large deviations are still reported simply because the same calculation procedures are used for both prediction and correlation, which are good examples to show the deficiencies of the corresponding parameter sets and the significances of correlation, i.e. using the binary interaction parameter k_{ij}.

As reported in Table 2.5, the parameter sets AG (4C) and W3B_C give the best predictions for VLE of binary systems of water with methanol and with ethanol, respectively. The parameter sets GS (2B) and AG (4C) give the best predictions for VLE of water with 1-propanol. It can be seen from Table 2.6 that the parameter sets GS (2B) and W3B_C show comparable and better predictions than the other sets for the VLLE of water with 1-butanol, while GS (2B) has best predictions for the system of water with 1-pentanol. It is surprising to see that the parameter sets with the best description of vapor pressure of water, i.e. NVS (4C), show worst predictions for all of these systems. It is worth noticing that the predictions of parameter sets W3B and W4C, both from Aparicio-Marínez et al. (2007), are not satisfactory, while the set W3B_C, with rescaling to the critical point and poor description of vapor pressure and liquid density, show comparably good prediction results.

Comparing the results in Tables 2.3, 2.5 and 2.6, the phase equilibria of water and 1-alcohols are easier to tune than the LLE of water and hydrocarbons, using either large or small k_{ij} values. The most obvious example is the parameter set NVS (4C), as indicated by the large k_{ij} values and simply demonstrated in Figure 2.33 (a), in which relatively large k_{ij} values are used to correlate the VLE of water and methanol for the parameter sets that show poor predictions for this system. The results from these two tables reveal that the parameters with 4C association schemes do perform better than those with 2B and 3B on correlating VLE of water with 1-alcohols if taking the deviations of the pressure or temperature and vapor composition into account.

As seen from Table 2.6, even though the parameters with the 2B and 3B schemes show acceptable deviations for the 1-alcohols rich phases, they have difficulties in describing this phase from the qualitative point of view, as shown in Figure 2.33 (b). Meanwhile the 4C sets, which have satisfactory description for the LLE of water with hydrocarbons, e.g. AG, DE and XL, could describe the 1-alcohols rich phases very well, but have difficulties in matching the water rich phase in the LLE of water with 1-alcohols, especially with 1-butanol. It is again surprising to see that the set NVS (4C) gives best results in balancing three phases with relatively large k_{ij} values. Lastly, it is interesting to note that the parameter set GS (2B) presents close to zero positive k_{ij} values, for water with 1-propanol and with 1-pentanol, while all of other sets give negative values.

In general, the new water parameter set (XL) shows quite satisfactory correlations for both VLE and VLLE of the binary systems of water with 1-alcohols, if compared to the results from the literature available parameters.

Table 2.5 %AAD for the VLE of water with methanol, ethanol or 1-propanol*

Models	dP (%) / dT (K)	dY (H_2O, %)	k_{ij}	dP (%) / dT (K)	dY (H_2O, %)
	Methanol (Experimental data in 298.15-373.15K) Butler et al. (1933), Griswold et al. (1952)				
GS	29.2	*9.63*	-0.0716	4.87	1.75
W2B	74.6	17.8	-0.1118	5.06	2.10
W3B	169	24.5	-0.1429	6.72	2.44
W3B_C	33.4	11.0	-0.0680	5.00	2.44
AG	***17.3***	***6.30***	-0.0585	3.81	0.99
DE	29.2	10.4	-0.0863	***3.52***	***0.79***
NVS	217	26.7	-0.1660	3.71	1.42
W4C	83.3	19.0	-0.1216	4.23	1.94
XL	32.0	11.1	-0.0852	*3.62*	*1.01*
XL (XL)+	*24.2*	*8.90*	-0.0657	*3.48*	*0.97*
CPA	***10.6***	***4.27***	-0.0748	***3.10***	***1.03***
	Ethanol (Experimental data in 298.14-363.15K) Phutela et al. (1979), Kurihara et al. (1995), Pemberton et al. (1978)				
GS	10.3	4.88	-0.0304	3.19	2.10
W2B	30.3	10.3	-0.0628	2.86	1.50
W3B	61.6	15.5	-0.0845	4.04	2.36
W3B_C	***6.25***	***2.93***	-0.0146	2.64	1.42
AG	*9.87*	*3.70*	-0.0359	1.83	0.86
DE	15.4	5.92	-0.0541	*1.46*	*0.53*
NVS	108	19.7	-0.1212	1.65	0.72
W4C	46.3	13.4	-0.0877	2.00	0.75
XL	16.5	6.34	-0.0532	*1.46*	*0.47*
XL (XL)	14.0	5.50	-0.0456	***1.31***	***0.52***
CPA	***4.48***	***2.52***	-0.0409	1.68	1.40
	1-Propanol (at atmospheric pressure, Udovenko et al. (1972)				
GS	*1.10*	*3.69*	0.0022	1.12	3.43
W2B	3.68	8.19	-0.0240	1.05	3.18
W3B	9.45	17.0	-0.0452	1.43	4.03
W3B_C	2.67	7.37	0.0239	0.71	2.74
AG	***1.87***	***1.77***	-0.0148	1.06	2.24
DE	3.96	5.89	-0.0334	1.08	2.23
NVS	21.4	27.1	-0.0874	***0.44***	***1.31***
W4C	9.13	14.8	-0.0512	*0.46*	2.12
XL	3.66	5.29	-0.0287	0.85	1.86
XL (AG)	2.65	3.74	-0.0215	0.69	*1.55*
CPA	*0.99*	*3.10*	-0.0300	1.37	4.08

* The mark for smallest (Bold and Italic) and largest (Highlight) deviations based on the sum.

+ TW_1 denotes the simplified PC-SAFT with the new proposed water parameters from this work and the 1-alcohol parameters from another source.

Table 2.6 %AAD for the VLE and LLE of water with 1-butanol or 1-pentanol*

Models	%AAD of x (H_2O) in each phase					%AAD of x (H_2O) in each phase			
	dT (K)	vapor	water	alcohol	kij	dT (K)	vapor	water	alcohol
	1-Butanol (at atmospheric pressure) [Boublik (1960), Sørensen et al. (1995)]								
GS	***1.41***	***3.69***	***1.39***	***21.7***	-0.0170	2.56	5.47	0.91	6.03
W2B	5.87	11.5	1.92	51.6	-0.0559	3.16	6.15	0.97	7.69
W3B	18.4	22.1	1.98	64.0	-0.0830	3.42	6.74	1.18	6.20
W3B_C	*1.39*	*4.23*	*0.93*	*24.7*	-0.0141	2.73	6.24	1.94	9.88
AG	2.81	3.62	0.53	46.1	-0.0360	0.83	2.54	8.38	3.81
DE	6.45	9.97	1.58	64.0	-0.0629	1.12	3.32	8.84	9.61
NVS	30.4	29.3	1.99	84.8	-0.1250	***0.87***	***2.42***	***2.52***	***2.29***
W4C	13.1	19.1	1.95	71.1	-0.0887	2.44	4.88	2.91	8.87
XL	5.96	9.22	1.64	61.3	-0.0585	*0.85*	*2.40*	*6.31*	*4.15*
XL (IK)	5.11	8.11	1.59	59.1	-0.0556	*1.05*	*2.25*	*6.07*	*2.98*
CPA	2.21	3.76	1.44	28.4	-0.0650	*2.95*	*5.61*	*0.70*	*3.64*
	1-Pentanol (at atmospheric pressure) [Beregovykh et al. (1971), Sørensen et al. (1995)]								
GS	***1.97***	***4.34***	***0.20***	***15.6***	0.0094	1.69	4.82	0.29	10.9
W2B	5.04	9.38	0.39	*23.5*	-0.0251	2.23	5.43	0.29	12.8
W3B	16.4	16.4	0.43	40.4	-0.0477	3.07	7.02	0.34	11.4
W3B_C	*2.84*	*5.61*	*0.71*	*26.1*	0.0137	0.92	3.17	0.28	13.2
AG	6.46	4.48	0.19	39.0	-0.0373	2.90	2.48	3.89	3.47
DE	10.4	9.81	0.24	56.0	-0.0603	3.40	2.85	4.37	1.64
NVS	33.2	24.7	0.43	76.8	-0.1060	*1.64*	*1.01*	*0.50*	*5.63*
W4C	15.5	16.9	0.41	57.5	-0.0692	0.77	3.02	0.48	13.1
XL	9.39	9.03	0.27	51.2	-0.0518	*2.65*	*2.05*	*2.52*	*2.82*
XL (AG)	11.4	12.2	0.36	54.0	-0.0640	***2.25***	***1.53***	***1.44***	***3.12***
CPA	***0.81***	***2.34***	***0.30***	***8.42***	-0.0370	1.44	3.62	0.15	6.16

* The mark for smallest (Bold and Italic) and largest (Highlight) deviations based on the sum.

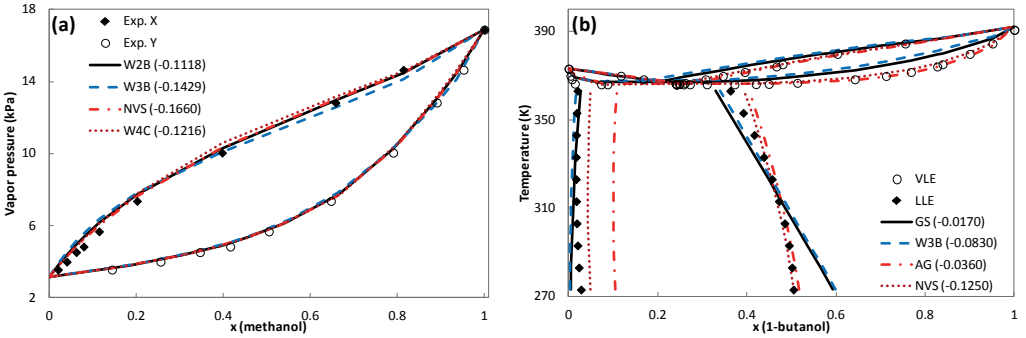

Figure 2.33 Experimental data and PC-SAFT correlations (k_{ij} shown in the parentheses) for the phase behavior of water with (a) methanol and (b) 1-butanol. The experimental data are taken from Butler et al. (1933), Griswold et al. (1952), Boublik et al. (1960), and DECHEMA data series [Sørensen et al. (1995)]. The names are explained in section 1.2.2 and Table 2.1.

2.4.2.2 Impacts of 1-alcohol parameters

The modeling of water and primary alcohols with PC-SAFT presented above has been conducted using the alcohol parameters from Gross and Sadowski (2002). There are some other parameters available for the 1-alcohols in the literature, which have shown good performance for some applications. In order to investigate if it is possible to have better description of water-alcohol systems, the same calculations are conducted for the alcohol parameters from other sources with the new proposed water parameters.

One result is reported for each system in Tables 2.5 and 2.6, using the name XL with the name of the alcohol parameters in the parentheses. The parameter values of each set can be found in Table 2.4. It can be seen that it is possible to have better the results with the new combinations than the original ones in terms of correlations, while it is worth pointing out that these alcohol parameters are obtained in different ways.

A typical example of correlating water and methanol mixtures with different parameter combinations is given in Table 2.7. These results deliver an important message that systematic investigations are needed to be conducted on alcohols as well. In the meantime, it is possible to conduct similar investigation as done for water above, since alcohols, as associating fluids, are modeled using five pure component parameters with the SAFT models.

Table 2.7 Correlation k_{ij} and %AAD of water + methanol*

Models (parameter sets)		kij	%AAD	
Water	Methanol		Sat. Press.	yH_2O in vapor
GS	GS	-0.0716	3.81	2.37
GS	XL	-0.0628	3.42	2.30
GS	XL2	-0.0585	3.36	2.33
AG	GS	-0.0585	2.69	1.81
AG	XL	-0.0539	2.56	1.80
AG	XL2	-0.0504	2.57	1.87
XL	GS	-0.0852	2.61	1.48
XL	XL	-0.0661	2.44	1.47
XL	XL2	-0.0594	2.40	1.51

* Experimental data are from Butler et al. (1933), Griswold(1952), Kurihara et al. (1995).

2.4.2.3 PC-SAFT versus CPA

The prediction and correlation of VLE and VLLE results for the binary mixtures of water and alcohols from CPA are also presented in Tables 2.5 and 2.6. Typical correlation results, from PC-SAFT with the new water parameters and from CPA, are compared in Figures 2.34 (a) and (b) for the systems of water with ethanol and with 1-pentanol, respectively.

In terms of predictions, on one hand, CPA shows much better accuracy than the simplified PC-SAFT with the new parameters for all systems, and with literature parameters for most of the systems as well. On the other hand, in terms of temperature or pressure in VLE correlations, PC-SAFT presents better results for the systems of water with ethanol, 1-propanol or 1-butanol, while CPA shows better performance for the systems of water with methanol and 1-pentanol. PC-SAFT with the new parameters, however, gives smaller deviations for vapor composition for all systems. CPA results in better LLE correlations of water with 1-butanol on both phases, while the two models describe best one of the two sides of the binodal for the LLE of water with 1-pentanol.

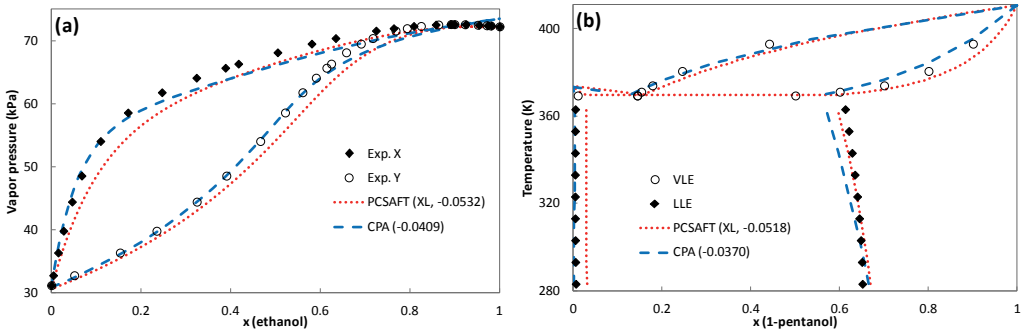

Figure 2.34 Phase behavior of water with (a) ethanol at 343.15K and (b) 1-pentanol at 1 atm. Experimental data from Pemberton et al. (1978), Beregovykh et al. (1971), and DECHEMA data series [Sørensen et al. (1995)]. The new proposed water parameters are used for PC-SAFT.

2.4.2.4 Water + MEG

The VLE correlation results of water and MEG are presented in Table 2.8 and Figure 2.35 from different parameter combinations. The correlations are all quite satisfactory. Though the AG-AG combination could give slightly better results than the XL-XL, the differences in the results are even smaller than experimental uncertainties.

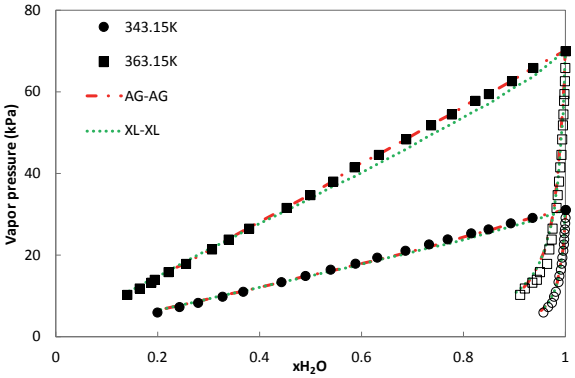

Figure 2.35 VLE of water and MEG. The experimental data are from Chiavone-Filho et al. (1993).

Table 2.8 Correlation k_{ij} and %AAD of water + MEG*

Models (parameter sets)		kij	%AAD	
Water	MEG		Sat. Press.	yH_2O
AG	AG	-0.0497	2.55	0.304
AG	XL	-0.0461	2.30	0.299
XL	AG	-0.0674	4.61	0.304
XL	XL	-0.0559	3.40	0.296

* Experimental data are from Chiavone-Filho et al. (1993).

2.4.2.5 Summary

With PC-SAFT, the phase behavior of binary aqueous systems with 1-alcohols is easier to be described (using one adjustable parameter) than the phase behavior of water-hydrocarbon mixtures. The PC-SAFT water parameters with the 4C association scheme seem to be more effective in obtaining better correlations of the phase equilibrium for aqueous 1-alcohols mixtures. It is necessary, however, to point out that for the 4C parameter sets presenting good description of the LLE for water with hydrocarbons, there is some space left for improving the descriptions of the water rich phase for the LLE of water with 1-butanol and with 1-pentanol. The fact that different results could be obtained by using different alcohol parameters suggest that systematic investigation needs to be conducted on alcohols as well, since they, as associating fluids, are also described using five pure component parameters with the SAFT theory. In general, CPA gives better predictions on the water and 1-alcohol binary systems studied in this section, but PC-SAFT with the new water parameters present comparably satisfactory VLE and VLLE correlations.

2.4.3 Water + Chemical + Inert ternary mixtures

2.4.3.1 Vapor-liquid equilibria

The prediction of the ternary systems of water, methanol and methane using the combinations of the water parameter sets AG and XL, and the methanol parameter sets GS and XL are presented in Figure 2.36. The results show that the three combinations from different parameter sets give equally reasonable results. As in the binaries, the composition of water and methanol in the vapor phase is mainly determined by the their parameters, e.g. the methanol parameter set GS predicts slightly lower composition of methanol in the vapor phase, while the water parameter set XL predicts slightly higher composition of water in the vapor phase, which is more close to the experimental data.

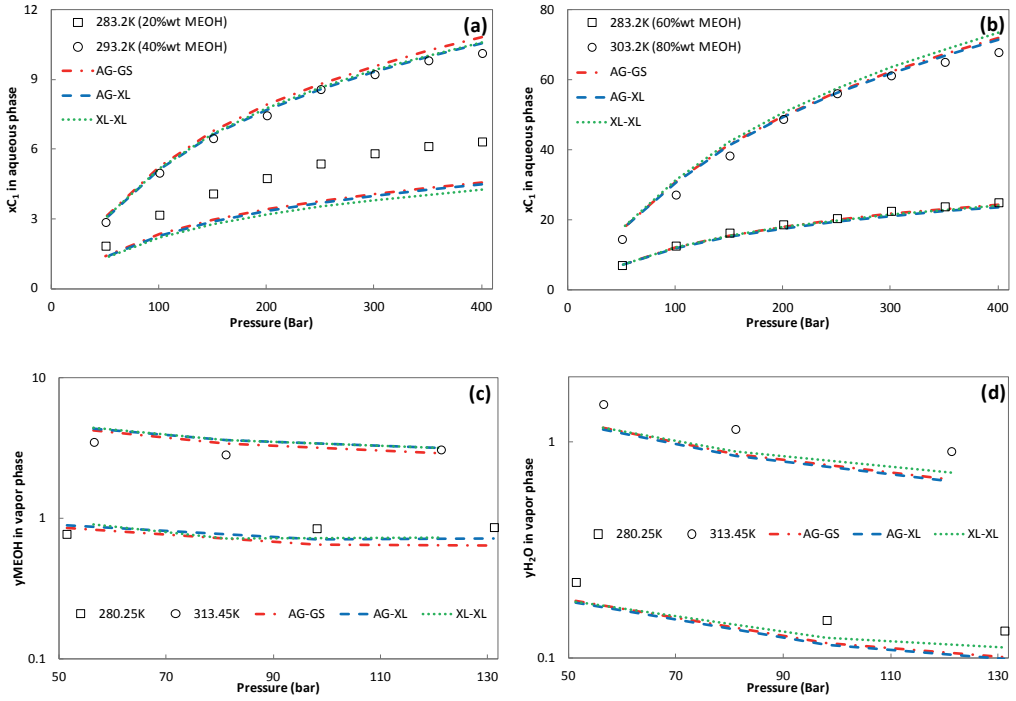

Figure 2.36 The predictions of the ternary systems of water + methanol + methane using the combinations of the water parameters from Grenner et al. (2006) and this work, and the methanol parameters from Gross and Sadowski (2002) and Liang et al. (2012). The data are taken from Wang et al. (2003) and Frost et al. (2014).

The predictions of the ternary mixture of water-MEG-methane using the combinations of the water and MEG parameter sets AG and XL are presented in Figure 2.37. The performance of these combinations is quite similar to what has been seen in the ternary mixture of water-methanol-methane, e.g. the MEG parameter set AG predicts slightly lower composition of MEG in the vapor phase, while the water parameter set XL predicts slightly higher composition of water in the vapor phase. There is no obvious evidence clarifying which combination is best.

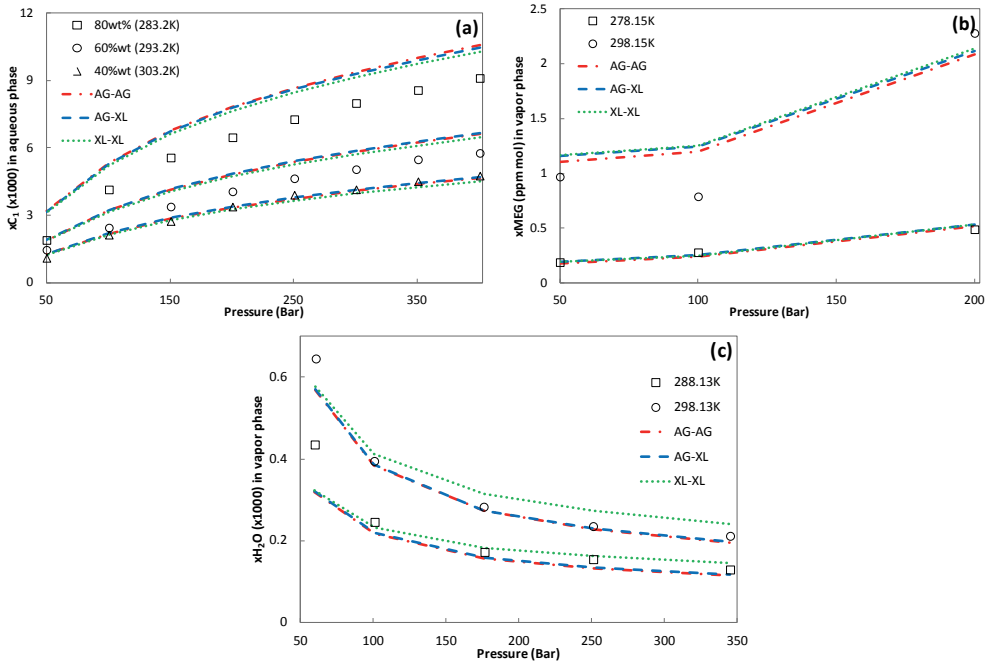

Figure 2.37 The predictions of the ternary systems of water + MEG + methane using the combinations of the water parameters from Grenner et al. (2006) and this work, and the MEG parameters from Tsivintzelis and Grenner (2008) and this work. The data are taken from Wang et al. (2003) and Folas et al. (2007).

2.4.3.2 Liquid-liquid equilibria

The prediction of the LLE of the ternary mixture water-methanol-heptane is presented in Figure 2.38. The combinations of water parameter sets AG and XL, and the methanol parameter sets GS and XL give similar prediction for the solubility of heptane in the polar phase, while the methanol parameter set XL presents higher prediction for the solubility of methanol in the organic phase than the parameter set GS. As shown in Figure 2.38 (b), if the experimental data is fully reliable, the

parameter set XL shows better performance in the high solubility region and the parameter set GS performs better in the low solubility region.

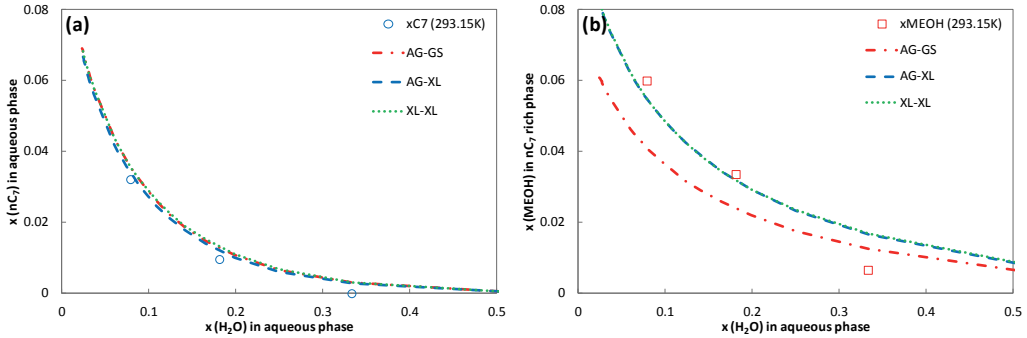

Figure 2.38 The predictions of the ternary systems of water + methanol + heptane using the combinations of the water parameters from Grenner et al. (2006) and this work, and the methanol parameters from Gross and Sadowski (2012) and Liang et al. (2012). The experimental data are taken from Letcher et al. (1986).

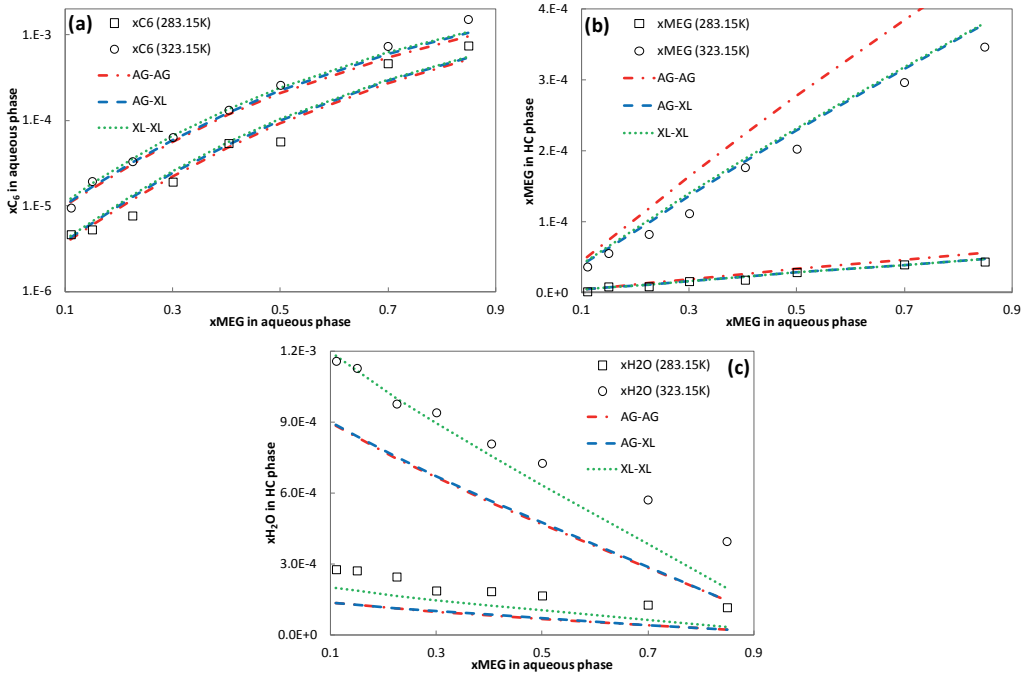

Figure 2.39 The predictions of the ternary systems of water + MEG + hexane using the combinations of the water parameters from Grenner et al. (2006) and this work, and the MEG parameters from Tsivintzelis and Grenner (2008) and this work. The data are taken from Razzouk et al. (2010).

The prediction of the LLE of the ternary mixture water-MEG-hexane is presented in Figure 2.39. As expected, the combinations of water and MEG parameter sets AG and XL give quite similar prediction for the solubility of hexane in the polar phase. Both water and MEG parameters from this work show better predictions of the solubility of water and MEG in the organic phase than the AG parameter set. This might be due to the usage of the relevant LLE data in the parameter estimation.

2.5 Conclusions

The binary systems of water and hydrocarbons, without accounting for cross association (solvation), present a good way to investigate the effect of the self-association interactions of water. An interactive step-wise optimization procedure has been developed to take LLE of water with non-aromatic hydrocarbons into account when estimating the pure component parameters for water with the simplified PC-SAFT EOS. This approach is similar to the one used for CPA.

The PC-SAFT EOS with the newly developed parameters and the CPA EOS, on one hand, give equally good description of the vapor pressure and saturated liquid density of water, and present quite satisfactory VLE/LLE/VLLE correlations for binary and ternary systems containing water, hydrocarbons, and chemicals. On the other hand, both models have difficulties in describing the second-order derivative properties, e.g. residual isochoric heat capacity and speed of sound. The significant deficiency of these perturbation theory based models on residual isochoric heat capacity indicates that the temperature dependency is not described well within the current frameworks. The temperature dependency of the speed of sound in saturated water on temperature is abnormal – there is a maximum around 350K, and different approaches give quite similar results. These observations suggest that it is not recommended to directly put these two properties in the parameter estimation for water.

Chapter 3. Petroleum fluid characterization

The PC-SAFT EOS has shown promising results for describing complex phase behaviors and high pressure properties of various systems. It has been proposed as an alternative to the classical cubic equations of state in the petroleum industry. However, it is far from a simple task to develop successful oil characterization methods for the PC-SAFT EOS.

The purpose of this study is: (1) to discuss the influence of different options in the characterization procedure, including the molar composition distribution, the density correlation, the number of pseudo-components, the estimation method of PNA contents and the binary interaction parameters, on PVT calculations; (2) to investigate the significance of fitting model parameters during characterization, and how to choose the fitting parameters for accurate descriptions of saturation pressure and density; (3) to propose general petroleum characterization methods with the PC-SAFT EOS; (4) to show the advantages and limitations of the PC-SAFT EOS.

3.1 Introduction

Characterization is always needed for applying thermodynamic models for phase behavior and property calculations of petroleum fluids. This is due to the facts that (1) a complete identification and quantification of all the species in the petroleum fluids is not feasible; (2) the properties to be used as model parameters, e.g. critical properties for cubic EOS models, are largely missing for most species; (3) it is impractical to perform phase equilibrium calculations for thousands of substances in process and/or reservoir simulations or online control [Pedersen et al. (2007a), Whitson et al. (2000), Riazi (2005)]. The characterization procedure is to represent the petroleum fluids with a reasonable number of pseudo-components and to find the EOS model parameters for each of them. In this way, we have an engineering solution that enables the application of theoretical thermodynamic models to ill-defined petroleum fluid mixtures. Fluid characterization is now an indispensable part in simulations involved in both upstream and downstream scenarios of the oil industry.

The most widely used characterization procedures in the petroleum industry are those proposed by Pedersen et al. (1983, 1984) and Whitson et al. (1983, 1989), which were originally developed in connection with the Soave-Redlich-Kwong (SRK) EOS [Soave (1972)] and the Peng-Robinson (PR) EOS [Peng and Robinson (1976)]. These two cubic EOS are the standard models for pressure-volume-temperature (PVT) modeling of reservoir fluids and compositional reservoir simulations, and they have been so for decades. Recently, the PC-SAFT EOS has been proposed as a potential next generation model, because of its performance for phase equilibrium calculations of highly asymmetric systems, high pressure density and second-order derivative properties, for instance compressibility and speed of sound, are superior to what are calculated from cubic EOS [Gross and Sadowski (2001), von Solms et al. (2006a), Pedersen et al. (2007b), Kontogeorgis et al. (2010a), de Villiers (2011), de Hemptinne et al. (2012)].

Pedersen and Sørensen (2007b) proposed to use linear functions of molecular weight to represent m and mε/κ for the paraffinic-naphthenic and the aromatic parts of single carbon number (SCN) fractions heavier than n-hexane, and then these two parts are combined by using the paraffinic-naphthenic-aromatic (PNA) estimation with the procedure of van Nes and van Western (1951). The adjustable coefficients are regressed to match the saturation points of 10 different reservoir fluids and the experimental asphaltenes precipitation onset pressures for 3 different oils. The segment diameter parameter (σ) is fitted to match the specific gravity (SG, liquid density) of the SCN fraction at atmospheric pressure and 288.15K. The C_{50+} SCN fractions are split into two asphaltene and non-asphaltene pseudo-components when modeling behaviors of asphaltene, such as precipitation. Recently, Pedersen et al. (2012) updated the characterization method by introducing molecular weight and liquid density of each SCN fraction directly in expressions of m and mε/k. The PNA content estimations only went into the C_7 fraction, which is assumed to be composed of n-heptane, cyclo-hexane and benzene. This characterization procedure has been used to model enhanced-oil-recovery (EOR) PVT data [Pedersen et al. (2012)], and high pressure phase behavior and asphaltene precipitation onsets of Gulf of Mexico (GoM) oil mixed with nitrogen [Hustad et al. (2013)]. Leekumjorn et al. (2013) commented that reliable and generally applicable petroleum fluid characterization methods are still needed to be developed for the PC-SAFT EOS.

Yan et al. (2010) developed a characterization method for the PC-SAFT EOS by combining the procedure proposed by Pedersen et al. (1983, 1984) with a set of new correlations for the model parameters. The new correlations are developed in a two-step perturbation approach: first, the

reference parameters are calculated from the linear correlation functions of molecular weight for the corresponding normal alkane; then, the parameters of the SCN fraction are estimated using a perturbation relation of SG. The correlations for these parameters were developed using 29 normal alkanes and 210 other hydrocarbons from the DIPPR database (2012).

Chapman and coworkers have shown promising results for asphaltene modeling with the PC-SAFT EOS [Ting (2003), Gonzaléz (2008), Vargas (2010), Panuganti et al. (2012, 2013), Punnapala et al. (2013)]. Their characterization method was based on saturates-aromatics-resins-asphaltene (SARA) analysis. Only three pseudo-components, i.e. saturates, aromatics + resins and asphaltene, were proposed to represent the stock tank oil (STO), and well-behaved correlation sets between pure component parameters and molecular weight were developed for saturates, aromatics and resins. The aromatics and resins were then combined by introducing an extra aromaticity parameter γ, which is fitted to the saturation pressure and STO density of the reservoir fluids. The parameters of asphaltene are considered to be adjustable, and are in general fitted to the measured precipitation onset data with or without gas injection.

The characterization methods for the PC-SAFT EOS discussed above can be summarized: (1) well-behaved correlations between model parameters and molecular weights could be established for different homologous series; (2) PNA or SARA analysis could be used to combine the parameters for each SCN fraction or pseudo-component; (3) SG could be used to correct or tune the parameters; (4) one extra pseudo-component could be introduced if necessary when modeling asphaltene.

In this study, it is assumed that only molecular weight and SG and/or true boiling point (Tb) are directly used in the characterization. We will review firstly the two widely used petroleum fluid characterization procedures, and in the meantime propose a third one by combining these two. Then, the well-behaved linear correlations for model parameters, the binary interaction parameters and the estimation method of PNA contents will be discussed, and six candidate methods will be proposed to estimate the model parameters by combining simple correlations with the PNA content estimations, and/or by fitting model parameters. Thirdly, the performance of these six candidate methods is investigated for predicting the saturation pressure and density of various petroleum fluids, and a new compromise general method is proposed. Finally, the behavior of the best four methods is further studied on PVT simulation, phase envelope and activity coefficients.

3.2 Entire C_{7+} characterization procedure

The petroleum fluid characterization procedures aim to provide the necessary information for EOS calculations from limited experimental data. In a full petroleum characterization, the components are normally classified into three categories [Pedersen et al. (2007a)]: (1) defined components whose properties are well known, such as N_2, CO_2, H_2S, C_1, C_2, C_3, iC_4, nC_4, iC_5, nC_5 and C_6; (2) Tb fractions, whose molecular weight and SG are either measured or estimated within a given temperature interval; (3) the plus (C_{N+}) fraction whose average molecular weight and SG are normally available. The characterization is in general used for the fractions in categories (2) and (3), which involve mainly C_{7+} fractions, so the petroleum fluid characterization procedure is sometimes called C_{7+} characterization procedure.

The characterization procedure proposed by Pedersen et al. (1983, 1984) is based on an exponential decay distribution of molar composition against molecular weight of SCN fractions, and in general C_{80} is the heaviest SCN fraction considered. The SCN fraction lumping is needed. This procedure consists of four steps: (1) calculating the mole fraction of SCN fraction by assuming a linear relationship between the logarithm of molar composition and the carbon number for SCN heavier than C_{N+} depending on users' specification; (2) calculating the liquid density of SCN fractions by assuming a linear relationship between the liquid density and the logarithm of carbon number; (3) estimating the required properties or parameters of the chosen EOS model for each SCN fraction, e.g. critical properties for cubic EOS; (4) lumping the SCN fractions and their properties into a user-specified number of pseudo-components with some given rules, for instance, approximate equal mass fraction.

Another well-known characterization procedure, which was developed by Whitson is based on a gamma type distribution of molar composition against molecular weight [Whitson et al. (1983, 1989)]. It consists of the following four steps: (1) calculating the characteristic parameters of the gamma distribution function, which is used to describe the relationship between molar composition and molecular weight in a continuous space; (2) creating a user-specified number of pseudo-components with either the equal mass fraction or the Gaussian quadrature approach; (3) calculating the SG by using a sophisticated correlation whose characteristic coefficient is fitted to the property of C_{7+} fraction [Søreide (1989), Whitson et al. (2000)]; (4) estimating the required properties or parameters of the chosen EOS model for each pseudo-component.

These two characterization procedures are compared in Table 3.1, and they are named as the exponential and gamma characterization procedures in the following discussions. It can be seen that there are two adjustable parameters in describing molar composition distribution in both characterization procedures if the experimental M_{C7+} is used in gamma characterization procedure, while there are one or two adjustable coefficients for the liquid density function or the SG correlation. Ghasemi et al. (2011) showed that the exponent constant in the Søreide correlation [Søreide (1989)] can also be used as an additional adjustable parameter. The known molecular weight and SG information of the C_{7+} fractions is used to estimate these parameters. The fitting makes little meaning when the C_{N+} fraction dominates the C_{7+} fraction, i.e. $z_{C_{N+}}/z_{C_{7+}} > 0.95$, in the gamma characterization procedure, so the recommended values of characteristic parameters ($\alpha = 1;\ \eta = 90$) will be used to create pseudo-components for these cases.

Table 3.1 Comparison of the exponential and gamma characterization procedures

Property or rule	Exponential	Gamma
molecular weight	$M_i = 14 \times C_i - 4$	$M_i = \dfrac{\left[\int_{\eta}^{M_{bi}} Mp(M) - \int_{\eta}^{M_{bi-1}} Mp(M)\right]}{\left[\int_{\eta}^{M_{bi}} p(M) - \int_{\eta}^{M_{bi-1}} p(M)\right]}$
mole composition	$lnz_i = A + B \times C_i$	$z_i = z_{C_{7+}}\left[\int_{\eta}^{M_{bi}} p(M) - \int_{\eta}^{M_{bi-1}} p(M)\right]$
specific gravity	$SG_i = C + D \times lnC_i$	$SG_i = 0.2855 + C_f(M_i - 66)^{0.13}$
combining rule (Exp) OR characteristic function (Gamma)	$\Omega_i = \sum_{j=i_m}^{i_n}(w_j\Omega_j) \Big/ \sum_{j=i_m}^{i_n}(w_j)$ $w_j = z_j \ or \ z_jM_j$	$p(M) = \dfrac{(M-\eta)^{\alpha-1}exp((\eta - M)/\beta)}{\beta^{\alpha}\Gamma(\alpha)}$ $\beta = \left(M_{C_{7+}} - \eta\right)/\alpha$, Γ is gamma function

Pedersen et al. (1992, 2007) showed that the performance of these two procedures was very similar based on an analysis of the mathematical expressions and the extended compositional analysis. Zuo and Zhang (2000), however, stated that the characterization procedure proposed by Pedersen et al. (1983, 1984) usually gives better predictions than those of Whitson et al. (1983, 1989) if no EOS tuning is undertaken.

In this study, both characterization procedures have been implemented and used with the PC-SAFT EOS. In order to investigate the individual influence from different options in the first two steps of

characterization, i.e. the molar composition distribution and the SG correlation strategy, a third characterization procedure has also been implemented – the Søreide correlation is used to calculate the SG for the lumped pseudo-components in the exponential characterization procedure. The entire flowchart is shown in Figure 3.1. All of these three characterization procedures are so general that only the step of estimating model parameters should be changed for different EOS models or different approaches for the same EOS model. In many cases, it is common or necessary to tune the model parameters to match experimental data, such as saturation pressure, oil density and precipitation onset pressure of asphaltene [Pedersen et al. (2007a)].

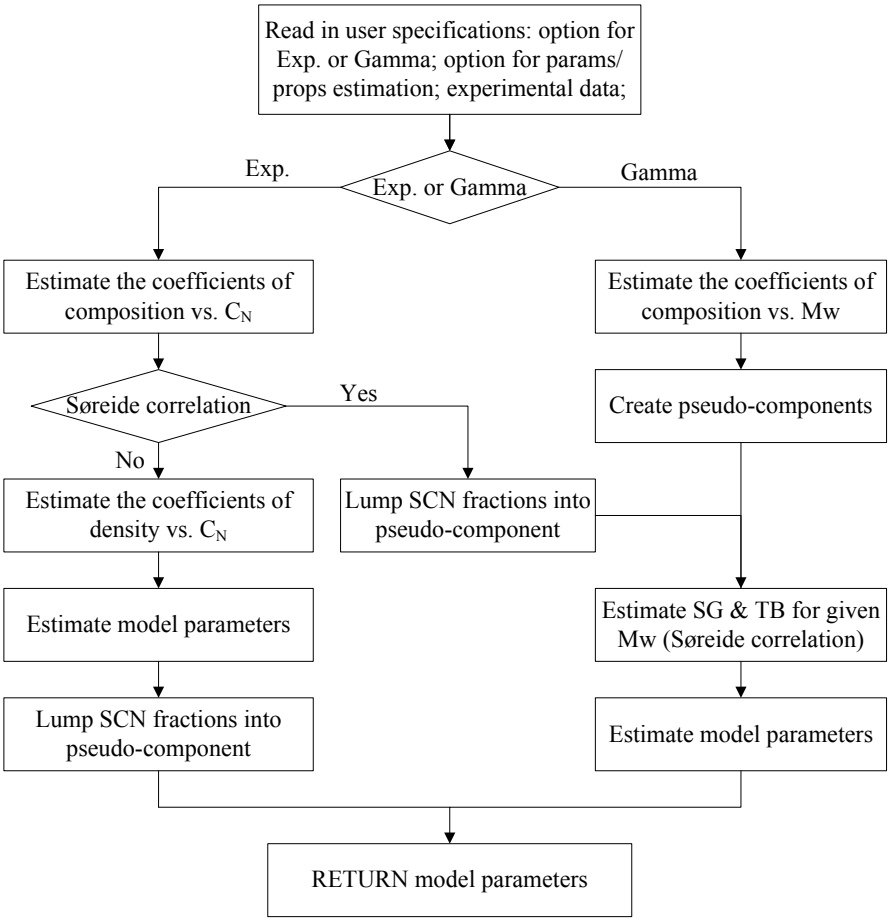

Figure 3.1 Entire C_{7+} characterization procedure

3.3 Model parameter estimation for pseudo-components

3.3.1 Model parameters

As discussed in the Chapter 2, the PC-SAFT EOS has three model parameters, i.e. the number of segments (m), the diameter of the segment (σ), and the segment self-interaction energy (ε/k), for each non-associating compound. Two other parameters are needed for the associating fluids. The pseudo-components are normally assumed to be non-associating in petroleum fluid characterization.

When using the PC-SAFT EOS with the general characterization procedures discussed above, correlations or fitting approaches are needed to estimate the model parameters m, σ and ε for SCN fractions or pseudo-components. Simple correlations between the model parameters and molecular weight for n-alkanes or other homologous hydrocarbon series are available in the literature [Tihić et al. (2006, 2008), Yan et al. (2010)], which provide a feasible basis to apply the PC-SAFT EOS for the petroleum fluids. It is most common to express the model parameters or their combinations m, $m\sigma^3$ and $m\varepsilon/k$ as linear functions of molecular weight [Tihić et al. (2006), Liang et al. (2012)]. Based on the model parameters given by Gross and Sadowski (2001), Tihic et al. (2006) and Yan et al. (2010), linear correlations for n-alkanes, cyclo-alkanes and benzene derivatives are refitted and listed in Table 3.2 and shown in Figure 3.2. The model parameters of methane are not used in the regression.

Table 3.2 Correlations of PC-SAFT model parameters against molecular weight for different homologous hydrocarbons families*

Properties	n-alkanes (Paraffins)	cyclo-alkanes (Naphthenes)	benzene series (Aromatics)
m	0.02569Mw + 0.8709	0.02254Mw + 0.6827	0.02576Mw + 0.2588
$m\sigma^3$ (Å^3)	1.7284Mw + 18.787	1.7115Mw + 1.9393	1.7539Mw - 21.324
$m\varepsilon/k$ (K)	6.8248Mw + 141.14	6.4962Mw + 154.53	6.6756Mw + 172.40

* The parameter values are taken from Gross and Sadowski (2001), Tihić et al. (2006, 2008).

There are alternatives for estimating the model parameters of ill-defined SCN fractions or pseudo-components. Based on the analysis of the relationships between different combinations of parameters and properties, Yan et al. (2010) proposed the following equation to correlate $m\sigma^3$ using a kind of perturbation expansion procedure.

$$\frac{(m\sigma^3)_0}{m\sigma^3} - 1 = 0.86381 \times \left(\frac{SG}{(SG)_0} - 1\right) \tag{3.1}$$

where subscript 0 denotes the parameter ($m\sigma^3$) or property (SG) of the corresponding n-alkanes which have the same molecular weight or Tb of the SCN fraction or pseudo-component being estimated for the parameters. The details of the calculation procedure can be found in the work of Twu (1984) or Yan et al. (2010).

In this study, a further analysis has been conducted for 310 hydrocarbons heavier than benzene, and it is found that a very good linear relationship exists for mε/k and Mw, as shown in Figure 3.3.

$$m\,\varepsilon/k = 6.8311 \times Mw + 124.42 \tag{3.2}$$

The properties of these hydrocarbons are taken from DIPPR database (2012), and the three model parameters are regressed to the correlated vapor pressure and saturated liquid density data available in DIPPR database (2012).

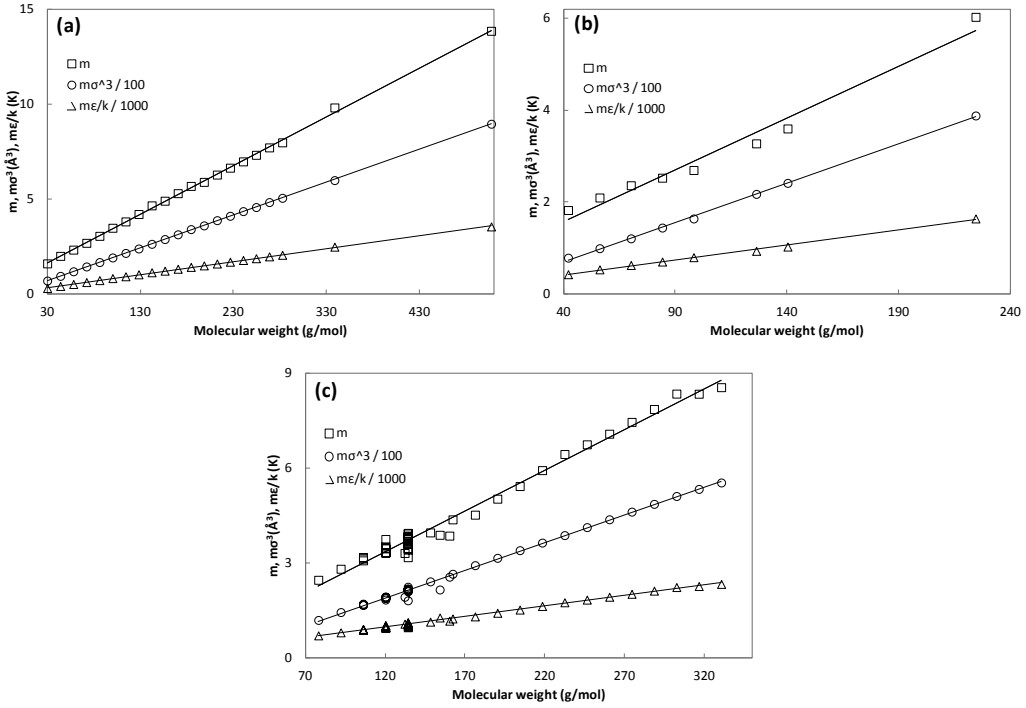

Figure 3.2 Linear correlations of m, $m\sigma^3$ and mε/k against molecular weight for (a) n-alkanes, (b) cyclo-alkanes, and (c) benzene derivatives.

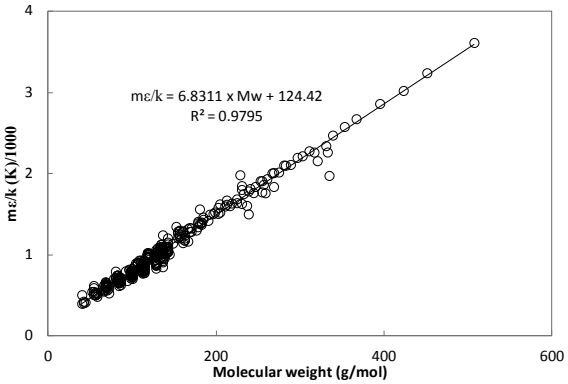

Figure 3.3 Simple correlations of mε/k against molecular weight for 310 hydrocarbons from DIPPR database (2012).

3.3.2 PNA estimations

For the prediction of thermodynamic properties of ill-defined petroleum fractions, knowledge of the PNA distribution of each SCN fraction or pseudo-component is usually helpful if it is available. In this study, two estimation methods of the PNA contents have been implemented. One method was developed by van Nes and van Western (1951), which is normally called as n-d-M method. The other one is from the work of Riazi and Daubert (1986), which will be denoted as Riazi method hereafter. The detailed calculation procedures of these two methods can be found in the book of Riazi (2005).

The PC-SAFT EOS model parameters can be combined using the following equation.

$$\Omega_i = \Omega_i^P \times x_i^P + \Omega_i^N \times x_i^N + \Omega_i^A \times x_i^A \tag{3.3}$$

where Ω represents m, $m\sigma^3$ or mε/k, and x_i^P, x_i^N, x_i^A are the percentages of P, N and A contents in each SCN fraction or pseudo-component, which fulfill the following summation constraint.

$$x_i^P + x_i^N + x_i^A = 1 \tag{3.4}$$

The model parameters of the P, N and A contents are represented, respectively, by n-alkanes, cyclo-alkanes and benzene derivatives in this study, for which the correlations are given in Table 3.2.

3.3.3 Binary interaction parameters (BIP) k_{ij}

In general, a binary interaction parameter (k_{ij}) is needed for polar or highly asymmetric binaries to correct the segment-segment interactions when using the PC-SAFT EOS. The k_{ij} values for the same binary mixtures are different for the original and simplified versions [von Solms et al. (2003)]. Fortunately, a lot of work has been done for the simplified PC-SAFT EOS in the past decade. Yan et al. (2010) reported an optimal k_{ij} table for the possibly most important binary pairs in reservoir fluids. These pairs include N_2-X, CO_2-X and C_1-X, where X is another compound in the reservoir fluid. Tihić et al. (2006, 2008)also studied the vapor-liquid equilibria of binary systems of heavy hydrocarbons and light alkanes or gases. In this work, the k_{ij} values are mainly taken from the work of Yan et al. (2010), while the following three changes are made: (1) negative k_{ij} values of hydrocarbon pairs, which are not common, have been removed or replaced by the values from Tihić's work (2006, 2008); (2) the available k_{ij} between H_2S and other components are added; and (3) the k_{ij} of N_2-C_{7+}, CO_2-C_{7+}, and C_1-C_{7+} are taken the reasonable values in the middle of those from Yan et al. (2010) and Tihić et al. (2006, 2008), since Yan et al. (2010) considered the n-alkanes only up to n-decane. The modified k_{ij} values are compared with the old ones in Table 3.3, and the k_{ij} for other pairs could be found in the work of Yan et al. (2010). More discussions will be given for the modification (3) in the following section.

Table 3.3 The modified k_{ij} values from the k_{ij} table reported in work of Yan et al. (2010)

Comp. 1	Comp. 2	k_{ij} (old)	k_{ij} (new)
N_2	C_{7+}	0.055	0.08
CO_2	C_{7+}	0.07	0.06
H_2S	iC_4	0.00	0.026
H_2S	nC_4	0.00	0.045
H_2S	nC_6	0.00	0.048
H_2S	C_{7+}	0.00	0.03
C_1	C_2	-0.0058	0.0
C_1	nC_4	-0.0159	0.0041
C_1	C_{7+}	0.016	0.02

3.3.4 Candidate methods (CM)

It is shown earlier that simple correlations for the model parameters can be readily established for homologous series, and the PNA contents can be easily estimated as well. Therefore, it is possible to develop approaches for estimating model parameters based on combining the simple correlations

with the estimated PNA contents. In order to investigate the feasibility of using linear correlations for model parameters, and/or the significances of fitting approaches, six methods are proposed to estimate the model parameters during the characterization procedure.

The brief descriptions of the main ideas of these six candidate methods are presented in Table 3.4. The basic procedure is to choose homologous series with well-behaved correlations to represent the PNA contents, and to combine the models parameters with the estimated PNA contents, and then to fit zero, one or two parameters to the known physical properties, i.e. SG and/or Tb, of each SCN fraction or pseudo-component. The details of how they are implemented are shown in the flowchart Figure 3.4, and more discussions are given for each method in the following sections.

Table 3.4 Description of the candidate methods for estimating model parameters

Candidate Method	Description
CM1	combination of correlations from Table 3.2 using equations (3.3 and 3.4)
CM2	P and N percentages are tuned to match Tb and SG with equation (3.4)
CM3	m and ε are from CM1 and σ from equation (3.1)
CM4	m and ε are tuned to match Tb and SG with σ from equation (3.1)
CM5	σ is tuned to match SG with m from CM1 and ε from equation (3.2)
CM6	m and σ are tuned to match Tb and SG and ε from equation (3.2)

3.4 Results and discussion

3.4.1 Petroleum fluids database

In order to investigate and compare the overall performance of different candidate methods, a petroleum fluid database covering wide ranges of composition, temperature and pressure is needed. In this work, 80 petroleum fluids have been collected from different sources [Wu et al. (1999), Jaubert et al. (2002), Al-Ajmi et al. (2011), Yan et al. (2013), CERE Internal Databank (2013)]. As listed in Appendix Table A, it can be seen that different types of petroleum fluids, from gas condensate to quite heavy oil, are included. It is readily seen that the plus fractions are starting from C_7, C_{11} or C_{20} for most of the fluids. Various experimental data from different measurements, such as Constant Mass Expansion (CME), Differential Liberation (DL), and/or separator test, are available for many of the fluids in this database.

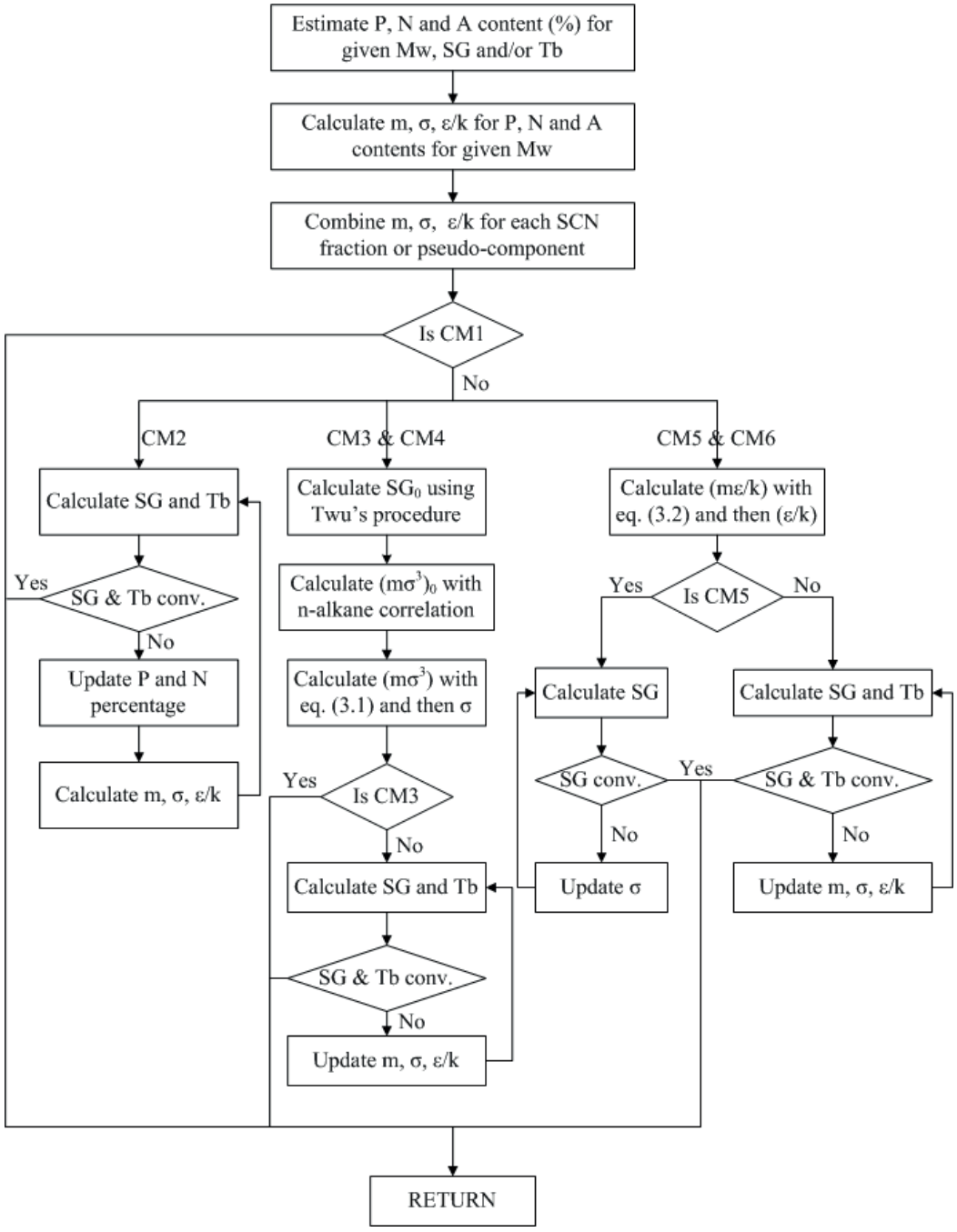

Figure 3.4 Implementation flowchart of the six candidate characterization methods

3.4.2 Saturation pressure and density

PVT modeling is used to study the volumetric behavior of the petroleum fluids as a function of temperature and pressure. Density is an essential property for petroleum fluids PVT measurements. Saturation pressure is another essential PVT property, especially the one at the reservoir temperature. A second phase starts to form after the reservoir pressure reaches the saturation pressure, which makes the produced fluid composition change significantly. These two properties play a crucial role in petroleum engineering calculations and production decision makings. They are used as the first criterion to choose proper characterization methods for further analysis. Density in this work includes liquid density of oils in both single-phase and two-phase regions, and density of gas condensates above dew pressure.

Table 3.5 The %AADs for saturation pressure of 80 petroleum fluids from different characterization procedures and number of pseudo-components

Char. Proc.	Numb. Pseudo.	%AAD of saturation pressure								
		CM1	CM2	CM3	CM4	CM5	CM6	Yan	SRK	PR
Pedersen	5	16.0	10.7	6.91	12.5	5.70	5.97	9.51	7.01	8.10
	7	16.0	10.8	6.89	12.4	5.69	5.94	9.89	7.10	8.26
	10	15.9	10.8	6.87	12.3	5.69	5.91	10.3	7.16	8.34
Whitson	5	15.4	9.04	6.73	11.8	5.62	5.97	8.14	8.06	9.38
	7	15.3	9.12	6.71	11.8	5.60	5.97	8.41	8.14	9.45
	10	15.3	9.28	6.70	11.8	5.60	5.94	8.62	8.13	9.37
Pedersen (Søreide)	5	15.4	9.19	6.81	12.0	5.57	6.07	8.24	7.01	8.10
	7	15.4	9.20	6.77	12.0	5.53	5.98	8.51	7.10	8.26
	10	15.3	9.31	6.76	12.1	5.55	5.93	8.71	7.16	8.34

Table 3.6 The %AADs for density of 80 petroleum fluids from different characterization procedures and number of pseudo-components with the PC-SAFT EOS

Char. Proc.	Numb. Pseudo.	%AAD of density						
		CM1	CM2	CM3	CM4	CM5	CM6	Yan
Pedersen	5	8.05	6.00	2.09	1.60	1.27	1.27	2.81
	7	8.04	6.00	2.09	1.60	1.26	1.27	2.31
	10	8.04	6.00	2.08	1.60	1.26	1.26	2.03
Whitson	5	7.90	5.46	2.17	1.60	1.29	1.30	1.67
	7	7.89	5.48	2.16	1.59	1.28	1.29	1.65
	10	7.88	5.52	2.15	1.59	1.28	1.29	1.63
Pedersen (Søreide)	5	7.91	5.50	2.17	1.60	1.28	1.28	1.61
	7	7.90	5.48	2.15	1.60	1.27	1.28	1.61
	10	7.89	5.49	2.15	1.60	1.27	1.28	1.60

Table 3.7 The percent deviations of saturation pressure for individual fluids

Fluid	CM1	CM2	CM3	CM4	CM5	CM5 (Whit.)	CM5 (nc=10)	CM5 (Riazi)	CM6	Yan	SRK
F01	6.08	0.15	2.43	9.69	2.37	5.05	0.53	2.00	2.38	10.6	9.23
F02	2.01	3.10	2.45	3.02	2.08	3.12	4.30	3.06	2.18	6.52	0.57
F03	2.58	9.72	6.69	3.32	7.71	8.06	10.1	10.1	6.25	15.6	4.90
F04	10.2	1.15	6.69	11.4	5.51	7.17	0.16	2.68	6.97	10.4	4.30
F05	0.45	9.45	5.16	4.54	6.67	4.96	12.1	9.79	4.53	23.2	0.08
F06	18.3	9.04	6.64	23.8	3.44	2.87	2.87	2.83	3.91	3.73	19.3
F07	12.0	6.83	4.15	10.4	2.78	2.01	2.44	1.76	2.97	4.98	2.52
F08	6.58	0.14	1.47	4.87	2.99	1.40	3.49	7.07	2.55	22.4	1.59
F09	1.52	4.78	2.11	0.11	1.38	4.29	1.07	3.03	1.51	30.0	5.35
F10	1.88	3.05	0.29	1.71	0.62	1.48	0.95	1.57	0.70	13.1	5.28
F11	0.24	3.36	0.67	0.57	0.18	1.81	0.47	2.00	0.26	15.9	3.95
F12	9.30	4.06	1.09	3.91	0.19	1.57	0.27	4.97	0.07	5.19	1.64
F13	16.5	11.5	8.51	11.0	7.22	5.97	7.13	2.75	7.42	2.02	1.63
F14	16.4	11.7	8.31	11.0	7.00	5.75	6.91	2.49	7.19	1.78	2.22
F15	17.9	13.5	9.45	15.1	8.05	6.92	7.95	3.70	8.22	1.95	4.45
F16	17.6	13.2	10.7	12.9	9.58	8.42	9.43	5.76	9.85	4.83	4.12
F17	20.4	15.8	12.9	15.7	11.7	10.5	11.5	7.65	12.0	7.24	6.70
F18	15.4	10.6	7.07	12.6	5.65	4.41	5.50	1.48	5.94	0.03	2.70
F19	19.5	14.9	12.3	14.8	11.1	9.93	11.0	7.24	11.5	6.81	6.43
F20	13.2	8.27	4.86	10.9	3.40	2.19	3.25	0.69	3.78	2.12	1.94
F21	14.9	10.2	6.50	12.4	5.00	3.75	4.85	0.87	5.39	0.71	2.71
F22	3.01	3.29	4.99	0.59	6.50	7.62	6.64	10.4	5.75	10.7	9.19
F23	5.11	0.64	4.98	1.72	6.94	8.27	7.09	11.8	6.24	13.5	8.10
F24	18.9	13.8	10.1	12.6	8.40	7.07	8.29	3.62	9.02	2.43	0.11
F25	19.9	14.2	12.2	14.4	10.6	9.6	10.5	6.73	11.6	6.51	4.63
F26	14.1	1.11	5.74	7.21	3.99	4.58	3.99	1.21	4.50	0.43	4.88
F27	7.94	2.07	1.71	2.98	0.78	0.62	0.54	3.53	1.34	14.5	9.15
F28	34.1	26.9	20.4	25.4	17.8	17.5	17.8	10.7	18.3	2.28	1.28
F29	17.4	4.55	4.11	8.55	1.33	1.44	1.33	4.26	2.04	10.0	3.48
F30	13.1	6.76	4.51	13.8	3.05	2.75	2.78	1.17	3.52	6.96	8.88
F31	19.5	13.4	10.8	20.8	9.54	9.41	9.35	6.15	10.1	1.42	11.9
F32	13.2	2.05	2.26	3.01	5.56	5.26	5.57	11.6	4.25	19.5	9.10
F33	12.4	6.15	2.80	11.8	1.47	1.11	1.33	2.14	2.16	6.14	0.39
F34	19.8	10.2	3.79	9.91	0.41	0.11	0.40	7.43	1.08	16.1	7.53
F35	20.6	12.7	10.3	21.7	8.37	8.27	8.13	4.98	9.31	1.02	13.0
F36	22.6	14.0	7.90	21.1	4.92	4.76	4.68	0.76	5.73	8.58	6.09
F37	21.9	13.0	10.5	23.8	8.14	8.22	7.92	5.02	9.19	0.68	16.6
F38	30.5	23.1	15.3	24.2	12.0	12.7	11.9	4.44	12.6	4.78	5.28
F39	18.3	13.2	9.33	12.9	7.69	6.96	7.45	1.57	8.24	9.36	7.18
F40	23.2	14.6	8.22	21.1	5.04	4.87	4.82	0.72	6.05	8.89	6.48
F41	18.1	8.49	4.74	18.2	2.06	2.07	1.86	2.20	3.26	8.56	5.83

F42	24.8	16.8	9.34	23.3	6.09	5.78	5.84	0	7.02	8.73	7.47
F43	31.9	26.8	16.9	27.3	13.9	13.2	13.8	6.37	14.8	2.83	0.70
F44	23.7	14.0	9.68	22.8	6.62	6.56	6.44	2.03	7.90	4.40	9.54
F45	19.4	13.3	3.66	14.0	0.56	0.44	0.42	6.63	1.54	14.7	10.4
F46	27.8	21.4	7.56	21.3	3.06	3.13	2.95	8.16	4.14	24.1	5.69
F47	37.2	29.5	23.4	33.3	20.2	20.6	20.1	14.5	21.4	6.67	20.9
F48	29.7	23.2	10.3	23.1	5.77	6.14	5.66	4.45	6.96	18.0	0.10
F49	26.2	20.7	9.82	19.6	6.41	6.34	6.28	1.87	7.35	13.2	6.86
F50	30.0	23.0	10.8	24.3	6.28	6.79	6.15	3.14	7.66	16.0	2.47
F51	17.4	10.8	6.36	10.2	4.08	3.56	4.01	0.91	5.20	4.36	6.62
F52	8.34	2.35	1.67	5.91	0.26	0.19	0.13	1.73	1.75	2.98	2.04
F53	29.7	24.7	13.2	22.7	9.38	9.06	9.24	1.42	10.7	8.64	4.10
F54	5.95	4.62	5.19	2.6	8.21	7.63	8.28	10.8	5.51	12.2	8.81
F55	13.1	6.37	2.54	5.04	6.24	6.18	6.28	13.0	4.86	20.7	14.7
F56	28.1	23.0	10.3	20.0	6.08	5.67	5.90	2.88	7.58	13.7	9.14
F57	39.0	35.8	19.2	27.4	14.4	11.9	14.4	2.23	15.6	15.8	11.3
F58	35.9	32.0	14.7	21.8	9.11	9.58	9.07	5.45	10.6	25.0	19.4
F59	11.5	3.85	0	5.86	3.14	4.01	3.18	6.44	0.67	11.5	0.02
F60	26.2	22.4	2.66	4.71	3.71	7.51	3.72	21.1	2.01	45.1	44.7
F61	22.1	16.7	7.02	8.21	2.74	1.11	2.70	4.03	5.23	12.3	17.8
F62	10.0	5.38	7.14	10.8	7.68	7.79	7.79	6.79	7.85	6.61	12.3
F63	10.3	2.64	2.85	9.72	1.00	1.18	0.69	1.14	2.14	4.42	9.56
F64	8.10	1.76	0.16	9.44	1.32	1.26	1.66	4.03	0.59	8.51	5.77
F65	7.24	1.31	1.17	8.29	0.90	0.89	1.10	2.73	0.83	4.87	15.6
F66	4.09	1.61	4.27	4.83	5.17	4.21	5.33	4.22	4.94	17.1	5.86
F67	0.03	9.01	8.17	1.08	10.5	10.3	11.0	13.5	9.07	18.0	0.39
F68	7.66	0.21	0.60	5.07	2.62	3.06	3.03	5.96	1.74	9.86	0.28
F69	19.8	14.4	10.8	15.2	8.92	8.17	8.54	4.94	9.39	0.13	3.82
F70	5.87	2.48	4.22	7.26	6.63	6.37	6.95	9.74	4.33	15.4	2.88
F71	11.6	4.74	6.54	9.06	5.29	5.41	5	3.41	6.12	1.23	10.1
F72	7.66	1.31	2.14	6.19	0.84	0.92	0.57	1.28	2.01	3.74	6.35
F73	11.1	2.3	0.73	11.8	1.87	1.65	2.27	4.64	1.05	13.2	9.81
F74	8.21	0.55	0.42	6.47	3.19	2.81	3.58	5.75	1.66	10.5	8.25
F75	22.2	16.4	14.5	18.8	12.4	12.1	12.2	10.3	14.1	6.99	13.0
F76	9.81	4.26	1.32	5.65	1.25	1.72	1.52	3.24	0.53	6.57	1.49
F77	8.10	2.21	0.87	3.34	1.82	3.46	2.26	2.49	0.58	0.38	FAIL
F78	23.3	15.6	10.4	19.7	7.73	6.89	7.59	1.86	8.35	2.82	3.19
F79	19.0	14.3	8.17	14.4	5.21	4.76	5.03	1.04	6.81	3.34	0.94
F80	21.0	16.6	9.28	20.3	6.09	6.14	5.75	1.55	7.45	4.75	11.0
avg	16.0	10.7	6.91	12.5	5.70	5.62	5.69	4.87	5.97	9.51	7.01
>10*	57	41	21	47	10	8	12	11	12	32	17

* Number of cases whose calculated saturation pressure deviation is larger than 10%.

The %AADs for saturation pressure and density are respectively listed in Tables 3.5 and 3.6 for these 80 petroleum fluids. The comparisons are made in four aspects, i.e. molar composition distributions, SG correlations, numbers of pseudo-components and EOS models or estimation methods of model parameters for the same EOS. The PNA distributions are estimated by the n-d-M method. The second column indicates how many pseudo-components are used to represent the C_{7+} fraction. The results from SRK and PR are also presented as references, for which the critical properties are calculated by the method developed by Twu (1984) and the acentric factor is calculated from the Lee-Kesler correlations [Lee et al. (1975), Kesler et al. (1976)].

The %AAD of saturation pressure for individual fluids are presented in Table 3.7. The results with different characterization procedures, number of pseudo-components and PNA content estimation methods are given for the candidate method CM5, while the standard exponential characterization procedure [Pedersen et al. (1983, 1984, 2007a)] is used for other methods. Both of the average values of %AAD and the number of cases with deviation larger than 10% are given for comparison. As seen from Table 3.5 and the work of Yan et al. (2010), SRK and PR perform quite similarly, and SRK gives slightly smaller overall deviations of saturation pressure. Thus the results of individual fluids from SRK are presented here for comparison.

It can be seen from Tables 3.5 and 3.6 that there are small variations of the overall %AAD of both saturation pressure and density among different characterization procedures, and these differences mainly come from different SG approaches, rather than from the molar composition distributions. The further comparison of these two characterization procedures, however, as presented in Table 3.7, shows that they have noticeable differences for individual oil fluids with plus fractions starting from seven or with extremely heavy plus fraction, for example F57, F60, F61 and F77. This is because default characteristic parameters are used for these fluids in the gamma characterization procedure. However, the overall %AADs for vapor pressure of fluids F57, F60, F61, F77 and those with plus fraction starting from seven are, respectively, 5.73% and 5.52% for the exponential and the gamma characterization procedures. All of these results confirm the conclusion made by Pedersen et al. (2007a) that the exponential and gamma characterization procedures perform quite similarly. Tables 3.5 and 3.6 also show that the variations of overall %AADs for saturation pressure and density among different number of pseudo-components are even smaller compared to those from different characterization procedures. However, the number of pseudo-components has significant impact on the dew points of gas condensate fluids as shown in Table 3.7. This could

probably be explained that the more pseudo-components used to represent the plus fraction, the heavier the last component would be, and the easier it would get condensed. The results indicate that five pseudo-components for the plus fraction seem to be enough to get satisfactory predictions of saturation pressure and density for oils, which is consistent to the statements about how many components to group from Whitson et al. (2000) and Riazi (2005). It is also meaningful for modeling and simulation of petroleum fluids, since the overall computational load increases significantly with the total component numbers.

The results from CM1 have much larger %AAD than those from other candidate methods in terms of both saturation pressure and density, which means that it is not the correct way to produce the model parameters. In order to eliminate the effects of PNA content estimations, the percentages of P and N are tuned to match the SG and Tb of the SCN fractions or pseudo-components in CM2. It can be seen that the predictions of both saturation pressure and density are much improved, while they are still unsatisfactory. This reveals that combination of the correlations of n-alkanes, cyclo-alkane and benzene derivatives are not good enough for producing all of the model parameters. Meanwhile it also indicates that it would not be generally applicable to have simple linear correlations for the three model parameters suitable for all different types of petroleum fluids.

The correlation equation (3.1) is used in CM3, CM4 and Yan's method [Yan et al. (2010)]. As shown in Tables 3.5 and 3.6, CM3 and Yan's method yield comparable descriptions of saturation pressure to those given by SRK and PR. The results of %AAD of density are also acceptable. In order to investigate if it is possible to further improve the descriptions of density within this framework, the parameters m and ε in CM4 are tuned to match the SG and Tb of SCN fractions and pseudo-components while keeping using equation (3.1) to calculate the parameter σ. This method shows significant deterioration of the predictions of saturation pressure with small improvements on density descriptions.

The simple equation (3.2) is used to calculate ε/k in both CM5 and CM6. The parameter m is from PNA combination, and the parameter σ is tuned to match SG in CM5, while both parameters m and σ are tuned to match SG and Tb in CM6. Even compared to the results calculated with the SRK and PR EOS, the results from these two methods are quite promising, with the %AADs for saturation pressure and density less than 6.0% and 1.3%, respectively, and more than 85% possibility to predict the saturation pressure within 10%. The method CM5 inspires us to fit the parameter σ to match SG in CM3. The %AADs for saturation pressure and density are respectively 5.67% and

1.28%, which are very close to those from CM5. This confirms to some extent that it is possible to use a simple correlation for the model parameter combination mε/k. These results indicate that it is feasible to use linear correlations for one or two of these parameters, while the remaining one(s) is/are tuned to SG and/or Tb.

The results and discussions presented above suggest on one hand that it is crucial to tune the model parameters to SG and/or Tb to have precise description of density, which could simultaneously improve the descriptions of saturation pressure further. On the other hand, it is very important to choose the right parameters for fitting purposes.

Since the percentages of PNA contents are used directly or indirectly in the process of estimating model parameters, it is useful to compare the two PNA content estimation methods themselves. The %AADs for saturation pressure and density are compared in Figures 3.5 (a) and (b) for all the candidate methods. The results of individual fluids are also given for CM5 in Table 3.7. The exponential characterization procedure [Pedersen et al. (1983, 1984, 2007a)] with five pseudo-components is used here, which will be the default procedure for the following discussions. It is clearly shown that the results from these two estimation methods are quite different. The comparisons in Figures 3.5 (a) and (b) show that the Riazi method [Riazi et al. (1986)] gives slightly smaller overall %AADs for both saturation pressure and density, while it can be seen from Table 3.7 that it really depends on the fluids under investigation. It is not surprising to see that these two PNA estimation methods give quite close results for CM4 and CM6. This is because the same parameters (m and σ) are tuned to the same data (SG and Tb), only with different initial guesses from these two PNA estimation methods.

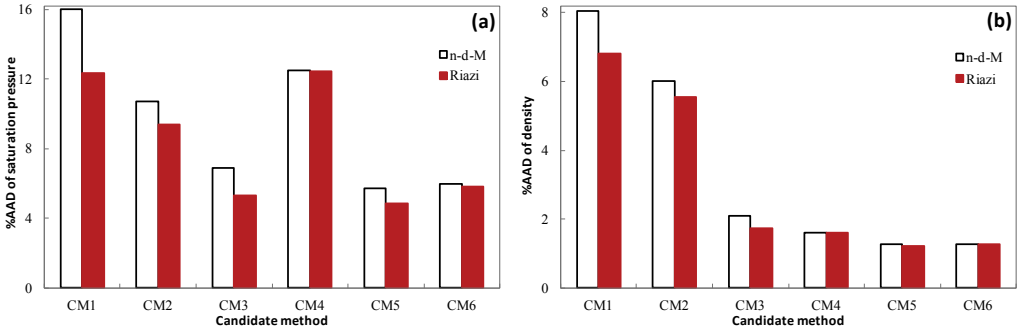

Figure 3.5 Comparison of the impacts of the estimations methods of PNA contents on the %AADs for (a) saturation pressure and (b) density of 80 petroleum fluids

It is quite demanding to investigate the effects of binary interaction parameters for these candidate methods. The %AADs for saturation pressure and density are compared in Figures 3.6 (a) and (b) for all candidate methods with the two available k_{ij} sets. It can be seen that k_{ij} values have, respectively, large and negligible impacts on the description of the saturation pressure and density. This is because k_{ij} values are mainly for the pairs containing light gases and/or methane, and these light components have large impacts on the saturation pressures of petroleum fluids, which makes k_{ij} values a powerful tool to tune the EOS model to match the saturation pressure. Most of the fluids considered in this work are oil samples, and the light components are too light to affect the oil density.

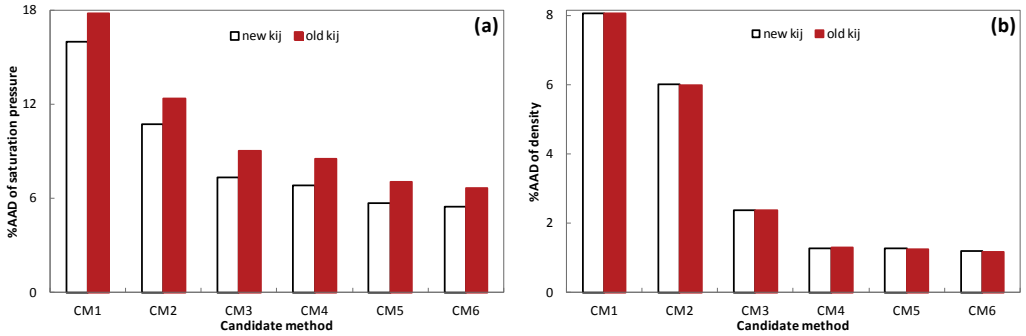

Figure 3.6 Comparison of the effects of binary interaction parameters on the %AADs for (a) saturation pressure and (b) density of 80 petroleum fluids.

As seen from Table 3.7, the saturation pressures of the N_2 and/or CO_2 rich fluids are predicted with satisfactory accuracy, which indicates, to some extent, that the k_{ij} values for pairs containing N_2 or CO_2 are reasonable. These k_{ij} values will not be further investigated in this work also because of lack of enough cases. It is, however, a good opportunity to study the influence of the k_{ij} of pairs containing C_1 on PVT calculations. We proposed to conduct the investigations with the scenarios by sequentially setting $k_{ij}(C_1,C_{2\text{-}6})=0.0$, $k_{ij}(C_1,C_{7+})=0.01$, $k_{ij}(C_1,C_{7+})=0.03$, or using the following correlation:

$$1000\times k_{ij}(C_1, C_{7+}) = 0.070199 \times Mw_{C_{7+}} + 5.4229 \tag{3.5}$$

This correlation is regressed from the values published by Yan et al. (2010) and Tihić et al. (2006, 2008). The difference between the %AAD of these k_{ij} values and the one with $k_{ij}(C_1,C_{7+})=0.02$ are plotted against the fluid number in Figure 3.7, where the %AAD from each scenario are also given.

It is readily seen that the $k_{ij}(C_1,C_{2-6})$ and $k_{ij}(C_1,C_{7+})$ have, respectively, quite small and fairly significant impacts on prediction of saturation pressure, even though quite close %AAD are obtained by using 0.02, 0.03 and equation (3.5) for $k_{ij}(C_1,C_{7+})$. The results suggest that more extensive investigations should be further conducted if the k_{ij} values are indirectly used to develop 'general' correlations for new characterization methods, as in the work of Pedersen et al. (2007b).

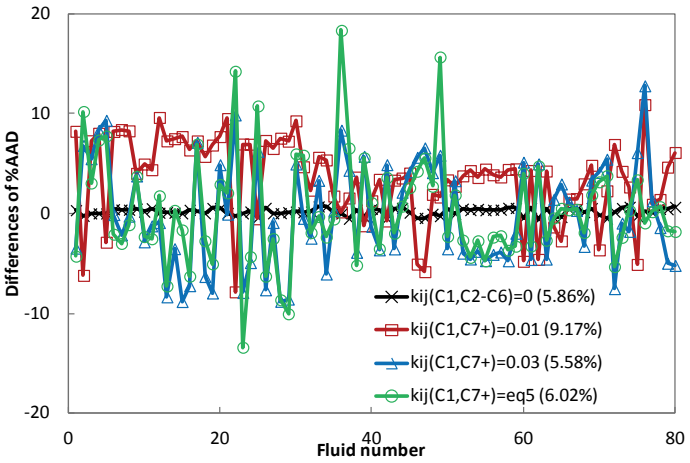

Figure 3.7 The difference between the %AAD of these k_{ij} values and the one with $k_{ij}(C_1,C_{7+}) = 0.02$. The average %AAD values of each k_{ij} are also listed in the legend for comparison.

3.4.3 A compromise method (CM7)

The candidate methods CM5 and CM6 have better overall performance on the prediction of saturation pressure and density. The two PNA content estimation methods (n-d-M and Riazi) have overall comparable performance for CM5, and the one with the Riazi method will be denoted as CM5 (R) hereafter.

As listed in Table 3.7, the candidate methods give comparable average deviations of the saturation pressure prediction, while the predictions for the individual case are quite different. It inspires us to investigate if it is possible to have simple (linear) correlations for m and $m\sigma^3$ as well. The strategy is to put the parameters which give the best prediction for each case together, and to analyze their relationships with molecular weight. The results are presented in Figure 3.8. It can be seen that the correlation of m is quite satisfactory, while the correlation of $m\sigma^3$ shows a bit more scatter for heavy pseudo-components.

The prediction of the saturation pressure of the aforementioned 80 fluids from this new method is compared with the ones from CM5 and CM6 in Table 3.8. Since the correlation of $m\sigma^3$ is not satisfactory at the heavy component ends, fitting σ to the specific density, as done before, has also been tried. The equation (3.2) is used for ε. The results show that it is necessary to fit the parameter σ for accurate description of density, and then the new method performs as satisfactory as the other ones.

In order to test the predictive capability of these methods, the predictions of the saturation pressure of the 55 fluids from Elsharkawy (2003) are conducted for these methods. The results are also reported in Table 3.8. The results for the additional 55 fluids, reported in this work, are assuming to use nC_4 and nC_5 for C_4 and C_5, but as we have found that there are no observable differences to use normal-hydrocarbons or iso-hydrocarbons. It can be seen that these methods show equally good predictions. The new method is named CM7, and it will be investigated, along with the other methods, further for three fluids for which extensive PVT experimental data is available.

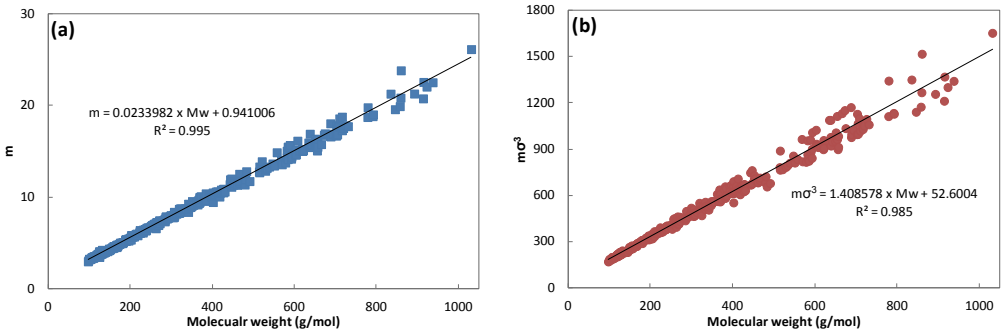

Figure 3.8 Correlations of m and $m\sigma^3$ from the best candidate methods for each fluid

Table 3.8 Comparison of the new method with CM5 and MC6 on saturation pressure and density

fluid number	CM5	CM5 (R)	CM6	CM7	
				fitting σ	no fitting
80	5.70	4.87	5.97	5.12 (1.27)*	6.69 (2.49)
80+55	6.33	6.79	6.44	6.60	7.31

* The values in the parentheses are the deviations of density.

3.4.4 Applications

3.4.4.1 PVT simulations

The methods CM5, CM5 (R), CM6 and CM7 are further tested using the three fluids from the book of Pedersen and Christensen (2007a) without tuning against the experimental PVT data. The first fluid is a gas condensate, and three experimental CME data sets are available. The second fluid is an oil sample, for which there are three CME data sets and five DL data sets available. The third fluid is also an oil sample, and four-stage separator test experimental data are available. The definitions of these experiments and associated properties, composition and experimental data can be found in the chapter 3 of the book [Pedersen et al. (2007a)].

The characterized fluid composition and model parameters of C_{7+} pseudo-components can be found in Tables 3.9 and 3.10. The model parameters of the defined components are taken from the work of Gross and Sadowski (2001). The model parameters of the first four pseudo-components of fluid F04 are the same in CM5 and CM6 as listed in Table 3.10, which means that no further fitting is needed to match SG and Tb for them.

Table 3.9 Mole composition of the three fluids (F04, F63, F64) after characterization

Comp.	Fluid F04		Fluid F63		Fluid F64	
	Mw (g/mol)	z%	Mw (g/mol)	z%	Mw (g/mol)	z%
N2		0.60		0.39		0.59
CO2		3.34		0.30		0.36
C1		74.167		40.2		40.81
C2		7.901		7.61		7.38
C3		4.15		7.95		7.88
iC4		0.71		1.19		1.20
C4		1.44		4.08		3.96
iC5		0.53		1.39		1.33
C5		0.66		2.15		2.09
C6		0.81		2.79		2.84
P1	97.36	2.35	111.00	14.14	117.58	14.44
P2	125.19	1.13	173.58	7.66	175.40	6.21
P3	161.09	1.06	253.29	4.815	239.32	5.483
P4	218.25	0.681	392.91	3.439	379.43	3.433
P5	362.00	0.471	674.59	1.896	665.62	1.994

The simulated CME results of fluid F04 from these four methods are compared with the experimental data in Figures 3.9 (a), (b) and (c). It can be seen that these characterization methods give quite similar overall results for these three CME measurements, except for the starting point of the drop liquid volume percentage. The simulated and experimental relative volumes agree very well in the whole pressure range, and the simulated Z factor matches the experimental data nicely with some small deviations in the high pressure range. The simulated percent liquid dropout volumes seem to be much lower than the experimental data in the low pressure range. These results, however, are comparable to those from SRK and PR with volume translations, for which simulation results are available in the chapter 7 of the book [Pedersen et al. (2007a)].

Table 3.10 Model parameters of C_{7+} pseudo-components for the three fluids (F04, F63, F64)

Fluid F04			Fluid F63			Fluid F64		
m	σ (Å)	ε/k (K)	m	σ (Å)	ε/k (K)	m	σ (Å)	ε/k (K)
CM5								
3.0956	3.7943	255.04	3.5110	3.8159	251.41	3.7341	3.8293	248.42
3.8148	3.8244	256.80	5.0837	3.8671	257.73	5.1551	3.8721	256.56
4.7700	3.8590	256.79	7.0736	3.9035	262.20	6.7153	3.8973	261.97
6.1859	3.8958	261.13	10.6916	3.8904	262.68	10.3516	3.8836	262.41
9.8645	3.9181	263.30	17.3748	3.9121	272.38	17.1599	3.8982	272.23
CM5 (R)								
3.1334	3.7755	251.96	3.4770	3.8310	253.87	3.6572	3.8619	253.64
3.7573	3.8480	260.73	4.9420	3.9115	265.11	4.9598	3.9331	266.67
4.6126	3.9117	265.55	7.0323	3.9128	263.74	6.6856	3.9043	263.14
6.1425	3.9069	262.97	10.3733	3.9386	270.74	10.0264	3.9345	270.92
9.7006	3.9450	267.74	17.1037	3.9373	276.70	16.8016	3.9319	278.03
CM6								
3.0956	3.7943	255.04	3.5110	3.8159	251.41	3.8172	3.7950	243.01
3.8148	3.8244	256.80	5.0973	3.8629	257.03	5.2882	3.8323	250.10
4.7700	3.8590	256.79	7.1122	3.8949	260.78	6.7133	3.8978	262.06
6.1859	3.8958	261.13	10.7823	3.8770	260.47	10.4212	3.8730	260.66
9.9855	3.8986	260.11	17.9459	3.8604	263.71	17.7040	3.8484	263.86
CM7								
3.2191	3.7339	245.26	3.5383	3.8038	249.47	3.6921	3.8470	251.24
3.8703	3.8020	253.12	5.0025	3.8924	261.90	5.0451	3.9061	262.16
4.7103	3.8787	260.04	6.8676	3.9505	270.06	6.5407	3.9391	268.97
6.0477	3.9316	267.10	10.1344	3.9762	277.12	9.8190	3.9680	276.64
9.4112	3.9939	275.98	16.7251	3.9736	282.96	16.5154	3.9598	282.85

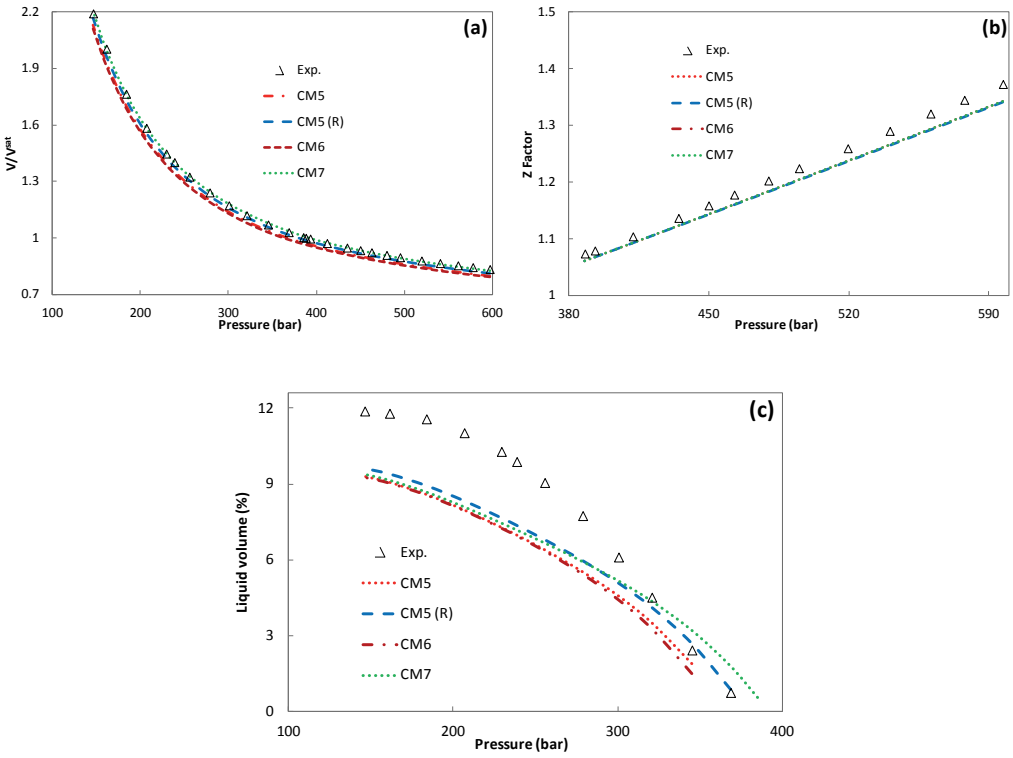

Figure 3.9 Simulation CME results of fluid F04 with characterization methods CM5, CM5 (R), CM6 and CM7. (a) Relative volume; (b) Z factor above dew point; (c) Liquid dropout volume (%). The experimental data are from the book of Pedersen et al. (2007a).

The simulated DL and CME results of fluid F63 are presented in Figure 3.10. It can be seen from Figure 3.10 (a) that these methods represent the oil density perfectly at all pressure steps. As seen from Figure 3.10 (b), however, they have difficulties in describing the liberated gas phase compressibility factor (Z factor) at high pressures.

The simulated Y-factor is compared with the experimental data in Figure 3.10 (c), which shows that the different methods do not predict as similar results as those they do for oil density and Z factor. The method CM6 gives best match to the experimental data. The simulated compressibility results are presented in Figure 3.10 (d). The similar scatter results as for Y-factor are seen, but the method CM6 presents the largest deviation from the experimental data for this property.

The simulated compressibility from PR are also plotted in Figure 3.10 (d), which is taken from the book of Pedersen and Christensen (2007a), where they showed that PR gave much better results

than SRK for this case. There is no doubt that PC-SAFT significantly improves the descriptions of compressibility. Similar results were reported by Pedersen et al. (2007b) and Leekumjorn et al. (2013), and this seems to be natural since cubic EOS have inherent deficiency in the compressibility description. However, the simulated compressibility values from PC-SAFT still show some deviations from the experimental data at high pressure range, from both quantitative and qualitative points of view. This phenomenon is consistent to what was seen in previous works [Pedersen (2007b), de Villiers (2011), Liang et al. (2012), Leekumjorn et al. (2013)], and it is because PC-SAFT EOS has difficulties in describing the derivatives of pressure with respect to volume in wide range of temperature, which can be somehow improved by refitting the universal constants [Liang et al. (2012)].

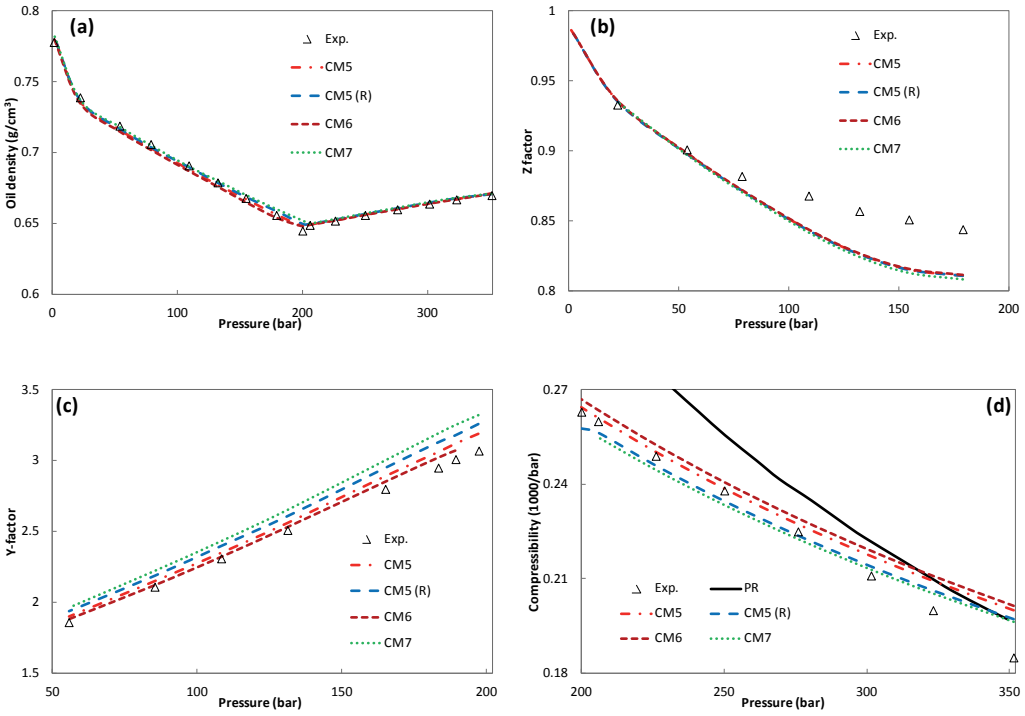

Figure 3.10 Simulation DL and CME results of fluid F63 with characterization methods CM5, CM5 (R), CM6 and CM7. (a) Oil density; (b) Z factor of liberated gas; (c) Y-Factor; (d) Compressibility above saturation pressure. The experimental data is from Pedersen et al. (2007a).

The %AAD of simulation results from the properties measured in CME and DL for fluids F04 and F63 are presented in Table 3.11. It can be seen that the simulation deviations are reasonably satisfactory except for the percent liquid dropout volume.

Table 3.11 %AADs for properties measured in CME and DL for fluid F04 and fluid F63

Methods	%AAD of properties											
	Fluid F04 CME			Fluid F63 CME			Fluid F63 DL					
	Rel. V	Liq. V	Z fact.	Rel. V	Y Fact.	Com. c_0	Bo	Rs	Oil ρ	Bg	Z fact.	G.G.
CM5	3.47	25.7	1.62	0.48	2.78	2.31	3.51	4.77	0.20	2.47	2.34	0.93
CM5 (R)	1.85	19.8	1.67	0.28	4.91	2.21	2.84	5.82	0.25	2.46	2.36	0.86
CM6	4.31	28.4	1.61	0.67	1.28	3.16	3.63	4.42	0.28	2.41	2.28	0.90
CM7	0.45	32.7	1.62	0.37	6.59	2.33	3.46	5.61	0.26	2.57	2.23	0.86

It has been shown that these methods have quite similar quantitative and qualitative behaviors for CME and DL results, and the same conclusion is true for the separator test experiments here. So the separator test results calculated only by the candidate method CM5 (R) and CM7 will be presented. The simulated separator test results of fluid F64 from both the simplified PC-SAFT and SRK EOS are presented in Table 3.12 along with the experimental data. Simulation results with both five and ten pseudo-components are available for the simplified PC-SAFT EOS. Since SRK and PR EOS give quite close results, which can be also seen from the Pedersen et al. (2007a), only the ones from SRK are presented. It can be seen that the simulated results from these two EOS models are quite close except for the composition of C_{7+}, if the same number of pseudo-components is used. It shows that the composition of C_{7+} could be largely affected by the number of pseudo-components for the plus fraction. This might be explained that the more pseudo-components are used to represent the plus fraction, the lighter the first C_{7+} component would be, and the tendency to enter the vapor phase would be easier. However, there is really small impact on the composition of the defined components when changing the number of pseudo-components for the plus fraction. This is consistent with the aforementioned statement that the number of pseudo-component has little effect on bubble points of oil samples. It is also seen that the simulated compositions of C_5 and C_6 are larger than the experimental results at the final stage for both EOS models, which might be tuned by binary interaction parameters.

Table 3.12 Comparison of simulated and experimental composition at each stage in separator test

Comp.	stage 1	stage 2	stage 3	stage 4	stage 1	stage 2	stage 3	stage 4
	Experimental data*				SRK (nc=5)			
N_2	1.07	0.42	0.01	0.00	1.32	0.61	0.16	0.02
CO_2	0.49	0.62	0.60	0.28	0.57	0.69	0.65	0.29
C_1	77.43	64.63	36.04	8.89	78.44	65.40	37.45	8.89
C_2	9.56	14.42	20.23	16.19	9.13	14.14	20.02	15.68
C_3	6.70	12.01	24.89	35.52	6.21	11.49	23.32	33.69
iC_4	0.71	1.30	3.13	5.74	0.64	1.23	2.84	5.52
nC_4	2.01	3.65	9.02	17.22	1.80	3.42	8.20	17.32
iC_5	0.44	0.74	1.86	3.77	0.39	0.70	1.73	4.23
nC_5	0.59	0.98	2.31	4.61	0.52	0.93	2.34	5.86
C_6	0.47	0.66	1.28	2.92	0.38	0.62	1.52	4.01
C_{7+}	0.53	0.57	0.63	4.86	0.59	0.78	1.76	4.50
	CM5 (R) (nc=5)				CM5 (R) (nc=10)			
N_2	1.31	0.53	0.12	0.01	1.31	0.53	0.12	0.01
CO_2	0.59	0.68	0.62	0.27	0.59	0.68	0.61	0.26
C_1	78.31	65.79	38.09	9.36	78.18	65.60	37.74	9.06
C_2	9.13	14.13	20.31	16.59	9.13	14.12	20.21	16.20
C_3	6.32	11.41	23.07	33.77	6.33	11.41	23.02	33.26
iC_4	0.68	1.24	2.84	5.48	0.68	1.24	2.84	5.43
nC_4	1.84	3.38	8.06	17.13	1.84	3.39	8.07	17.02
iC_5	0.40	0.71	1.76	4.29	0.40	0.71	1.76	4.28
nC_5	0.54	0.93	2.32	5.83	0.54	0.93	2.33	5.83
C_6	0.40	0.62	1.53	4.03	0.40	0.62	1.53	4.04
C_{7+}	0.48	0.58	1.28	3.25	0.59	0.77	1.78	4.61
	CM7 (nc=5)				CM7 (nc=10)			
N_2	1.30	0.52	0.12	0.01	1.30	0.52	0.12	0.01
CO_2	0.59	0.68	0.62	0.26	0.59	0.68	0.61	0.26
C_1	78.24	65.68	37.90	9.24	78.11	65.49	37.56	8.95
C_2	9.15	14.16	20.32	16.50	9.16	14.15	20.22	16.13
C_3	6.34	11.44	23.12	33.71	6.35	11.44	23.07	33.21
iC_4	0.68	1.25	2.85	5.49	0.68	1.25	2.85	5.44
nC_4	1.84	3.39	8.09	17.15	1.85	3.40	8.09	17.04
iC_5	0.40	0.71	1.76	4.30	0.40	0.71	1.77	4.29
nC_5	0.54	0.94	2.33	5.84	0.54	0.94	2.34	5.84
C_6	0.40	0.62	1.53	4.04	0.40	0.62	1.54	4.06
C_{7+}	0.50	0.61	1.36	3.45	0.62	0.80	1.84	4.77

* The experimental data is taken from Pedersen et al. (2007a).

3.4.4.2 Phase envelope

The phase envelopes of fluids F04 and F63 from the PC-SAFT EOS with the characterization methods CM5, CM5(R), CM6 and CM7, and the PR EOS are presented in Figure 3.11. It can be seen that PC-SAFT predicts a bit larger phase envelopes for these two fluids than PR, among which the method CM7 gives the largest ones. These characterization methods present similar predictions around the experimental points, so it is hard to say which characterization method is superior to others if based on one saturation pressure data point only.

Both PC-SAFT and PR predict liquid-liquid like phase split at the low temperature regions for fluid F04, though temperature regions are much different, i.e. the liquid-liquid like phase split from PC-SAFT appears 80K higher than those from PR. PC-SAFT predicts liquid-liquid like phase split for fluid F63 as well, however, PR does not give the same prediction. The experimental data are extremely scarce at these temperature ranges, e.g. below 250K, so it is hard to determine whether this is a physical or non-physical prediction.

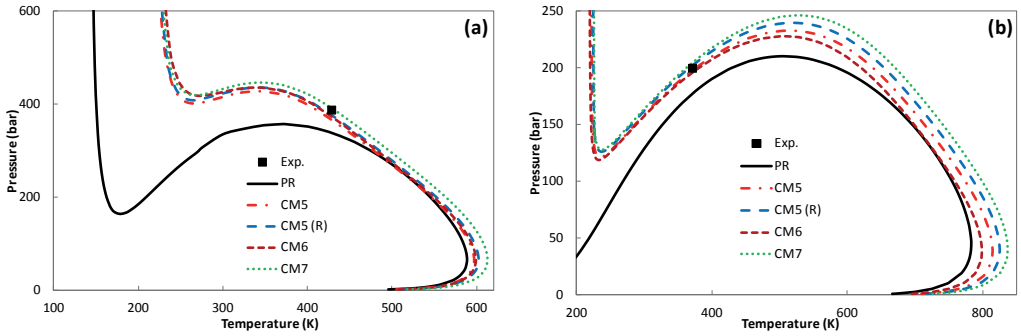

Figure 3.11 Phase envelopes of F04 (a) and F63 (b) from the PC-SAFT and PR EOS

3.4.4.3 Activity coefficients

The activity coefficients are good measures to roughly indicate the solution behavior of the heavy components. The activity coefficients of the pseudo-components have been calculated for 55 fluids, for which the DL/CME experimental data is available. The calculations have been conducted under the same temperature, pressure and composition conditions as those in the DL/CME experiments, and the results are shown in Table 3.13.

On one hand, the average activity coefficients for all the pseudo-components from different characterization methods are not far from unity, indicating that our models predict a near-ideal solution behavior for the pseudo-components in the tested systems. On the other hand, as the pseudo-component becomes heavier, the activity coefficient generally decreases, showing a shift towards the athermal solution behavior, which to some extent largely depends on the oil types, as indicated by the increasing standard deviations.

Table 3.13 Average activity coefficients of pseudo-components from four characterization methods

Comp.	CM5	CM5 (R)	CM6	CM7
P1	1.03 (0.038)*	1.03 (0.036)	1.02 (0.038)	1.02 (0.031)
P2	1.03 (0.050)	1.04 (0.059)	1.04 (0.051)	1.03 (0.049)
P3	0.98 (0.095)	1.00 (0.083)	0.99 (0.098)	1.01 (0.087)
P4	0.88 (0.125)	0.96 (0.127)	0.87 (0.132)	0.98 (0.133)
P5	0.82 (0.151)	0.91 (0.215)	0.74 (0.144)	0.92 (0.205)

* The numbers in the parentheses are standard deviations along with the averages

3.5 Conclusions

In this work, six candidate methods are proposed for estimating model parameters during petroleum fluid characterization procedures for the PC-SAFT EOS, in which the model parameters are produced by combining well-behaved simple correlations of homologous series with the estimated PNA contents, and/or by using different approaches fitted to match SG and/or Tb. The performance of these candidate methods is investigated for predicting the saturation pressure and density of 80 petroleum fluids over wide temperature, pressure and composition conditions, along with different options in characterization procedures, including the molar composition distribution function, the SG correlation, the number of pseudo-components, the PNA content estimation method and the binary interaction parameters.

The results show that the characterization procedures have small impact on saturation pressure and density for all of the proposed candidate methods, so does the number of pseudo-components for oil fluids. However, the number of pseudo-components has significant impact on saturation pressure of the gas condensates. The investigations of PNA content estimation methods reveal that they could lead to quite different results, which suggests that precautions should be taken when the PNA content estimations are directly used in producing model parameters. The binary interaction

parameters have significant effects on saturation pressure and quite small impact on density, and more extensive investigations are recommended if the k_{ij} values are indirectly used to develop 'general' correlations for new characterization methods. The candidate methods CM5 and CM6 show better overall performance than other methods, with %AAD less than 6.0% and 1.3% of saturation pressure and density, respectively, and with 85% possibility to predict saturation pressure within 10%.

A further analysis has been conducted for the generated parameters from the best candidate methods for each fluid, and a new compromise method is proposed with a simple linear correlation for the model parameter *m*, named as CM7, which gives quite similar predictions for saturation pressure and density as those from CM5 and CM6.

The methods CM5, CM6 and CM7 are further studied on simulating experimental CME, DL and separator test data for three petroleum fluids. These methods show overall similar performance. The simulated relative volumes and density of both gas condensate and oil fluids match the experimental data quite well. These methods, however, have difficulties in describing the percent volumes of dropped liquid from gas condensate, Z factor of liberated gas from oil, and the compressibility of oils at high pressure range from the qualitative point of view. The simulated separator test results from the simplified PC-SAFT EOS and the SRK EOS are quite close except for the composition of C_{7+}, which seem to be largely influenced by using different number of pseudo-components for the plus fraction. Compared to the simulation results available in the literature with volume corrected cubic EOS models [Pedersen et al. (2007a)] or the PC-SAFT EOS [Pedersen et al. (2007b)], the results presented in this work are quite promising.

This work provides valuable information for developing general characterization methods for the PC-SAFT EOS, i.e. (1) simple linear correlations could be used for model parameter m and the combination $m\varepsilon/k$; and (2) fitting the parameter σ to match SG could give an accurate description of density, and improve the prediction of saturation pressure further.

As seen in previous works [de Villiers (2011), Liang et al. (2012)], the PC-SAFT EOS has difficulties in describing the speed of sound in fluids, especially for those containing long-chain components. In this work, the similar deficiency of the PC-SAFT EOS has been seen in the description of isothermal compressibility. Both properties are directly linked to the derivative of pressure with respect to the total volume, when the density could be accurately modeled. Liquid-

liquid phase split has been predicted by PC-SAFT, but not by cubic EOS for some cases, at low temperature region, which needs to be further investigated.

Based on the feedback from one of the reviewers of the published article [Liang et al. (2014)] who stated that the pseudo-components in oils show near-ideal solution behavior, the methods CM5 (R) and CM7 are proposed for further use in modeling oil-water-chemical systems in the next chapter.

Chapter 4. Modeling oil-water-chemical systems

Compared to other applications, the PC-SAFT EOS has not been extensively applied to model petroleum fluids, which might be due to the complex and ill-defined nature of oils. It is a critical test for PC-SAFT to model the systems of oil plus water and/or chemicals, since sophisticated characterization methods and robust parameters are needed for oils and polar compounds.

The purpose of this work is to apply the PC-SAFT EOS into modeling oil-water-chemical systems, with the newly developed model parameters of polar compounds, interaction schemes from well-defined mixtures, and the characterization methods in the previous chapters.

4.1 Introduction

The complex phase behavior between petroleum fluids and polar compounds such as water, methanol and glycols has become more and more important as the offshore reservoirs represent one of the major growth areas of the oil and gas industry, which often mean extreme and complicated conditions, the use of hydrate inhibitors, etc. It is a reasonable approximation to deal with water and petroleum fluids as totally immiscible systems at low to moderate temperature and pressure conditions. However, the mutual solubility of petroleum fluid and water will considerably increases when chemicals are involved, the petroleum fluid is highly aromatic, or at high temperature and pressure regions. For instance, the addition of methanol or glycols into unprocessed well streams during subsea pipelines is necessary to inhibit gas hydrate formation, for which modeling the phase behavior of oil-water-chemicals is very important for the viewpoints of economical operation and environmental safety.

It is hard and often unreliable to use conventional cubic EOS, which have been standard models for the oil and gas industry for decades, for such complex systems containing petroleum fluids, water and/or chemicals, even with quite large binary interaction coefficients for water and hydrocarbons. The association models, explicitly accounting for hydrogen bonding interactions, show advantages over cubic EOS, especially for predictive calculations [Kontogeorgis et al. (2010a)]. In this chapter, the developments from the previous chapters will be applied to model the phase behavior of oil plus water and/or chemical systems.

4.2 Data

Seven petroleum fluids, two live oils and five dead oils, are studied in this work. The compositions of these fluids are listed in Table 4.1, and it can be seen that the fluid Light-1 is a quite heavy oil. The composition of N_2, CO_2 and hydrocarbons up to six carbon numbers in general are kept no change during the characterization procedure, and the model parameters of these components are taken from the original literature [Gross et al. (2001)], so the related information will not be duplicated in the characterization results hereafter.

Table 4.1 Composition of petroleum fluids

Comp.	Live Oil 1[*]	Live Oil 2[+]	Cond-1[#]	Cond-2[#]	Cond-3[#]	Light-1[#]	Light-2[#]
N2	0. 369	0.64	0.0	0.0	0.0	0.0	0.0
CO2	4.113	3.10	0.0	0.0	0.0	0.0	0.0
C1	69.242	72.733	0.0	0.0	0.0	0.04	0.0
C2	8.732	8.009	0.004	0.0	0.0	0.30	0.17
C3	4.27	4.26	0.0896	0.0	1.04	0.81	2.35
iC4	0.877	0.73	2.382	0.015	5.23	0.41	1.83
nC4	1.641	1.49	7.813	0.527	6.33	1.02	6.47
iC5	0.625	0.53	5.502	10.2	5.86	0.74	4.13
nC5	0.720	0.64	7.275	12.174	5.55	0.90	5.73
C6	0.972	0.81	10.292	14.289	13.98	1.92	8.41
C7	2.499	1.08	16.046	20.837	26.65	4.92	13.69
C8	0.732	1.20	16.632	18.433	21.81	6.21	14.27
C9	0.637	1.08	8.903	8.558	6.69	6.09	8.38
C10+	4.571	3.70	24.254	14.966	6.86	76.64	34.57

Data are from [*] Pedersen et al. (1996); [+] Pedersen et al. (2001); [#] Riaz M. (2011).

4.3 Results and Discussions

4.3.1 Live Oil 1 + Water

The characterization results of Live Oil 1 with the PC-SAFT EOS, using the two characterization methods CM5 (R) and CM7 are plotted in Figure 4.1. The detailed information, i.e. molar fraction, molecular weight and model parameters, of each pseudo-component are reported in Table B.1 (Appendix B).

It can be seen that these two methods produce considerably different parameters, i.e. CM5 (R) gives smaller segment number, larger segment size and larger dispersion energy, respectively, but similar trends are observed for all three parameters. The quantities ($m\sigma^3$) and ($m\varepsilon/k$) are reported in Figures 4.1 (c) and (e). These two characterization methods show quite similar values for the quantity ($m\sigma^3$),

and almost identical results for the quantity (mε/k). The later one is expected, since the same linear correlation $m\,\varepsilon/k = 6.8311 \times Mw + 124.42$ is used in both methods (see in Chapter 3), so it will not be reported for other cases hereafter. These similar trends lead to similar phase envelopes, as shown in Figure 4.2, from the qualitative point of view. CM7 presents a bit larger phase envelope than CM5 (R), as discussed in Chapter 3.

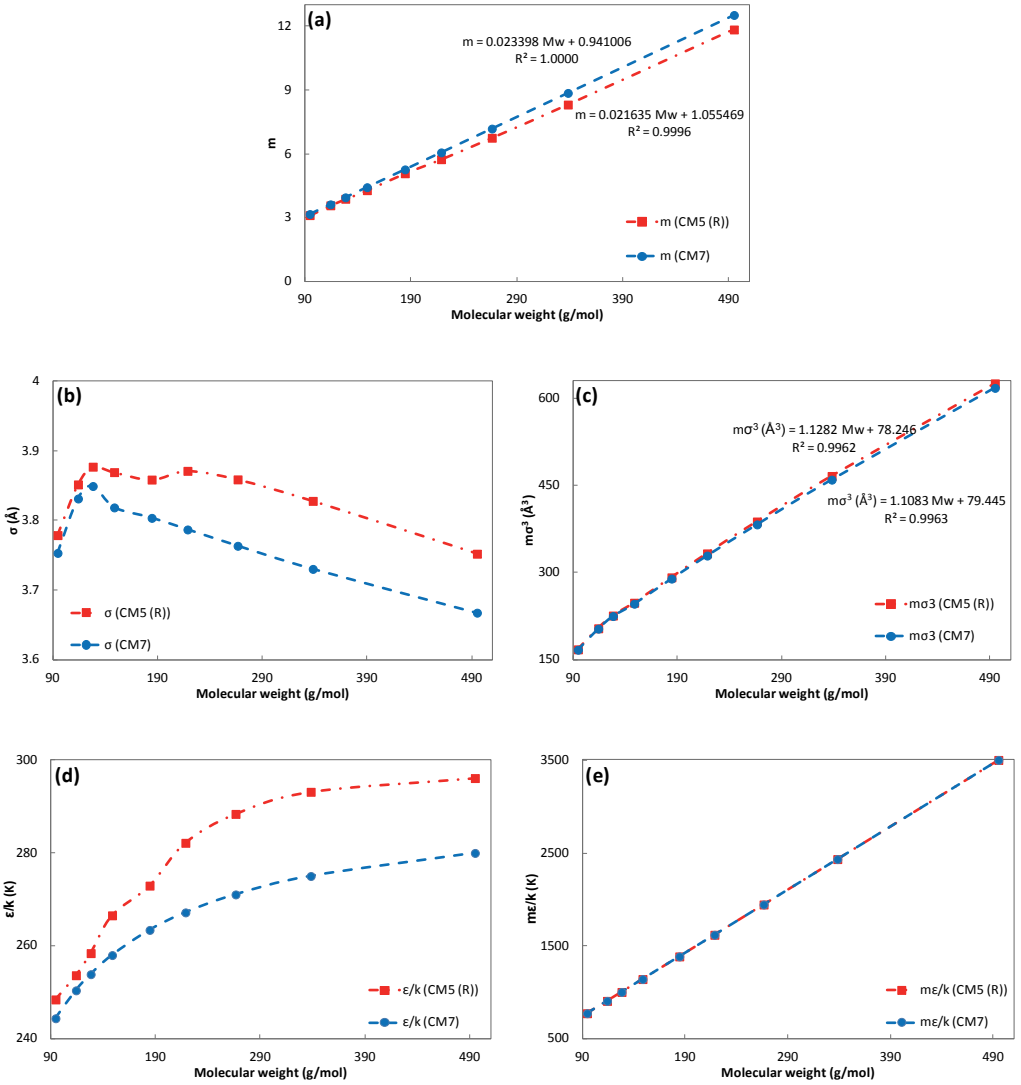

Figure 4.1 Characterized PC-SAFT parameters of pseudo-components for Live Oil 1. (a) Segment number (m), (b) segment size (σ), (c) quantity ($m\sigma^3$), (d) segment energy (ε/k), (e) quantity (mε/k).

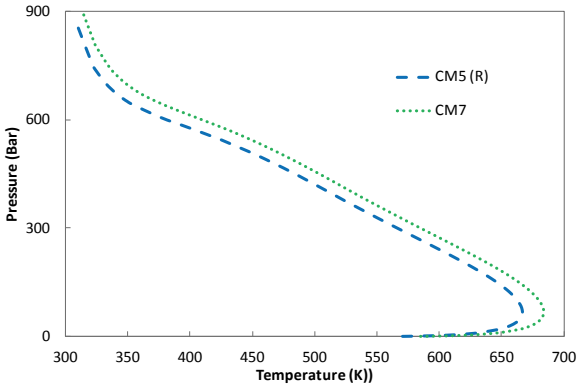

Figure 4.2 Phase envelopes of Live Oil 1 with PC-SAFT using characterization methods CM5 (R) and CM7

The modeling results with PC-SAFT are reported in Table 4.2. Two water parameter sets are used in the calculations. One is from Grenner et al. (2006), which is named as AG, and the other one is developed in Chapter 2, which is given the name XL. These two sets will be used throughout this chapter. The temperature dependent k_{ij} of methane-water are applied in both cases. The simple linear correlation of k_{ij} against molecular weight (carbon number) between pseudo-components and water is used for the AG parameters, and zero k_{ij} is used for the XL parameters. The details of these binary mixtures are available in Chapter 2.

As shown in Table 4.2, in general, this system could be satisfactorily modeled with both water parameter sets AG and XL, while the set XL performs better on predicting the mutual solubility of the Live Oil 1 and water, especially the solubility of hydrocarbons in the polar phase. The parameter set AG over-predicts the solubility of hydrocarbons in the polar phase at all conditions, while the XL set presents predictions cross the experimental points. Both parameter sets noticeably under-predict the solubility of water in organic phase at all conditions.

The method CM5 (R) predicts three liquid phases at 308.15K and 100MPa, as presented in Table 4.3. This is a non-physical prediction, though the phase fraction is quite small. It can be seen that the new small amount phase is rich in heavy ends. It could be anticipated that the three phase split might be due to the high dispersion energy produced by method CM5 (R) for these heavy pseudo-components, as seen from Figure 4.1 (d) and Table B.1.

Table 4.2 The experimental and calculated composition (×1000) of Live Oil 1 + Water

T (K)	P (MPa)	Char. Method	xC1			xHC			yH2O		
			Exp.	AG*	XL*	Exp.	AG	XL	Exp.	AG	XL
308.15	100	CM5 (R)	3.42	4.09	3.73	5.67	6.20	5.50	0.55	0.298	0.366
		CM7		4.09	3.73		6.18	5.49		0.300	0.370
393.15	100	CM5 (R)	4.31	4.49	4.22	6.28	6.73	6.26	7.53	5.05	5.51
		CM7		4.48	4.21		6.71	6.24		5.07	5.61
473.15	100	CM5 (R)	7.46	9.35	8.48	10.02	12.5	11.4	46.83	35.2	35.6
		CM7		9.32	8.46		12.4	11.3		35.4	36.2
473.15	70	CM5 (R)	6.01	7.85	7.25	8.19	10.5	9.72	57.25	45.1	46.6
		CM7		7.83	7.23		10.5	9.69		45.2	47.2
%AAD		CM5 (R)		20.0	11.3		17.3	8.91		31.2	25.7
		CM7		19.7	11.2		16.8	8.86		30.9	24.5

* AG denotes the results are calculated using the water parameters from Grenner et al. (2006), and XL is using the water parameters developed in Chapter 2.

Table 4.3 Phase equilibrium results of the Live Oil 1 + Water at 308.15K and 100MPa *

Comp.	feed	CM7		CM5 (R)		
		organic	polar	organic 1	organic 2	polar
phase fraction		4.03E-01	5.97E-01	2.00E-03	4.01E-01	5.97E-01
Composition						
H2O	5.93E-01	3.70E-04	9.95E-01	4.06E-04	3.66E-04	9.94E-01
N2	1.50E-03	3.70E-03	1.35E-05	1.80E-03	3.71E-03	1.36E-05
CO2	1.67E-02	3.91E-02	1.61E-03	3.60E-02	3.91E-02	1.63E-03
C1	2.82E-01	6.92E-01	3.73E-03	4.38E-01	6.94E-01	3.73E-03
C2	3.55E-02	8.78E-02	1.18E-04	7.82E-02	8.79E-02	1.18E-04
C3	1.74E-02	4.30E-02	1.38E-05	4.00E-02	4.30E-02	1.39E-05
iC4	3.57E-03	8.84E-03	3.96E-07	7.72E-03	8.85E-03	3.97E-07
nC4	6.67E-03	1.65E-02	1.23E-06	1.63E-02	1.65E-02	1.23E-06
iC5	2.54E-03	6.30E-03	7.81E-08	6.46E-03	6.30E-03	7.84E-08
nC5	2.93E-03	7.26E-03	1.06E-07	7.49E-03	7.25E-03	1.06E-07
nC6	3.95E-03	9.80E-03	3.62E-08	1.08E-02	9.79E-03	3.63E-08
P1	1.02E-02	2.52E-02	1.99E-07	3.52E-02	2.51E-02	2.00E-07
P2	2.98E-03	7.38E-03	5.13E-09	1.05E-02	7.36E-03	5.19E-09
P3	2.59E-03	6.42E-03	1.27E-09	9.76E-03	6.40E-03	1.30E-09
P4	6.35E-03	1.57E-02	1.50E-09	2.98E-02	1.57E-02	1.59E-09
P5	2.98E-03	7.38E-03	1.02E-10	1.88E-02	7.30E-03	1.11E-10
P6	3.16E-03	7.84E-03	2.02E-11	2.77E-02	7.71E-03	2.40E-11
P7	2.60E-03	6.45E-03	1.91E-12	3.55E-02	6.25E-03	2.43E-12
P8	2.17E-03	5.39E-03	8.46E-14	5.76E-02	5.02E-03	1.14E-13
P9	1.31E-03	3.25E-03	2.22E-16	1.32E-01	2.36E-03	2.59E-16

* The results presented here are calculated with the XL water parameters, and the same three liquid phase split is obtained with the AG water parameters.

In general the two characterization methods present very close modeling results, especially for the solubility of hydrocarbons in the aqueous phase. As compared in Figure 4.3, there are, however, systematic differences between these two methods – CM7 predicts the solubility of petroleum fluid in polar phase smaller and the solubility of water in organic phase larger, respectively, than CM5 (R). They have larger impacts on the solubility of water in the organic phase than on the solubility of petroleum fluid in the polar phase, and on the XL parameter set than on the AG one, with 1.0% larger on average.

The following quantity is used for comparison of these two characterization methods through this chapter:

$$(CM5\ (R)\ -\ CM7)/CM7 = (x_1 - x_2)/x_2 \times 100\% \qquad (4.1)$$

where, x_1 and x_2 are the solubilities from characterization method CM5 (R) or CM7, respectively.

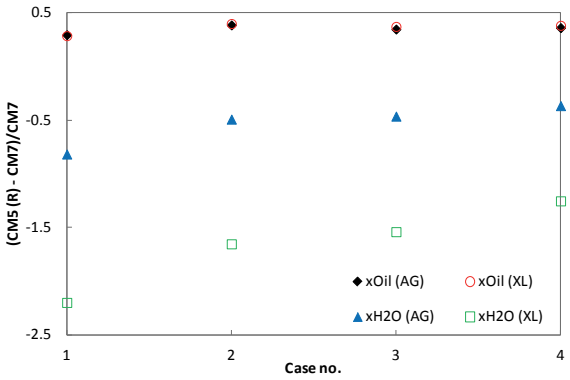

Figure 4.3 Comparisons of the two characterization methods on the solubilities with both AG and XL water parameter sets (see explanation in content or Table 4.2). The quantity *(CM5 (R) – CM7)/CM7* is defined in equation (4.1).

4.3.2 Live Oil 2 + Water + Methanol

The characterization results of Live Oil 2 are plotted in Figure 4.4, and the detailed results can be found in Table B.2. In this case, the parameters from the two characterization methods are closer to each other, if compared to those of Live Oil 1, but the trends of individual segment energy and segment size parameters are not as similar as what seen in Live Oil 1. The segment number and quantity ($m\sigma^3$) are following quite similar trends, and the quantity ($m\varepsilon/k$) of course has the same function of molecular weight.

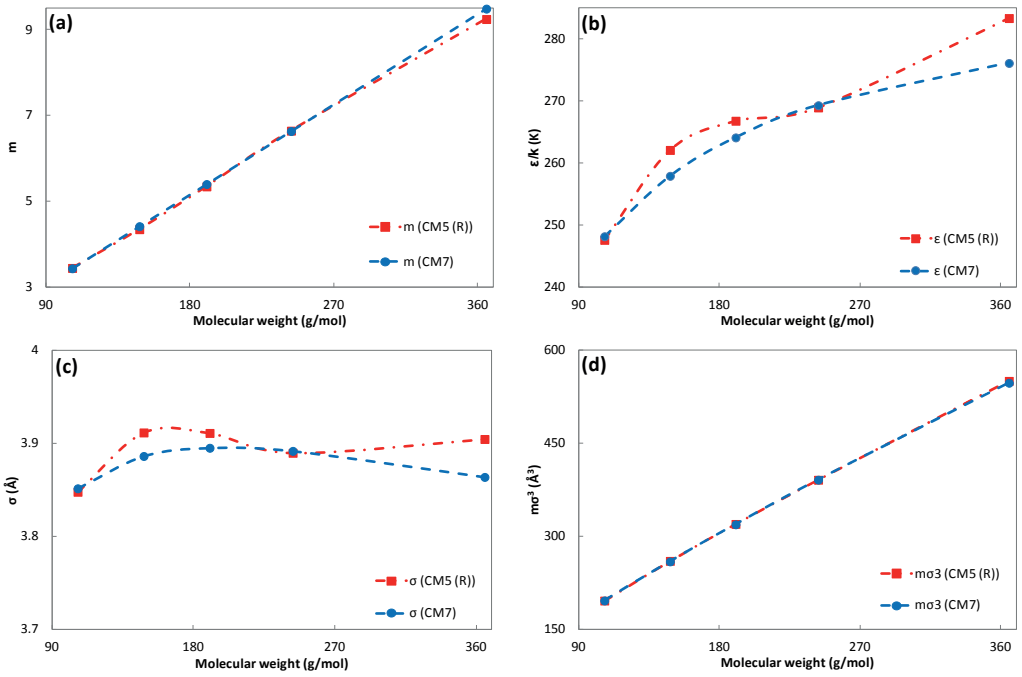

Figure 4.4 Characterized PC-SAFT parameters of pseudo-components for Live Oil 2. (a) Segment number (m), (b) segment energy (ε/k), (c) segment size (σ), (d) quantity ($m\sigma^3$).

The modeling results are presented in Table 4.4. The CPA modeling results are taken from Yan et al. (2009). The calculations with PC-SAFT are performed by applying two parameter combinations. One combination is the water parameter set AG and the methanol parameters from Gross and Sadowski (2002), so the combination is named as AG-GS. The other combination is the parameters of both components from this work, named as XL-XL. The temperature independent k_{ij} of methane-methanol and water-methanol are used for both parameter combinations as discussed in Chapter 2, and the same interaction strategy of normal hydrocarbon-water k_{ij} is adopted here. Almost the same results are obtained for the two characterization methods.

It can be seen that the experimental solubility data are only available for methanol in the vapor and organic liquid phases. CPA predicts closer results, especially for the solubility of methanol in the organic phase. As shown in Table 4.4, some amounts of water are predicted from both CPA and PC-SAFT in the two phases, and as discussed in Chapter 2, water will be presented in the vapor phase in the methane-water binary, and in the organic phase in the normal hydrocarbon-water binaries. Therefore the deviations of the results with PC-SAFT from those with CPA are calculated,

along with the %AADs of methanol composition from experimental data at two temperatures. The parameter combination XL-XL gives closer prediction to those from CPA and the parameter combination AG-GS for all the composition except the water content in the vapor phase. It can be seen that the CPA and PC-SAFT with the approach XL-XL give almost the same prediction of the solubility of petroleum fluid in the polar phase.

Table 4.4 The experimental and calculated composition (×1000) of Live Oil 2 + Water + Methanol[*]

Type	Solubility at (276.75K and 60.3Bar)				%RD to CPA	
	Exp.	CPA	AG-GS[+]	XL-XL	AG-GS	XL-XL
yH2O	0	0.152	0.164 (0.164)	0.166 (0.166)	7.89	9.21
yMEOH	0.429	0.452	0.382 (0.382)	0.414 (0.414)	-15.5	-8.63
xH2O	0	0.163	0.132 (0.132)	0.184 (0.185)	-19.0	13.5
xMEOH	2.01	1.83	0.708 (0.710)	1.041 (1.042)	-61.2	-43.2
xOil	0	6.02	6.511 (6.510)	6.025 (6.025)	8.14	0.00
Solubility at (280.85K and 149.9Bar)						
yH2O	0	0.140	0.142 (0.142)	0.166 (0.166)	1.43	18.6
yMEOH	0.687	0.638	0.430 (0.430)	0.515 (0.515)	-32.6	-19.3
xH2O	0	0.204	0.163 (0.163)	0.226 (0.226)	-20.1	10. 8
xMEOH	1.88	1.99	0.814 (0.815)	1.174 (1.176)	-58.8	-40.7
xOil	0	8.76	9.065 (9.064)	8.596 (8.596)	3.42	1.83
%AAD[#]		6.82	42.4	28.5	22.8	16.6

[*] The values in parentheses are calculated using characterization method CM7, and the deviations are made only for the characterization methods CM7.

[+] AG-GS denotes the parameter combination of water parameters from Grenner et al. (2006) and methanol parameters from Gross and Sadowski (2002). XL-XL means both are from this project.

[#] The %AAD is calculated for two temperatures.

4.3.3 Dead Oils + MEG

The detailed characterization results of the five dead oils are given in Table B.3. The typical results for petroleum fluids Cond-1, Light-1 and Light-2 are plotted in Figures 4.5-4.7. The results of Cond-2 and Cond-3 are very similar to those of Cond-1, from the qualitative point of view. There is an obvious turning-point for segment energy parameter from the characterization method CM5 (R) for all the fluids, while is not true for those from the method CM7. This is because the method CM5 (R) uses the PNA analysis, estimated by molecular weight and specific gravity of the pseudo-components, to combine the model parameters m and $m\varepsilon/k$ from three hydrocarbon series, and the method CM7 uses linear correlations for m and $m\varepsilon/k$. A very similar turning-point is also observed

for the segment size parameter from the method CM5 (R). The turning-point in these two parameters indicates that they are to some extent coupling with each other, especially the quantity ($m\sigma^3$) shows quite similar values from the two characterization methods, as seen from the two live oils above.

The modeling results of the mutual solubility of petroleum fluids and MEG with PC-SAFT, using the characterization method CM7, are plotted in Figure 4.8, and the detailed results with the two characterization methods can be found in Appendix B.4. The %AAD results with PC-SAFT and CPA are presented in Table 4.5. The CPA modeling results are taken from Riaz et al. (2011a, 2011b, 2014), and Frost et al. (2013). Two MEG parameter sets are applied for PC-SAFT. One is from Tsivintzelis and Grenner (2008), which is named as AG as well. The other one from this thesis is named as XL. Linear correlations of k_{ij} between pseudo-components and MEG against molecular weight, developed in Chapter 2, with 0.0 as the truncation are used for the both MEG parameter sets.

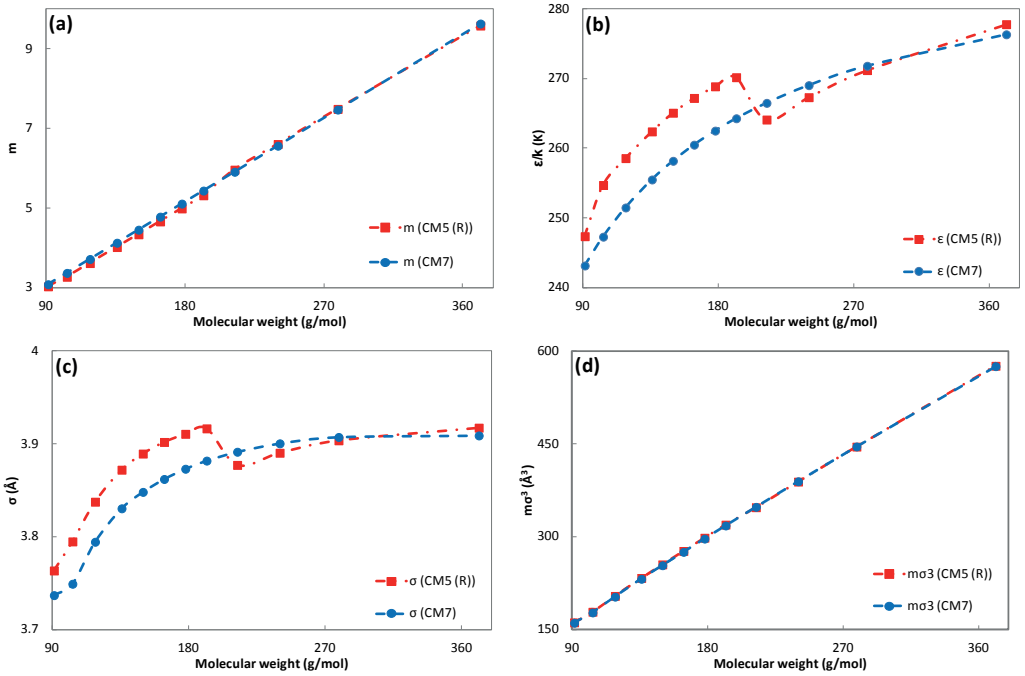

Figure 4.5 Characterized PC-SAFT parameters of pseudo-components for petroleum fluid Cond-1. (a) Segment number (m), (b) segment energy (ε/k), (c) segment size (σ), (d) quantity ($m\sigma^3$).

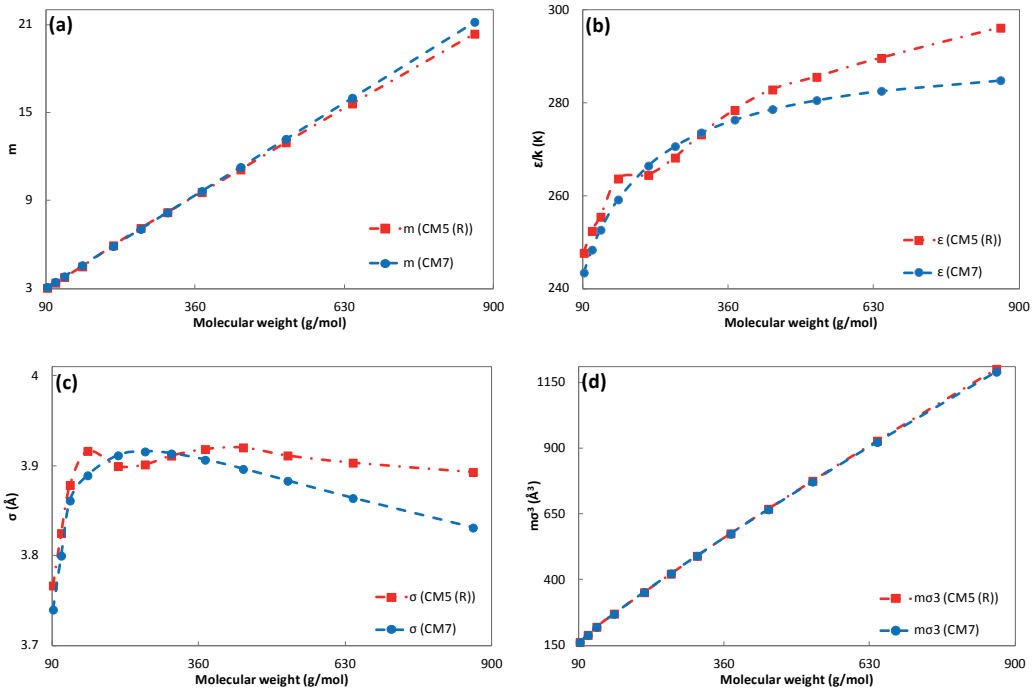

Figure 4.6 Characterized PC-SAFT parameters of pseudo-components for petroleum fluid Light-1. (a) Segment number (m), (b) segment energy (ε/k), (c) segment size (σ), (d) quantity ($m\sigma^3$).

In general, both CPA and PC-SAFT could reasonably model the petroleum fluid + MEG systems, except for the petroleum fluid Light-1, for which the models significantly under-predict the solubility of MEG in the organic phase. It can be seen from Table 4.5 that in general the CPA predicts the solubility of the petroleum fluids in the polar phase better, but PC-SAFT wins the other side, i.e. the solubility of MEG in the organic phase.

Though the parameter set XL correlates the LLE of MEG and normal hydrocarbons better as discussed in Chapter 2, the two parameter sets give similar prediction of the solubility of the petroleum fluids in the MEG rich phase, as seen from Figure 4.8 (a) and Table 4.5. The parameter set XL presents smaller overall deviation for the prediction of the solubility of MEG in the organic phase, as presented in Table 4.5. As shown in Figure 4.8 (b), however, the performance largely depends on the type of petroleum fluids. In general, the results from Table 4.5 reveal that the parameter set XL performs better for the condensate gas, while the MEG parameter set AG gives better predictions for oils on the solubility of MEG in organic phases. This might be because the

parameter set AG always predicts higher solubility of MEG in the organic phase than those from the parameter set XL, as seen in Figure 4.8.

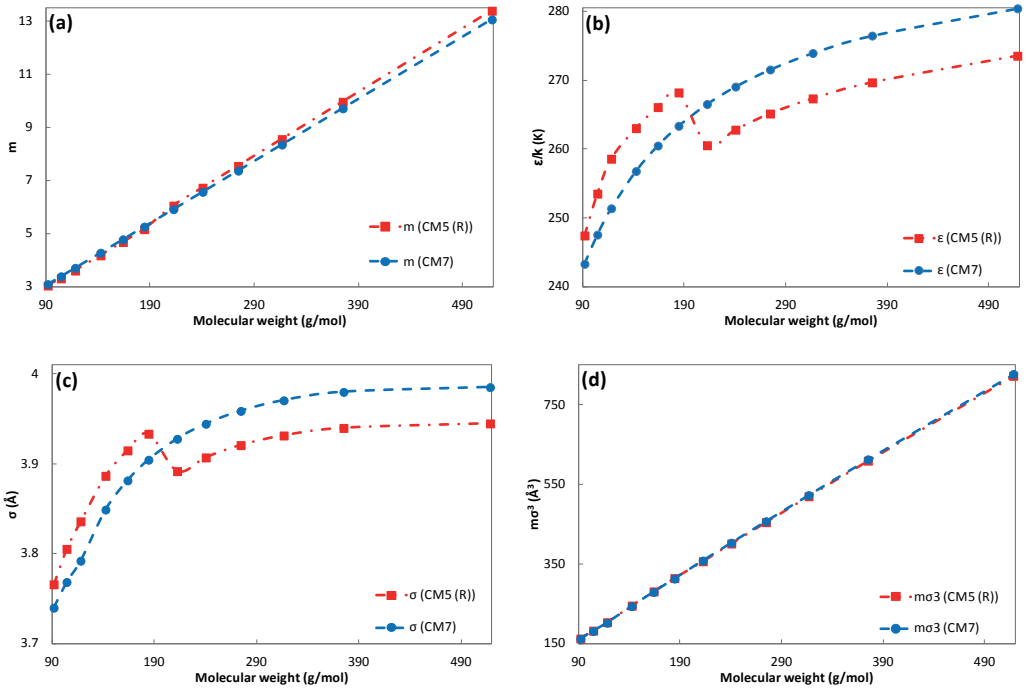

Figure 4.7 Characterized PC-SAFT parameters of pseudo-components for petroleum fluid Light-2. (a) Segment number (m), (b) segment energy (ε/k), (c) segment size (σ), (d) quantity ($m\sigma^3$).

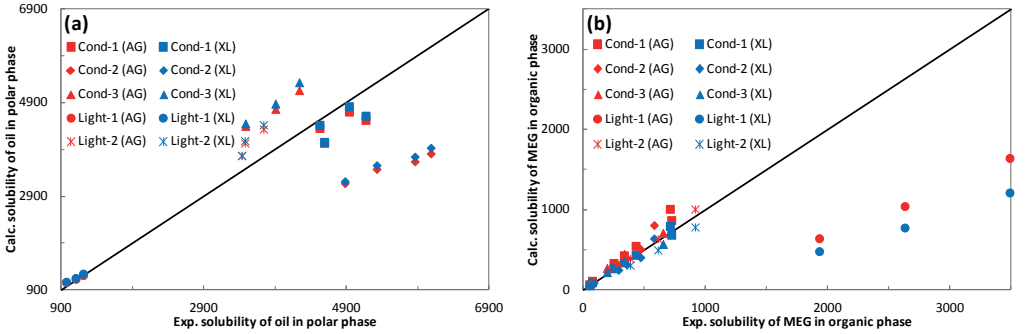

Figure 4.8 Modeling results of the mutual solubility of petroleum fluids and MEG with PC-SAFT using the two characterization methods. The experimental data are taken from Riaz et al. (2011a, 2011b, 2014), and Frost et al. (2013). The detailed modeling results can be found in Appendix B.4.

Table 4.5 %AADs for the mutual solubility of petroleum fluids and MEG from different models*

Fluid	Oil fluids in polar phase			MEG in organic phase		
	CPA	AG +	XL +	CPA	AG	XL
Cond-1	11.0	7.12 (8.18)	5.77 (6.66)	12.0	33.9 (33.6)	8.57 (8.47)
Cond-2	17.0	35.5 (36.2)	34.6 (34.6)	None	18.6 (18.5)	8.99 (8.99)
Cond-3	None	24.9 (23.4)	27.4 (26.2)	None	27.2 (26.7)	11.0 (10.9)
LightOil-1	1.00	5.77 (4.13)	7.42 (5.95)	82.0	60.3 (60.0)	70.5 (70.3)
LightOil-2	13.0	14.6 (13.9)	15.8 (15.3)	21.0	5.02 (5.13)	17.8 (17.7)
avg. %AAD	10.3	17.6 (17.2)	18.2 (17.7)	36.7	29.0 (28.8)	23.4 (23.3)

* Values in parentheses are from CM7.

+ AG denotes that the PC-SAFT parameters of MEG from are Tsivintzelis and Grenner (2008), and XL means that the parameters are from this thesis.

As seen from Table 4.5 and Appendix B.4, the two characterization methods present similar overall modeling results, especially for the solubility of MEG in the organic phase. The similar systematic differences, as seen from the case Live Oil 1 + Water, are observed in this case for the solubility of petroleum fluid in polar phase – CM7 predicts smaller solubility than CM5 (R). They have slightly larger impacts on the AG parameter set than on the XL one for this solubility. There seem no systematic differences for the solubility of MEG in the organic phase, but the impacts on it are smaller than on the solubility of petroleum fluid in the polar phase from the two characterization methods. Largest impacts are seen for Light-1. These results are demonstrated in Figure 4.9.

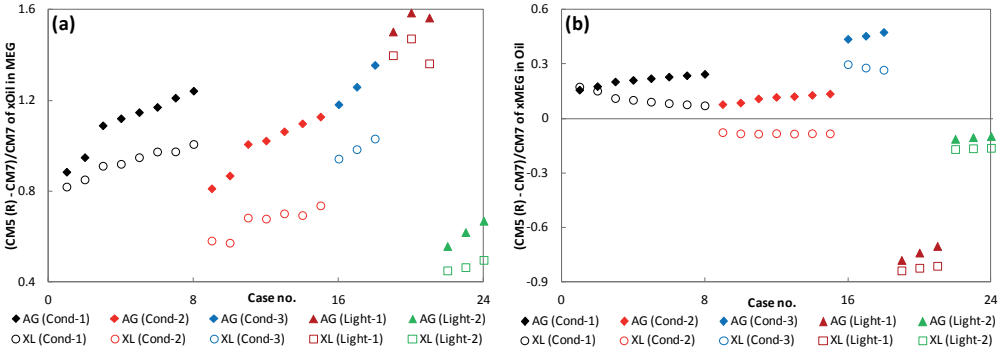

Figure 4.9 Comparisons of the two characterization methods on the solubilities from both AG and XL MEG parameter sets. The quantity *(CM5 (R) – CM7)/CM7* is defined in equation (4.1). The x-axis 'Case no.' can be found in Table Appendix B.4, which is corresponding to the conditions of each petroleum fluid.

4.3.4 Dead Oils + Water + MEG

The modeling results of petroleum fluid + water + MEG systems with the PC-SAFT EOS, using the characterization method CM7, are presented in Figure 4.10, and the detailed results with the two characterization methods are given in Table Appendix B.5. The calculations with the PC-SAFT EOS are performed with two options of the parameters: (1) the parameters of water and MEG are from Grenner et al. (2006) and Tsivintzelis and Grenner (2008), which option is denoted as AG; and (2) the parameters of both compounds are from this project, which option is denoted as XL.

The %AADs for the modeling results from CPA and PC-SAFT are compared in Table 4.6. The CPA modeling results are taken from Riaz et al. (2011a, 2011b, 2014), and Frost et al. (2013). The percentage relative deviations (%RD) are reported for each case, and the calculations of PC-SAFT are using the characterization method CM7. The %AADs for all the conditions are presented at the end of the table, for which the results from both characterization methods are reported.

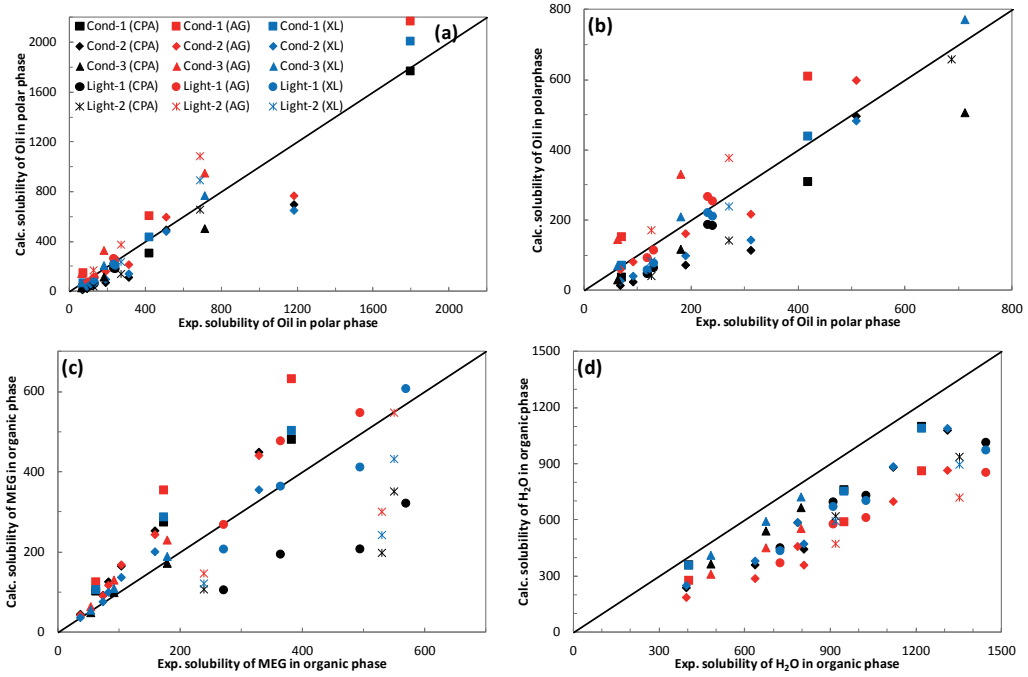

Figure 4.10 Modeling results of the solubility of petroleum fluids, MEG and water from CPA and PC-SAFT with the characterization method CM7. Figure (b) is rescaled from Figure (a), and the legend is the same in all four figures. The experimental data are taken from Riaz et al. (2011a, 2011b, 2014), and Frost et al. (2013). The detailed modeling results can be found in Appendix B.5.

Table 4.6 Deviations of the solubility of petroleum fluids, MEG and water from different models

Case no.	T (K)	Oil in polar phase			MEG in organic phase			H_2O in organic phase		
		CPA*	AG#	XL#	CPA	AG	XL	CPA	AG	XL
					Cond-1					
1	323.15	-43	123	5	70	108	76	-10	-29	-10
2	323.15	-26	47	6	61	107	68	-19	-37	-20
3	323.15	-1	21	12	27	66	32	-10	-30	-10
					Cond-2					
4	303.15	-78	-10	-59	27	21	4	-45	-55	-41
5	303.15	-61	-14	-47	27	27	6	-43	-54	-40
6	303.15	-2	18	-5	61	64	34	-39	-52	-36
7	323.15	-72	-10	-54	55	44	23	-17	-34	-17
8	323.15	-63	-30	-54	61	55	28	-21	-37	-21
9	323.15	-41	-35	-45	37	35	9	-25	-41	-25
					Cond-3					
10	313.15	-29	34	9	-3	30	7	-23	-35	-14
11	313.15	-35	84	17	10	44	21	-19	-33	-12
12	313.15	-50	135	15	-6	22	6	-16	-30	-9
					LightOil-1					
13	313.15	-18	17	-3	-58	11	-16	-37	-48	-39
14	313.15	-58	-19	-49	-61	0	-23	-23	-36	-26
15	323.15	-22	7	-11	-43	43	7	-28	-40	-31
16	323.15	-49	-10	-39	-46	32	1	-29	-41	-32
					LightOil-2					
17	323.15	-4	59	30	-36	0	-21	-32	-48	-35
18	323.15	-47	40	-11	-62	-43	-54	-30	-47	-34
19	323.15	-66	38	-33	-54	-37	-48	-34	-49	-37
%AAD (CM7)		40.3	39.5	26.5	42.4	41.5	25.5	26.3	40.9	25.7
%AAD (CM5 (R))			40.0	26.3		41.6	25.5		41.5	26.5

* The CPA results are from Riaz et al. (2011a, 2011b, 2014) and Frost et al. (2013). The k_{ij} of MEG and HC are 0.0 and 0.4 for Cond-2 and Cond-3, respectively, and it is 0.02 for other cases.

AG uses the PC-SAFT parameters of water and MEG from Grenner et al. (2006) and Tsivintzelis and Grenner (2008). XL uses the parameters of both components from this project.

The prediction of the mutual solubility of petroleum fluids and polar compounds, i.e. water and MEG, highly depend on the types of petroleum fluids and the conditions, as seen from Figure 4.10, Tables 4.6 and Appendix B.5. As shown in Table 4.6, PC-SAFT with the parameter option XL presents generally the best overall predictions. It predicts the solubility of petroleum fluids in the polar phase and the solubility of MEG in the organic phase better than both CPA and PC-SAFT with the parameter option AG. The parameter option XL gives quite similar prediction of the water solubility to CPA, and much better prediction than the parameter option AG for all the cases. It is interesting to see that the prediction of the solubility of MEG in the organic phase for Light-1 is

quite reasonable, where the models have difficulties in predicting this solubility in the systems of Light-1 + MEG, as discussed above.

It is worth noticing that both CPA and PC-SAFT under-predict the solubility of water in the organic phase. This is because the water parameters are obtained by taking account the LLE data of water with non-aromatic hydrocarbons into the estimation procedure. Very recently, it has been shown internally the prediction from CPA could be improved by using different binary interaction parameter approach, but it is not true for PC-SAFT if good prediction of the solubility of petroleum fluid in the polar phase needs to be kept. This is because, as discussed in Chapter 3, the solubility lines of hydrocarbons and water always go the same direction by tuning the interaction parameter. As a feasible solution, the prediction is anticipated to be improved for heavy oils by taking the aromatic compounds into accounts explicitly, for which the solvation interactions will bring more water into the organic phase. The solubility of water in normal hexane, cyclo-hexane and benzene are presented in Figure 4.11, which shows that the solubility of water in benzene is much higher than those in non-aromatic hydrocarbons, especially at low temperature ranges.

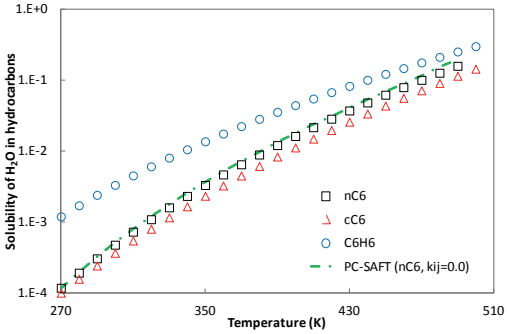

Figure 4.11 Comparison the solubility of water in different hydrocarbons. The dash-dot line is the prediction from PC-SAFT for water-nC6 binary system.

The two characterization methods present very similar modeling results, especially for the solubility of the petroleum fluids in the polar phase and the MEG solubility in the organic phase, as seen from Table Appendix B.5. The method CM7 presents slightly better results than CM5 on the water solubility in the organic phase. The similar systematic differences, as seen from previous cases, appear in this case as well – CM7 predicts the solubility of petroleum fluid in polar phase smaller and the solubility of water in organic phase larger, respectively, than CM5 (R). These results are demonstrated in Figure 4.12. It shows that the impacts, respectively, are largest for the water

solubility and smallest for the MEG solubility. In this case, the differences of the impacts on the water solubility between these two water parameters are not as large as what have been seen in the case Live Oil 1 + Water. The two characterization methods show larger impacts on the solubility of petroleum fluids in the polar phase for this case than for the case Live Oil 1 + Water.

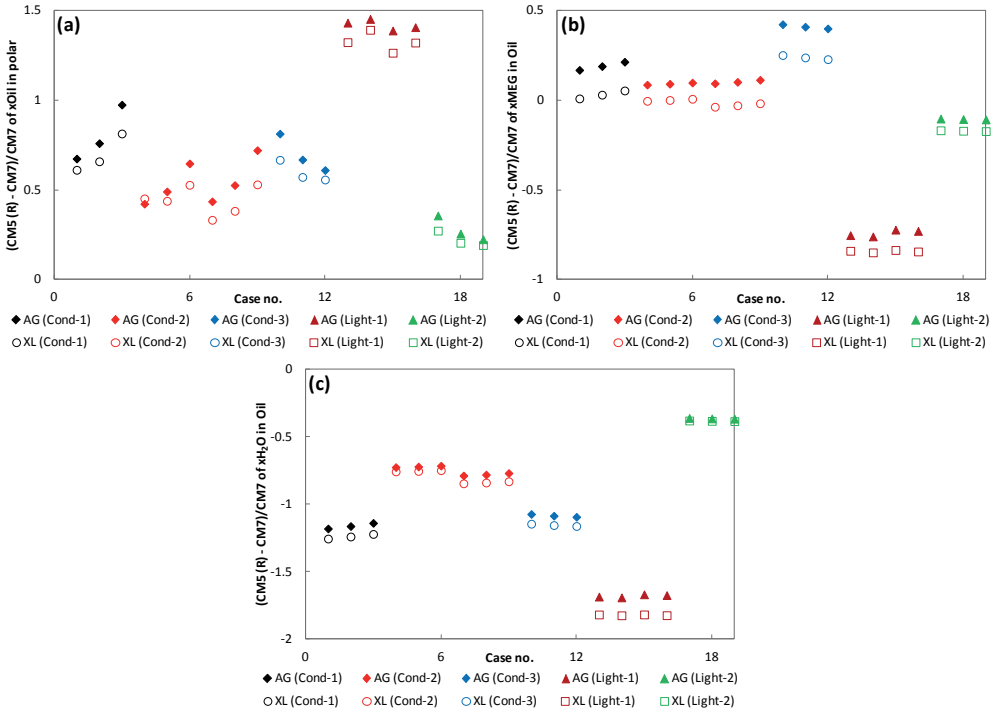

Figure 4.12 Comparisons of the two characterization methods on the solubilities from both AG and XL parameter combinations. The quantity *(CM5 (R) – CM7)/CM7* is defined in equation (4.1). The x-axis 'Case no.' can be found in Table Appendix B.5, which is corresponding to the conditions of each petroleum fluid.

4.4 Conclusions

In this work, the PC-SAFT EOS with the newly developed parameters of water, methanol and MEG, and the general petroleum fluid characterization methods is applied to model the phase behavior of oil plus water and/or chemical systems. The modeling results for most systems are satisfactory. The PC-SAFT EOS with the newly developed water and MEG parameters give quite promising prediction on the mutual solubility of the oil-water-MEG systems, compared to those from CPA and PC-SAFT with other literature available parameters. The results also show that the current PC-

SAFT parameters under-predict the water solubility in the organic phase, which suggest that the explicit inclusion of the aromatic compounds might improve the modeling results by introducing the solvation interactions.

The two characterization methods CM5 (R) and CM 7, developed in the Chapter 3, on one hand, produce quite different PC-SAFT model parameters (segment number, segment size and segment energy) of pseudo-components for individual cases. On the other hand, they show quite similar trends for the segment number and the quantity ($m\sigma^3$) against molecular weight. In the meantime, the same linear equation is used for the quantity ($m\varepsilon/k$) in both characterization methods. These similar or same trends lead to quite similar overall modeling results for almost all of the considered systems in this work, but systematic differences are observed between these two characterization methods. CM7 predicts the solubility of petroleum fluid in the polar phase smaller and the solubility of water in the organic phase larger, respectively, than CM5 (R). It is also found that both these two characterization methods have, respectively, largest and smallest impacts for the water solubility and for the MEG solubility. These systematic differences lead the method CM7 to give slightly better overall predictions, but these differences are much smaller than experimental uncertainties. So the modeling of the mutual solubility of oil plus water and/or chemicals would still not be the excellent criterion to select the characterization methods from the quantitative point of view. It is worth pointing out that, however, these two characterization methods predict different phase splits at some specific conditions. For instance, non-physical liquid-liquid-liquid phase equilibrium is predicted by CM5 (R) for the case Live Oil 1 + Water at low temperature. The characterization method CM7 might be recommended as the default method, but other alternative approaches for model parameters are possible, especially for segment size, which will be the future work due to the time limitation.

Chapter 5. Data and correlations of speed of sound

Volumetric properties and phase equilibria data are commonly used to tune the thermodynamic models. It is preferable, however, to include the derivative properties into the parameter fitting procedures, if the model is going to be extended to calculate derivative properties, e.g. speed of sound, as in this project.

The purpose of this work is (1) to review and analyze the speed of sound data of hydrocarbons, alcohols and their mixtures including petroleum fluids; (2) to review correlations for the speed of sound data, and develop general correlations for speed of sound in pure hydrocarbons and 1-alcohol.

5.1 Introduction

Speed of sound is a thermo-physical property that can be accurately determined in wide temperature and pressure ranges. The usage of ultrasound has been moving from the exploratory stage to systematic applications in various fields, such as fundamental researches on intermolecular interactions, and online monitor of industrial processes. In oil industry, acoustic measurements are helpful on obtaining phase behavior and physical properties of reservoir fluids, e.g. estimating the density of downhole reservoir fluids, and on in-situ measurement or characterization of the heterogeneous or homogenous mixtures in reservoirs [Meng et al. (2005, 2006), Goodwin (2003), Machefer et al. (2007), Durackova (1995)]. Specifically SONAR (Sound Navigation and Ranging) uses sound propagation to navigate, communicate with or detect objects on or under the surface of the water, and it can even provide some measurements of the echo characteristics of the "targets" [Automatic Leak Detection Sonar (2012)].

As discussed in Chapter 1, within the framework of general thermodynamic rules, on one hand, speed of sound is related with other thermodynamic properties such as density, isobaric and isochoric heat capacities, and isothermal compressibility. Moreover, speed of sound measurements have found wide acceptance as a satisfactory and relatively simple method to obtain thermodynamic data of liquids, since it is possible to derive equations of state for liquids from these experimental results. As the direct determination of properties such as density and heat capacity can be quite difficult at elevated pressures, some people claim that it is more reliable to calculate these properties

from the speed of sound data by combining direct measurements of density and heat capacity at atmospheric pressure. Moreover, speed of sound is a valuable property for developing thermodynamic model as a supplement property or a discriminating reference quantity, since it can be measured to a high degree of accuracy, even in high pressure regions.

5.2 Data

The following sections will be organized based on pure fluids, binary mixtures, ternary mixtures, and oil or gas mixtures.

5.2.1 Pure fluids

5.2.1.1 Normal hydrocarbons

Hydrocarbons are the primary constituents of reservoir fluids, and are commonly categorized as paraffins, naphthenes and aromatics. They range from the lightest components, which at normal conditions are gases, such as methane and ethane, to extremely heavy components, for instance asphaltenes or bituminous residues [Pedersen et al. (2007a)].

Normal hydrocarbons are very important constituents in crude oils, and extensive speed of sound measurements have been done, especially for the short chain ones. Comprehensive data reviews can be found in the works of Khasanshin et al. (2001), Oakley et al. (2003) and Padilla-Victoria et al. (2013). The speed of sound database for pure hydrocarbons from this work is given in Appendix C (Table C.1). Detailed reviews will not be duplicated anymore, but more efforts will be put to show that the high degree of accuracy of speed of sound measurements, the impacts of temperature, pressure and chain length on speed of sound, and the performance of NIST [REFPROP (2010)] reference equations of state for speed of sound in short chain n-alkanes.

Methane (C1) is probably the most important single compound in the oil and gas mixtures. The speed of sound in gaseous and liquid methane had been extensively measured in wide temperature and pressure ranges since 1960s because of the petroleum industry development [van Itterbeek et al. (1967), Straty (1974), Gammon et al. (1976), Baidakov et al. (1982), Kortbeek et al. (1990)]. The speed of sound in saturated liquid methane and compressed liquid methane are shown in Figure 5.1. On one hand, it is shown that the speed of sound measurements are highly reproduced among different groups, indicating the high degree of experimental accuracy. On the other hand, the NIST reference equation of state [REFPROP (2010)] represents the speed of sound in C1 very well.

Normal hexane (nC6) is another extensively studied hydrocarbon, an important constituent of fuel, and a widely in-use solvent. Many groups conducted speed of sound measurements for n-hexane [Boelhouwer (1967), Daridon et al. (1998), Ball et al. (2001), Khasanshin et al. (2001), Plantier et al. (2003/2004)]. It can be seen from Figure 5.2 (a) that high reproducibility is again shown for the speed of sound in liquid n-hexane, but the NIST [REFPROP (2010)] reference equation of state does not seems to perform as well as for methane. The speed of sound in n-nonane is supplemented in Figure 5.2 (b) to show that the accuracy of NIST [REFPROP (2010)] reference equations of state are compound dependent rather than a systematic error along with chain length. The speed of sound in both n-hexane and n-nonane show similarly smooth functionalities of temperature and pressure.

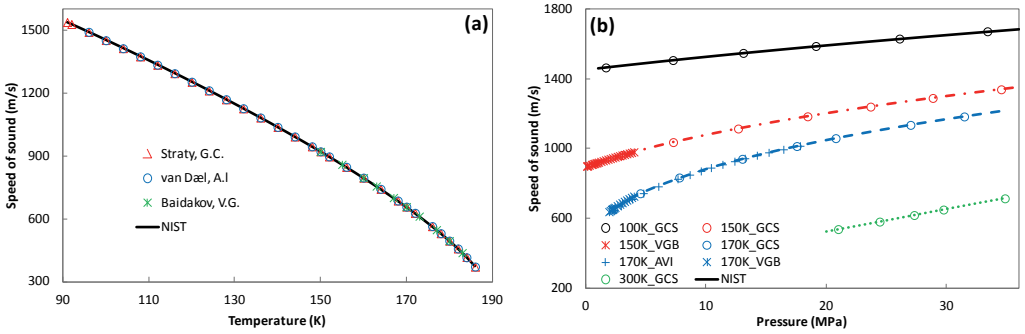

Figure 5.1 (a) The speed of sound in saturated methane. Data are taken from van Itterbeek et al. (1967), Straty (1974), and Baidakov et al. (1982), respectively. (b) The speed of sound in condensed liquid methane. Data are taken from Straty (1974). Lines are data from NIST [REFPROP (2010)].

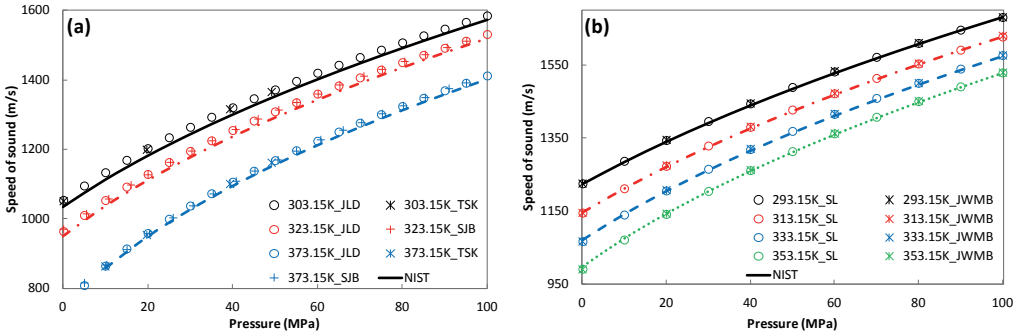

Figure 5.2 (a) The speed of sound in liquid nC6. Data are taken from Daridon et al. (1998a), Khasanshin et al. (2001), and Ball et al. (2001). (b) The speed of sound in liquid nC9. Data are taken from Boelhouwer (1967) and Lago et al. (2006). Lines are data from NIST [REFPROP (2010)].

Khasanshin et al. (2001, 2002, 2003, 2009) made many speed of sound measurements for n-alkanes, shorter than n-hexadecane. During the same period, Daridon et al. (2000, 2002) and Dutour et al. (2000, 2001a, 2001b, 2002) systematically measured the speed of sound in n-alkanes up to n-hexatriacontane. The pressure dependence of the speed of sound in n-dodecane, n-octadecane, n-tetracosane and n-hexatriacontane at 373.15K is plotted in Figure 5.3. It can be seen that the speed of sound in n-alkanes increase as the chains get longer, and show qualitatively similar functions of pressure, which makes it possible to use a generalized expression to correlate the speed of sound as a function of chain length [Khasanshin et al. (2000, 2001), Padilla-Victoria et al. (2013)].

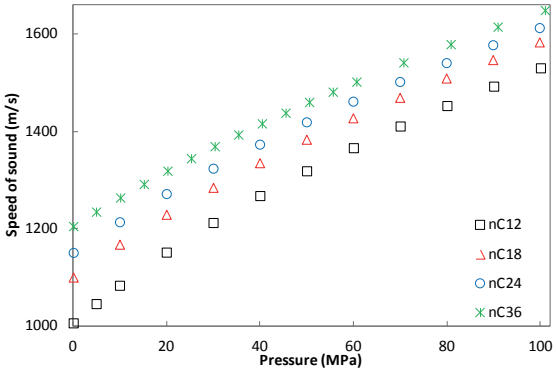

Figure 5.3 The speed of sound in liquid nC12, nC18, nC24 and nC36 at 373.15K. Data are taken from Khasanshin et al. (2003) and Dutour et al. (2000, 2001b, 2002).

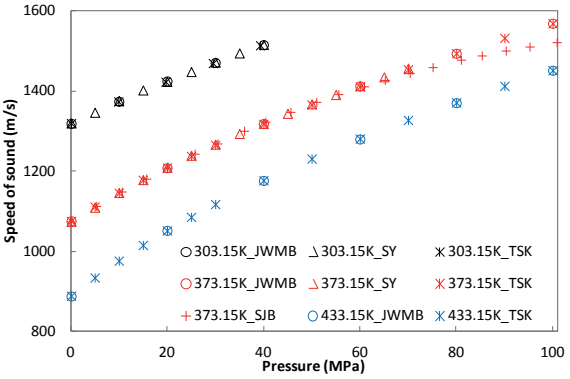

Figure 5.4 The speed of sound in liquid nC16. Data are taken from Boelhouwer (1967), Ye et al. (1990), Ball et al. (2001), and Khasanshin et al. (2001).

The speed of sound measurements have high degree of accuracies, which can be seen from high reproducibility of the experimental results from different groups. It is, however, not always true. Figure 5.4 presents that the speed of sound in n-hexadecane at 373.15K measured by Ball et al. (2001) deviate from other three sets [Boelhouwer (1967), Khasanshin et al. (2001, 2009)] under elevated pressures, which suggest that careful selections or evaluations of experimental data should be undertaken when more than one data sets are available.

5.2.1.2 Cyclohexane, Benzene and Toluene

Cyclohexane, benzene and toluene are common constituents of petroleum fluids. Cyclohexane and toluene are important solvents, while benzene is one of the most elementary petrochemicals.

Sun et al. (1987) measured the speed of sound in cyclohexane in the temperature range from 283.15 to 323.06 K and pressure range up to 85 MPa. Takagi et al. (2002) reported the speed of sound in cyclohexane at temperatures between 283.15K and 333.15K and pressures up to 20 MPa. The speed of sound in cyclohexane at three temperatures is plotted in Figure 5.5 (a) together with the data calculated from NIST [REFPROP (2010)] reference equation of state. It shows again that the NIST [REFPROP (2010)] reference equation of state does not perform very well for cyclohexane from the qualitative point of view, especially for those above room temperature.

Bobik (1978) measured the speed of sound in benzene at temperatures between 283K and 463 K and pressures from the coexistence region up to 62 MPa. Takagi et al. (1984, 1987, 2004c) reported the speed of sound in benzene in temperature ranges 283.15-333.15K and pressure ranges 0.1-170MPa in three works. Sun et al. (1987) also reported the speed of sound in benzene in temperature range from 283.143 to 323.125 K and pressure up to 170 MPa in the same work in which they published the data for cyclohexane. In Figure 5.5 (b), it can be seen that the experimental data from different groups are consistent to each other, and NIST [REFPROP (2010)] reference equation of state gives perfect description of the speed of sound in benzene.

Hawley et al. (1970) reported the speed of sound in nine liquids, in which the data of toluene were measured at temperatures 303 to 348 K and pressures between 0.1 to 522 MPa. Takagi et al. (1984) measured the speed of sound in toluene at temperatures 293.15K, 298.15K and 303.15K and in the pressure range from 0.1 to 160 MPa. Muringer et al. (1985) measured the speed of sound in toluene up to 263.5 MPa and at temperatures from 173.18 to 320.3 K. Comprehensive speed of sound measurements in toluene were carried out very recently by Meier et al. (2013) at the temperatures

between 240 and 420 K with the pressure range from 0.1 to 100 MPa, in which they summarized the reference of experimental works on speed of sound measurements for toluene. Figure 5.5 (c) shows the data from different groups and NIST [REFPROP (2010)] reference equation of state.

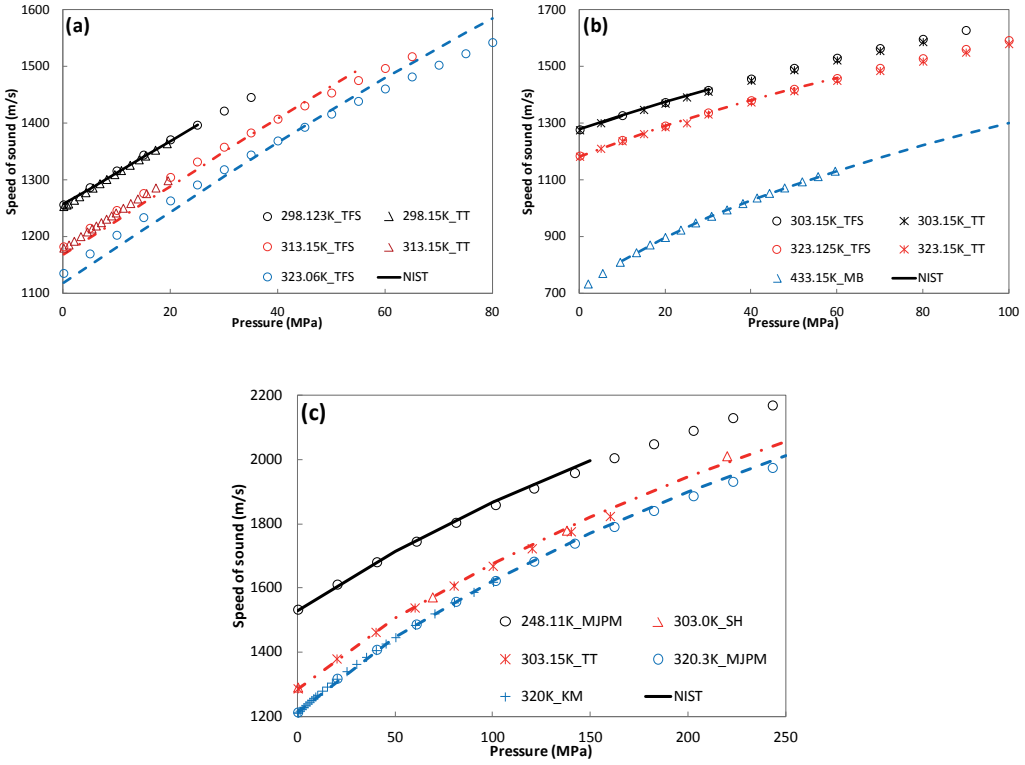

Figure 5.5 (a) The speed of sound in cyclo-C6. Data are taken from Sun et al. (1987) and Takagi et al. (2002). (b) The speed of sound in benzene. Data are taken from Sun et al. (1987), Bobik (1978), and Takagi et al. (1987). (c) The speed of sound in toluene. Data are taken from Takagi et al. (1984), Hawley et al. (1970), Muringer et al. (1985), and Meier et al. (2013). Lines are data from NIST [REFPROP (2010)].

5.2.1.3 1-Alcohols

1-Alcohols are important biologically and industrially amphiphilic additives in the oil production and petrochemical industries [Abida et al. (2003), Dubey et al. (2008c)]. They are also very good candidates to investigate the association phenomena.

There were some systematic investigations on acoustic properties of monatomic saturated alcohols. Wilson et al. (1964) measured the speed of sound in four primary alcohols, i.e. methanol, ethanol, 1-propanol and 1-butanol, at temperatures from 273.15 to 323.15 K and pressures up to 96.5 MPa. Sun et al. (1988, 1991) measured the speed of sound in methanol and ethanol, respectively, at temperatures from 274.74 to 332.95 K and from 193.4 to 263.05 K up to 280 MPa. Khasanshin et al. (1992) proposed a correlation expression for the speed of sound in the series of normal alcohols from C_4 to the higher homologs in the region of liquid state within temperatures range 303-405K and pressures below 100 MPa. The speed of sound in methanol, 1-butanol and 1-octanol was reported in the temperature range from 303.15 to 373.15 K and pressure range up to 50 MPa by Plantier et al. (2002b), which data was used to determine the nonlinear acoustic parameter. In their systematic work of thermodynamics properties of organic liquids using the acoustic methods, Dzida et al. (2000, 2007, 2009a, 2013) reported the speed of sound data for 1-propanol, 1-pentanol to 1-decanol in the temperature range from 293 to 318 K and pressures up to above 100 MPa.

The speed of sound in 1-alkanols, from methanol to 1-decanol, at 313.15K are presented in Figure 5.6 (a). It can be seen that a similar trend is obtained as the speed of sound in n-alkanes. The speed of sound, on one hand, shows a simple and smooth function of temperature and pressure, and on the other hand, the slower the speed of sound increases as the chains get longer. Figure 5.6 (b) shows that the NIST [REFPROP (2010)] reference equation of state represents the speed of sound in methanol with a perfect accuracy.

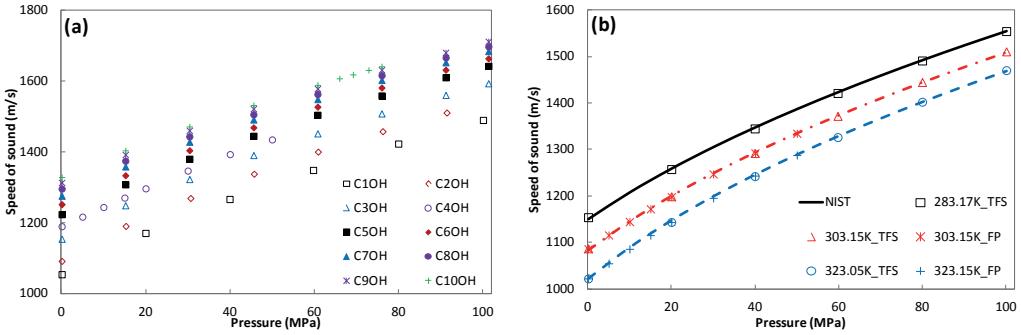

Figure 5.6 (a) The speed of sound in 1-alkanols at 313.15K. Data are taken from Sun et al. (1988), Marczak et al. (2000), Plantier et al. (2002b), Dzida et al. (2005, 2007, 2009a, 2013); (b) The speed of sound in methanol. Data are taken from Sun et al. (1988), and Plantier et al. (2002b). Lines are data from NIST [REFPROP (2010)].

5.2.2 Binary systems

The investigation on physical and transport properties of binary mixtures are of considerable interest to fundamental researches and industrial applications. On one hand, the experimental excess properties (deviations from ideal mixing) provides information about intermolecular interactions, e.g. packing efficiencies taking place when mixing the pure compounds into a solution, effects of temperature and pressure, and changes with respect to composition. The phase behavior information, on the other hand, can be used to validate the predictive capabilities of thermodynamic models or adjust the binary interaction parameters for engineering applications [Dubey et al. (2008a, 2008c), Dzida et al. (2008)].

There is no ideal mixing concept for speed of sound, but in order to analyze the limit of the speed of sound in mixtures, the following equation is used for representing the ideal limit (ideal mixing):

$$u^{id} = \sum_{i=1}^{n} x_i u_i \tag{5.1}$$

where x and u are the molar fraction of and speed of sound in the pure compound i. In the meantime, the concepts of positive and negative deviations from this ideal limit will be introduced for binary and ternary mixtures.

5.2.2.1 Hydrocarbon + hydrocarbon

Thermodynamic and acoustic properties of binary hydrocarbons mixtures are very important to petroleum industries. Meanwhile binary mixtures of hydrocarbons, especially alkanes, are very important systems to investigate the impacts of temperature and pressure on the thermodynamic properties through the effects of short-range interactions, such as dispersion force, chain length and mixing behaviors of asymmetric molecules, from a theoretical point of view.

A summary of temperature range, pressure range and references of the experimental speed of sound data in binary hydrocarbons mixtures, available in our data base, is given in Appendix C, Table C.2. The impacts of temperature, pressure and molecular asymmetry on speed of sound will be investigated through the discussions of speed of sound for some typical systems.

Figure 5.7 presents the speed of sound in two gaseous binary systems dominated by methane at three temperatures [Lagourette et al. (1994)]. It can be seen that the speed of sound curves at low

pressure regions are intersecting each other or having a minimum against pressure, which is because the gaseous mixtures are moving from a vapor-like state to a liquid-like state. This behavior might introduce difficulties in correlating speed of sound as a function of pressure by a universal form.

Figure 5.8 presents the speed of sound in binary series of n-hexane with moderate (n-heptane) to long chain (n-hexadecane) normal alkanes at 298.15 K and atmospheric pressure [Tourino et al. (2004), Bolotnikov et al. (2005)]. The speed of sound in these systems show positive deviations from ideal limit, and as expected, the deviations increase as the asymmetry of the corresponding pure compounds become larger.

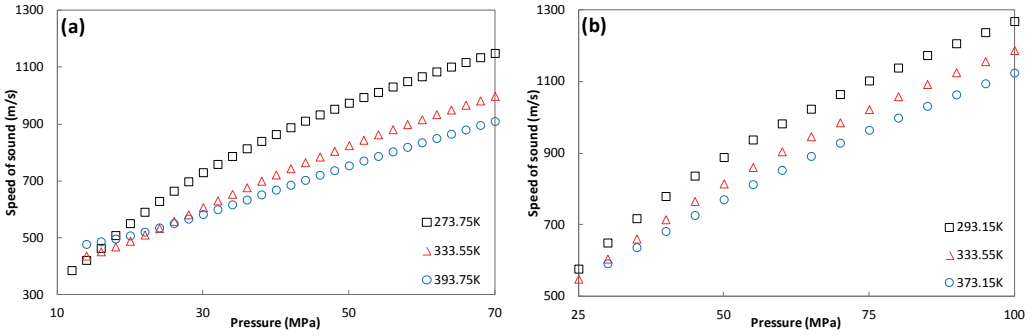

Figure 5.7 The speed of sound in gaseous binary systems of (a) {0.8998 methane + 0.1002 propane} and (b) {0.98 methane + 0.02 nC8}. Data are taken from Lagourette et al. (1994).

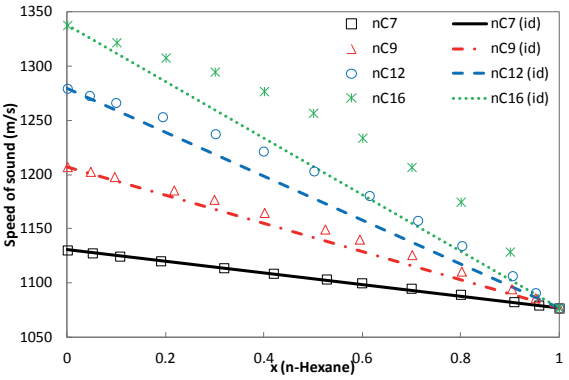

Figure 5.8 The speed of sound in binary systems of n-hexane + n-heptane, n-nonane, n-dodecane or n-hexadecane at 298.15K and atmospheric pressure. Data are taken from Tourino et al. (2004) and Bolotnikov et al. (2005). Lines are from equation (5.1).

In order to investigate the impacts of temperature, pressure and compound asymmetry on deviation from ideal limit, three speed of sound data sets are presented in Figure 5.9 for each binary system, (a) methane + n-hexadecane at 298.15K [Ye et al. (1992b)], (b) n-hexane + n-hexadecane at 323.15K [Ye et al. (1992b)], (c) n-hexane + n-hexadecane at 10 MPa [Ye et al. (1992b)], and (d) n-heptane + n-dodecane at 298.15K [Dzida et al. (2008)]. It can be known from these figures that asymmetry plays a better important role than temperature and pressure on deviations from ideal limit, which are positive and become smaller as temperature and/or pressure increase. The ideal limit gives satisfactory description of the speed of sound in the binary mixture of n-hexane and n-hexadecane at high temperature and pressure, as shown in Figure 5.9 (b) and (c). It performs very well for the speed of sound in the binary mixture of n-heptane and n-dodecane, as seen from Figure 5.9 (d). These results tell us that, for such kinds of binary systems, good prediction results can be obtained if correlations of speed of sound in the corresponding pure fluids are available.

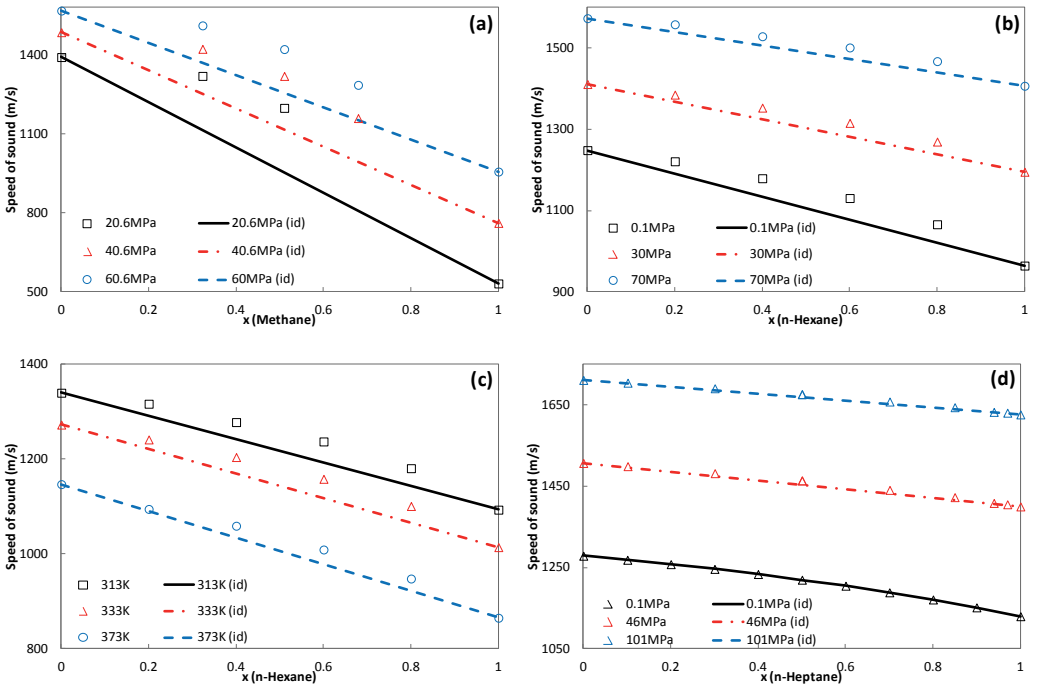

Figure 5.9 The speed of sound in binary systems (a) methane + n-hexadecane at 313.25K; (b) n-hexane + n-hexadecane at 323.15K; (c) n-hexane + n-hexadecane at 10MPa; (d) n-heptane + n-dodecane at 298.15K. Data are taken from Ye et al. (1992b), Bolotnikov et al. (2005) and Dzida et al. (2008). Lines are from equation (5.1).

Figure 5.10 (a) presents the speed of sound in binary mixtures of n-hexane + cyclohexane at 303.15K [Oswal et al. (2002)] and n-hexane or cyclohexane + benzene or toluene at 313.15K [Calvar (2009a, 2009b)]. All measurements are made at atmospheric pressure. The speed of sound in these binary systems shows negative deviations from the ideal limit. The negative deviations in the binary mixture of n-hexane and cyclohexane are smaller than those in the systems with benzene or toluene, which compounds have similar performance on the systems when they are mixing with n-alkanes or cyclohexane. The speed of sound in binary series of benzene with n-hexane to n-nonane is shown in Figure 5.10 (b), which indicates that the deviations from ideal limit become more negative when the normal alkane gets heavier.

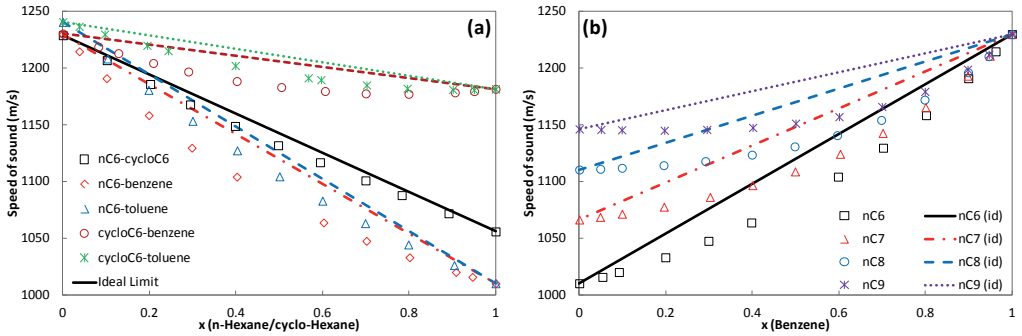

Figure 5.10 (a) The speed of sound in binary systems of n-hexane + cyclohexane at 303.15K and n-hexane or cyclohexane + benzene or toluene at 313.15K and atmospheric pressure. Data are taken from Oswal et al. (2002) and Calvar et al. (2009a, 2009b). (b) The speed of sound in binary systems of benzene + n-hexane, n-heptane, n-octane and n-nonane at 313.15K and atmospheric pressure. Data are taken from Calvar et al. (2009b). Lines are from equation (5.1).

5.2.2.2 Hydrocarbon + 1-alcohol

Systematic studies have been made extensively on binary mixtures of 1-alkanols with hydrocarbons, especially with alkanes. This is mainly because binary mixtures of alcohols and alkanes, as pointed by many researchers [Nath (1998b), Dubey et al. (2008c, 2008d), Dzida (2009b)], are convenient model systems for studying association phenomena, solvation and nonspecific physical interactions, which are essential for developing and testing of advanced general theoretical models, such as SAFT models [Chapman et al. (1988, 1990), Jackson et al. (1988)], considering intermediate range forces, e.g. hydrogen bonding, in an explicit way.

During their systematic investigations on the volumetric properties of binary mixtures of 1-alkanol + n-alkane, Benson and co-workers [Kiyohara et al. (1979), Benson et al. (1981), Handa et al. (1981)] measured the speed of sound in binary mixtures of methanol to 1-hexanol, 1-octanol and 1-decanol with n-heptane, in binary mixtures of 1-hexanol with n-pentane, n-hexane, n-octane and n-decane, and in binary mixtures of 1-decanol with n-pentane, n-hexane, n-octane, n-decane and n-hexadecane, over the whole molar composition range at 298.15K and atmospheric pressure. In their measurements, special attention was paid to the high dilute regions with respect to 1-alkanols.

In their systematic studies on thermodynamics of alcohol + alkane binary mixtures by measuring scarcely available physical and transport properties, such as dielectric constants, refractive indices and viscosities, Sastry et al. (1996a, 1996b) reported the speed of sound in binary mixtures of 1-propanol or 1-butanol + n-heptane at 298.15K and 308.15K, and 1-heptanol + n-hexane or n-heptane at 303.15K and 313.15K, all at atmospheric pressure.

During the continuous work series of the program on thermodynamic properties and phase behavior of binary and ternary nonelectrolyte systems related to homogeneous and heterogeneous extractive distillation, Orge et al. (1995, 1999) reported the speed of sound, as a function of mole fraction, in binary mixtures of (benzene or cyclo-hexane) with 1-pentanol at 298.15K, (methanol, ethanol or 1-propanol) with (n-pentane, n-hexane, n-heptane or n-octane) at 298.15K, and (methanol or ethanol) with (hexane, heptane or octane) at temperatures from 303.15 to 318.15 K. All are at atmospheric pressure. Recently, new speed of sound data in binary mixtures of ethanol with (n-hexane, n-heptane, n-octane or n-nonane) at temperatures from 288.15 to 323.15K over the whole composition range was reported by Gaycol et al. (2007), with co-authors of the works presented above.

Oswal et al. (1998) measured the speed of sound in ten binary mixtures of ethanol to 1-decanol, and 1-dodecanol with cyclo-hexane over the whole composition range at temperature 303.15K and atmospheric pressure.

To study intermolecular interactions predominated by hydrogen bonding, chain length and temperature dependence of excess thermodynamic properties, Nath (1997, 1998a, 2000, 2002a, 2002b) carried out systematic measurements on the speed of sound in binary mixtures of (1-butanol, 1-hexanol, 1-heptanol and 1-octanol) with (n-pentane to n-octane) at temperature range from 288.15 to 303.15K and atmospheric pressure.

The speed of sound in binary mixtures of 1-pentanol and n-nonane was reported at temperature from 293.15 to 313.15K over the whole composition range by Gepert et al. (2003)

Recently, along with density and viscosity, speed of sound in binary mixtures (1-butanol, 1-hexanol, 1-octanol or 1-decanol) with (n-hexane, n-octane or n-decane), and (1-butanol or 1-octanol) with (n-hexadecane or squalane) were measured at temperatures 298.15K, 303.15K and 308.15K and atmospheric pressure in the series of work by Dubey et al. (2008a-f). They adopted the Redlich–Kister type mathematical formula to correlate the excess properties, and used the Prigogine-Flory-Patterson (PFP) theory to analyze excess volume and to estimate the speed of sound and the isentropic compressibilities in these systems.

Experimental speed of sound data of 1-alkanol and alkanes binary mixtures at high pressures is rather scarce. To fill this gap and to provide a way to calculate properties such as density and heat capacity at high pressures, Dzida et al. (2003, 2005, 2009b) measured the speed of sound in binary systems of (ethanol, 1-propanol and 1-decanol) with n-heptane at the temperatures from 293 to 318K and pressures up to over 90MPa. These experimental results provide valuable information to study both the temperature and pressure dependence of excess properties and to test theoretical models [Dzida et al. (2003)].

The speed of sound in binary mixtures of, respectively, methanol + n-hexane at 298.15K, 308.15K and 318.15K at atmospheric pressure, and 1-propanol + n-heptane at 298.15K at 0.1MPa, 46MPa and 101MPa pressures are presented in Figure 5.11. It could be seen that these systems show negative deviations from ideal limit, and temperature and pressure do not show significant impacts.

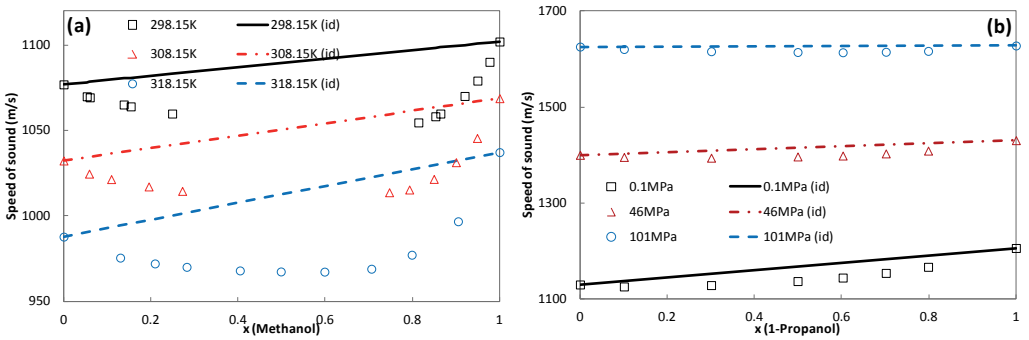

Figure 5.11 The speed of sound in binary system of (a) methanol + n-hexane at 298.15K, 308.15K and 318.15K and atmospheric pressure; (b) 1-propanol + n-heptane at 298.15K under 0.1MPa, 46MPa and 101MPa pressures. Data are taken from Orge et al. (1997, 1999) and Dzida et al. (2003). Lines are from equation (5.1).

The speed of sound in binary systems of, respectively, 1-butanol + (n-hexane, n-decane, n-hexadecane or squalane) at 298.15K, n-heptane + (ethanol, 1-propanol, 1-heptanol or 1-decanol) at 293.15K, and cyclo-hexane + (ethanol, 1-propanol, 1-heptanol or 1-dodecanol) at 303.15K is presented in Figures 5.12 (a), (b) and (c), all at atmospheric pressure. These figures all show that the deviations of the speed of sound in 1-alkanol + hydrocarbon binary systems change from negative to positive as the chain differences become larger. Figure 5.12 (d) presents the speed of sound in binary systems of 1-pentanol with benzene or cyclo-hexane at 298.15K and atmospheric pressure, which shows similar negative deviations.

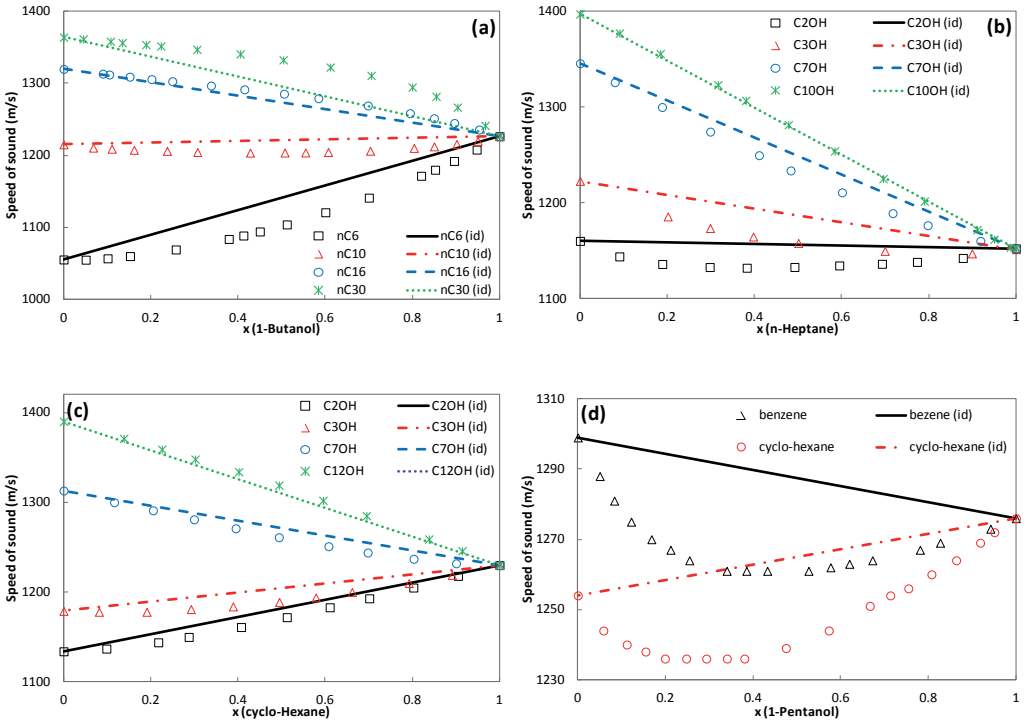

Figure 5.12 The speed of sound in binary systems of (a) 1-butanol + n-hexane, n-decane, n-hexadecane or squalane at 298.15K; (b) n-heptane + ethanol, 1-propanol, 1-heptanol or 1-decanol at 293.15K; (c) cyclo-hexane + ethanol, 1-propanol, 1-heptanol or 1-dodecanol at 303.15K. All are at atmospheric pressure. Data are taken from Dubey et al. (2008b, 2008c). (d) The speed of sound in binary systems of 1-pentanol and benzene or cyclo-hexane at 298.15K and atmospheric pressure. Data are taken from Orge et al. (1995). Lines are from equation (5.1).

5.2.2.3 1-Alcohol + 1-Alcohol

The speed of sound measurements in binary mixtures containing only 1-alkanols are scarce, at least not as extensive as other mixtures presented above. Gepert et al. (2003, 2006) reported the speed of sound in binary mixtures of 1-pentanol with 1-octanol at temperature from 293K to 313K, binary mixtures of 1-propanol with 1-hexanol, 1-pentanol with 1-nonanol, and 1-pentanol with 1-decanol at 298.15K, all over whole composition range, which are shown in Figure 5.13.

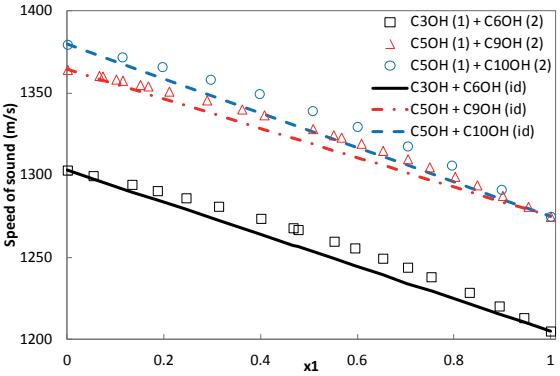

Figure 5.13 The speed of sound in the binary 1-alcohols. Data are taken from Gepert et al. (2006).

5.2.3 Multicomponent systems

5.2.3.1 Ternary mixtures

It is a common and economically attractive practice to add a new compound in azeotropic mixture separations. To study the capability of using 1-pentanol as such a candidate for benzene and cyclohexane mixture, Orge et al. (1995) measured different properties, including speed of sound, for this ternary system at 298.15K over wide composition ranges.

To explore molecular interactions in ternary liquid mixtures using empirical, semi-empirical and statistical theories, Rai et al. (1989) measured the speed of sound in ternary mixtures of (n-pentane + n-hexane + benzene), (n-hexane + cyclohexane + benzene), and (cyclohexane + n-heptane + toluene) at 298.15 K and atmospheric pressure. Later, Pandey et al. (1999) adopted these theories to predict the speed of sound in ternary mixtures of (toluene + n-heptane + n-hexane), (cyelohexane + n-heptane + n-hexane) and (n-hexane + n-heptane + n-deeane), which were compared with their experimental results.

In order to possess experimental information covering the temperature and pressure conditions encountered at all stages in petroleum production, Daridon, Lagourette and their co-workers carried out systematic acoustic measurements for synthetic mixtures in wide temperature and pressure ranges. They measured the speed of sound in ternary mixtures of (0.88methane + 0.10propane + 0.02n-octane) at the temperatures from 293.15 to 373.15K and pressures from 25 to 100MPa [Lagourette et al. (1995)]. They also measured the speed of sound in ternary mixtures of (carbon dioxide + methane + n-hexadecane) in the temperature range 313.15 to 393.15K and pressure up to 70MPa for three composition {0.12, 0.10, 0.78}, {0.10, 0.46, 0.44} and {0.44, 0.11, 0.45} [Daridon et al. (1996a)]. Later, they reported the speed of sound in four synthetic systems which were representative of distillation cuts with high bubble points in even wider temperature and pressure ranges. The speed of sound data, together with the density data at atmospheric pressure, were used to calculate densities and isentropic and isothermal compressibilities under evaluated pressures. [Daridon et al. (1998b, 1999)]

It is not easy to show the deviations from ideal limit in a two-dimension figure for a ternary system, so the average relative deviations of some typical systems are calculated and reported in Appendix C (Table C.3). It can be seen that the ideal limit can describe well for systems consisting of similar compounds, such as n-hexane, n-heptane and cyclo-hexane, but it gives unsatisfactory results for some other systems depending on the composition, temperature and pressure.

Figure 5.14 shows the speed of sound in ternary systems of methane + propane + n-octane with fixed composition {0.88, 0.10 and 0.02} as a function of pressure, which shows similar behaviors in the low pressure region as those in binary mixtures predominated by methane in Figure 5.7.

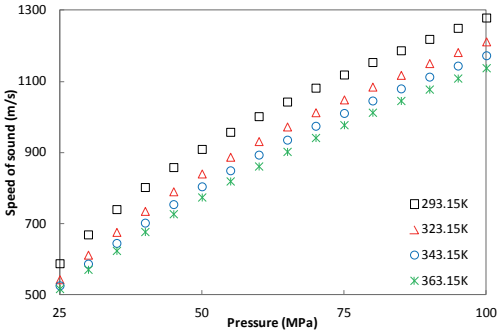

Figure 5.14 The speed of sound in a ternary mixture {0.88 methane + 0.10 propane + 0.02 n-octane} as a function of pressure at 293.15K, 323.15K, 343.15K and 363.15K. Data are taken from Lagourette et al. (1995).

5.2.3.2 Oils and gases

To fill the void of experimental data of acoustic properties in crude oils, Wang et al. (1990) measured the speed of sound in three light oils, two refined oils, five heavy oils and one live oil, covering a wide API gravity range from 5 to 62 degrees, in wide temperature and pressure ranges. They made correlations between speed of sound, temperature, pressure and API gravity, so empirical equations were available to calculate the speed of sound in oils with known API gravities.

To meet the challenges from the increasing number of hyperbaric oil reservoirs, Daridon and co-workers [Labes et al. (1994), Daridon et al. (1996b, 1998c), Barreau et al. (1997), Lagourette et al. (1999), Plantier et al. (2008)] made systematic studies on the thermodynamic properties and fluid behaviors of reservoir fluids by speed of sound measurements in the wide ranges of temperature, pressure and petroleum fluid types. They conducted a series of systematic acoustic measurements on pure, binary, ternary and other synthetic hydrocarbons mixtures, as discussed above, and also they measured the speed of sound in reservoir fluids from condensate gases to heavy oils. The composition, temperature and pressure information of the speed of sound measurements in oils, available in our data base, is summarized in Appendix C (Table C.4).

Figure 5.15 (a) presents the speed of sound in one condensate gas, one hyperbaric oil and one heavy oil as a function of pressure at 313.15K, which shows that the speed of sound in heavy oil are higher, but they show a similar trend versus pressure from the qualitative point of view. Figure 5.15 (b) presents the speed of sound in two extremely heavy oils, which show very close values above room temperature, but they get diverged at low temperatures.

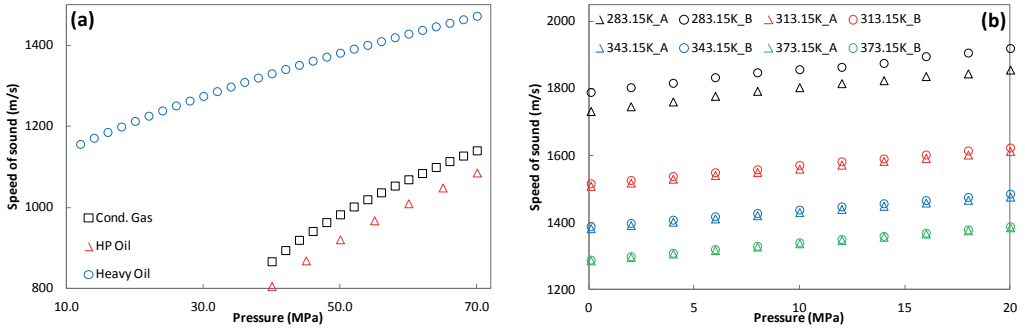

Figure 5.15 (a) The speed of sound in a condensate gas, a hyperbaric oil and an under-saturated heavy oil as a function of pressure at 313.15K. Data are taken from Daridon et al. (1998c). (b) The speed of sound in two very heavy oils. Data are taken from Plantier et al. (2008).

5.3 Correlations

In order to interpolate and extrapolate experimental data to given conditions, and also for compact and smooth representations, it is a common practice to correlate the measured speed of sound data to mathematical expressions. This also makes it possible for people to compare their own data with the published values at the exactly same conditions, i.e. temperature, pressure and/or composition. Depending on the number of free variables, different mathematical expressions are used to correlate the experimental data, among which the combination of polynomials are most popular.

Equation (5.2) is a general expression for one free variable situation.

$$u = \sum_{i=0}^{n} a_i \Omega^i \tag{5.2}$$

where Ω is temperature, pressure or concentration in binary mixtures, and a_i are coefficients.

This equation can be used to represent the speed of sound as a function of temperature along isobaric or co-existence lines, a function of pressure along isothermal lines for pure fluids or mixtures with fixed composition, or a function of the concentration of one compound in binary mixtures at constant temperature and pressure [Del Grosso et al. (1972), Straty (1974), Bobik (1978), Oswal et al. (2002)]. Oakley et al. (1991) used this type expression up to third degree for the speed of sound as a function of pressure for 68 different organic liquids. Wang et al. (1991) even correlated the speed of sound as a linear function of temperature for 26 pure hydrocarbons samples at atmospheric pressure with satisfactory accuracy. It is also common to express the pressure as a function of speed of sound using the same type formula [Sun et al. (1987), Muringer et al. (1985)].

Besides equation (5.2), many researchers [Nath (1997), Oswal et al. (2002), Dzida et al. (2003), Dubey et al. (2008e)] have expressed the speed of sound deviation from the ideal limit as a function of concentration, which makes it clear to show the non-ideality of the binary mixtures from the viewpoint of speed of sound.

$$\left(u - u^{id}\right) = x(1-x) \sum_{i=1}^{n} a_i \, (2x-1)^i \tag{5.3}$$

$$u^{id} = x_1 \times u_1 + x_2 \times u_2 \tag{5.4}$$

where *x* could be molar composition or volume fraction.

Several mathematical formulas were proposed by different researchers to express the speed of sound in pure fluids or mixtures with fixed composition as a function of temperature and pressure. The most popular one is the following equation [Wilson (1959), Bobik (1978), Niepmann et al. (1987), Takagi et al. (1992, 1997), Żak et al. (2000), Khasanshin et al. (2002)]:

$$u^{\alpha} = \sum_{i=0}^{n_i} \sum_{j=0}^{n_j} a_{ij} (P - P_0)^i (T - T_0)^j \tag{5.5}$$

where a_{ij} are correlation coefficients, and T_0 and P_0 are arbitrarily chosen independent constants. T and P could be absolute or reduced variables over critical values or some given constants, such as 1000 for temperature and 100 for pressure. Normally the exponent factor of speed of sound α is 1, while -2 was used by Żak et al. (2000) for the speed of sound in water.

As done for the one variable situation, Sun, Biswas and their co-workers [Marczak et al. (2000), Sun et al. (1987, 1988, 1991)], Dzida and co-workers [Dzida et al. (2003, 2005, 2008, 2009b)] have extensively used the following expressions to correlate the experimental speed of sound data.

$$P - P_0 = \sum_{i=0}^{n_i} \sum_{j=0}^{n_j} a_{ij} (u - u_0)^i T^j \tag{5.6}$$

where P_0 normally is an arbitrarily chosen constant, but the most common one is 0.1MPa, and u_0 is the corresponding speed of sound.

A more complex expression, ratio of two polynomials, was adopted by Lainez, Zollweg and their co-workers [Lainez et al. (1989, 1990), Guedes et al. (1992)], Takagi et al. (2002, 2004a-c).

$$\left(\frac{u}{u_0}\right)^{\alpha} = \frac{\sum_{i=0}^{n_i} \sum_{j=0}^{n_j} a_{ij} (P - P_0)^i (T - T_0)^j}{\sum_{l=0}^{n_l} \sum_{k=0}^{n_k} a_{lk} (P - P_0)^l (T - T_0)^k} \tag{5.7}$$

where the meanings of symbols are the same as those in equation (5.5) , while α could be 1 or 2. If α is chosen to be 2, u_0 would usually be set to 1.

The same idea of equation (5.7) was adopted in the works of Daridon, Lagourette and their co-workers [Daridon et al. (1998a, 1998b, 2000, 2002), Dutour et al. (2000, 2001), Lagourette et al. (1999)], but the cross terms of temperature and pressure were not considered and only linear terms were in the denominator. This expression could lead to a straightforward and analytical form of the

integral of $1/u^2$, which is useful when calculating the density and/or heat capacity under high pressures.

$$u^{-2} = \left(\sum_{i=0}^{n_i} a_i T^i + \sum_{j=0}^{n_j} b_j P^j \right) \Big/ (1 + c \times T + d \times P) \tag{5.8}$$

where a_i, b_j, c and d are adjustable coefficients.

Recently, the following more complex expression, not a combination of pure polynomials anymore, was adopted by Khasanshin et al. (2006, 2009) to correlate the speed of sound in 1-hexadecene and n-hexadecane, in which it was used to calculate other properties under high pressures as well.

$$\frac{10^6}{u^2} = A + \frac{B}{C + P/100} + \frac{D}{E + P/100} \tag{5.9}$$

$$C = c_0 + c_1 \left(\frac{T}{100} \right)^{\alpha} \tag{5.10}$$

$$D = d_0 + d_1 \left(\frac{T}{100} \right) \tag{5.11}$$

$$E = e_0 + e_1 \left(\frac{T_c - T}{100} \right) + e_1 \left(\frac{T_c - T}{100} \right)^{\gamma} \tag{5.12}$$

where A, B, c_0, c_1, d_0, d_1, e_0, e_1, e_2 and α, γ are adjustable coefficients.

In order to calculate the speed of sound in binary mixtures of ethanol or 1-decanol + n-heptane at atmospheric pressure for any given temperature and composition, equation (5.3) were extended by Dzida et al. (2005, 2009) to include temperature dependence in a straight forward way.

$$\left(u - u^{id}\right) = x(1 - x) \sum_{i=1}^{n_i} \sum_{j=0}^{n_j} a_{ij} (2x - 1)^i T^j \tag{5.13}$$

Hasanov (2012) successfully correlated the speed of sound in the binary mixture of n-heptane and n-octane in wide ranges of temperature and pressure, over the whole composition range by the following equation.

$$u = \sum_{i=0}^{5} \sum_{j=0}^{4} \sum_{k=0}^{2} a_{ijk} P^i (100x)^j T^k \tag{5.14}$$

Khasanshin et al. (1992, 2000, 2001) attempted to develop generalized correlations to predict the speed of sound in n-alkanes and 1-alkanols.

$$ln(u) = ln(u_0) + A \times N^{\alpha} \tag{5.15}$$

where $ln(u_0)$ and A is expressed by equation (5.5), N is carbon number and α is -1 or -1/2.

Very recently, Padilla-Victoria et al. (2013) proposed the following Tait type expression to correlate the speed of sound in normal alkanes and their binary mixtures with carbon number ≥5.

$$\frac{u - u_0}{u} = D \times log\left(\frac{E + P}{E + P_0}\right) \tag{5.16}$$

D is a function of temperature, pressure and carbon number, while E is a function of temperature and carbon number only. The detailed mathematical expressions will not be duplicated here.

5.4 Conclusions

The experimental speed of sound data of pure hydrocarbons, pure 1-alcohols, binary mixtures, ternary systems, oil and gas mixtures have been reviewed and analyzed. The results have shown that the speed of sound measurements have high accuracy, and the speed of sound in binary mixtures to some extent are good candidates to show the deviations from 'ideal solution', even though there is no real ideal mixing or excess property concept for speed of sound.

The empirical correlations for the speed of sound data have been collected as well, most of which are suitable for fixed composition or simple binary mixtures. The only one that is used to correlate the speed of sound, composition, temperature and pressure simultaneously for the binary mixture of nC7 and nC8 needs 90 coefficients. These results indicate that it is not very realistic to use speed of sound to build general equations of state for predictive purpose over wide ranges of compounds, temperature and pressure.

Based on equation (5.8), the correlations for the speed of sound in pure normal hydrocarbons up to nC36, cyclo-hexane, benzene, toluene and 1-alcohols are developed. The coefficients are given in Appendix C (Table C.5), and the corresponding temperature and pressure conditions and statistics are given in Appendix C (Table C.6).

Chapter 6. Modeling speed of sound

Within the thermodynamics framework, speed of sound is directly related to the density or volume, heat capacities, and isothermal compressibility. As a second-order derivative property, it is one of the most demanding tests to check the performance limits for a thermodynamic model. The speed of sound, on one hand, is a valuable property for thermodynamic model developments as a supplement property or a discriminating reference quantity, since it can be measured to a high degree of accuracy, even in high pressure regions. On the other hand, an EOS model that can describe the speed of sound for a wide range of mixtures accurately would be very helpful on in-situ characterization of the research objects, for example, in the petroleum industry, by combining the acoustic measurements and seismic data analysis.

The purposes of this work are (1) to compare SRK, CPA and PC-SAFT on modeling speed of sound in pure substances; (2) to propose approaches to improve the speed of sound description within the PC-SAFT framework; (3) to evaluate the performance of the new approach on predicting speed of sound in a wide range of mixtures; (4) to investigate the possibility or cost of simultaneous modeling phase behavior and speed of sound; (5) to study the association term of the PC-SAFT framework using pure 1-alcohols and 1-alcohol + hydrocarbon binary systems as research objects.

6.1 Introduction

The calculation of speed of sound needs first and second order derivatives of Helmholtz free energy with respect to both temperature and total volume, so it is a second-order derivative property. As pointed out by Gregorowicz et al. (1996), the precise description of the second derivative properties is a challenge for any EOS model. For instance, most of the classical EOS, such as SRK [Soave (1972)] and PR [Peng and Robinson (1976)], fail in describing speed of sound reliably in wide temperature and pressure ranges [Gregorowicz et al. (1996), Ye et al. (1992b), Faradonbeh et al. (2014)]. This may be due to the intrinsic nature of these EOS, usually applied only to phase equilibria calculations, to the sensitivity of the second-order derivative properties performed to a given function, or to the physics behind these models and properties. A way to discern some of these uncertainties could be to use a molecular-based EOS – these equations retain the microscopic contributions considered when building the equation. Meanwhile it needs to be kept in mind that the

second-order derivative properties should not be improved at the expense of significant deterioration of the primary properties, such as vapor pressure and liquid density. Some of the applications of the SAFT family EOS for speed of sound calculations are reviewed below.

Lafitte et al. (2006, 2007) proposed the SAFT-VR Mie approach to simultaneously describe phase equilibria and derivative properties. In the first paper, they preliminarily checked the performance of the models PC-SAFT, SAFT-VR, and SAFT-VR LJC [Davies et al. (1998)] to describe the derivative properties with molecular parameters fitted to the vapor-liquid equilibrium data only, i.e. vapor pressure and saturated liquid densities, which aims to identify the limitations of these models. Poor agreement of the results from these models with the experimental data made them conclude that all these models fail to describe the speed of sound. As discussed in the article, a feasible solution might be to recalculate molecular parameters for these models by taking into consideration isothermal compressibility data (or speed of sound) in the fitting procedure to overcome this problem. The reported results of these tests indicated a slight improvement on isothermal compressibility estimation results with an important deterioration of the vapor-liquid equilibrium curve. Hence, by assuming that the problem in accurately describing the derivative properties was the choice of the intermolecular potential used to model the repulsion and dispersion interactions between the monomers forming the chain, they modified the potential term in the SAFT-VR approach, and proposed the SAFT-VR Mie model. The new model introduces an extra compound specific parameter related to the shape of the repulsive part of the potential. In addition, they proposed new fitting procedures to include two types of properties, vapor-liquid equilibrium data, i.e. vapor pressure and liquid density, and the speed of sound in the condensed liquid phase. The results of both first and second derivative properties were shown better agreements with the experimental data than the other SAFT models with original parameters. The mentioned %AAD for speed of sound was around 2%. This work showed the capability of the SAFT-type models for describing both first and second derivative properties with good accuracy simultaneously. In the second article [Lafitte et al. (2007)], they extended this approach to model vapor-liquid equilibria behavior and second-order derivative properties of alcohols and 1-alcohol + n-alkanes mixtures simultaneously. The extra nonconformal parameter characterizing the repulsive interaction between the monomer segments greatly enhanced the performance of the SAFT-VR theory for the prediction of second derivative properties of the 1-alcohol substances with around 2.5%AAD for speed of sound. This was due to the fact that in SAFT theory the contact segment-segment radial distribution

function plays a fundamental role not only in the chain contribution but also in the association contribution with the free energy [Lafitte et al. (2007)].

In order to get a more precise speed of sound prediction for mixtures from the SAFT-VR Mie model, Khammar and Shaw (2010) translated isentropic compressibility estimations for a mixture at a specific composition by adding the molar average error of the predicted pure components isentropic compressibility to the isentropic compressibility of the mixture predicted from SAFT-VR Mie EOS, which has been tested for binary mixtures of 1-alcohol and n-alkane.

Llovell et al. (2006a, 2006b) argued that inclusion of properties other than vapour pressure and saturated liquid density data in the fitting procedure would reduce the predictive capability of the model. So they performed calculations with soft-SAFT [Blas et al. (1997, 1998)] on second derivative properties with the pure component parameters fitted to vapour pressure and saturated liquid density data only to show the physical soundness of the theory and to address specifically the transferability of the parameters. In addition, the soft-SAFT is able to accurately capture the density singularities related to the critical region by using a crossover treatment which explicitly incorporates a renormalization group term with two extra parameters [Llovell et al. (2004)]. Pure n-alkanes and 1-alkanols were modeled in their first article [Llovell et al. (2006b)]. Their work provided a clear insight into the capability of the SAFT theory to capture simultaneously the vapor-liquid and derivative properties of an associating fluid, but the %AADs for speed of sound in n-hexane and n-heptane at T_r=1.1 are around 20%. In the later work [Llovell et al. (2006a)], the %AADs of speed of sound for n-heptane at 0.1MPa and 101.3MPa is about 6%.

Diamantonis et al. (2010) evaluated the performance of SAFT and PC-SAFT on derivative properties in a wide range of conditions for six fluids that are of interest to the Carbon Capture and Sequestration (CCS) technology. They used a similar approach, as that proposed by Llovell et al. (2006b), to predict the second-order derivative properties using the pure component parameters fitted to VLE data only. The results revealed that both models performed well, especially away from the critical region. PC-SAFT was shown to be more accurate than SAFT for CO_2, H_2S and H_2O, while two models give comparable accuracies for other components. The average %AAD of the PC-SAFT model on the speed of sound for the six fluids is 2%. These results are not consistent with the point of view of Lafitte et al. (2006), who said that PC-SAFT was not able to describe the speed of sound well, but the author argued that direct comparisons are difficult, since the fluids and

conditions examined are not the same. We agree partly with this argument, and also want to point out that the studied six fluids are all composed of small molecules.

Very recently, to address the numerical pitfalls, unphysical predictions and wrong estimations of the pure components' critical properties of the SAFT approaches, Polishuk (2011b) proposed a SAFT plus Cubic approach, where in SAFT the attractive term of cubic EoS is attached. As pointed out by the author, unlike other SAFT variants, SAFT + Cubic relies on generalizing the regularities exhibited by experimental data rather than approximating the results of molecular simulations. The authors concluded several merits of this approach: (1) free of the well-known disadvantages characteristic for several SAFT approaches, such as the inability to correlate the critical and subcritical pure compound data simultaneously and generating artificial unrealistic phase equilibria; (2) free of numerical pitfalls; (3) the smaller number of the pure compound adjustable parameters due to solving the critical conditions to obtain three of the five parameters (for most pure alkanes, one more parameter could be estimated by a empirical expression) when critical properties are available; (4) relatively modest numerical contribution. This approach demonstrated its superiority on speed of sound calculation compared to SAFT-VR Mie, PC-SAFT and SBWR for the selected systems both on curvature and accuracy from the figures in their published articles [Polishuk et al. (2011a-d)]. Unfortunately, they presented very limited %AAD data explicitly, and also there is very little information about the vapor pressure prediction accuracy. This SAFT + Cubic approach has five parameters for non-associating compounds and seven for associating ones.

In order to provide a comprehensive understanding of the potentials and limitations of the advanced SAFT family EOS and their improvements over classical models, de Villiers et al. (2011, 2013) have studied the performance of SRK, PR, CPA, SAFT and PC-SAFT on derivative properties for different component families, i.e., non-polar, polar non-associating, and associating, in both the compressed liquid and near-critical regions. Based on the fact that the total Helmholtz free energy is expressed as summation of separate contributions and all of the derivative properties could be calculated explicitly from one or more Helmholtz free energy derivatives with respect to temperature or total volume, they analyzed the contributions of individual terms on the final derivative properties and single derivatives. They concluded that, in general, the performance of PC-SAFT is superior in correlating most of the second-order derivative properties of investigated alkanes. A major improvement of the SAFT and PC-SAFT over CPA is its ability to give a better description of the dP/dV derivative. However, as pointed out by the authors, this improvement is

still not sufficiently significant and is the primary reason why the models are not able to correlate the speed of sound accurately. They further pointed out that a similar approach as SAFT-VR Mie [Lafitte et al. (2006, 2007)] seems to be necessary in order to accurately predict speed of sound, since the *dP/dV* derivative is predominantly influenced by the hard-sphere term and its incorrect slope with respect to pressure is possibly caused by the chain term, both of which are largely influenced by the radial distribution function. The similar incorrect slope of residual isochoric heat capacity and isothermal compressibility with respect to molar density from the chain term contribution were shown in the work of Llovell and Vega (2006b), in which they conducted the same term contribution analysis for these two properties for short and long, non-associating and associating chain compounds. They concluded from this analysis that association played a dominant role in heat capacities (and other energetic properties) for relatively short associating chains.

Based on the literature investigations above, the SAFT-type models (the SAFT framework) seem to provide a 'theoretically correct' approach to describe the first and second-order derivative properties simultaneously. The differences depend mostly on segment potentials, parameter estimation procedures and the number of adjustable parameters used.

6.2 Comparison of SRK, CPA and PC-SAFT

Although some calculations of SRK, CPA and PC-SAFT EOS have been reported for speed of sound for alkanes [de Villiers (2011)], it is worth performing an extensive comparison for these models over wide temperature and pressure ranges. In this work, the performance of these three models on speed of sound is evaluated for normal paraffins from methane to n-eicosane (n-C_{20}), n-tetracosane (n-C_{24}) and n-hexatriacontane (n-C_{36}) over wide temperature and pressure ranges against the experimental or correlation data based on the available literature. The pure component parameters of CPA can be found in the book of Kontogeorgis and Folas (2010), and those of PC-SAFT can be found in the original literature [Gross et al. (2001), Ting et al. (2003)]. The vapor pressure and saturated liquid density data are taken from the DIPPR correlations [DIPPR Database (2012)] in the reduced temperature range T_r=[0.45, 0.9] for consistency and easy comparison with other models, while the speed of sound data of methane to n-decane is taken from the NIST database [REFPROP (2010)], and those of other long chain molecules are taken from the literature.

The typical shapes of the isothermal speed of sound curves from the three models are shown in Figure 6.1, from which it can be seen that PC-SAFT performs better on capturing the curvature.

According to the investigation of de Villiers et al. (2011, 2013), it is due to the fact that PC-SAFT provides a good description of the derivative of pressure with respect to total volume, which is the dominant term in the speed of sound calculation. Not surprisingly, CPA performs significantly better to SRK as liquid density is used in the parameter fitting procedure. This is because density is directly used in the speed of sound calculation, as expressed in equation (1.7). It is shown in Figure 6.1 (d), however, that the superiority of CPA over SRK is much smaller than that of PC-SAFT over CPA, which indicates that the model itself is more important than the parameter fitting. The detailed %AAD information of vapor pressure, liquid density and speed of sound of these three models are supplied in Table 6.1. It is worth pointing out that SRK or CPA could have a smaller %AAD in narrow low pressure ranges for some cases, such as hexane at 300K in Figure 6.1 (b), because the cancellation of the errors from the under-predicted to over-predicted regions.

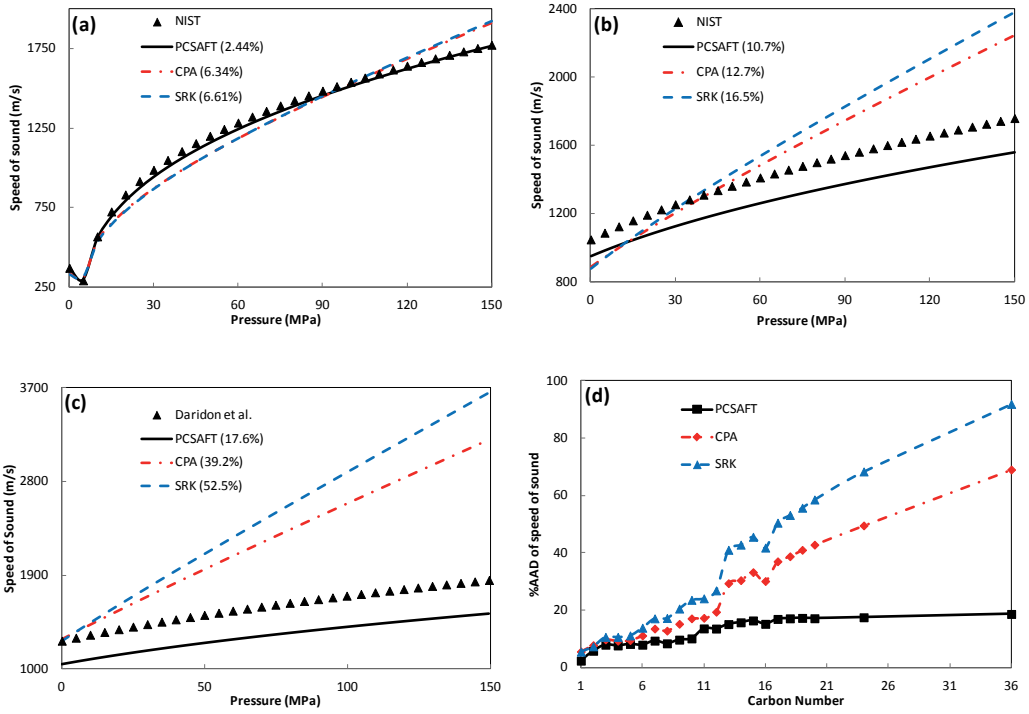

Figure 6.1 Speed of sound in (a) methane (C1) at T=200K (T_r=1.05), (b) nC6 at T=300K (T_r=0.59), (c) nC15 at T=313.15K (T_r=0.44). (d) The %AAD of speed of sound from SRK, CPA and PC-SAFT against carbon number. Dash line, dash dot line and solid line are results of SRK, CPA and PC-SAFT, respectively, and data for C1 and nC6 are taken from NIST [REFPROP (2010)], and data of nC15 are from Daridon et al. (2002).

Table 6.1 %AADs for vapor pressure, liquid density and speed of sound from different models

Comp	SRK			CPA			PC-SAFT			T of u (K)	P of u (MPa)	np [+]
	P	*ρ*	*u*	*P*	*ρ*	*u*	*P*	*ρ*	*u*			
C1 [*,1]	1.67	2.73	5.51	0.51	1.77	5.55	0.21	0.49	2.36	100-350	0.1-150	25
C2 [1]	1.87	5.18	7.36	0.32	1.23	7.77	0.25	0.68	5.80	150-500	0.1-150	30
C3 [1]	1.20	6.81	10.7	3.43	1.90	9.75	0.19	0.51	7.92	150-500	0.1-150	30
C4 [1]	1.79	8.04	10.7	0.63	4.07	9.31	0.33	0.50	7.66	200-550	0.1-150	30
C5 [1]	1.66	9.91	11.2	0.63	0.75	9.52	0.29	1.35	8.18	250-550	0.1-150	30
C6 [1]	1.94	11.6	13.9	2.61	0.55	11.1	1.05	0.66	7.92	250-600	0.1-150	30
C7 [1]	1.13	13.0	17.1	1.65	0.60	13.6	0.26	0.94	9.34	250-600	0.1-150	30
C8 [1]	1.76	14.5	17.2	0.77	0.77	12.8	0.44	0.82	8.40	300-600	0.1-150	30
C9 [1]	1.60	15.5	20.5	1.54	0.92	15.2	0.77	0.62	9.69	300-600	0.1-150	30
C10 [1]	2.03	16.5	23.6	1.92	0.99	17.1	0.84	0.61	10.1	300-650	0.1-150	30
C11 [2]	1.36	17.8	24.1	2.07	1.34	17.3	1.79	0.67	13.6	303.15-413.15	0.1-118	91
C12 [3]	1.79	18.6	26.9	1.79	1.53	19.4	1.29	0.79	13.6	293.15-433.15	0.1-140	112
C13 [4]	1.05	20.1	41.0	1.92	2.26	29.4	1.89	1.18	15.1	293.15-433.15	0.1-150	294
C14 [4]	1.34	21.7	42.8	1.75	2.19	30.4	2.69	0.74	15.7	293.15-433.15	0.1-150	269
C15 [5]	0.46	22.3	45.6	1.16	2.07	33.2	2.24	0.79	16.4	293.15-383.15	0.1-150	170
C16 [6]	1.42	23.0	41.8	2.97	2.43	30.1	2.51	0.63	15.2	303.15-433.15	0.1-140	58
C17 [5]	1.56	22.8	50.5	1.41	2.27	37.0	2.95	0.58	16.9	303.15-383.15	0.1-150	151
C18 [7]	1.91	23.4	53.2	1.49	2.52	38.8	3.01	0.51	17.1	313.15-383.15	0.1-150	141
C19 [7]	1.91	23.9	55.7	2.74	2.70	41.0	3.71	0.51	17.3	313.15-383.15	0.1-150	134
C20 [8]	4.90	23.5	58.6	3.08	2.79	42.8	4.17	0.79	17.2	323.15-393.15	0.1-150	129
C24 [9]	8.84	25.4	68.4	2.52	3.34	49.5	1.28	0.41	17.5	333.15-393.15	0.1-150	105
C36 [10]	22.1	26.6	91.0	33.3	5.07	68.3	19.43	1.49	18.7	363.15-403.15	0.1-151	76
Avg.	2.97	16.9	33.5	3.19	2.00	25.0	2.34	0.74	12.4			

[*] The reduced temperature ranges of vapor pressure and liquid density is Tr=[0.45, 0.9], while for methane it starting from 100K.

[+] *np* denotes the number of evenly spread vapor pressure and liquid density data used to evaluate the %AAD. The same data is used in parameter estimation and universal constants regression.

The vapor pressure and liquid density of C1 to C10 and C11 to C36 are from NIST [REFPROP (2010)] and DIPPR Database (2012) , respectively.

Speed of sound reference: (1) REFPROP (2010); (2) Badalyan et al. (1971); (3) Khasanshin et al. (2003); (4) Daridon et al. (2000); (5) Daridon et al. (2002); (6) Boelhouwer (1967); (7) Dutour et al. (2000); (8) Dutour et al. (2001a); (9) Dutour et al. (2001b); (10) Dutour et al. (2002).

6.3 Improve PC-SAFT for modeling speed of sound

6.3.1 Approaches

As discussed above, PC-SAFT could be taken as a good start to calculate the speed of sound due to its capability of capturing the curvature as discussed above, but the quantitative performance is not good enough. By inspired the fact shown in Figure 6.1 (b), in order to improve the description of speed of sound with PC-SAFT, an intuitively feasible approach is to take the speed of sound data into consideration in the parameter fitting procedure, as discussed by Laffite et al. (2006). This is named as ***OrgSS*** (original one with speed of sound).

The speed of sound calculated from the PC-SAFT model does not deviate qualitatively very much from the experimental data curve. Thus, it is speculated whether it is possible to 'rotate' or 'move' somewhat the calculated curve in order to match the experimental results better by putting the speed of sound data into the universal constants regression, and the pure component parameters are then estimated with the new universal constants. This is named as ***NewUC***, and the original one with literature available parameters is given the name ***OrgUC***.

It can be seen from equations (2.11) and (2.12) that 14 numbers, i.e. $\{a_{0i}\}$ and $\{b_{0i}\}$, of the 42 universal constants need to be fitted for methane if its segment number is fixed to 1. On the other hand, as shown Figure 6.1 (a), PC-SAFT can predict the speed of sound for methane with good accuracy. So we propose to fit the universal constants and pure component parameters in two steps. In the first step, the universal constants and pure component parameters are regressed for methane using an iterative procedure as shown below:

(1) Estimate the pure component parameters with original universal constants
(2) Regress the coefficients $\{a_i\}$ and $\{b_i\}$ for each component
(3) Estimate the pure component parameters with the new universal constants
(4) Repeat steps (2) to (3) until convergence is obtained

The original $\{a_{0i}\}$ and $\{b_{0i}\}$ provide good initial estimates for the regression. In the second step, only the differences of the coefficients from those of methane need to be regressed, i.e., the sum of the last two terms of equations (2.11) and (2.12). The same procedure is applied for ethane to n-decane, but an additional step is needed to fit the coefficients to segment number *m* after getting the individual coefficients, in which step 28, i.e. $\{a_{1i}, a_{2i}\}$ and $\{b_{1i}, b_{2i}\}$ in equations (2.11) and (2.12),

of the 42 universal constants can be fitted. This procedure makes it possible to use the original universal constants as initial values.

Convergence here means that the changes of overall %AAD of the three properties or the changes of the pure component parameters are smaller than given tolerance. It is unavoidable to arrive to multiple local minimum points when the problem has several parameters, as discussed later. Thus it is a good strategy to decrease the tolerance in the convergence criteria error gradually and to keep the curves on reasonable trends which can be controlled by carefully choosing boundaries for the coefficients. The new universal constants are reported in Table 6.2.

Table 6.2 The newly developed universal constants with speed of sound in regression*

First dispersion term universal constants (I1)

i	a_{0i}	a_{1i}	a_{2i}
0	0.836215101666	-0.411727190935913	0.0319867672916212
1	2.201683842453	2.37426400571265	-2.75137756155503
2	-11.25210310939	-21.0620603419144	25.7581175334397
3	37.841836899902	105.65718855671	-103.082737163044
4	-68.035304263396	-298.665894225644	239.569856365622
5	69.952369867326	468.695983731173	-320.622085430506
6	-42.828905226651	-316.673589664169	186.50494276364

Second dispersion term universal constants (I2)

	b_{0i}	b_{1i}	b_{2i}
0	0.627209841336118	-0.622507280536237	-0.0303061275320169
1	4.02517816132384	1.86478114256654	2.59554209415371
2	-22.6660554011051	-22.5660800172653	11.5803588817289
3	70.0153445172765	153.069895818654	-145.915305288352
4	-129.548046066679	-321.710866534244	354.901071174401
5	150.197401680241	453.083735030445	-151.675970200232
6	-86.9664928046989	-233.232187026907	-282.837925415568

* The vapor pressure, liquid density and speed of sound data of ***saturated*** methane to decane are used in the regression.

6.3.2 Objective function and data

The objective function used in this work is:

$$f_{min} = w_P \sum_{i=1}^{N_P} \left(\frac{P_i^{exp} - P_i^{calc}}{P_i^{exp}} \right)^2 + w_\rho \sum_{i=1}^{N_\rho} \left(\frac{\rho_i^{exp} - \rho_i^{calc}}{\rho_i^{exp}} \right)^2 + w_u \sum_{i=1}^{N_u} \left(\frac{u_i^{exp} - u_i^{calc}}{u_i^{exp}} \right)^2 \quad (6.1)$$

Where P, ρ and u are vapor pressure, liquid density and speed of sound respectively; N and w with the corresponding subscript are total experimental points and weights of the objective function respectively.

This objective function is minimized by applying a Levenberg-Marquardt algorithm [Móre (1977)] for both universal constant regression and pure component parameter estimation. Equal points of vapor pressure, liquid density and speed of sound of ***saturated*** methane to n-decane are used for both universal constants regression and pure component parameters estimation. Equal weights, i.e. $w_P = w_\rho = w_u = 1$, are used for the three properties, although Laffite et al. (2006, 2007) suggested using half weight for the speed of sound in their parameter fitting procedure. The information of data points can be found in Table 6.1.

For other components, the number points of experimental vapor pressure and liquid density data used in the pure component parameter estimations depend on the available compressed liquid speed of sound data, for which the ranges of temperature and pressure and how many data points can be found in Table 6.1 as well.

6.4 Results and discussion on speed of sound

6.4.1 Pure substances

6.4.1.1 Hydrocarbons

The pure component parameters from these two approaches OrgSS and NewUC are compared with the original ones (OrgUC) in Table 6.3. Due to their sound physical meanings and the same framework of PC-SAFT, it can be seen that the three pure component parameters obtained from all three approaches follow similar trends against molecular weight. As shown in Figure 6.2, the parameters m, $m\sigma^3$ and $m\varepsilon/k$ from the approach NewUC show good linear functions of molecular weight, as the original ones discussed in other works [Tihić et al. (2006, 2008), Yan et al. (2010)].

Table 6.3 PC-SAFT pure component parameters estimated from different approaches

Alkanes	OrgUC			OrgSS			NewUC		
	m	σ (Å)	ε/k (K)	m	σ (Å)	ε/k (K)	m	σ (Å)	ε/k (K)
C1	1.0	3.7039	150.03	1.0	3.7040	150.07	1.0	3.7030	149.98
C2	1.6069	3.5206	191.42	1.63742	3.4994	189.26	1.61691	3.5225	190.52
C3	2.002	3.6184	208.11	2.03288	3.5938	206.27	2.01124	3.6106	207.51
C4	2.3316	3.7086	222.88	2.41443	3.6633	218.20	2.32230	3.7129	223.40
C5	2.6896	3.7729	231.20	2.83126	3.6936	224.64	2.68579	3.7666	231.41
C6	3.0576	3.7983	236.77	3.29163	3.7014	227.18	3.04140	3.8083	237.15
C7	3.4831	3.8049	238.40	3.67278	3.7374	231.17	3.52812	3.7800	236.67
C8	3.8176	3.8373	242.78	4.23567	3.7096	229.48	3.89759	3.8137	239.76
C9	4.2079	3.8448	244.51	4.25860	3.8174	243.24	4.14894	3.8713	246.14
C10	4.6627	3.8384	243.87	4.90831	3.7797	237.26	4.62216	3.8560	244.73
C11	4.9082	3.8893	248.82	5.13150	3.8375	243.25	5.01574	3.8706	245.86
C12	5.3060	3.8959	249.21	5.48676	3.8548	245.09	5.36078	3.8888	247.74
C13	5.6877	3.9143	249.78	5.93966	3.8553	244.53	5.75866	3.8981	248.13
C14	5.9002	3.9396	254.21	6.26516	3.8737	246.61	6.06497	3.9194	250.39
C15	6.2855	3.9531	254.14	6.59888	3.8927	248.09	6.36243	3.9441	252.37
C16	6.6485	3.9552	254.70	6.95948	3.8986	249.12	6.74213	3.9457	252.77
C17	6.9809	3.9675	255.65	7.36130	3.9032	249.42	7.07933	3.9592	253.97
C18	7.3271	3.9668	256.20	7.73947	3.9077	249.59	7.43336	3.9661	254.25
C19	7.7175	3.9721	256.00	8.18528	3.8975	249.10	7.86483	3.9567	253.66
C20	7.9849	3.9869	257.75	8.53672	3.9155	249.90	8.19382	3.9759	254.60
C24	9.8220	3.9370	253.18	9.86769	3.9474	252.69	9.41287	4.0195	258.08
C36	13.86	4.0140	256.37	15.5707	3.8376	245.21	14.8457	3.9188	250.19

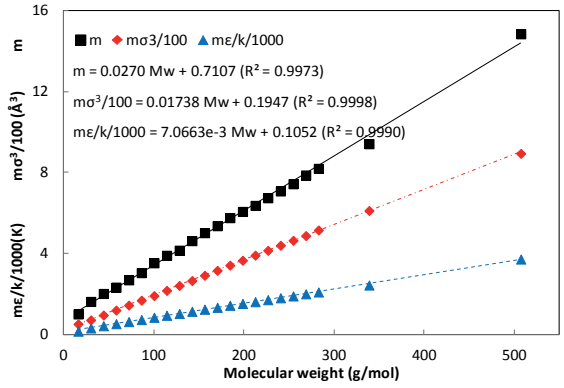

Figure 6.2 The parameter groups m (cycle), $m\sigma^3$ (square) and $m\varepsilon/k$ (triangle) from the approach NewUC as linear functions of molecular weight for n-alkanes up to n-C_{36}.

The %AAD of vapor pressure (P^{sat}), density (ρ), speed of sound (u) are reported in Table 6.4. There are two columns for speed of sound in Table 6.4, and the one with *u(s)* presents that the %AAD is calculated for saturated speed of sound data, since this data is used to fit the parameters for methane to n-decane. The two *Avg.* rows in Table 6.4 are for methane to n-decane and for methane to n-hexatriacontane, respectively, since the data of methane to n-decane are used to readjust the universal constants. The large %AAD vapor pressure of n-hexatriacontane is mainly because its vapor pressure from DIPPR correlation is very low, about 4.0E-4 Pa at T_r=0.45. Similar results were reported for SAFT-VR and SAFT-VR Mie [Lafitte et al. (2006)]. The speed of sound in saturated and compressed nC6, and in compressed nC15 are shown in Figures 6.3 and 6.4 with the three approaches.

Table 6.4 %AADs for vapor pressure, liquid density and speed of sound from different approaches

Comp.	OrgUC *				OrgSS				NewUC			
	P	*ρ*	*u(s)*+	*u*	*P*	*ρ*	*u(s)*	*u*	*P*	*ρ*	*u(s)*	*u*
C1	0.21	0.49	2.38	2.36	0.26	0.50	2.33	2.35	0.52	0.83	1.26	2.52
C2	0.25	0.68	7.83	5.80	0.50	0.40	7.79	5.75	0.68	1.75	0.90	3.69
C3	0.19	0.51	8.69	7.92	0.62	0.39	8.59	8.00	0.65	1.90	1.54	3.55
C4	0.33	0.50	8.55	7.66	1.62	0.72	8.57	7.73	0.72	1.80	1.34	3.32
C5	0.29	1.35	8.84	8.18	1.86	0.69	8.58	8.42	0.58	1.59	1.68	3.51
C6	1.05	0.66	7.04	7.92	2.74	1.25	6.79	7.99	1.74	1.49	0.58	2.97
C7	0.26	0.94	8.40	9.34	2.61	1.73	8.44	9.42	1.13	1.63	1.52	3.47
C8	0.44	0.82	7.33	8.40	4.32	2.48	6.78	8.34	1.16	1.56	0.41	2.69
C9	0.77	0.62	8.73	9.69	0.99	0.61	8.56	9.82	1.40	1.82	2.30	2.91
C10	0.84	0.61	8.42	10.1	3.02	1.91	8.23	10.1	1.28	1.59	1.54	3.93
C11	1.79	0.67		13.6	1.32	1.44		13.3	1.52	1.41		2.03
C12	1.29	0.79		13.6	1.25	1.40		13.3	1.52	1.41		2.07
C13	1.89	1.18		15.1	1.29	1.70		14.8	1.37	1.37		2.24
C14	2.69	0.74		15.7	1.43	1.70		15.1	1.43	1.37		2.52
C15	2.24	0.79		16.4	1.13	1.78		16.0	1.11	1.37		2.94
C16	2.51	0.63		15.2	1.39	1.54		14.8	1.77	1.33		2.79
C17	2.95	0.58		16.9	1.26	1.80		16.4	1.54	1.29		3.26
C18	3.01	0.51		17.1	1.20	1.82		16.5	1.49	1.28		3.47
C19	3.71	0.51		17.3	1.70	1.73		16.7	2.21	1.26		3.66
C20	4.17	0.79		17.2	1.86	1.82		16.4	2.71	1.24		3.46
C24	1.28	0.41		17.5	1.09	1.76		17.3	2.57	1.25		4.25
C36	19.4	1.49		18.7	16.5	2.23		17.5	17.2	1.91		5.10
Avg.[1]	0.46	0.72	7.62	7.74	1.85	1.07	7.47	7.79	0.99	1.60	1.31	3.26
Avg.[2]	2.34	0.74		12.4	2.27	1.43		12.1	2.10	1.48		3.20

* The original parameters are from Gross and Sadowski (2001) and Ting et al. (2003).

+ *u* with *s* in parentheses denote the %AAD value only for saturated data of C1 to C10. Avg.[1] and Avg.[2] denote the average deviations from C1 to C10 and from C1 to C36, respectively. The ranges of temperature and pressure; and the references can be found in Table 6.1.

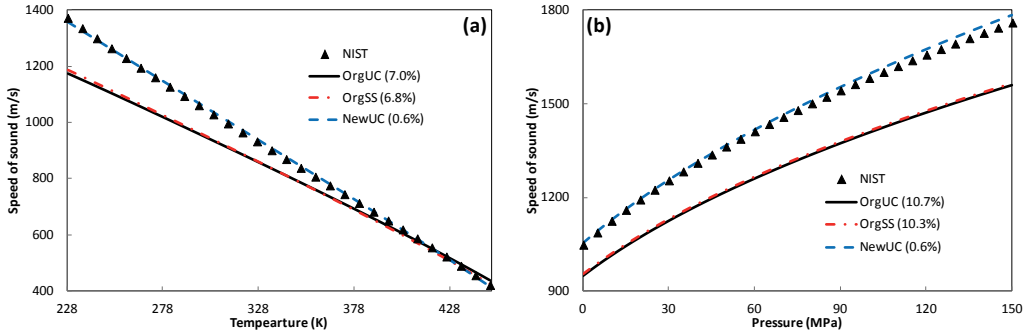

Figure 6.3 Speed of sound in liquid nC6 at saturated state (a) and 300K (b) with parameters from different approaches. Triangles mark data are from NIST [REFPROP (2010)]. The solid lines, dash dot lines and dash lines are the results of the approaches OrgUC, OrgSS and NewUC, respectively.

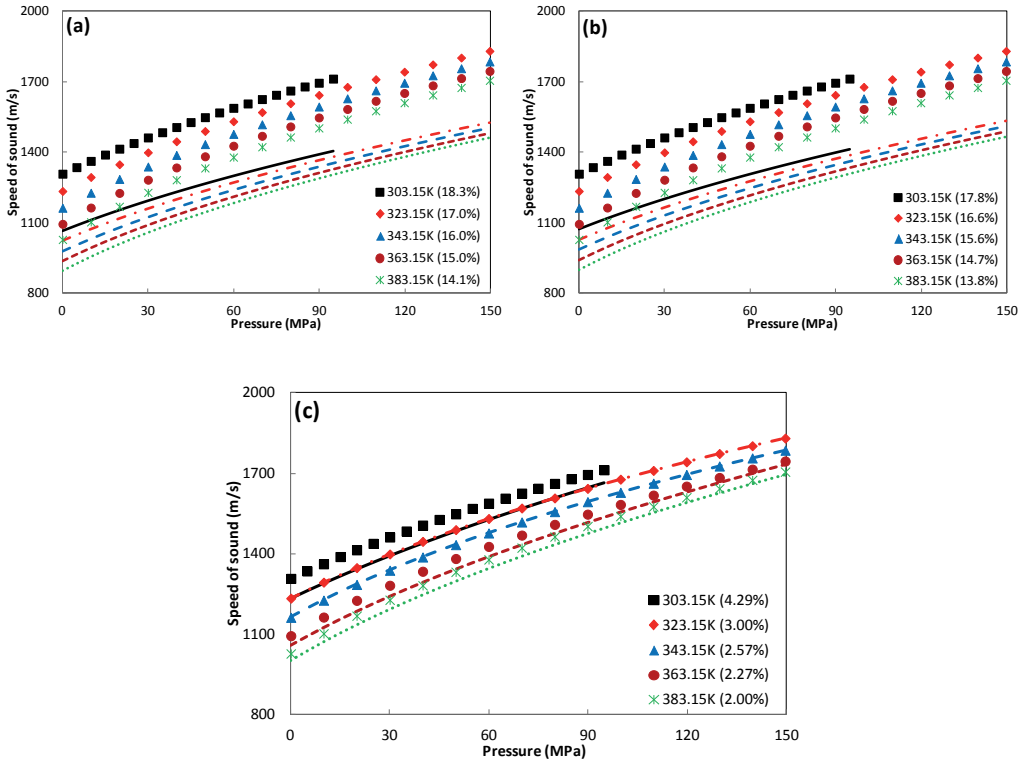

Figure 6.4 Speed of sound in nC15 from different approaches, (a) OrgUC, (b) OrgSS and (c) NewUC. The experimental data are from Daridon et al. (2002).

As shown in Table 6.4 and Figures 6.3-6.4, the approach OrgSS offers small improvements on speed of sound, but yields poor vapor pressures and liquid densities. Similar results were obtained in the works of de Villiers (2011, 2013) and Laffite et al. (2006). However, with the approach NewUC, significant improvements are obtained both in terms of accuracy and reproducing the curvature of the speed of sound with a reasonable loss in accuracy for vapor pressures and liquid densities. Compared to the SAFT-VR Mie model [Lafitte et al. (2006)], our approach is slightly inferior on both saturated liquid density and speed of sound based on the limited data from their work, but is better on vapor pressures. The average %AAD of vapor pressure and liquid density of the same n-alkanes from SAFT-VR Mie model are 5.0% and 0.6% respectively, while the reported average %AAD of speed of sound was close to 2%. (The condensed liquid density data was used in parameter estimation SAFT-VR Mie). Our approach captures the speed of sound curvature quite well with only three pure component parameters for non-associating fluids.

6.4.1.2 1-Alcohols

1-Alcohols are good candidates to investigate the association phenomena, and to check the capability of the association models, so it is worth investigating the impact of the new universal constants on the speed of sound in 1-alcohols. The performance of PC-SAFT on modeling 1-alcohols containing systems has been extensively studied by different researchers. It is also a good opportunity to thoroughly compare the pure component parameters from different sources.

The parameters of methanol to 1-nonanol from Gross and Sadowski (2002), the methanol parameters of Avlund (2010), and the two parameter sets of ethanol to 1-decanol from Grenner et al. (2007a) are investigated along with the two sets obtained in this work. As done for hydrocarbons, on one hand, we use OrgUC, OrgSS and NewUC to present the parameters from different fitting methods when it is clear to distinguish parameter sets. On the other hand, since there are four or five parameter sets for each 1-alcohol, when it is necessary, we use #1 to designate the pure component parameters from Gross and Sadowski (2002), #2 and #3 for the two new sets fitted in this work with the original (OrgSS) and new universal constants (NewUC), respectively, and #4 or #5 for the parameters from other sources for easy reference.

More specifically, the methanol parameters of Avlund (2010) will be denoted as #4. The optimized and general parameters of ethanol to 1-decanol from Grenner et al. (2007a) will be labeled as #4 and #5, respectively. Only four parameter sets for methanol and 1-decanol are discussed in this

work, since methanol was not included in the work of Grenner et al. (2007a) and 1-decanol was not included in the work of Gross and Sadowski (2002). The parameter sets of methanol and 1-decanol fitted by the approaches OrgSS (#2) and NewUC (#3) are presented in Table 6.5. Readers are referred to the original literature for the detailed values of other parameter sets.

Table 6.5 Simplified PC-SAFT parameters for methanol to 1-decanol fitted to vapor pressure, liquid density and speed of sound data with the original and new universal constants.

1-Alkanols	Approach (#set)	pure component parameters (2B)				
		m	σ (Å)	ε/κ (K)	$\varepsilon^{A_iB_j}/\kappa$ (K)	$\kappa^{A_iB_j}$
C1OH	OrgSS (#2)	1.88238	3.0023	181.77	2738.03	0.1044
	NewUC (#3)	1.55166	3.2335	190.66	2864.78	0.06861
C2OH	OrgSS (#2)	2.63505	3.0577	191.90	2574.01	0.07885
	NewUC (#3)	2.35339	3.1692	186.65	2798.79	0.06446
C3OH	OrgSS (#2)	2.71906	3.3512	231.50	2464.16	0.03183
	NewUC (#3)	3.08888	3.1645	191.02	2650.96	0.08001
C4OH	OrgSS (#2)	2.49226	3.7399	270.25	2697.72	0.009106
	NewUC (#3)	3.47445	3.2843	201.87	2560.02	0.085351
C5OH	OrgSS (#2)	4.11911	3.2902	235.95	2023.36	0.02862
	NewUC (#3)	3.46732	3.5058	223.66	2419.99	0.07999
C6OH	OrgSS (#2)	5.10492	3.1827	229.55	2321.46	0.005552
	NewUC (#3)	2.99576	3.9046	265.71	2760.01	0.016547
C7OH	OrgSS (#2)	5.84139	3.1989	225.25	2750.51	0.001318
	NewUC (#3)	3.21685	4.0278	278.17	2979.98	0.006001
C8OH	OrgSS (#2)	6.13366	3.2477	228.96	2750.00	0.001162
	NewUC (#3)	3.50513	4.0364	280.88	2950.02	0.006099
C9OH	OrgSS (#2)	6.16014	3.3524	236.73	3397.23	2.3176e-4
	NewUC (#3)	3.89104	4.0105	282.08	3079.98	0.003519
C10OH	OrgSS (#2)	6.45578	3.4215	238.95	3460.17	1.9464e-4
	NewUC (#3)	4.26982	4.0240	280.00	3091.77	0.003339

Pure component parameters from all these sets are plotted against molecular weight in Figure 6.5, in which segment size and dispersion energy are expressed as $m\sigma^3$ and mε/k, respectively. The parameters of methanol are not shown for sets #4 and #5, and the parameters of 1-decanol are not shown for set #1, for reasons explained above. In general, the pure component parameters show similar overall trends. The segment number (m), segment size ($m\sigma^3$), and segment dispersion energy (mε/k) increase with the molecular weight. The association energy ($\varepsilon^{A_iB_j}$) and association volume ($\kappa^{A_iB_j}$), except those from parameter sets #2 (OrgSS), show small variations for heavy 1-alkanols, e.g. starting from 1-heptanol. To some extent, the phenomena indicate that the association term does not play as important role for heavy 1-alkanols as for light ones.

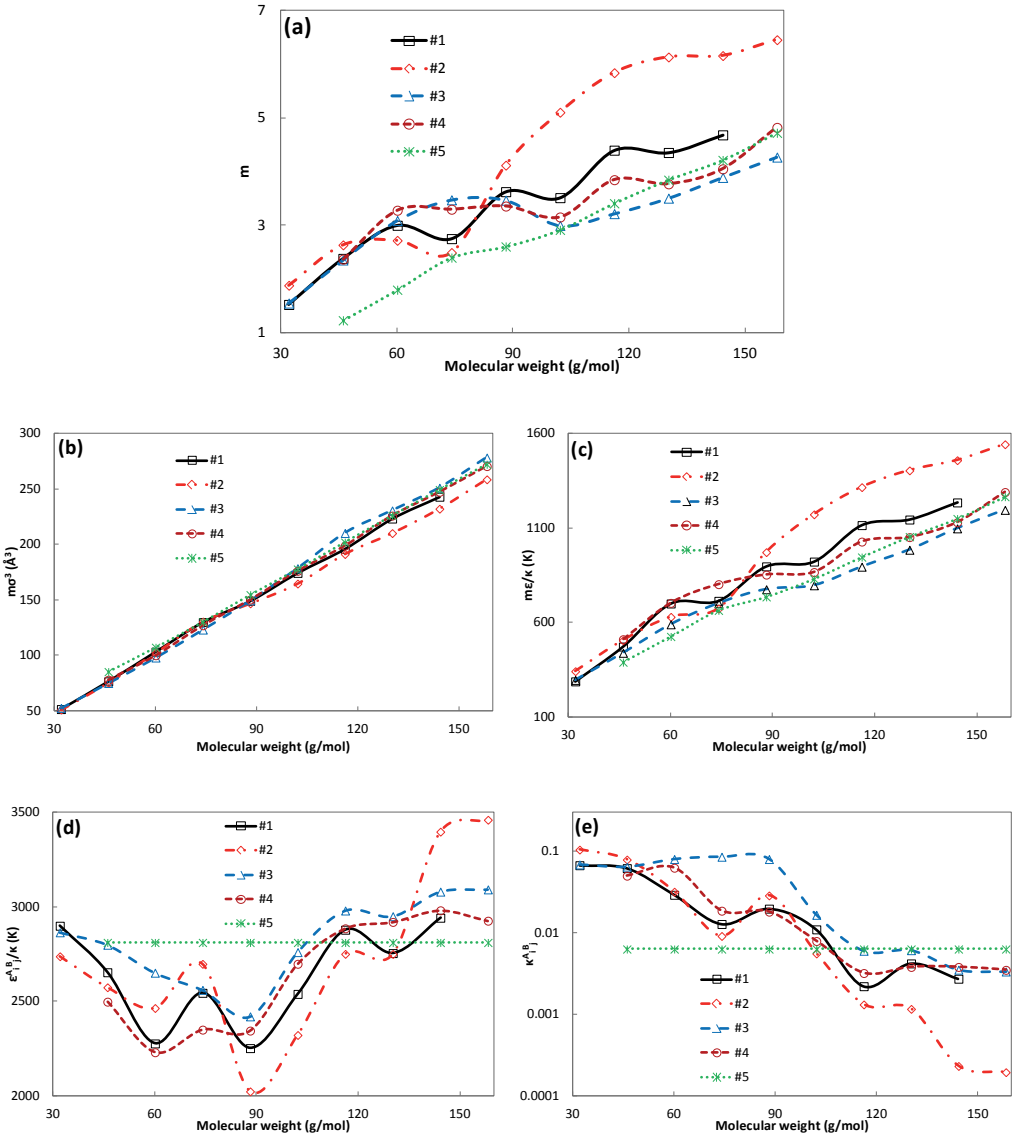

Figure 6.5 Relationships of pure component parameters against molecular weight for all parameter sets (#1, #2, #3, #4, #5). (a) segment number (m), (b) segment number times cubic segment size ($m\sigma^3$), (c) segment number times dispersion energy ($m\varepsilon/k$), (d) association energy ($\varepsilon^{A_iB_j}/k$), (e) association volume ($\kappa^{A_iB_j}$). Pure component parameters of methanol are not shown for sets #4 and #5, and those of 1-decanol are not included in parameter set #1.

It is also noticed that different sets show quite different parameter values or trends for 1-butanol to 1-hexanol. The segment number (m) of 1-butanol is smaller than that of 1-propanol in both parameter set #1 and #2 (OrgSS). This could be attributed to the coupling of parameters, i.e. the non-association and association terms are competing to dominate the interactions, which makes the parameter fitting more difficult, e.g. more sensitive to the input data.

As expressed in equation (2.17), association energy and association volume only appear in the association strength term, which means that these two association parameters are highly coupled from a mathematical point of view. Figure 6.6 presents the relationship between the quantity $\Delta^{A_iB_j}/g^{hs}$, the combination of segment size, association energy and association volume, and temperature for ethanol and 1-octanol. Parameter set #2 (OrgSS) gives values very close to those from parameter set #1 for ethanol, while larger differences result from other parameter sets for 1-octanol. This suggests again that, as expected, the association term plays a more important role for small associating fluids than for long chain associating ones. Figure 6.6 also shows that parameter sets #4 and #5 give values very close to each other for 1-octanol, but not for ethanol. However, the quantity $\Delta^{A_iB_j}/g^{hs}$ shows, as expected, qualitative similarity as a function of temperature for all parameter sets.

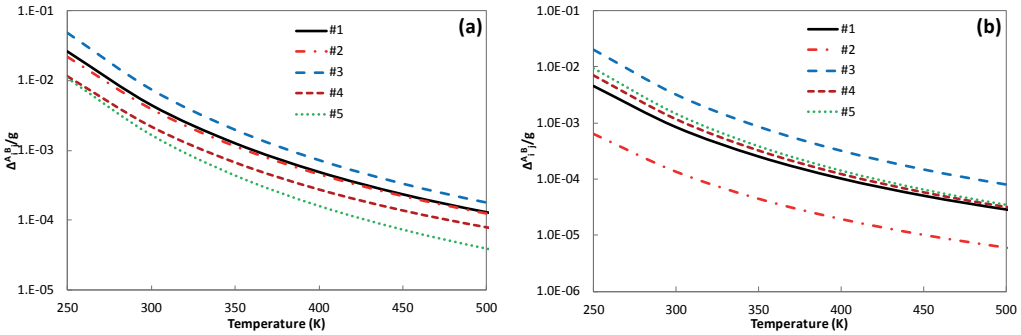

Figure 6.6 Relationships of the combinations of segment size, association energy and association volume (i.e. $\Delta^{A_iB_j}/g^{hs}$) against temperature for parameter sets (#1, #2, #3, #4, #5). (a) ethanol, (b) 1-octanol. Square dot (dense dash line), dash dot line, solid line, dash line and dot line are for parameter sets #1, #2, #3, #4 and #5 respectively.

The clear trends of pure component parameters combinations $m\sigma^3$, $m\varepsilon/k$ and $\Delta^{A_iB_j}/g^{hs}$ might provide ideas to simplify the parameter fitting procedure for a specific class of compounds. One such example was the work of Grenner et al. (2007a), in which constant association energy and

association volume values were used for all the 1-alkanols (except for methanol) in the parameter estimation. This strategy help avoiding the sensitivities of the parameter estimation to the input data when association and non-association compete to dominate the contributions, since as shown in Chapter 2, there is a unique solution for three parameters fitted to vapor pressure and liquid density. According to the investigations above, however, there would be other alternatives for the starting points and association parameters.

Table 6.6 %AAD of vapor pressure, liquid density and speed of sound from different parameter sets

C.N.[+]	Percentage Average Absolute Deviation (%AAD)														
	Vapor Pressure (P)					Liquid Density (ρ)					Speed of Sound (u)				
	#1	#2	#3	#4	#5	#1	#2	#3	#4	#5	#1	#2	#3	#4	#5
1	1.86	1.39	1.54	0.76	NA	0.53	0.22	0.58	0.10	NA	5.52	1.19	0.73	23.4	NA
2	1.01	0.37	1.15	0.38	0.86	0.55	0.13	1.00	0.69	2.23	2.44	1.56	0.8	5.04	6.83
3	1.02	0.38	2.21	0.36	0.84	1.21	0.53	0.88	0.14	1.27	4.58	1.97	0.53	2.38	2.21
4	0.97	0.41	3.65	0.30	2.30	0.78	0.75	0.94	0.64	0.89	2.14	1.80	0.90	4.27	1.86
5	0.74	0.50	3.59	0.86	3.19	0.36	0.69	1.02	0.17	0.33	2.96	2.02	1.53	4.02	7.39
6	1.74	1.45	3.97	1.49	3.55	0.50	1.85	1.36	0.30	0.23	7.38	2.56	2.60	8.76	9.56
7	2.16	2.41	2.45	1.81	2.71	2.06	0.46	2.80	2.58	2.72	7.14	4.02	3.27	8.99	11.2
8	3.43	2.59	1.29	3.33	4.07	0.56	1.27	1.81	0.40	0.38	10.4	6.64	1.95	12.3	12.4
9	1.63	3.08	1.21	1.54	2.24	0.98	1.83	0.92	0.50	1.33	12.1	9.02	1.57	14.2	13.8
10	NA	3.02	0.23	1.24	1.17	NA	1.48	1.00	0.52	0.47	NA	10.6	0.71	14.0	14.6
Avg.[*]	1.59	1.58	2.19	1.26	2.33	0.88	1.00	1.30	0.66	1.09	6.14	4.47	1.54	8.22	8.87

[+] C.N. designates Carbon Number of 1-Alkanols.

[*] Average is for ethanol to 1-decanol, since the parameter set #4 is taken from a different source.

Reference: the vapor pressure and liquid density are from DIPPR Database (2012); the speed of sound data are from Sun et al. (1991); Wilson et al. (1964), Marczak et al. (2000), Plantier et al. (2002), Dzida (2007, 2009b) and Chorazewski et al. (2013).

The %AAD of vapor pressure, liquid density and speed of sound with the different parameter sets are compared in Table 6.6. It can be seen that different parameter sets give overall comparable %AAD results in vapor pressure and liquid density. The parameter set #3 (NewUC) reproduces these two properties well, as shown in Figure 6.7. The correlations of the speed of sound in the 1-alcohols with parameter set #3 (NewUC) are quite satisfactory. However, it has difficulties in simultaneously reproducing the vapor pressure, liquid density and speed of sound for 1-butanol to

1-heptanol. Along with the observation that the association volumes of 1-butanol to 1-hexanol from parameter set #3 (NewUC) are much larger than those from other parameter sets, as shown in Figure 6.5 (e), it can be concluded that, to balance the non-association and association terms, parameterization should be carried out carefully for 1-butanol to 1-heptanol. The parameterization could be pure component parameters fitting, and/or further changes of universal constants in dispersion term or other parts of the model.

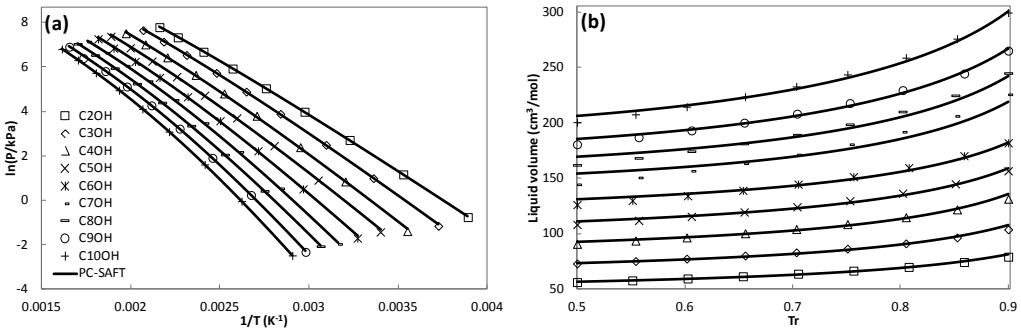

Figure 6.7 Vapor pressure and liquid volumes of saturated 1-alkanols (ethanol to 1-decanol) with new universal constant PC-SAFT (parameter set #3). Data are taken from DIPPR database (2012).

The speed of sound calculated with parameter set #3 (NewUC) shows the smallest %AAD among all sets in Table 6.6. This is further confirmed in Figure 6.8, which presents the speed of sound in methanol at four temperatures from the approaches OrgUC, OrgSS and NewUC, and the speed of sound in 1-propanol and 1-nonanol at 308.15 K, and 1-decanol at 30 MPa. The approach NewUC (parameter set #3) remarkably improves the description of speed of sound from both quantitative and qualitative points of view.

It is seen from Table 6.6 that parameter set #2 (OrgSS) gives satisfactory description of the three properties, i.e. vapor pressure, liquid density and speed of sound, for methanol, as observed by de Villiers (2011). These results are comparable to those calculated from SAFT-VR Mie model [Lafitte et al. (2007)], with one more model parameter. Similarly, the parameter sets #2 (OrgSS), #4 and #5 give acceptable deviations for these three properties of ethanol to 1-pentanol. As concluded in the work of Llovell and Vega (2006b), the association plays an important role in the derivative properties for short associating compounds. From the parameter estimation point of view, two additional parameters give significant flexibility to fit the experimental data. As shown in Table 6.6, parameter set #2 (OrgSS) yields better overall %AAD than those of parameter set #1 (OrgUC) and

parameter set #3 (NewUC) for methanol to 1-pentanol. In the Chapter 2, it has been shown that the parameters of methanol from parameter set #2 (OrgSS) could improve the description of LLE of methanol with normal hydrocarbons. These results reveal that it is possible to find a better compromise of parameters by using more inherently different constraints, for instance by putting second-order derivative properties into the parameter estimation, when there are extra parameters and they play important role, such as association energy and association volume in SAFT EOS.

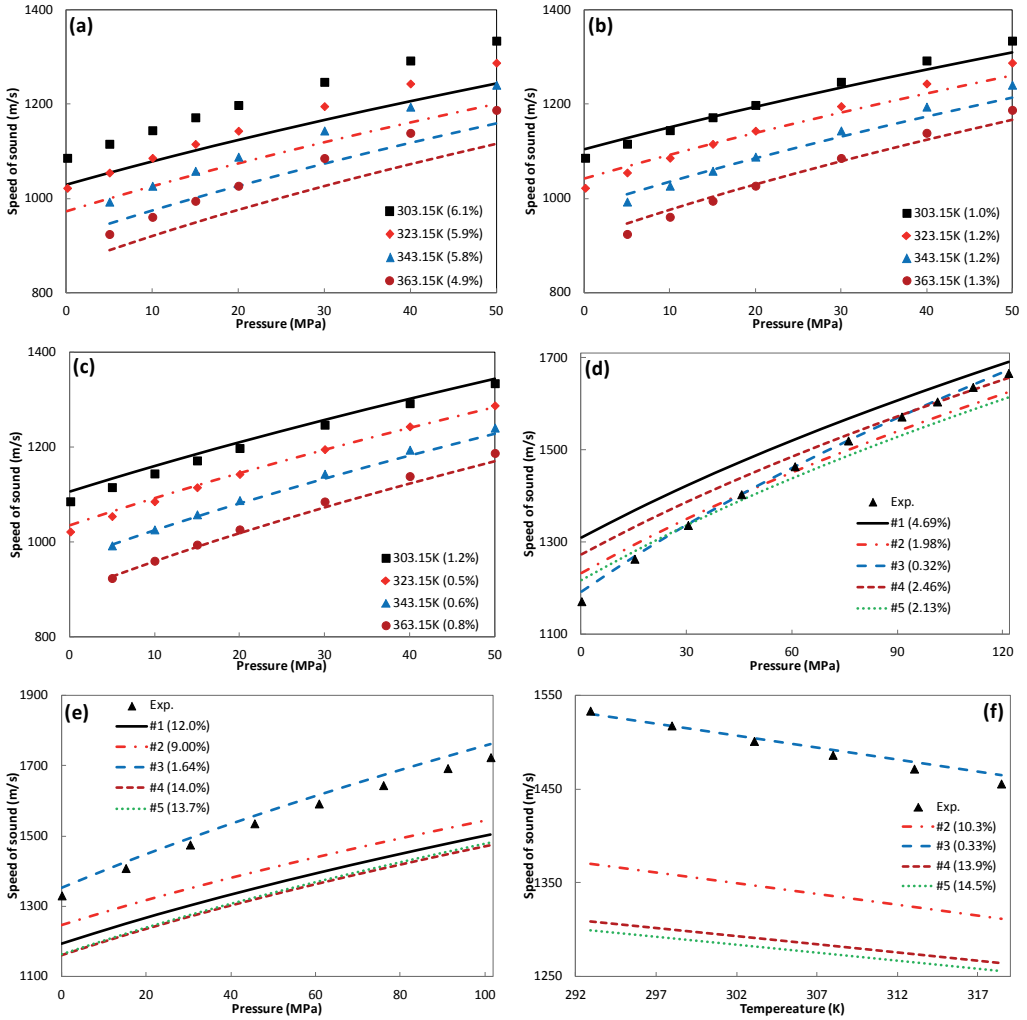

Figure 6.8 The speed of sound in methanol with parameters from different approaches, (a) OrgUC, (b) OrgSS and (c) NewUC; and the speed of sound in (d) 1-propanol at 308.15K; (e) 1-nonanol at 308.15K; (f) 1-decanol at 30 MPa with different parameters. Comparison to the experimental data from Plantier et al. (2002).

As argued by Lafitte et al. (2007), however, any theory with a certain degree of complexity including several characteristic parameters must face the presence of several local minima for the fitted parameters. The resulting values after any correlation depend to a great extent on a priori conditions imposed on the parameters, as their physical meanings and the choice of the objective functions. Hence, the values of the parameters will depend strongly on what we want to estimate and to the expected degree of accuracy. Similar discussions were reported by Avlund (2011). As shown in Figure 6.8 (d) for the speed of sound in 1-propanol, none of the sets performs correctly from a qualitative point of view, even with quite satisfactory accuracy for some sets. Moreover, the pressure dependence is not as good as what has been seen for alkanes from the qualitative point of view, which is seen for the long chain fluids as well, as presented in Figure 6.8 (e) for the speed of sound in 1-nonanol.

As listed in Table 6.6 and shown in Figure 6.5, parameter set #2 (OrgSS) is characterized by the pure component parameters that are very different from other parameter sets for 1-alkanols heavier than 1-pentanol. As shown in Figures 6.8 (e) and (f), the results also reveal that the predictions by PC-SAFT can not be improved by including the speed of sound data into the common parameter estimation procedure for considerable long chain 1-alcohols, for which the chain term becomes the dominant contribution. This is the same conclusion as we arrived to for normal hydrocarbons. This is because the dominant contribution is turned to be the chain length for long chain molecules, which is consistent with the results of Llovell and Vega (2006b).

6.4.1.3 Water

The speed of sound in saturated water has been calculated with different approaches, and the results are presented in Figure 6.9. The data show a complicated temperature dependence of the speed of sound, i.e. there is a maximum around 350K, and the results reveal that none of the approaches or models is able to capture the curvature correctly, though they could give comparable quantitative deviations. The parameters of OrgUC are taken from Diamantonis and Economou (2010), as these parameters give smallest deviation of the speed of sound in saturated water as shown in Chapter 2. The two approaches OrgSS and NewUC give similar results. As the curves intersect the data, PC-SAFT is able to satisfactorily predict the speed of sound around some specific temperature points.

The liquid-liquid equilibria of water containing systems are of high interest to this project, so the same procedure, developed for estimating water parameters by taking LLE data into account, is also

applied to the new universal constants. The speed of sound from the parameters with both original and new universal constant are quite similar, as compared in Figure 6.9 (b). The performance on phase behavior will be discussed later in this chapter.

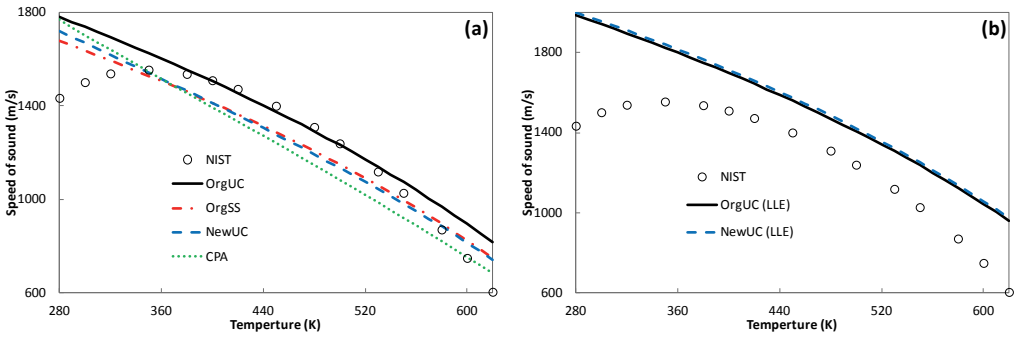

Figure 6.9 Speed of sound in saturated pure water, (a) comparison of the three approaches and CPA, and (b) comparison of parameters with LLE data in parameter estimation. The water parameters with OrgUC are taken from Diamantonis and Economou (2010), and the data are taken from NIST [REFPROP (2010)]

6.4.2 Binaries

In this work, the speed of sound in most pure fluids are used to fit the pure component parameters, so it is very demanding to test the predictive capability of the approach by applying it to mixtures.

6.4.2.1 Hydrocarbon + Hydrocarbon

The speed of sound in hydrocarbon binaries have been calculated using the original parameters and the two approaches proposed in this work. The binary mixtures cover normal hydrocarbons, cyclic hydrocarbons and aromatic hydrocarbons. The speed of sound data are, for most of the binary mixtures, measured at atmospheric pressure. The deviations are reported in Table 6.7. As an example, the speed of sound in the binary of nC6 and nC16 are presented in Figure 6.10.

It can be seen from Table 6.7 and Figure 6.10 that the approach NewUC significantly improves the description of speed of sound for all of these mixtures – deviations are more than 4 times smaller. The Figures 6.10 (a) and (b) show the speed of sound against pressure at temperature 323.15K and 373.15K, respectively. The prediction from the approach NewUC at high temperature is quite satisfactory, but it deviates from the experimental data noticeably in the nC16 rich mixtures, especially at low temperatures. While the temperature dependence of the speed of sound at different

pressures are quite similar, as shown in Figures 6.10 (c) and (d), which present the speed of sound at 5MPa and 40MPa, respectively. From the qualitative point of view, the results also show that the approach NewUC significantly improves the pressure dependence of the speed of sound to a satisfactory degree, while it does not improve the temperature dependence enough, especially in the nC16 rich ends. This might be due to the temperature dependence of the framework of PC-SAFT, which will be discussed more in the later chapter.

It is worth pointing out that the description of the speed of sound in nC6 or cC6 containing binary mixtures might be able to be slightly improved by using the experimental speed of sound data in the parameter estimation, since the speed of sound in these fluids from NIST [REFPROP (2010)] do not match the experimental data perfectly, as discussed in Chapter 5.

Table 6.7 %AADs for speed of sound in binary hydrocarbons from different approaches

Comp1	Comp2	OrgUC	OrgSS	NewUC	T range (K)	P range (MPa)	np	Ref.
nC6	nC7	11.9	11.5	1.53	298.15	0.1	11	1
nC6	nC8	12.5	11.9	1.88	298.15	0.1	11	1
nC6	nC9	13.2	12.8	2.30	298.15	0.1	11	1
nC6	nC10	13.9	13.1	2.53	298.15	0.1	11	1
nC6	nC11	14.3	13.8	2.86	298.15	0.1	11	1
nC6	nC12	14.5	14.1	2.99	298.15	0.1	11	1
nC6	nC16	14.3	13.9	2.49	298.15-373.15	0.1-70	340	2
nC7	nC12	14.2	12.5	2.05	293-318	0.1-100	485	3
nC6	Benzene	10.2	9.68	0.59	313.15	0.1	12	4
nC7	Benzene	10.9	10.5	0.59	313.15	0.1	13	4
nC8	Benzene	11.7	10.9	0.98	313.15	0.1	13	4
nC9	Benzene	12.3	11.9	1.39	313.15	0.1	13	4
nC6	Toluene	10.6	10.2	0.49	313.15	0.1	11	4
nC7	Toluene	11.4	11.2	0.64	313.15	0.1	12	4
nC8	Toluene	12.2	11.6	1.09	313.15	0.1	13	4
nC9	Toluene	12.8	12.5	1.53	313.15	0.1	12	4
cC5	Benzene	11.5	11.0	1.72	313.15	0.1	13	5
cC5	Toluene	12.0	11.7	1.75	313.15	0.1	13	5
cC6	Benzene	13.0	12.2	2.48	313.15	0.1	13	5
cC6	Toluene	13.4	12.8	2.43	313.15	0.1	13	5

Reference: (1) Tourino et al. (2004), (2) Ye et al. (1992), (3) Dzida et al. (2008), (4) Calvar et al. (2009b), (5) Calvar et al. (2009a)

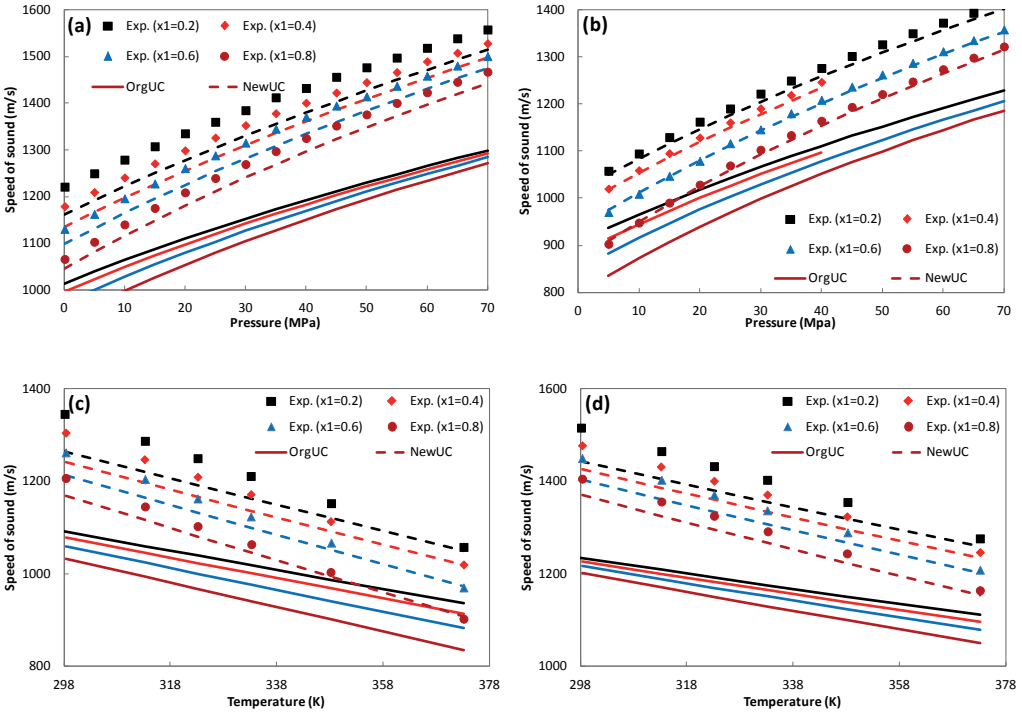

Figure 6.10 The speed of sound in the binary of nC6 and nC16 at (a) 323.15K and (b) 373.15K, (c) 5MPa and (d) 40MPa. Solid line and dash lines are from the parameters with the original and new universal constants, respectively. The experimental data are from Ye et al. (1992).

6.4.2.2 Hydrocarbon + 1-Alcohol

The prediction of the speed of sound in 29 binary systems of 1-alkanol and n-alkanes at atmospheric pressure are presented in Table 6.8. The calculations of the speed of sound in the binary systems of ethanol, 1-propanol and 1-decanol with n-heptane are performed in the temperature range of 293-318K, and pressure ranges of 0.1-91MPa, 0.1-122MPa and 15-101MPa, respectively, and the deviations at constant 1-alkanol composition are summarized in Table 6.9. The modeling results of the speed of sound in the binary mixtures of 1-alkanol and cC6 are reported in Table 6.10. All these results show that the approach NewUC (parameter set #3) considerably improves the description of speed of sound.

Table 6.8 %AADs for the speed of sound in binary systems of 1-alkanol + n-alkane [*]

1-Alcohol	n-Alkane	Deviations with different sets					T (K)	Data Points	Ref.
		#1	#2	#3	#4	#5			
C1OH	nC5	6.67	4.49	2.02	14.0	NA	298.15	12	1
	nC6	7.44	5.01	1.49	13.6	NA	298.15-318.15	54	1,2
	nC7	8.32	5.95	1.71	17.6	NA	298.15-318.15	43	1,2
	nC8	9.28	6.75	1.95	18.7	NA	298.15-318.15	42	1,2
C2OH	nC5	3.86	4.15	2.15	6.04	6.43	298.15	12	1
	nC6	4.74	4.68	1.23	6.16	6.73	298.15-318.15	56	1,2
	nC7	6.08	5.91	0.89	6.72	7.29	298.15-318.15	55	1,2
	nC8	7.41	6.80	1.13	7.53	8.14	298.15-318.15	55	1,2
C3OH	nC5	6.93	4.49	2.55	5.78	4.16	298.15	12	1
	nC6	7.23	5.04	1.68	6.19	5.00	298.15	11	1
	nC7	6.76	5.51	1.40	6.09	5.64	298.15	12	1
	nC8	7.96	6.38	1.39	7.36	6.82	298.15	11	1
C4OH	nC6	4.24	3.98	2.18	5.03	4.19	298.15-308.15	48	3
	nC8	6.38	6.32	1.32	6.6	6.74	298.15-308.15	48	3
	nC10	7.99	8.23	1.71	7.81	8.46	298.15-308.15	48	3
C6OH	nC6	6.41	3.92	2.40	7.35	7.91	298.15-308.15	48	4
	nC8	8.65	5.72	1.73	9.49	9.99	298.15-308.15	48	4
	nC10	10.2	7.43	1.91	10.9	11.4	298.15-308.15	48	4
C7OH	nC5	4.94	2.53	3.44	6.33	8.07	293.15	26	5
	nC6	6.23	3.85	2.72	7.59	9.27	293.15	27	5
	nC7	7.47	5.28	2.06	8.79	10.4	293.15	27	5
	nC8	8.37	5.93	1.71	9.67	11.3	293.15	27	5
C8OH	nC6	8.18	5.42	1.97	9.52	9.66	298.15-308.15	48	6
	nC8	10.2	7.53	1.30	11.4	11.5	298.15-308.15	48	6
	nC10	11.6	9.28	1.56	12.7	12.8	298.15-308.15	48	6
C10OH	nC6	NA	8.05	1.16	10.8	11.2	298.15-308.15	47	7
	nC7	NA	9.17	0.99	11.3	11.7	298.15-308.15	66	8
	nC8	NA	9.86	0.66	12.5	12.9	298.15-308.15	48	7
	nC10	NA	11.3	1.25	13.6	14.0	298.15-308.15	48	7
Avg. [#]		7.34	6.17	1.71	8.53	8.87	293.15-318.15	1123	

[*] All measurements are made at atmospheric pressure.

[#]Averages for parameter sets #4 and #5 cover ethanol to 1-decanol.

Reference: (1) Orge et al. (1997), (2) Orge et al. (1999), (3) Dubey et al. (2008c), (4) Dubey et al. (2008e), (5) Nath (1998), (6) Dubey et al. (2008d), (7) Dubey et al. (2008f), (8) Dzida (2009b).

Table 6.9 %AADs for the speed of sound in binary systems of C2OH, C3OH or C10OH + nC7

x1	Deviations with different sets					T range (K) & P range (MPa)	Data Points
	#1	#2	#3	#4	#5		
C2OH (1) + nC7 (2) [Dzida et al. (2005)]							
0.1214	11.6	11.3	0.95	11.3	11.4	293.0-318.2K 0.1-91MPa	90
0.2279	10.9	10.6	0.85	10.3	10.5		90
0.3054	10.4	9.98	0.75	9.42	9.75		90
0.4045	9.63	9.12	0.65	8.20	8.6		89
0.4966	9.06	8.45	0.79	7.15	7.58		90
0.7016	6.65	5.73	0.41	3.47	3.7		90
0.8123	5.18	4.05	0.31	1.71	1.58		75
0.9157	3.76	2.57	0.41	1.94	2.81		89
avg.	8.40	7.73	0.64	6.69	6.99		703
C3OH (1) + nC7 (2) [Dzida et al. (2003)]							
0.1008	11.2	11.2	0.79	11.3	11.6	293.2-318.2K 0.1-122MPa	59
0.3008	8.66	9.38	0.47	9.07	9.91		54
0.4992	5.71	7.27	0.47	6.52	8.00		54
0.6027	4.14	6.01	0.51	5.00	6.83		54
0.7016	2.91	4.8	0.57	3.82	5.67		54
0.7986	1.97	3.78	0.62	2.69	4.50		54
avg.	5.77	7.07	0.57	6.40	7.75		329
C10OH (1) + nC7 (2) [Dzida (2009b)]							
0.0111	NA	12.1	1.05	12.4	12.4	292.8-318.2K 15-101MPa	45
0.0147		12.1	0.93	12.3	12.4		43
0.0508		11.8	0.73	12.3	12.3		43
0.153		11.3	0.45	12.1	12.1		44
0.2911		10.9	0.66	12.1	12.3		43
0.5159		10.6	1.12	12.5	12.8		44
0.6924		10.5	1.17	13.0	13.4		43
0.8616		10.4	0.72	13.6	14.1		30
avg.		11.2	0.85	12.5	12.7		335

Table 6.10 The speed of sound in binary of cC6 + 1-alcohol at 303.15K and atmospheric pressure

1-Alochol	OrgUC	OrgSS	NewUC	1-Alochol	OrgUC	OrgSS	NewUC
C2OH	8.76	7.88	2.49	C3OH	8.23	7.12	2.45
C4OH	7.25	7.41	2.27	C5OH	6.9	6.21	2.11
C6OH	9.62	6.02	2.29	C7OH	9.2	6.72	2.34
C8OH	11.7	8.66	1.85	C9OH	12.5	9.8	1.76
C10OH	13.9	10.9	1.76	Experimental data are from Oswal et al. (1998)			

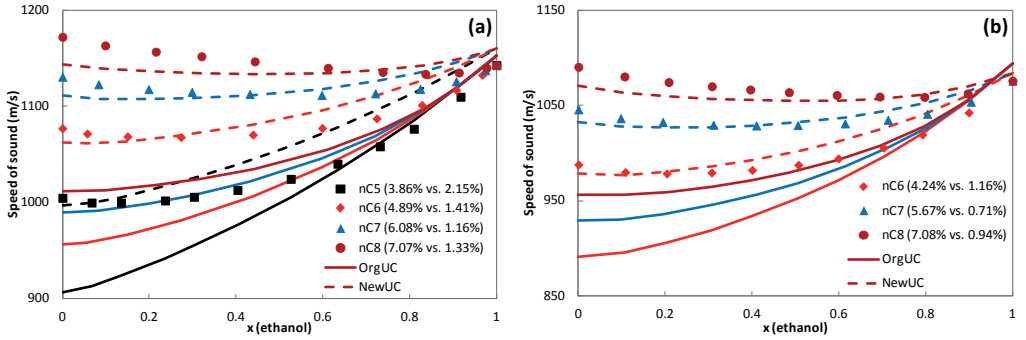

Figure 6.11 Speed of sound in the binary mixture of ethanol and n-alkanes at (a) 298.15K and (b) 318.15K. Filled square, diamond, triangle and circle markers indicate the speed of sound in nC5, nC6, nC7 and nC8, respectively (from top to bottom). Dash line and solid line represent the results from the approach OrgUC (first number in the parentheses is the corresponding %AAD) and the approach NewUC (second number in the parentheses is the corresponding %AAD), respectively. The experimental data are from Orge et al. (1997, 1999).

Figure 6.11 shows the measured and predicted speed of sound in the binary system of ethanol with n-alkanes at 298.15K (a) and 318.15K (b) at atmospheric pressure. The speed of sound results from the parameter sets using the original universal constants are qualitatively similar, as illustrated in Figure 6.8, and quantitatively comparable, as summarized in Table 6.6, so only one result from the approach OrgUC are compared with those from the new approach NewUC. Both parameter sets capture to some extent the local minimum in the variation of the speed of sound with the composition. The deviation from the approach OrgUC becomes larger as the n-alkane gets heavier, but the approach NewUC does not show the same trend. Even though there is no doubt that the approach NewUC shows better quantitative speed of sound description, it does not perform very well from a qualitative point of view. This is mainly because the approach NewUC fails to describe the speed of sound in pure ethanol and n-alkanes with high accuracy, especially in nC8.

This can be improved by the approach proposed by Khammar and Shaw (2010), which is to translate the isentropic compressibility estimation for a mixture by adding the molar average error of the pure component isentropic compressibility predicted from an EOS model, more specifically, SAFT-VR Mie in their work. This 'translation' approach was applied to the simplified PC-SAFT models with the parameters from approaches OrgUC and NewUC for the speed of sound in the binary mixtures of ethanol + n-octane, by using the correlations developed in Chapter 5. Figure 6.12 shows that this strategy works well for both appraoches. The root mean square deviations of this

system are 13.9 m/s and 3.69 m/s, respectively, for the approach OrgUC and the approach NewUC in the temperature range from 298.15 to 318.15K over the whole composition range. These deviations are comparable to the results 6.4 to 7.1 m/s reported by Khammar and Shaw (2010) for the same system under the same conditions with SAFT-VR Mie. This 'translation' strategy, however, needs experimental density and speed of sound data, or reliable correlations, of the pure substances at the same temperature and pressure as inputs, which are not always available.

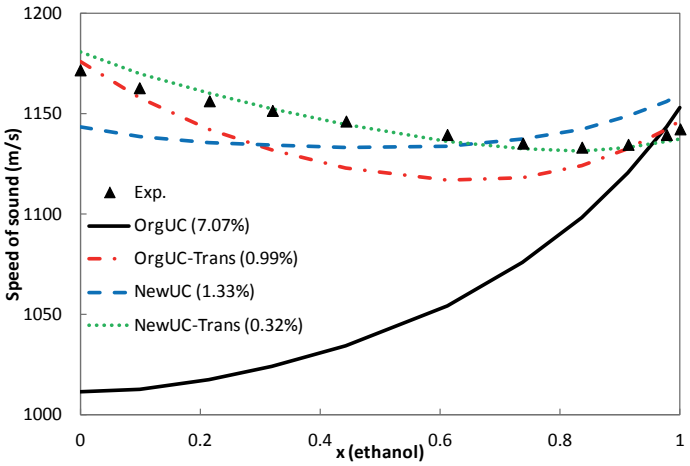

Figure 6.12 Speed of sound in the binary mixtures of ethanol + nC8 at 298.15K and 0.1MPa. The suffix '-Trans' represent the results calculated from the 'Translation' approach proposed by Khammar and Shaw (2010). The experimental data are from Orge et al. (1997).

Some typical results of the speed of sound in the binary systems of 1-propanol and 1-decanol with n-heptane at different temperature and pressure conditions are plotted in Figures 6.13 and 6.14. It is clearly seen that the approach NewUC leads to a significantly improved prediction of the speed of sound both qualitatively and quantitatively, and the improvements become more pronounced as the chain length gets longer.

By comparing Figure 6.14 with Figure 6.13, it can be seen that the approach OrgUC results in better qualitative behavior in the systems with 1-decanol than in the systems with 1-propanol, due mainly to overestimation and underestimation of speed of sound in the two pure compounds. This behavior also because to some extent the association term plays a more important role for 1-propanol, while different combining rules are used for the parameters in the association and dispersion terms.

For the speed of sound in the binary system of 1-propanol with n-heptane, as shown in Figure 6.13, the deviations from the approach NewUC become smaller as the pressure increases at constant temperature, but this is not the case for the approach OrgUC. The speed of sound in the binary system of 1-decanol with n-heptane is shown in Figure 6.14. The deviations from calculations with the approach OrgUC become smaller and those from the approach NewUC become larger as the temperature increases at constant pressure. However, the deviations do not vary very much with temperature and pressure. It can be anticipated that the approach NewUC can predict the speed of sound in other mixtures of 1-alcohols and n-alkanes with equally good accuracy.

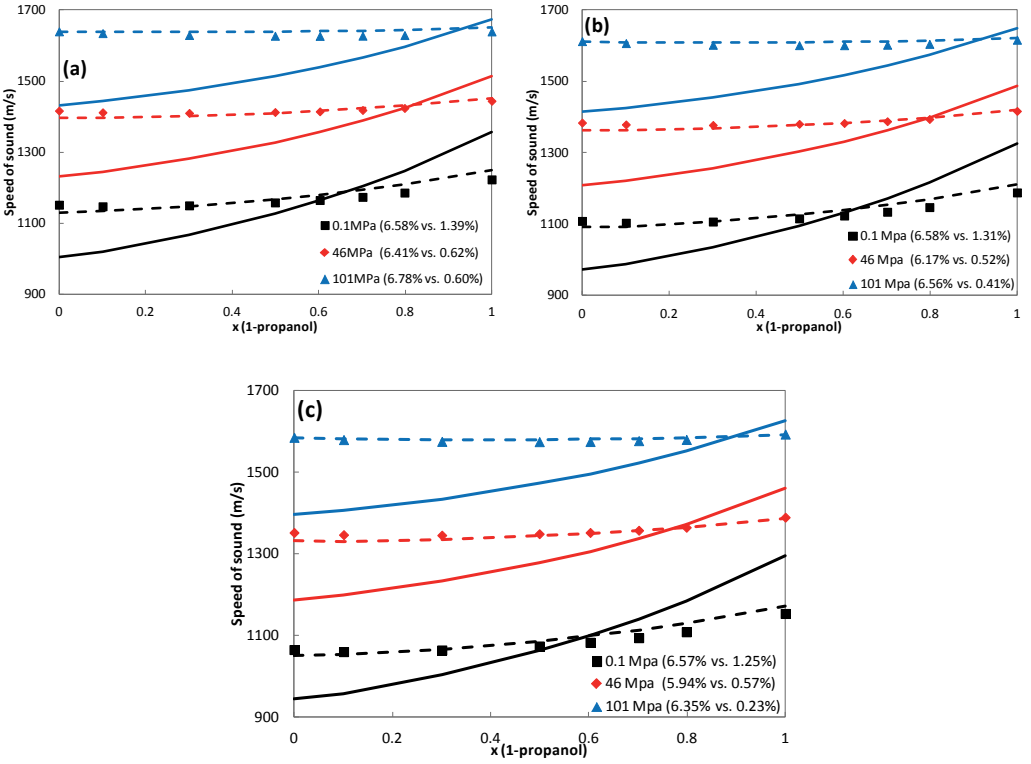

Figure 6.13 Temperature effects on speeds of sound in the binary mixtures of 1-propanol + n-heptane. (a) 293.15K; (b) 303.15K; (c) 313.15K. Filled triangle, square and circle mark indicate the speeds of sound at 0.1MPa, 46MPa and 101MPa at constant temperatures respectively (from bottom to top). Same curves and %AAD designations as Figure 6.11 are used. The experimental data are from Dzida et al. (2003).

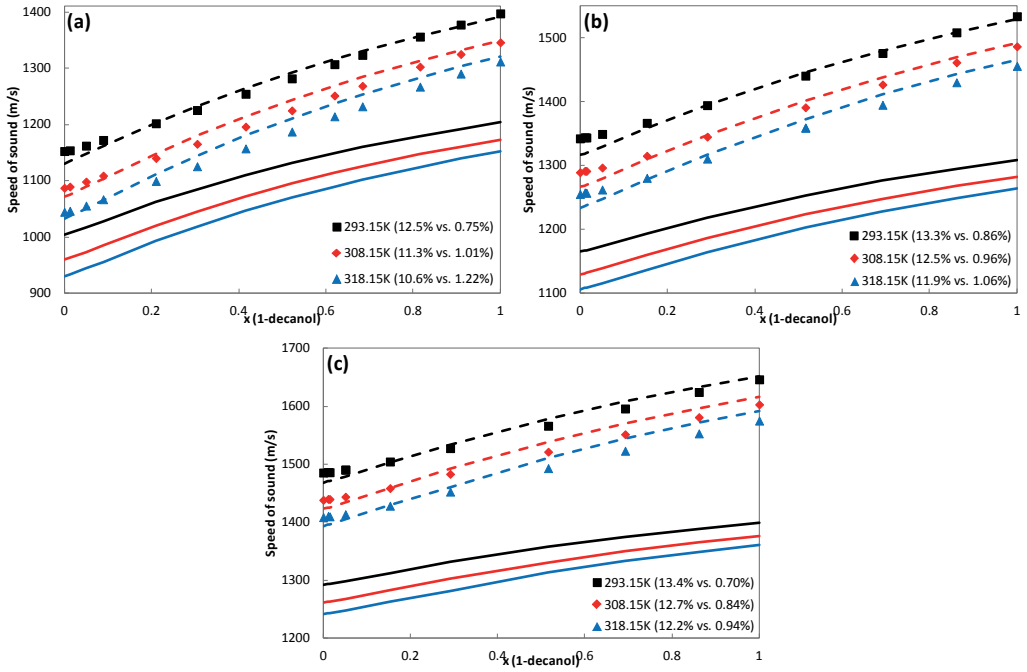

Figure 6.14 Pressure effects on speeds of sound in binary mixtures of 1-decanol + n-heptane, (a) 0.1MPa, (b) 30MPa, (c) 61MPa. Filled triangle, square and circle mark the speeds of sound at 293.15K, 308.15K and 318.15K at constant pressures respectively (from top to bottom). Same curves and %AAD designations as Figure 6.11 are used. The experimental data are from Dzida et al. (2009b).

With SAFT-VR Mie, having an extra pure component parameter, Lafitte et al. (2007) correlated vapor pressure and liquid density of saturated pure 1-alkanols from ethanol to 1-decanol with average %AAD 1.35% and 0.81%. These deviations are smaller than those from parameter sets #1, #2, #3 and #5 studied in this work. The speed of sound in binary mixtures of methanol + n-pentane, methanol + n-hexane, 1-propanol + n-pentane and ethanol + n-octane were predicted with deviations 4.07%, 4.10%, 3.45% and 4.96% respectively in the temperature range 298-318K at atmospheric pressure. The %AAD of the speed of sound in the binary mixture of ethanol + n-heptane was 1.83% in the temperature and pressure range of 293-318K and 0.1-90MPa. As seen from Tables 6.8 and 6.9, the parameter #3 (NewUC) presents smaller deviations of the speed of sound in the same systems. As discussed above, the 'translation' strategy proposed by Khammar and Shaw (2010) can be generalized to PC-SAFT as well, and even smaller deviations are obtained for the binary systems of ethanol + n-octane.

6.4.2.3 1-Alcohol + 1-Alcohol

The experimental results of the speed of sound in the binary 1-alcohol + 1-alcohol mixtures are scare. The prediction for three such binary systems from the three approaches is reported in Table 6.11. It can be seen again that the approach NewUC improves the description of speed of sound, but not as pronounced as those seen for other systems discussed above. However, it is worth pointing out that, as shown in Figure 6.15 (a), the results from the approach OrgUC are qualitatively incorrect. This is because the investigated 1-alcohols parameters with the approach OrgUC did not predict the trend of speed of sound against chain length of 1-alcohols correctly, as presented in Figure 6.15 (b). The results also suggest more investigations for the approach NewUC.

Table 6.11 Speed of sound in binary 1-alcohol + 1-alcohol at 298.15K and atmospheric pressure*

Binary	OrgUC	OrgSS	NewUC
C3OH + C6OH	4.21	3.39	2.03
C5OH + C9OH	6.45	3.57	1.47
C5OH + C10OH	7.90	4.76	0.73

*The experimental data are from Gepert et al. (2006).

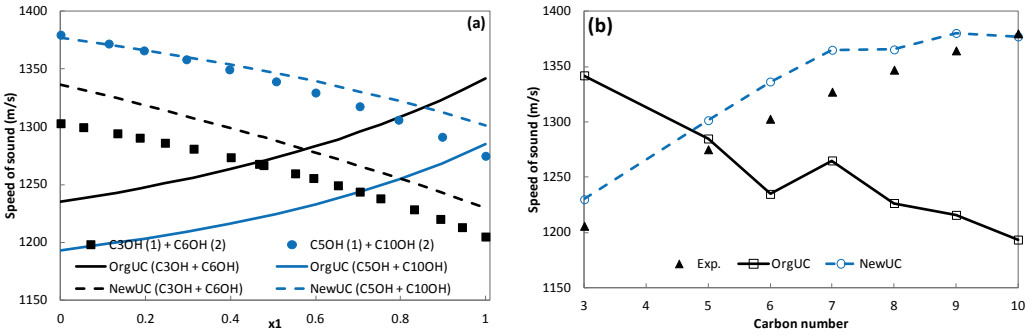

Figure 6.15 (a) The speed of sound in 1-alcohol binaries. Black and blue data and lines are speed of sound in C3OH + C6OH and C5OH + C10OH, respectively. The experimental data are from Gepert et al. (2006). (b) The speed of sound versus carbon number at 298.15K and atmospheric pressure.

6.4.3 Ternary

The speed of sound in ternary mixtures have been predicted with PC-SAFT, and the deviations are reported in Table 6.12. The approach NewUC considerably improves the description of the speed of sound in most of the systems, except in the methane rich (xC1=0.88) mixture. As shown above, the original PC-SAFT has already had good description of the speed of sound in methane.

Table 6.12 %AADs for speed of sound in ternary mixtures from different approaches

Comp1	Comp2	Comp3	OrgUC	OrgSS	NewUC	T (K)	P (Mpa)	np	Ref.
C1	C3	nC8	3.12	3.08	3.62	293.15-373.15	25-100	144	1
nC6	nC7	nC10	9.59	9.04	1.87	298.15	0.1	15	2
nC6	nC7	cC6	12.9	12.5	2.43	298.15	0.1	15	2
nC6	nC7	Tol	11.8	11.5	0.97	298.15	0.1	15	3
cC6	Ben	C5OH	7.36	6.07	1.05	298.15	0.1	41	5

Reference: (1) Lagourette et al. (1995), (2) Pandy et al. (1999), (3) Ria et al. (1989), (4) Orge et al. (1995).

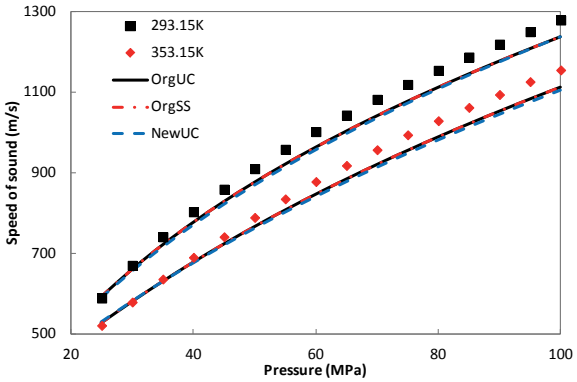

Figure 6.16 The speed of sound in the ternary mixture C1 (0.88) + C3 (0.10) + nC8 (0.02) from the three approaches. The data are taken from Lagourette and Daridon (1995).

6.4.4 Petroleum fluids

The speed of sound prediction is performed for the petroleum fluids for which basic information of composition and molecular weight, necessary for petroleum fluid characterization, is available. The composition information and the molecular weight of the plus fraction are listed in Table 6.13. Data for one condensate gas, one light oil and three heavy oils are available.

In order to calculate the speed of sound with the new universal constants, it is necessary to have characterization methods to estimate the model parameters. The petroleum fluid characterization methods discussed and developed in Chapter 3, however, are for the original PC-SAFT. Since in general the speed of sound data is not available or not measured as commonly as density, it is not straightforward to develop similar general characterization procedures for such a new model. So we propose a procedure to convert the model parameters from the original universal constants to the new ones, based on the fact that linear correlations against molecular weight are used for m and $m\varepsilon/k$ in the characterization method CM7.

(1) Calculating the differences of the parameters m and $m\varepsilon/k$ of normal hydrocarbons from the original (OrgUC) and new universal constants (NewUC);
(2) Adding these differences to the correlations of m and $m\varepsilon/k$ in the characterization method CM7;
(3) Calculating the speed of sound in normal hydrocarbons with the same molecular weight of the pseudo-component by using the correlation developed in Chapter 5;
(4) Fitting the parameter σ to the specific gravity and speed of sound.

The prediction results with both OrgUC and NewUC are presented in Table 6.14, and two examples are plotted in Figure 6.17. Different characterization methods have been tested, which show that both the number of pseudo-components and characterization methods have small impact.

Table 6.13 Molar composition and molecular weight of the plus fraction of the petroleum fluids

Comp.	mole composition (%)				
	Condensate Gas [*]	Light Oil [*]	Heavy Oil 1 [*]	Heavy Oil 2 [#]	Heavy Oil 3 [#]
N2	0.497	0.556	0.506	0.000	0.000
CO2	2.13	2.897	1.337	0.000	0.000
C1	61.886	69.129	29.96	0.000	0.000
C2	9.35	8.156	6.845	0.000	0.012
C3	5.792	4.011	5.317	0.008	0.028
iC4	0.737	0.875	0.96	0.031	0.016
nC4	2.128	1.596	2.89	0.161	0.014
iC5	0.794	0.829	1.629	0.280	0.080
nC5	1.063	0.737	1.682	0.241	0.037
C6	2.316	1.521	4.672	0.867	0.245
C7	2.349	1.755	3.208	1.131	0.927
C8	1.716	1.563	3.445	0.994	1.229
C9	1.223	1.16	3.19	1.146	0.246
C10	0.675	0.909	3.248	1.404	0.878
C11+	7.34 (Mw=275)	4.305 (Mw=237.5)	31.11 (Mw=323)	93.737 (Mw=525)	96.288 (Mw=525)

Reference: [*] Daridon et al. (1998c), [#] Plantier et al. (2008)

It can be seen that the approach OrgUC performs even better than the approach NewUC for the condensate gas, which might be because it has considerably high methane concentration, as demonstrated above. Meanwhile the predictions for live oils from the approach NewUC are reasonably acceptable. Significant improvements for the prediction of the speed of sound have been seen in the extremely heavy oils, however, the results are not satisfactory enough. This is mainly because the correction being used is based only on the difference from normal hydrocarbons (for both parameters and fitting speed of sound data), and aromatic compounds generally appear considerable amounts in the quite heavy oils. So more sophisticated characterization procedures are needed for the approach NewUC for extremely heavy oils. It is a feasible engineering solution to predict the speed of sound in condensate gas with high methane content by the original PC-SAFT EOS, and the speed of sound in other live petroleum fluids by the procedures proposed here with the new universal constants (NewUC).

Table 6.14 %AADs for speed of sound prediction in petroleum fluids

Petroleum type	%AAD of speed of sound		T Range (T)	P Range (MPa)
	OrgUC	NewUC		
Condensate Gas	3.03	5.40	273.05-373.45	40-70
Light Oil	2.96	2.97	313.15-469.15	40-120
Heavy Oil 1	11.1	1.45	273.75-413.45	16-70
Heavy Oil 2	25.7	12.4	283.15-373.15	0.1-20
Heavy Oil 3	26.5	13.4	283.15-373.15	0.1-20

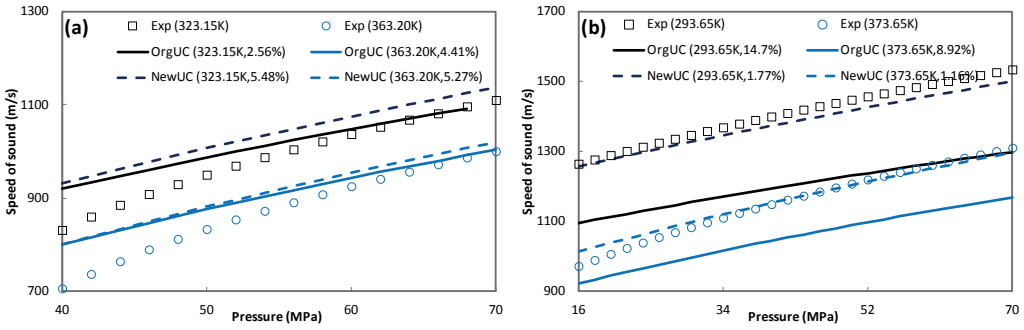

Figure 6.17 The speed of sound in the (a) condensate gas and (b) heavy oil from the two approaches OrgUC and NewUC. The data are taken from Daridon and Lagourette (1998).

6.5 Beyond speed of sound

As demonstrated above, the approach NewUC significantly improves the description of the speed of sound in various systems. Modeling speed of sound is a challenge for any equation of state, so it is demanding to investigate the possibility of simultaneous modelling the first- and second-order derivative properties within one framework, and to see what kind of price we have to pay if this is not possible. These investigations are valuable for further improvements of the framework.

6.5.1 Properties

6.5.1.1 Pure substances

In order to test the overall performance of the approach NewUC, we calculated the molar volumes, isochoric and isobaric heat capacity and the derivative of pressure with respect to volume in the same temperature and pressure ranges of speed of sound as in Table 6.1 for methane to n-decane. These properties are directly involved in the speed of sound calculation, i.e. the equations (1.7).

Table 6.15 %AADs for different properties with the approaches OrgUC and NewUC over wide temperature and pressure ranges

Alkanes	OrgUC					NewUC				
	ρ	u	C_V	C_P	dP/dV	ρ	u	C_V	C_P	dP/dV
C1	0.99	2.36	3.42	1.36	3.62	1.2	2.52	3.40	1.99	5.82
C2	1.74	5.80	4.77	1.23	4.76	1.85	3.69	5.05	3.65	11.15
C3	1.44	7.95	5.24	1.43	9.32	2.33	3.55	5.54	4.28	10.9
C4	1.40	7.66	4.91	1.44	9.47	2.23	3.32	4.76	3.37	9.72
C5	1.11	8.18	4.38	1.06	11.1	2.10	3.51	4.15	3.17	8.27
C6	1.35	7.92	3.82	1.25	10.4	2.14	2.99	3.48	3.14	8.82
C7	1.29	9.34	3.22	1.06	13.6	2.21	3.47	2.86	3.74	7.48
C8	1.31	8.40	1.99	0.82	12.0	1.69	2.69	1.70	3.43	6.59
C9	1.73	9.69	2.73	0.89	13.0	2.02	2.91	2.26	3.86	5.80
C10	1.63	10.12	2.60	0.96	14.5	2.10	3.93	2.13	3.62	5.39
Avg.	1.40	7.74	3.71	1.15	10.2	1.99	3.26	3.53	3.43	7.99

Reference: the data are from NIST [REFPROP (2010)].

As shown in Table 6.15, the approach NewUC improves the speed of sound and the derivative of pressure with respect to volume while deteriorating the molar volume and isobaric heat capacity. Both models give comparable isochoric heat capacity, which reveals that the new approach does have impact on the derivatives of Helmholtz free energy with respect to the volume, but less so on

the derivatives with respect to the temperature. It is worth noticing that the approach OrgUC describes the isobaric heat capacity for hydrocarbons quite well, but it can be shown that that the new approach gives comparable isobaric heat capacity results as SAFT-VR Mie [Lafitte and Bessieres (2006)], as reported in Table 6.16.

Table 6.16 %AADs for isobaric heat capacity from different models

Comp.	OrgUC		NewUC		SAFT-VR Mie		T range (K)	P range (MPa)
	C_P	C_P^r	C_P	C_P^r	C_P	C_P^r		
nC6 *	0.51	2.23	4.29	18.5	5.40	22.8	298.15-403.15	10-100
nC12 #	0.45	2.11	6.61	31.1	6.78	31.2	313.15-373.15	0.1-100
nC13 +	0.39	1.85	6.55	30.9	7.01	32.2	313.15-373.15	0.1-100

Reference: * Randzio et al. (1994), # Bessieres et al. (2000a), + Bessieres et al. (2000b)

6.5.1.2 Density of hydrocarbon + alcohol

The liquid density in 29 binary systems of 1-alkanol and n-alkanes are calculated at atmospheric pressure by the same various parameter sets, as done for the speed of sound above. The results are presented in Table 6.17.

It can be readily seen that the approach NewUC (parameter set #3) gives noticeably worse liquid density than the other parameter sets for the systems containing heavy 1-alkanols. The main reason is that, as illustrated in Figure 6.7 (b), the deviations of liquid density of pure 1-alkanols get larger at lower temperatures. However, the model accuracy for the liquid density of the systems containing light 1-alkanols is quite satisfactory. The parameter sets #4 and #5 show overall comparable accuracies of liquid density and speed of sound.

6.5.2 Phase behavior

6.5.2.1 VLE of hydrocarbon + alcohol

Vapor-liquid equilibria (VLE) of 35 binary systems of 1-alkanols and n-alkanes with total 1533 experimental data points were calculated in a predictive manner (i.e. binary interaction parameter k_{ij}=0) over the temperature range from 273 to 493K. The %AADs for the saturation pressure are summarized in Table 6.18. It can be seen that in general the prediction results are reasonably satisfactory with deviations lower than 10% for most of the systems.

Table 6.17 %AADs for liquid densities of the binary systems of 1-alkanol + n-alkane*

n-Alkanols	n-Alkanes	Deviations with different sets					T (K)	Data Points	Ref.
		#1	#2	#3	#4	#5			
C1OH	nC5	0.88	0.46	0.74	1.33	NA	298.15	12	1
	nC6	0.59	0.82	0.32	1.29	NA	298.15-318.15	54	1,2
	nC7	0.68	0.93	0.32	1.05	NA	298.15-318.15	43	1,2
	nC8	0.59	1.17	0.73	0.79	NA	298.15-318.15	42	1,2
C2OH	nC5	0.95	0.29	0.97	0.70	1.24	298.15	12	1
	nC6	0.72	0.69	0.54	0.49	0.94	298.15-318.15	56	1,2
	nC7	1.01	1.11	0.50	0.81	1.26	298.15-318.15	55	1,2
	nC8	0.97	1.50	0.71	0.80	1.2	298.15-318.15	55	1,2
C3OH	nC5	1.12	0.40	0.50	0.63	1.01	298.15	12	1
	nC6	0.95	0.76	0.23	0.42	0.8	298.15	11	1
	nC7	1.17	1.06	0.24	0.65	0.99	298.15	12	1
	nC8	1.15	1.4	1.01	0.62	0.94	298.15	11	1
C4OH	nC6	1.11	1.12	0.82	0.27	0.63	298.15-308.15	48	3
	nC8	1.15	1.65	1.48	0.39	0.69	298.15-308.15	48	3
	nC10	1.27	1.69	2.13	0.57	0.83	298.15-308.15	48	3
C6OH	nC6	0.43	1.46	1.70	0.34	0.26	298.15-308.15	48	4
	nC8	0.45	1.6	2.32	0.38	0.30	298.15-308.15	48	4
	nC10	0.50	1.55	2.89	0.44	0.40	298.15-308.15	48	4
C7OH	nC5	0.77	0.63	3.35	0.56	0.54	293.15	26	5
	nC6	0.71	0.59	3.87	0.50	0.30	293.15	27	5
	nC7	0.68	0.71	3.93	0.49	0.45	293.15	27	5
	nC8	0.64	0.87	4.61	0.45	0.33	293.15	27	5
C8OH	nC6	0.23	1.40	2.56	0.27	0.44	298.15-308.15	48	6
	nC8	0.28	1.50	3.14	0.31	0.46	298.15-308.15	48	6
	nC10	0.39	1.43	3.64	0.42	0.56	298.15-308.15	48	6
C10OH	nC6	NA	1.42	2.71	0.42	0.26	298.15-308.15	47	7
	nC7	NA	1.56	2.72	0.61	0.48	298.15-308.15	28	8
	nC8	NA	1.47	3.20	0.45	0.29	298.15-308.15	48	7
	nC10	NA	1.41	3.67	0.49	0.37	298.15-308.15	48	7
Avg.#		0.78	1.13	1.92	0.50	0.64	293.15-318.15	1085	

* The measurements are made at atmospheric pressures.

Averages for parameter sets #4 and #5 cover ethanol to 1-decanol.

Reference: (1) Orge et al. (1997), (2) Orge et al. (1999), (3) Dubey et al. (2008c), (4) Dubey et al. (2008e), (5) Nath (1998), (6) Dubey et al. (2008d), (7) Dubey et al. (2008f), (8) Sastry et al.(1996c).

Table 6.18 Prediction of vapor-liquid equilibria of the binary systems of 1-alkanol + n-alkane

1-Alkanol	n-Alkane	Deviations with different sets					T range (K)	Data Points	Ref.
		#1	#2	#3	#4	#5			
C1OH	C3	28.1	26.1	27.5	19.1	NA	310.7-373.15	55	1,2
	nC5	9.02	7.39	8.61	2.39	NA	372.7- 422.6	33	3
	nC6	11.3	10.1	10.8	4.80	NA	293.15- 333.15	74	4
C2OH	nC5	13.9	12.9	15.2	12.4	8.72	273.15-303.15	47	4
	nC6	6.39	5.55	6.22	6.20	3.55	298.15-333.15	50	4
	nC7	6.84	5.48	7.40	6.14	2.78	303.15-343.15	92	4
	nC8	7.12	6.46	7.95	6.35	3.66	313.15-348.15	56	4
	nC9	6.14	5.21	6.09	4.70	2.47	343.15	27	4
C3OH	nC6	5.09	5.31	3.91	2.83	4.77	298.15-313.15	36	4
	nC7	5.90	5.35	5.71	3.27	5.44	278.16-333.15	54	4,5
	nC8	6.17	6.80	5.33	3.34	5.44	313.15-363.15	63	4
	nC9	6.49	6.89	5.55	3.73	5.69	333.15-363.15	47	4
	nC11	8.70	8.64	6.87	4.88	8.14	333.15-353.15	34	4
C4OH	nC4	12.0	9.13	3.59	10.9	10.9	333.01-493.28	145	6
	nC5	6.99	6.73	8.37	3.16	6.71	303.15	15	4
	nC6	6.14	5.75	4.24	5.45	5.34	288.15-333.15	87	7,8
	nC7	7.24	5.71	4.90	6.72	7.34	313.15-363.15	69	4
	nC8	5.01	9.27	3.58	4.81	6.51	283.16-308.09	52	4,9
	nC10	4.73	4.79	5.15	4.64	5.72	358.15-388.15	42	4
C5OH	nC5	5.21	4.14	10.8	6.30	6.99	303.15	15	4
	nC6	7.17	6.72	8.47	7.73	7.61	303.15-323.15	30	4
	nC7	6.66	5.73	4.75	6.42	5.32	313.15- 368.15	65	4
	nC8	6.84	8.42	3.85	6.56	5.53	313.15-373.15	30	4
	nC10	5.19	5.81	3.93	4.81	3.54	363.27	13	4
C6OH	nC6	5.69	6.73	5.02	5.34	4.99	298.23-342.82	33	4
C8OH	nC6	5.83	8.06	5.01	4.09	3.81	313.15-333.15	34	4
	nC7	4.32	5.83	6.84	3.19	3.10	293.15-313.15	48	4
	nC8	8.77	11.1	3.72	6.55	6.06	373.15-383.15	27	10
	nC10	8.21	9.72	3.69	6.21	6.05	373.15-413.15	64	4,11
	nC11	10.7	12.0	6.87	9.08	9.29	393.15-413.15	32	4
	nC12	10.2	11.1	6.64	8.67	9.20	393.15-413.15	32	4
C10OH	nC6	NA	5.74	7.51	3.67	3.64	283.15- 323.15	32	4
avg.		7.13	7.28	6.11	5.80	5.80	273-493	1533	

Reference: (1) Galivel-Solastiouk et al. (1986), (2) Lev et al. (1992), (3) Wilsak et al. (1987), (4) Góral et al. (2002), (5) Lee et al. (1967), (6) Deak et al. (1995), (7) Rodriguez et al. (1993), (8) Heintz et al. (1986), (9) Gracia et al. (1992), (10) Plesnar et al. (1988), (11) Plesnar et al. (1989).

The predictions with parameter sets #3 (NewUC), #4 and #5, for which the same pure component experimental vapor pressure data is used in the parameter estimation, are generally giving lower %AAD than those with parameter set #1 from Gross and Sadowski (2002). However, this does not mean that one of the parameter sets performs clearly better than the others for all systems.

It is shown from Table 6.18 that the parameter set #4 of methanol from Avlund (2011) gives much better VLE results, while it performs worse for both speed of sound and liquid density as reported in Tables 6.8 and 6.17.

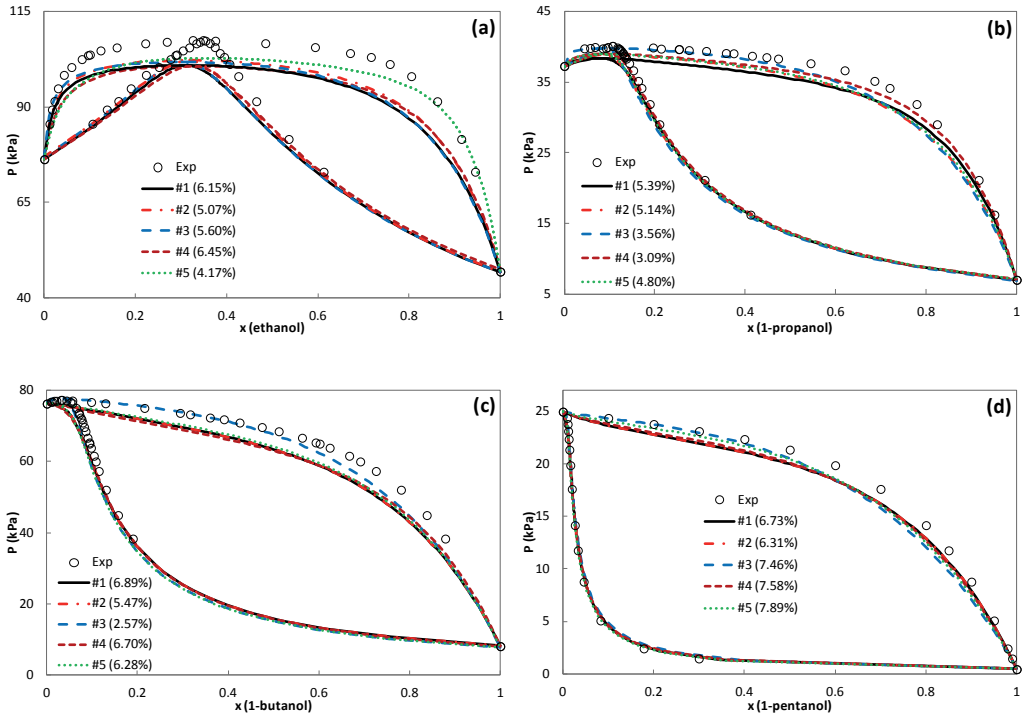

Figure 6.18 Predictions of vapor-liquid equilibria of 1-alcohols and n-hexane with parameters fitted in different ways. (a) ethanol at 333.15K [Góral et al. (2002)]; (b) 1-propanol at 313.15K [Góral et al. (2002)]; (c) 1-butanol at 333.15K [Rodriguez et al. (1993), Heintz et al. (1986)]; (d) 1-pentanol at 303.15K [Góral et al. (2002)].

Some typical VLE (Pxy) diagrams of 1-alkanols with n-hexane are given in Figure 6.18. Parameter set #5 shows much better results for the system of ethanol with n-hexane at 333.15K especially on the ethanol rich side, as shown in Figure 6.18 (a). It is shown in Figure 6.18 (b) that the parameter sets #3 (NewUC) and #4 perform better for the systems of 1-propanol with n-hexane at 313.15K, on

the n-hexane rich side and the 1-propanol rich side, respectively. For the VLE of 1-butanol with n-hexane at 333.15K in Figure 6.18 (c), parameter set #3 (NewUC) shows much better results in the whole composition range. The parameter sets #1 and #2 have slightly overall smaller deviations for the system of 1-pentanol with n-hexane at 303.15K, as seen from Figure 6.18 (d). However, they do not show better performance on the n-hexane rich side.

Figure 6.19 presents some example VLE (*Px*) diagrams of 1-octanol with nC7, nC8 and nC12 in wide ranges of temperature. It can be seen that parameter set #3 (NewUC) captures the non-ideality better than the other sets, especially for systems with long chain n-alkanes, while the predictions from the parameter sets #1, #4 and #5 get worse when the corresponding n-alkanes become heavier, where a binary interaction parameter is necessary. The parameter set #2 (OrgSS) performs worst, though it matches the ending points, i.e. the vapor pressures of pure fluids, equally well.

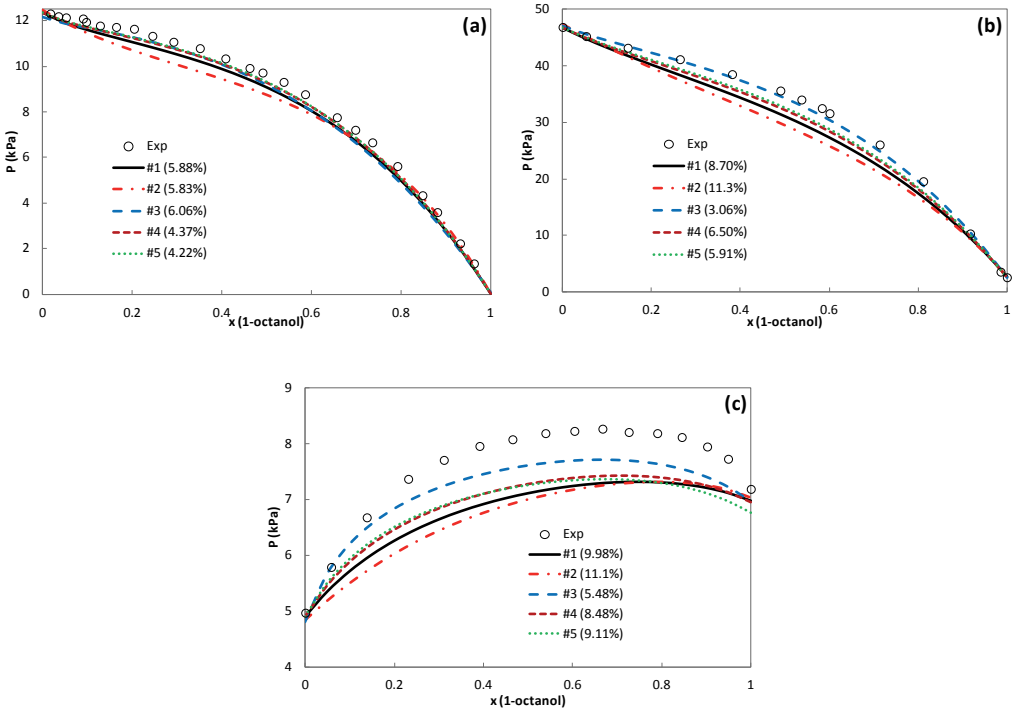

Figure 6.19 Predictions of vapor-liquid equilibria of the binary systems of 1-octanol and n-alkane with different parameters. (a) n-heptane at 313.15K [Góral et al. (2002)]; (b) n-octane at 373.15K [Plesnar et al. (1988)]; (c) n-dodecane at 393.15K [Góral et al. (2002)].

The parameter sets #4 and #5 show overall comparable predictions of the VLE, liquid density and speed of sound of the binary mixtures of 1-alcohols and normal hydrocarbons. This could be explained by the fact that they are fitted to the same experimental data. These observations reveal that it is possible to perform the pure component parameter fitting in a dimension-reduced space for a regular compound series during parameter estimation. For example, Grenner et al. (2007a) and Llovell et al. (2006b) used constant association energy and association volume for all of the 1-alkanols (except for very short molecules) to obtain the pure component parameters.

6.5.2.2 Water containing systems

As discussed in Chapter 2, water is a unique molecule, and it is not an easy task to model water with any thermodynamic model. The same procedure of fitting water parameters developed in Chapter 2 is applied to the new universal constants. The correlation results of the liquid-liquid equilibira of water with nC8 and with cC6 are presented in Figure 6.20. These two sets of the universal constants have almost identical correlation capability.

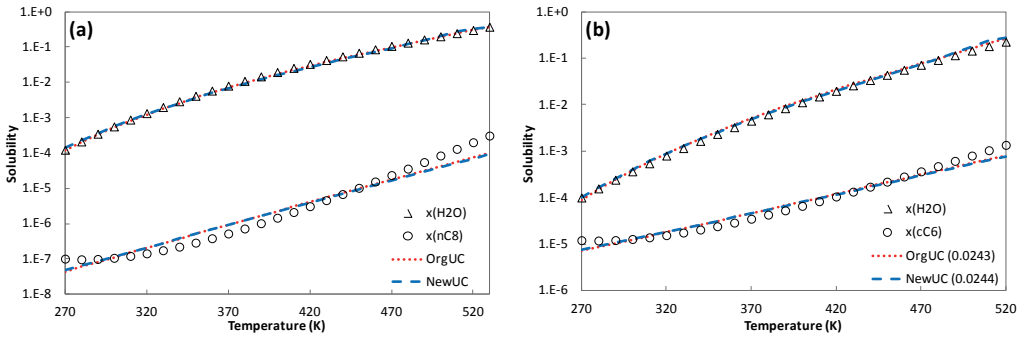

Figure 6.20 Correlations of the liquid-liquid equilibria of (a) water with nC8 and (b) water with cC6 from the approaches OrgUC and NewUC. The experimental data are from Tsonopoulos et al. (1983, 1985).

The prediction and correlation of the phase behavior of water and 1-alochols, as done in Chapter 2, are performed with the approach NewUC as well. The results are compared to those from the approach OrgUC in Table 6.19. The results show that these two approaches OrgUC and NewUC have comparable results, which is mainly due to the robustness of the association framework. It is worth pointing out that the vapor phase correlation of water + 1-butanol mixture from the approach NewUC is not satisfactory, which is mainly due to the poor performance for the vapor pressure description of pure 1-butanol, as shown in Table 6.6.

Table 6.19 VLE and VLLE of water with 1-alcohols from the approaches OrgUC and NewUC

Approach	dP (%) dT (K)	%AAD of x (H_2O)			k_{ij}	dP (%) dT (K)	%AAD of x (H_2O)		
		vapor	water	alcohol			vapor	water	alcohol
Methanol (T=298.15-373.15K) [Butler et al. (1933), Griswold et al. (1952)]									
OrgUC	32.0	11.1			-0.0852	3.62	1.01		
NewUC	26.7	7.39			-0.0847	2.38	1.42		
Ethanol (T=298.14-363.15K) [Phutela et al. (1979), Kurihara et al. (1995), Pemberton et al. (1978)]									
OrgUC	16.5	6.34			-0.0532	1.46	0.47		
NewUC	18.0	6.84			-0.0581	1.34	0.51		
1-Propanol (at atmospheric pressure) [Udovenko et al. (1972)]									
OrgUC	3.66	5.29			-0.0287	0.85	1.86		
NewUC	3.29	5.82			-0.0296	0.52	1.41		
1-Butanol (at atmospheric pressure) [Boublik (1960), Sørensen et al. (1995)]									
OrgUC	5.96	9.22	1.64	61.3	-0.0585	0.85	2.40	6.31	4.15
NewUC	5.11	8.11	1.59	59.1	-0.0597	2.36	2.99	5.36	3.44
1-Pentanol (at atmospheric pressure) [Beregovykh et al. (1971), Sørensen et al. (1995)]									
OrgUC	3.82	7.09	1.62	56.8	-0.0518	2.65	2.05	2.52	2.82
NewUC	8.44	10.1	0.35	46.9	-0.0640	0.70	1.58	0.92	8.35

6.6 Conclusions

In this work, firstly, the performance of the SRK, CPA and PC-SAFT EOS is evaluated for the speed of sound in normal alkanes. The results reveal that (1) none of the models could describe the speed of sound with satisfactory accuracy, over wide ranges of temperature, pressure and chain-length; (2) fitting parameters to experimental data could improve the description of the speed of sound for chain molecules, i.e. CPA performs better than SRK; (3) PC-SAFT is superior to SRK and CPA from both the accuracy and the curvature points of view over wide pressure ranges due to its theoretically more sound physical term. This indicates that the functional form of the model is more important than the parameter fitting strategy.

Secondly, the PC-SAFT model was chosen as the starting point to develop approaches for modeling speed of sound. The first approach is to include the speed of sound data into pure component parameters. The second approach is to integrate the speed of sound data into both the universal constants regression and the pure component parameters estimation. The new universal constants

regression was based on the data of saturated methane to decane. As the original parameters of normal hydrocarbons, the new ones exhibit good linear correlation functions for m, $m\sigma^3$ and $m\varepsilon/k$ against molecular weight due to the same framework. These two approaches have been applied to model the speed of sound in pure hydrocarbons, pure 1-alcohols, pure water, binary mixtures of hydrocarbons, binary mixtures of hydrocarbon + 1-alcohol, ternary mixtures and petroleum fluids.

The first approach could not improve the description of speed of sound for normal alkanes and heavy 1-alcohols, even at the cost of accuracy loss for vapor pressure and liquid density, but it does improve the speed of sound description for the short 1-alcohols, for which the association term plays an important role, from the quantitative point of view. This is mainly due to the significant improvements of the flexibility of parameter estimation with two extra parameters. As discussed in Chapter 2, the parameters with speed of sound data in estimation could improve the description of the liquid-liquid equilibria of methanol with normal hydrocarbons, which reveals that better compromise might be obtained by putting the second derivative properties into the parameter estimation if there are extra fitting parameters, i.e. association energy and volume here, when the association term plays an important role.

The second approach significantly improves the description of the speed of sound in most of the defined systems except for methane rich fluids and water, from both qualitative and quantitative points of view. For the methane rich fluids, the original PC-SAFT has already had good description of the speed of sound in methane, but it has to be pointed out that it is possible to have alternatives to offer better description of speed of sound in such fluids. The current PC-SAFT framework, however, is ***not*** able to model the speed of sound in water in wide temperature and pressure ranges, because the temperature dependence is complex. In this project, general petroleum fluid characterization methods have been developed for the original PC-SAFT EOS, but it is still far away to have such procedures for the new universal constants. This is because the speed of sound data is not available as commonly as density, which is necessary to characterize the model parameters with the new universal constants. A simple conversion procedure is proposed to connect the model parameters of the pseudo-components from the original PC-SAFT EOS to the new universal constants. It shows considerably improvements for the description of the speed of sound in heavy oils, but the results are not satisfactory enough for extremely heavy oils.

The new universal constants have been applied to model the phase equilibria of the binary systems containing n-alkanes, 1-alkanols and water, in which VLE, LLE and VLLE are covered. In general,

comparable results are obtained as those given by the original universal constants. This fact reveals that it is possible to have simultaneously satisfactory description of phase equilibria and speed of sound within the same PC-SAFT framework.

The two sets of universal constants present similar isochoric heat capacity results for the considered normal hydrocarbons, which show that the second approach has little impact on the derivatives of residual Helmholtz free energy with respect to temperature. However, the new universal constants perform less satisfactorily than the original ones for the isobaric heat capacity for the investigated normal hydrocarbons. The new universal constants have difficulties in simultaneously describing the vapor pressure, liquid density and speed of sound in the associating fluids with chain length around m=3, and they also have difficulties in reproducing the liquid density for both associating and non-associating long chain fluids. The results indicate that more systematic research needs to be done in the universal constants regression, if excellent accuracy in both first- and second-order derivative properties is desired.

The pure component parameters from different sources, fitted in different ways, are investigated with the original universal constants for 1-alcohols. They perform differently for specific systems, but they present overall comparable performance in terms of describing vapor-liquid equilibria, liquid densities, speed of sound for various systems in wide ranges of temperature and pressure. The results confirm that it is possible to use generalized parameter estimation schemes for 1-alcohols, but they also suggest that further systematic studies are needed.

Lastly, an important message from this chapter is that ***changing the universal constants is possible***!

Chapter 7. A new variant of the Universal Constants

As a popular and promising model, the PC-SAFT EOS has been applied into many different fields, including chemicals, polymers, biochemicals, pharmaceuticals, and so on. It has also been shown in the previous chapters that the PC-SAFT EOS is capable of modeling the phase behavior of oil and water containing systems, if appropriate parameters could be found for both well- and ill-defined systems. The PC-SAFT EOS has, however, been criticized for some numerical pitfalls especially during the recent years.

The purposes of this chapter are (1) to analyze the temperature and volume dependence of the PC-SAFT EOS in a somehow deterministic way; (2) to propose a new variant of universal constants which can avoid the numerical pitfalls; (3) to compare the universal constant sets and to investigate the possibility of using the original PC-SAFT parameters with the new universal constant set.

7.1 Introduction

As denoted by its name, the dispersion term of the PC-SAFT EOS is a perturbation for hard chains instead of hard spheres, but in fact it is represented by the interaction energy fitted to the real fluids in the form of 6^{th} degree polynomials of reduced density. There are in total 42 empirical coefficients in these 6^{th} degree polynomials, which are the so-called universal constants. In Chapter 6, the universal constants are readjusted because the original ones could not provide satisfactory correlation and/or prediction for the speed of sound in most systems, even with the pure component parameters fitted to the speed of sound data. The universal constants were obtained by including the vapor pressure, liquid density and speed of sound data of saturated methane to decane in the regression.

On one hand, it has been found that these new universal constants improve the description of the speed of sound in most systems from both qualitative and quantitative points of view, while keeping satisfactory description of phase equilibrium. Very recently, Polishuk et al (2013) have found that the universal constants, developed in our previous work, could practically avoid the numerical pitfalls of the additional fictitious critical point of the pure components.

On the other hand, it has also been found that these new universal constants perform worse for the density of long chain fluids and isobaric heat capacity. Polishuk showed, in a later article (2014), that these new universal constants give poor prediction for virial coefficients, even negative third virial coefficients at high temperatures. Moreover, it is not convenient to develop general characterization procedures for modeling ill-defined systems, e.g. petroleum fluids, since speed of sound used in the parameter estimation. Equally importantly, unrealistic phase behavior can be predicted by the original PC-SAFT EOS. All these inspired us to revisit the fundamentals of this model.

7.2 Analysis of the Original PC-SAFT EOS

7.2.1 Temperature and density dependences

The PC-SAFT EOS can be expressed as:

$$a^r = a^{hc} + a^{disp} = \left(a^{hs} + a^{chain}\right) + a^{disp} \tag{7.1}$$

If it is assumed, for a given temperature and density, that the reduced residual Helmholtz free energy can be calculated from a well-established model, for instance from NIST reference equations [REFPROP (2010)], and the hard-sphere chain contribution is calculated from PC-SAFT, the reduced dispersion term can be calculated:

$$a^{disp} = a^r - a^{hc} \tag{7.2}$$

First, the following variables are introduced for easy mathematic manipulations.

$$Q = a^{disp} = a^r(NIST) - a^{hc}(PCSAFT) \tag{7.3}$$

$$QV = \frac{\partial a^{disp}}{\partial (V/R)} = -\frac{P^r(NIST)}{T} - \frac{\partial a^{hc}}{\partial (V/R)}(PCSAFT) \tag{7.4}$$

$$QVV = \frac{\partial^2 a^{disp}}{\partial (V/R)^2} = -\frac{dPdV(NIST)}{T/R} - \frac{\partial^2 a^{hc}}{\partial (V/R)^2}(PCSAFT) \tag{7.5}$$

Furthermore, a new function F is defined as:

$$F = \left\{(-12I_1) \times \left(m^2 \frac{\varepsilon}{kT}\sigma^3\right) + (mC) \times (-6I_2) \times \left[m^2 \left(\frac{\varepsilon}{kT}\right)^2 \sigma^3\right]\right\} \tag{7.6}$$

Where the constant factor $\left(\frac{\pi}{6}\frac{N_A}{R}\right)$ is ignored here, so

$$Q = \frac{1}{V/R}F \tag{7.7}$$

$$QV = \frac{\partial Q}{\partial (V/R)} = \frac{1}{V/R}\left(\frac{\partial F}{\partial \eta}\frac{\partial \eta}{\partial (V/R)} - \frac{F}{V/R}\right) = \frac{1}{(V/R)}\left(\frac{\partial F}{\partial \eta}\frac{\partial \eta}{\partial (V/R)} - Q\right) \tag{7.8}$$

$$QVV = \frac{\partial^2 Q}{\partial (V/R)^2} = \frac{1}{(V/R)}\left(\frac{\partial^2 F}{\partial \eta^2}\left(\frac{\partial \eta}{\partial\, V/R}\right)^2 + \frac{\partial F}{\partial \eta}\frac{\partial^2 \eta}{\partial (V/R)^2} - 2 \times QV\right) \tag{7.9}$$

Then,

$$F = (V/R) \times Q \tag{7.10}$$

$$\frac{\partial F}{\partial \eta} = \{(V/R) \times QV + Q\} \times \left(\frac{\partial \eta}{\partial (V/R)}\right)^{-1} \tag{7.11}$$

$$\frac{\partial^2 F}{\partial \eta^2} = \left\{(V/R) \times QVV - \frac{\partial F}{\partial \eta}\frac{\partial^2 \eta}{\partial (V/R)^2} + 2 \times QV\right\} \times \left(\frac{\partial \eta}{\partial\, V/R}\right)^{-2} \tag{7.12}$$

If F is further formulated as:

$$F = F_A SS_1 + F_C F_B SS_2 \tag{7.13}$$

$$F_A = (-12I_1),\ SS_1 = \left(m^2 \frac{\varepsilon}{kT}\sigma^3\right) \tag{7.14}$$

$$F_C = (mC),\ F_B = (-6I_2),\ SS_2 = \left[m^2 \left(\frac{\varepsilon}{kT}\right)^2 \sigma^3\right] \tag{7.15}$$

Then,

$$F_A + F_B \frac{1}{F_C}\left(\frac{SS_2}{SS_1}\right) = \frac{F}{SS_1} \tag{7.16}$$

$$\frac{\partial F_A}{\partial \eta} + \left(\frac{-1}{(F_C)^2}\frac{\partial F_C}{\partial \eta}F_B + \frac{\partial F_B}{\partial \eta}\frac{1}{F_C}\right)\frac{SS_2}{SS_1} = \frac{1}{SS_1}\frac{\partial F}{\partial \eta} \tag{7.17}$$

$$\begin{aligned}\frac{\partial^2 F_A}{\partial \eta^2} + \left(\frac{2}{(F_C)^3}\left(\frac{\partial F_C}{\partial \eta}\right)^2 F_B + \frac{-1}{(F_C)^2}\frac{\partial^2 F_C}{\partial \eta^2}F_B + \frac{-2}{(F_C)^2}\frac{\partial F_C}{\partial \eta}\frac{\partial F_B}{\partial \eta} + \frac{\partial^2 F_B}{\partial \eta^2}\frac{1}{F_C}\right)\frac{SS_2}{SS_1} \\ = \frac{1}{SS_1}\frac{\partial^2 F}{\partial \eta^2}\end{aligned} \tag{7.18}$$

For a pure fluid,

$$\frac{SS_2}{SS_1} = \frac{\varepsilon}{kT} \tag{7.19}$$

The following three variables should be all linear functions of 1/T.

$$\frac{1}{SS_1}F, \quad \frac{1}{SS_1}\frac{\partial F}{\partial \eta}, \quad \frac{1}{SS_1}\frac{\partial^2 F}{\partial \eta^2} \tag{7.20}$$

In this way, it is possible to have a deterministic procedure to obtain the universal constants, as long as the framework and the assumed pure component parameters could fulfill the requirements that the three properties in equation (7.20) are all linear functions of 1/T. The procedure is documented in detail as below:

(1) Setup NIST and PC-SAFT for the specified compound

(2) Specify reduced density η and temperature T

(3) Setup PC-SAFT for temperature dependent parameters/variables, and calculate V from η and T by $V = \frac{\pi}{6}\frac{md^3}{\eta}$

(4) Call NIST to calculate the required properties ($a^r,\ P^r,\ dP/dV$)

(5) Call PC-SAFT to calculate the contributions of the hard-chain term

(6) Calculate the dispersion term from NIST and hard-chain term from PC-SAFT (equation 7.3-7.5)

(7) Calculate $F, \partial F/\partial \eta, \partial^2 F/\partial \eta^2$ from equations 7.10-7.12

(8) Calculate linear coefficients of $\frac{1}{SS_1}F, \frac{1}{SS_1}\frac{\partial F}{\partial \eta}, \frac{1}{SS_1}\frac{\partial^2 F}{\partial \eta^2}$ as a function of 1/T for the given η

(9) If we assume $\frac{1}{SS_1}F = A + B/T$, we could get $F_A = A;\ F_B = F_C\left(\frac{B}{\varepsilon/k}\right)$

(10) If we assume $\frac{1}{SS_1}\frac{\partial F}{\partial \eta} = C + D/T$, we could get $\frac{\partial F_A}{\partial \eta} = C;\ \frac{\partial F_B}{\partial \eta} = F_C\left(\frac{D}{\varepsilon} + \frac{1}{(F_C)^2}\frac{\partial F_C}{\partial \eta}F_B\right)$

(11) If we assume $\frac{1}{SS_1}\frac{\partial^2 F}{\partial \eta^2} = G + H/T$, we could get

$$\frac{\partial^2 F_A}{\partial \eta^2} = G;\ \frac{\partial^2 F_B}{\partial \eta^2} = F_C\left(\frac{H}{\varepsilon} - \frac{2}{(F_C)^3}\left(\frac{\partial F_C}{\partial \eta}\right)^2 F_B + \frac{1}{(F_C)^2}\frac{\partial^2 F_C}{\partial \eta^2}F_B + \frac{2}{(F_C)^2}\frac{\partial F_C}{\partial \eta}\frac{\partial F_B}{\partial \eta}\right)$$

(12) When all the information is available, the sixth polynomial coefficients could be fitted to be the universal constants

The examples of the converted dispersion term (eq. 7.16) of methane and propane are demonstrated for the volume dependence and temperature dependence, respectively, in Figures 7.1 and 7.2. It can be seen that the reduced density dependence, 6th degree polynomials, is sufficient, but the

temperature dependence is only valid either at low density region, or in a narrow range of temperature. This explains why PC-SAFT has difficulties in describing the highly temperature dependent properties, e.g. residual isochoric heat capacity, which solely depends on the derivatives of residual Helmholtz free energy with respect to temperature.

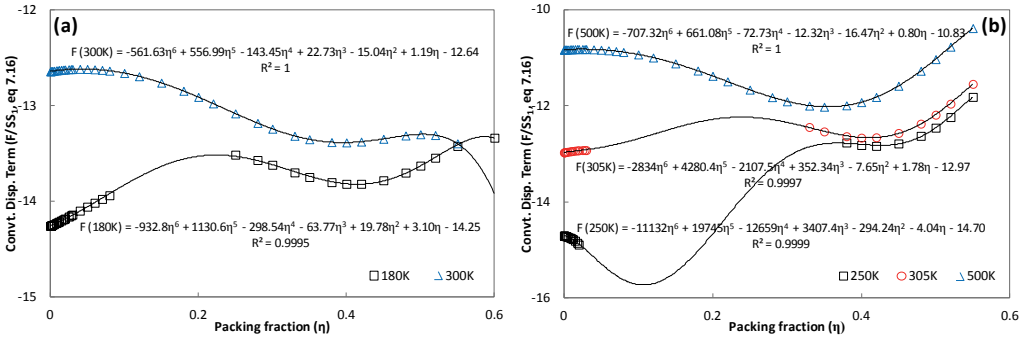

Figure 7.1 Volume (density) dependence of the converted dispersion term (eq. 7.16) for methane and propane. The reduced residual Helmholtz free energy is calculated by NIST [REFPROP (2010)].

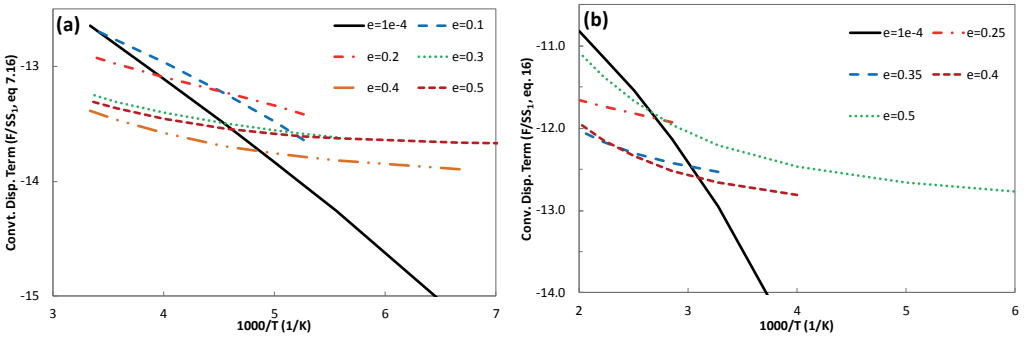

Figure 7.2 Temperature dependence of the converted dispersion term (eq. 7.16) for methane and propane. The reduced residual Helmholtz free energy is calculated by NIST [REFPROP (2010)].

7.2.2 Isothermal curves

It has been criticized that the original PC-SAFT EOS can give more than three volume roots at some temperature and pressure conditions. Privat et al. (2010) stated that it is a problem to have more than three volume roots, since the classical volume-root solvers only search for three roots. It could be argued that this issue can be solved by developing sophisticated volume-root solvers, e.g. setting limit values or checking the derivatives. The isothermal curves of C10 at 135K and C20 at

150K from the original PC-SAFT EOS are presented in Figure 7.3. The one of C10 was firstly reported by Privat et al. (2010), in which the detailed information of its curve shape in the low reduced density region can be found. It can be seen that it is possible to have two stable liquid volume roots in some pressure ranges, and there is only one single volume root locating in the very heavy reduced density region. More severely, the volume roots are not continuous as the pressure increases, so the volume-root solver will probably not be an appropriate solution anymore.

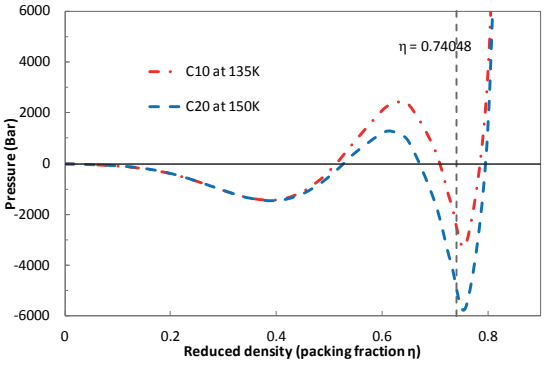

Figure 7.3 Isothermal curves of (a) C10 at 135K and (b) C20 at 150K from the original PC-SAFT EOS [Gross and Sadowski (2001)]. The curve of C10 was firstly reported by Privat et al (2010).

In order to have a more complete picture of the isothermal curves, the parameters and temperature are screened to test how many volume roots the original PC-SAFT EOS will have at most by using the following procedure.

(1) Produce the parameters from {m=[1:1:200], σ=3.8Å, ε/k=[100:10:1000]K}
(2) Produce the temperature from {T=[100:20:2000]K}
(3) Check the number of volume roots at P=0Bar, NVR(P=0), and P(η→0)
(4) If [NVR(P=0)] is zero, check the number of volume roots of dP/dV=0, NVR(dP/dV=0)
(5) If [NVR(P=0)] is two, check the number of volume roots of dP/dV=0, NVR(dP/dV=0) for P > 0
(6) LOOP step (1) to (5) until testing all the parameters

According to the work of Polishuk et al. (2013), the parameter σ is arbitrarily set to 3.8Å, which is a typical value for hydrocarbons. When the isothermal curve has zero or two volume roots at *P=0* Bar, it does not mean it is free from the numerical pitfalls, simply because the working pressure is not zero Bar. This is why it is checked in steps (4) and (5) for the number of volume roots of dP/dV=0.

Figure 7.4 presents the examples of the parameter combinations with which the original PC-SAFT EOS has one or three volume roots at *P=0* Bar when $P(\eta \to 0) > 0$ Bar. It can be seen that it is probably that no single solution will be found in most of the interested pressure ranges, while it could be argued that the dispersion energy (ε/k) has been too large and temperature has been too low for real applications, but this examination gives the limitations of the feasible ranges of the parameters, which is very useful for automatic parameter tuning in large scale simulations.

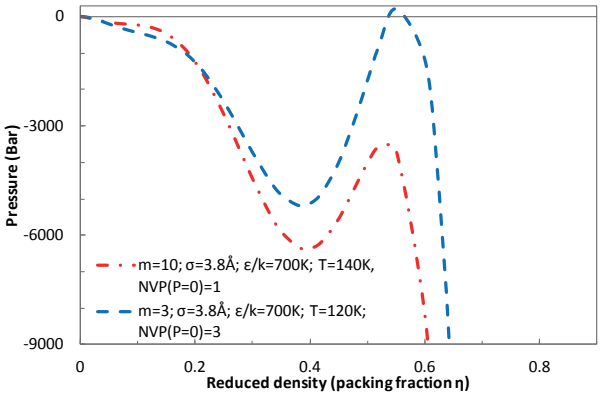

Figure 7.4 Isothermal curves from PC-SAFT (GS) with different parameter combinations. Red dash-dot line is for one root and blue dash line is for three roots at P=0 bar with $P(\eta \to 0) > 0$.

Figure 7.5 (a) and (b) present the examples of the parameter combinations with which the original PC-SAFT EOS has four volume roots at *P=0* Bar, and more than two volume roots satisfying *dP/dV=0* when the *NVR(P=0)* is two, respectively. It can be seen that the functionalities of pressure versus reduced density from these two situations are quite similar to those shown in Figure 7.3 for C10 and C20, i.e. two stable liquid volume roots exist at some ranges of pressure and the only valid liquid volume root locates in very high reduced density region for higher pressures. It can be also seen that some combinations have already located in the real application ranges. It is possible to use this procedure to define the application ranges of the original PC-SAFT EOS. For example, the ranges of segment number and dispersion energy parameters, with which these phenomena of Figure 7.5 will occur, are given in Figure 7.6 for the given segment size (3.8Å) and temperature (300K). Figure 7.6 (a) indicates that it is not recommended to use the dispersion energy higher than 460K if the segment number is larger than 10 at temperature 300K.

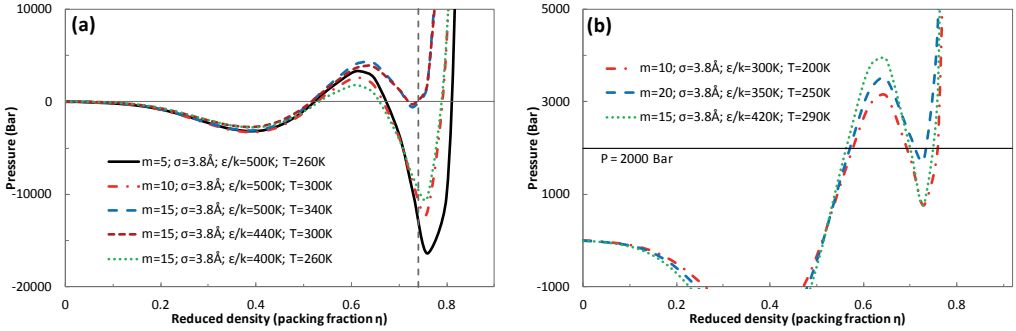

Figure 7.5 Isothermal curves from the original PC-SAFT EOS with different parameter combinations for the situations. (a) Four volume roots at P=0Bar, and (b) more than two volume roots satisfying dP/dV=0 when two volume roots at P=0Bar.

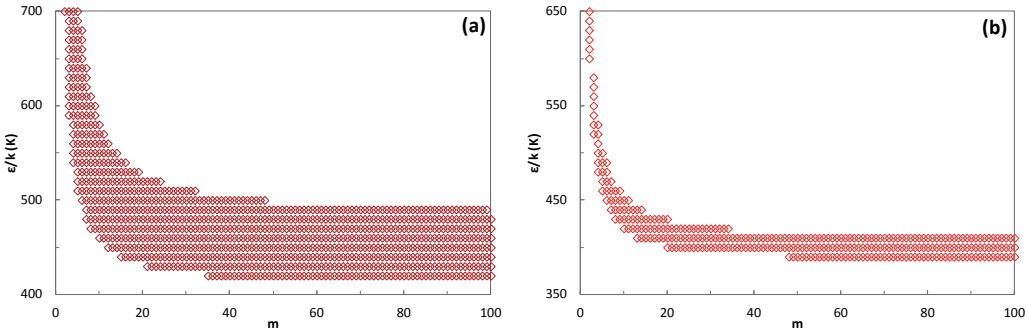

Figure 7.6 The ranges of m and ε/k for the original PC-SAFT EOS to have the same type of P-η curve as those presented Figure 7.5, with fixed σ=3.8Å at 300K.

7.3 New universal constants

On one hand, as discussed by Polishuk et al. (2013), it is a feasible approach to fix the numerical pitfalls by changing the universal constants. On the other hand, the PC-SAFT EOS has already been successfully applied into modeling various types of systems. It will fundamentally extend the application ranges of the PC-SAFT EOS if a new set of universal constants can avoid the numerical pitfalls and reuse the original parameters as much as possible.

7.3.1 A practical way

In Chapter 6, the universal constants are regressed with a step-wise procedure by assuming that the methane (C1) has a segment number parameter m=1. It is further assumed that propane (C3) has a segment number parameter m=2 to develop the following practical procedure.

(1) Estimate the pure component parameters for C1 to C10 with the original universal constants
(2) Regress the coefficients $\{a_{0i}\}$ and $\{b_{0i}\}$ from the properties of C1 with m = 1
(3) Regress the coefficients $\{a_{1i}\}$ and $\{b_{1i}\}$ from the properties of C3 with m = 2
(4) Regress the coefficients $\{a_{2i}\}$ and $\{b_{2i}\}$ from the properties of C4 to C10
(5) Estimate the pure component parameters for C1 to C10 with the new universal constants

In the previous work [Liang et al. (2012)], the universal constant regression and pure component parameter estimation are iterated, but the steps (2) and (5) are not repeated in this work, because we want to keep the most possibility of reusing the original PC-SAFT EOS parameters.

The following objective function is employed:

$$f_{min} = \sum w_k \frac{1}{N_k} \sum_{i=1}^{N_k} \left(\frac{\Omega_i^{exp} - \Omega_i^{calc}}{\Omega_i^{exp}} \right)^2 \tag{7.21}$$

Where Ω is vapor pressure and density (both saturated and isothermal-isobaric conditions), and second-order derivative property dP/dV.

For pure component parameter estimation, vapor pressure and saturated liquid density are the only properties used, but for the regression of the universal constants, dP/dV is included with a weight factor $w_k = 0.01$, as the objective function with vapor pressure and density only has a very flat respond surface. As demonstrated above, that the current PC-SAFT framework are not good enough for simultaneously accurate description of the first- and second-order derivative properties over wide ranges of temperature with the associated pure component parameters. This is one of the reasons why a small number (0.01) is used, and the other reason is to keep the possibility to reuse the original PC-SAFT parameters. The data are the same ones from NIST [REFPROP (2010)], and the details of the temperature and pressure ranges can be found in Chapter 6.

Table 7.1 The newly developed universal constants

i	The first dispersion term (I1)			The second dispersion term (I2)		
	a_{0i}	a_{1i}	a_{2i}	b_{0i}	b_{1i}	b_{2i}
0	0.961597	-0.333416	-0.0632483	0.548398	-0.277226	-0.150684
1	0.414449	0.358440	0.287134	2.07176	0.0621105	-0.507877
2	0.689253	-0.219088	-0.105309	-1.84013	4.29640	1.24227
3	-7.43899	0.285586	7.16607	-29.9683	-39.9453	-48.7052
4	31.8755	5.88256	-37.5008	160.445	214.911	63.1155
5	-54.8833	-22.4931	68.8002	-206.106	-232.563	205.380
6	27.3613	21.2109	-40.3177	51.6201	60.9734	-262.437

7.3.2 I1/I2 versus η

The obtained new universal constants are listed in Table 7.1. From the viewpoint of individual coefficients, it can be seen that these new universal constants are quite different from the original ones of Gross and Sadowski (2001) and the ones developed with speed of sound data in the regression [Liang et al. (2012)]. The later one will not be further discussed in this work, and its applications can be found in the previous chapters. In the following discussions, the PC-SAFT models with the original universal constants from Gross and Sadowski (2001) and the new ones from this work will be denoted as PC-SAFT (GS) and PC-SAFT (LK), respectively.

The curves of the dispersion terms I1 and I2 versus reduced density (packing fraction η) from the two universal constant sets are compared for m=[1, 1.5, 2, 3, 10, 10000] in Figures 7.7 and 7.8. It can be seen that, in general, the two universal constant sets produce similar I1 and I2 curves over a wide range of reduced density, i.e. η=0-1.0, from the qualitative point of view, except for m=1, and they give similar values in the typical range of liquid volume roots, i.e. η=0.25-0.40, except for I2 of m=1. However, the PC-SAFT (GS) gives, respectively, larger and smaller values for I1 and I2 than those from PC-SAFT (LK) in the high reduced density region, i.e. η=0.6-1.0, or in other words, the curvatures of I1 and I2 from these two universal constant sets occur in different reduced density regions, i.e. the PC-SAFT (LK) shifts the larger stationary point to a higher reduced density region.

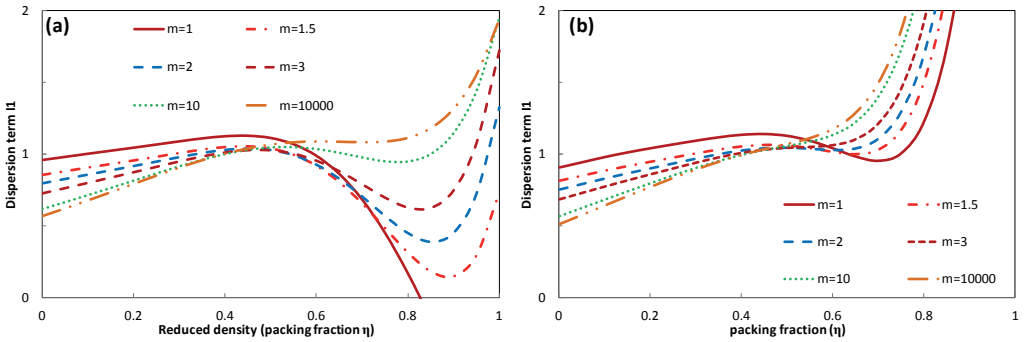

Figure 7.7 Comparison of dispersion term I1 from the two universal constant sets from (a) this work and (b) Gross and Sadowski (2001).

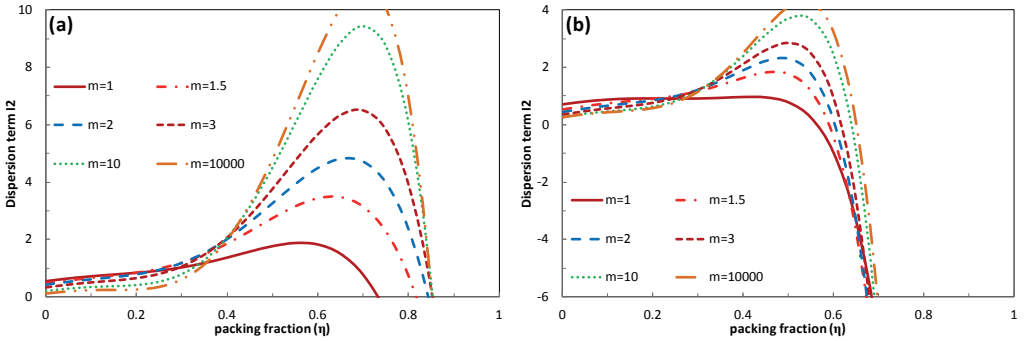

Figure 7.8 Comparison of dispersion term I2 from the two universal constant sets from (a) this work and (b) Gross and Sadowski (2001).

7.3.3 Parameters and physical properties

In order to have a fair comparison, the pure component parameters of normal hydrocarbons are refitted to the same vapor pressure and saturated liquid densitydata with both universal constant sets. The fitted parameters and corresponding deviations are listed in Appendix D, Tables D.1 and D.2, respectively. It is known from Table D.2 that PC-SAFT (GS) gives deviations 0.65% and 0.35%, respectively, for vapor pressure and density of the normal hydrocarbons from C1 to C20, and PC-SAFT (LK) gives deviations 0.30% and 0.27% for the corresponding properties. This illustrates that both universal constant sets provide very good correlating capabilities for the vapor pressure and saturated liquid density.

The differences of the pure component parameters from PC-SAFT with the two universal constants are compared in Figure 7.9 (a), which is defined as:

$$\%RD\ of\ parameters\ = \frac{LK\ -\ GS}{GS} \times 100\% \tag{7.22}$$

GS and LK are used instead of PC-SAFT (GS) and PC-SAFT (LK) just for simplicity, which will also be used in the following figures.

It can be seen that the PC-SAFT (LK) gives larger parameter *m* and smaller parameters σ and ε/k for all the investigated n-alkanes, except C1, but the differences are smaller than 1%, and the differences themselves have small variations for n-alkanes longer than C10.

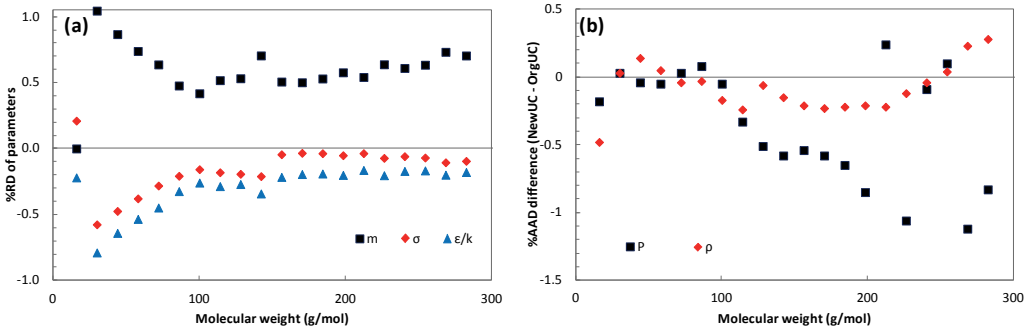

Figure 7.9 Comparisons of the PC-SAFT parameters and the corresponding %AADs for vapor pressure and liquid density of normal hydrocarbons (from C1 to C20). The experimental data are taken from NIST [REFPROF (2010)] for C1 to C10 and from DIPPR (2012) for C11 to C20.

The differences of the deviations for vapor pressure and saturated liquid density from PC-SAFT with the two universal constants are compared in Figure 7.9 (b), which is defined by:

$$\%AAD\ differences\ = LK\ -\ GS \tag{7.23}$$

It is shown in Figure 7.9 (b) that PC-SAFT (LK) presents a slightly better correlation for vapor pressure than the PC-SAFT (GS), whereas the two sets perform quite similarly for density.

The second-order derivative properties, speed of sound (*u*), *dP/dV*, residual isochoric and isobaric heat capacities (C_V *(r)* and C_P *(r)*), and Joule-Thomson (*JT*) coefficients are calculated from PC-SAFT with the two universal constants, and compared with the data from NIST [REFPROP(2010)]. The detailed deviations for all the properties are reported in Appendix D, Tables D.3 and D.4. The

deviations are compared for speed of sound and *dP/dV* in Figure 7.10 (a), and for residual and total isochoric and isobaric heat capacities in Figure 7.10 (b) by using equation (7.23) as well. It can be seen that the PC-SAFT (LK) gives better description of speed of sound and *dP/dV*, except for C1, and the PC-SAFT (GS) gives better prediction of residual isochoric heat capacity for short chain molecules. They present quite similar performance for residual isobaric heat capacities as well as the total heat capacities, both isochoric and isobaric ones.

The deviations of Joule-Thomson coefficients are compared in Figure 7.11 (a). It can be seen, from Figure 7.11 (a) and Tables S3 and S4, that the PC-SAF (LK) predicts quite large deviations for Joule-Thomson coefficients of saturated nC8. This is because one 'experimental' datum has a very small value, i.e. just around the point when the sign changes. The whole Joule-Thomson coefficient curves of saturated nC8 from these two models are plotted in Figure 7.11 (b), from which the two universal constant sets present quite similar results.

As discussed above, it is possible for different universal constants to have equally good correlations for vapor pressure and density, and it is possible to obtain different universal constants by taking different property combinations into account, which will give different balances on describing the properties depending on the designed objective function. To best of our experience, it seems not possible to find a unique set of universal constants, within the current framework, which is able to give absolutely better description for all the properties. It could be anticipated that it is a fundamental deficiency that the current PC-SAFT framework is not able to simultaneously describe all of the first- and second-order derivative properties, based on this work and the previous one.

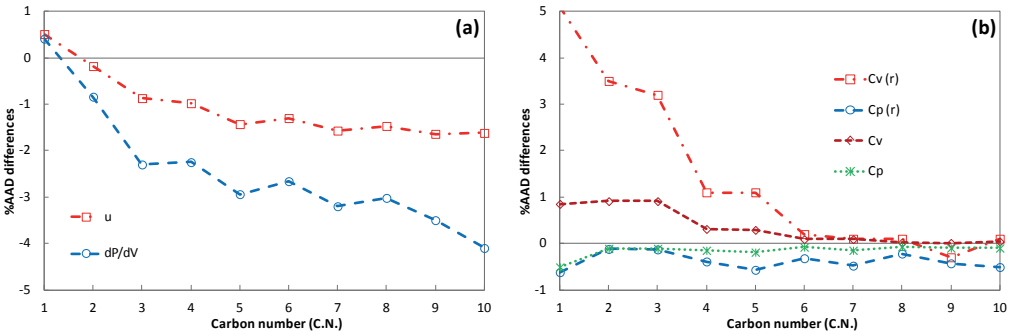

Figure 7.10 Comparisons of the %AADs from the two universal constants using equation (7.23). (a) speed of sound (u) and dP/dV, and (b) residual and total heat capacities of C1 to C10, over wide ranges of temperature and pressure. The experimental data are taken from NIST [REFPROP(2010)].

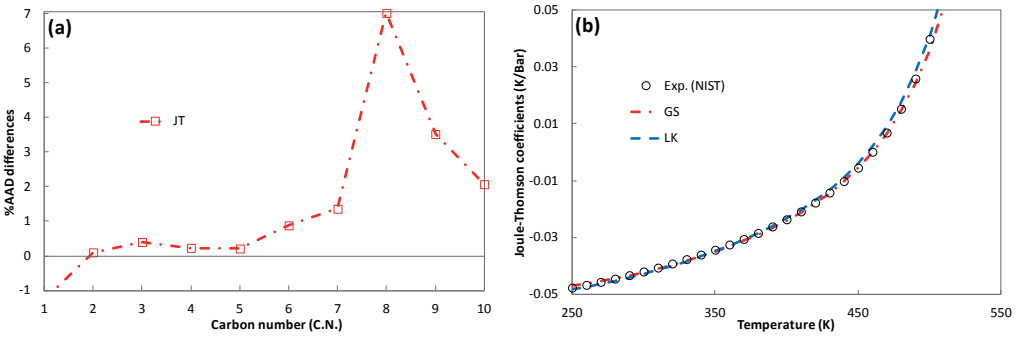

Figure 7.11 (a) Comparisons of the %AADs for Joule-Thomson (JT) coefficients of C1 to C10 over wide ranges of temperature and pressure using equation (7.23), and (b) Joule-Thomson coefficients of saturated nC8 from the two universal constants. GS and LK denote the universal constants from Gross and Sadowski (2001) and this work, respectively. The experimental data are taken from NIST [REFPROP (2010)].

7.3.4 Application ranges

The same procedure proposed in Section 7.2.2 is also conducted for the new universal constants. The results show that the behavior of having one or three volume roots at *P=0* Bar when $P(\eta \rightarrow 0) > 0$ Bar have not been observed, as those presented in Figure 7.4. It has also been found that it is possible to have at most two volume roots satisfying *dP/dV=0* when there are zero or two volume roots at *P=0* Bar, which means these are typical cubic-like P-η curves, so there will be no numerical pitfalls for these two situations as well.

In the entire investigated ranges of parameters and temperature, all possible combinations, with which the new universal constants give four volume roots at *P=0* Bar, are shown in Figure 7.12. It can be seen that it is not possible to have more than three roots, or two stable liquid volume roots, in the entire pressure range if the dispersion energy is not larger than 780K, or if the working temperature is higher than 120K. In another word, the PC-SAFT EOS with the new universal constants is practically free of numerical pitfalls of the presence of more than three volume roots.

However, it has to be pointed out that it is possible for the PC-SAFT (LK) to give at most six volume roots at *P=0* Bar if the working temperature is very low, e.g. smaller than 55K, which could be argued that it is out of the real application ranges for most interested processes. This can be improved by tuning the universal constants to obtain the I1 and I2 curves as those from our previous work [Liang et al. (2012)] or Polishuk (2014), but the ultimate solution is believed to use a fewer

degree polynomials, e.g. 4th degree, or other types of functions to represent the dispersion interactions. In this case, however, the model parameters are probably needed to be refitted.

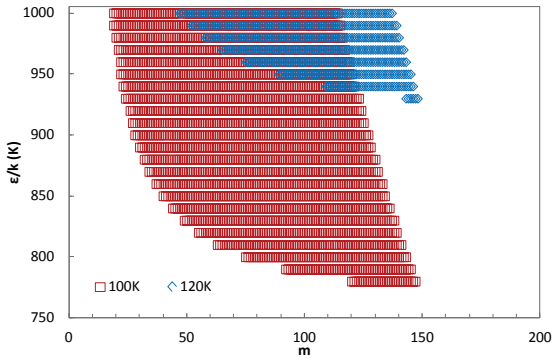

Figure 7.12 The ranges of *m* and *ε/k* for the PC-SAFT EOS with the new universal constants to have four volume roots at P=0Bar, which presents the potential risk to have more than three volume roots and discontinuity of the volume roots versus temperature or pressure when the parameters locate in these ranges.

7.3.5 A real example

It is a common practice to use large parameter values for dispersion energy and/or segment number when modeling asphaltene. For instance, Hustad et al. (2013) used the parameters {m=11, σ=4.53Å, ε/k=500K} for asphaltene. The isothermal curve of this asphaltene at 280K is shown in Figure 7.13 (a), and the one from the PC-SAFT (GS) has the typical behavior of four volume roots at *P=0* Bar. It can be seen that the discontinuity of the volume roots occurs when the pressure exceeds 600Bar, and the volume root will then locate in the very heavy reduced density area (η>0.74).

In order to study the relationship of isothermal curve and phase equilibrium, the isobaric-isothermal flash calculations have been conducted for the original reservoir fluid, i.e. without nitrogen injection, from 200 to 1000Bar at 280K. All the parameters, including the binary interaction parameters, are taken from Hustad et al. The molar numbers of the asphaltene in its rich phase are presented in Figure 7.13 (b). It can be seen that the two models give similar prediction below 600Bar, and the PC-SAFT (GS) predicts non-physical phase split results when the pressure exceeds 600Bar, i.e. one pure asphaltene phase, whereas the PC-SAFT (LK) gives a smooth prediction. The discontinuity of the volume roots versus pressure is believed to the reason for the discontinuous phase equilibrium results along the pressure curve.

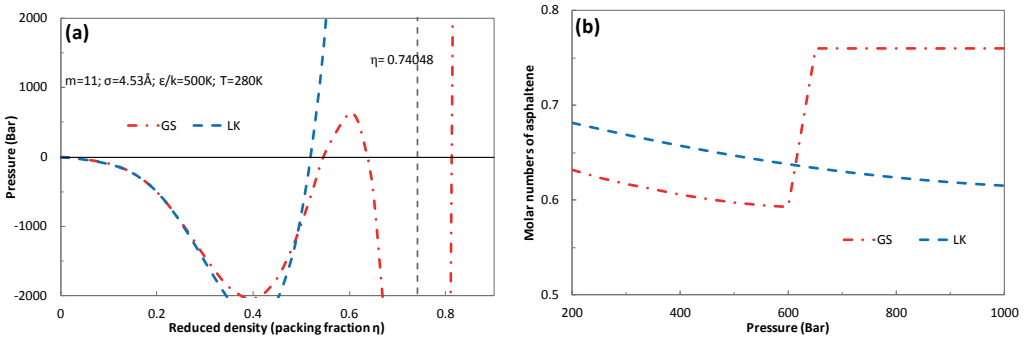

Figure 7.13 (a) Isothermal curves of asphaltene at 280K with the parameters from Hustad et al. (2013); (b) the molar numbers of asphaltene in its rich phase versus pressure. GS and LK denote the universal constants from Gross and Sadowski (2001) and this work, respectively.

7.4 Possibility to use the original PC-SAFT parameters

As discussed above, the same pure component parameters from the original universal constants are used when fitting the new universal constants, and the differences of the final pure component parameters of n-alkanes from these two universal constant sets are less than 1%. In this section, we will investigate the possibility of reusing the parameters from the original PC-SAFT EOS with the new universal constants.

7.4.1 Binary hydrocarbon systems

The VLE of the binary mixtures of C2 + nC10 and C3 + C6H6 have been modeled by PC-SAFT with both universal constant sets using the parameters from Gross and Sadowski. The results are presented in Figure 7.14. The k_{ij} is 0.0 in both cases. It can be seen that the phase diagrams from the two universal constant sets are quite similar to each other.

7.4.2 1-Alcohol + n-alkane mixtures

The VLE of the binary mixtures of ethanol + nC6 and 1-octanol + nC12 have been modeled by PC-SAFT with both universal constants. The results are presented in Figure 7.15. The k_{ij} is fitted to the data for the original parameters with the PC-SAFT (GS). Again it can be readily seen that the phase diagrams are almost identical.

The possibility of using the original parameters with the new universal constants is also checked for the LLE of methanol + n-alkanes (nC6, nC8 or nC10). The results with the same model parameters

and k_{ij} are presented in Figure 7.16 (a). The model parameters of methanol are from Liang et al. (2012), with speed of sound data in the parameter estimation. The k_{ij} is fitted to the data for the original parameters with the PC-SAFT (GS). It can be seen that the phase diagrams are similar, but the differences from the two universal constants are not as small as what have been seen in the aforementioned VLE modeling results. It is demonstrated in Figure 7.16 (b) that a slightly different k_{ij} could give almost identical phase diagrams.

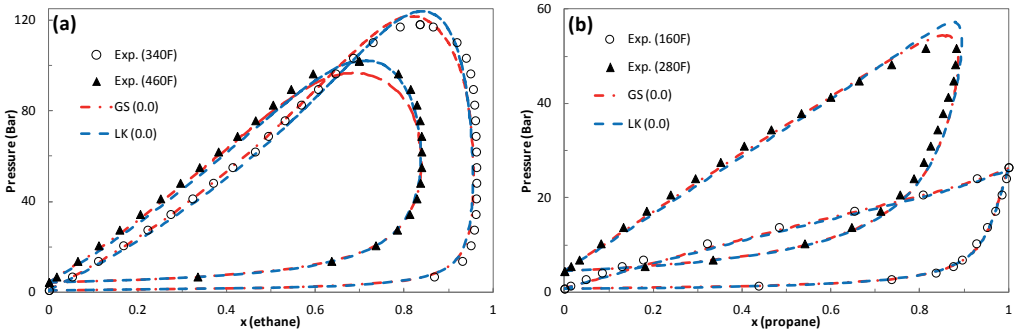

Figure 7.14 P-x diagrams of (a) ethane + n-decane. Data are from Reamer et al. (1962) and (b) propane + benzene. Data are from Glanville et al. (1950) The model parameters of all hydrocarbons are from Gross and Sadowski (2001). GS and LK denote the universal constants from Gross and Sadowski (2001) and this work, respectively.

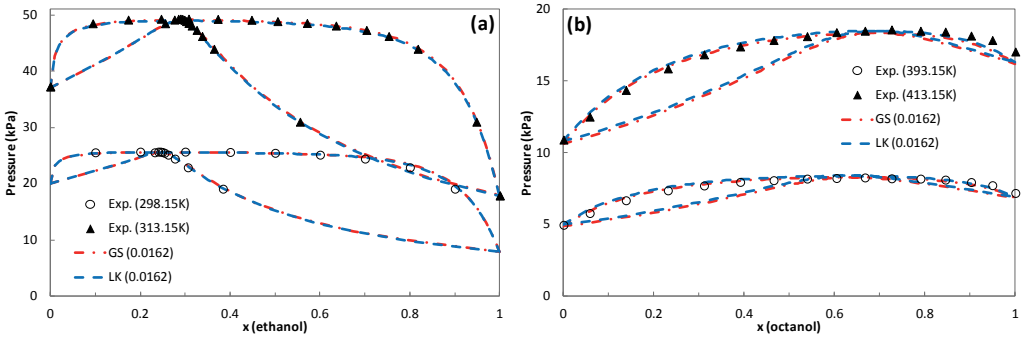

Figure 7.15 P-x diagrams of (a) ethanol + n-hexane and (b) 1-octanol + n-dodecane. The data are both from Góral et al. (2002), The ethanol and 1-octanol parameters are from Gross and Sadowski (2001) and Grenner et al. (2007a), respectively. The k_{ij} values are shown in the parenthesis. GS and LK denote the universal constants from Gross and Sadowski (2001) and this work, respectively.

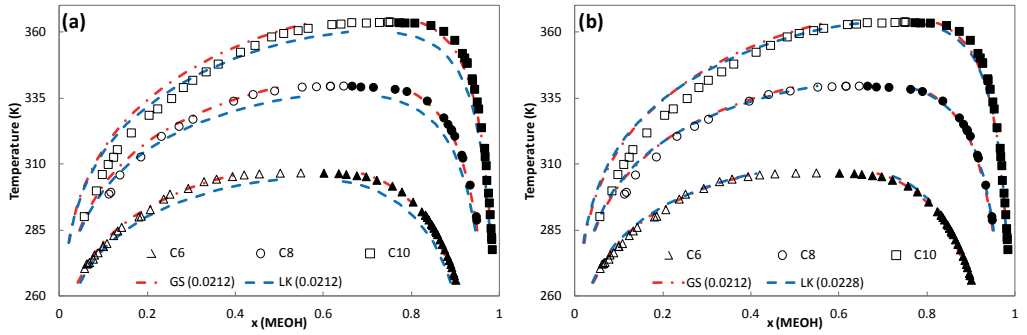

Figure 7.16 LLE of methanol with n-hexane, n-octane or n-decane, (a) same model parameters and k_{ij}, (b) same model parameters and different k_{ij}. The methanol parameters are from Liang et al. (2012) The experimental data are from Matsuda et al. (2002), Kurihara et al. (2002), and Matsuda et al. (2004) The k_{ij} values are shown in the parenthesis. GS and LK denote the universal constants from Gross and Sadowski (001) and this work, respectively.

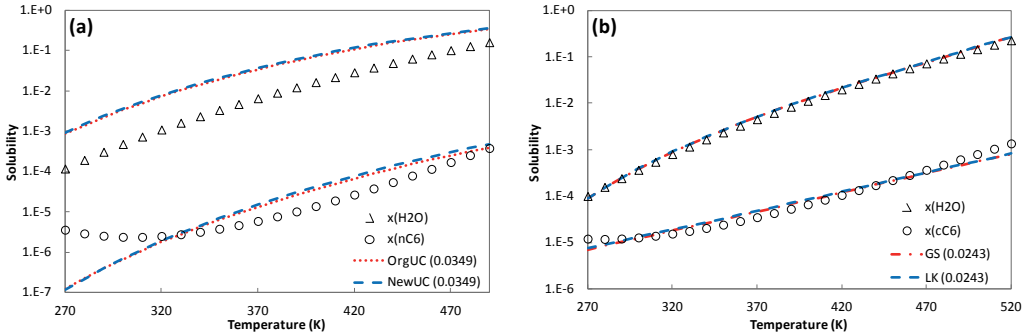

Figure 7.17 Phase equilibria of (a) water + n-hexane, data are from Tsonopoulos et al. (1983) and water parameters are from Gross and Sadowski (2002); (b) water + cyclo-hexane, data are from Tsonopoulos et al. (1985) and parameters from Liang et al. The k_{ij} values are shown in the parenthesis. GS and LK denote the universal constants from Gross and Sadowski (2001) and this work, respectively.

7.4.3 Water containing systems

From the phase equilibrium modeling point of view, the water containing systems are good candidates in order to investigate the possibility of using the original PC-SAFT parameters with the new universal constants, since water is a challenging molecule for any EOS. The PC-SAFT modeling results of the LLE of water + non-aromatic hydrocarbon (nC6 or cyclo-C6), VLE of water + mono-ethylene glycol (MEG), VLE and LLE of water + 1-butanol, and LLE of water + methanol + nC7 are presented in Figures 7.17-7.19 with both universal constants. All of the model parameters

and binary interaction parameters are based on the PC-SAFT (GS). The combining rule CR-1 is used for cross associations. It can be seen that the two models give similar results for all the systems, except for the 1-butanol rich phase in the water + 1-butanol binary mixture and the methanol solubility in the hydrocarbon rich phase of the ternary mixture, which can be tuned by the binary interaction parameters as discussed above for the methanol + n-alkane binary mixtures. It could be argued, however, that the deviations from these two universal constant sets are much smaller than the deviations of modeling results from the experimental data.

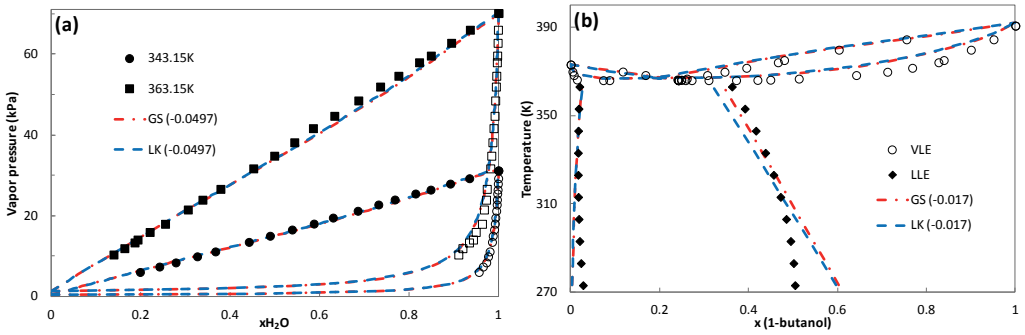

Figure 7.18 Phase equilibria (a) water with MEG. Data are from Chiavone-Filho et al. (1993) The model parameters of water and MEG are from Grenner et al. (1996) and Tsivintzelis et al. (2008), respectively. (b) water + 1-butanol. Data are from Boublik (1960) and Sørensen et al. (1995) The model parameters of water and 1-butanol are from Gross and Sadowski (2002). The k_{ij} values are shown in the parenthesis. GS and LK denote the universal constants from Gross and Sadowski (2001) and this work, respectively.

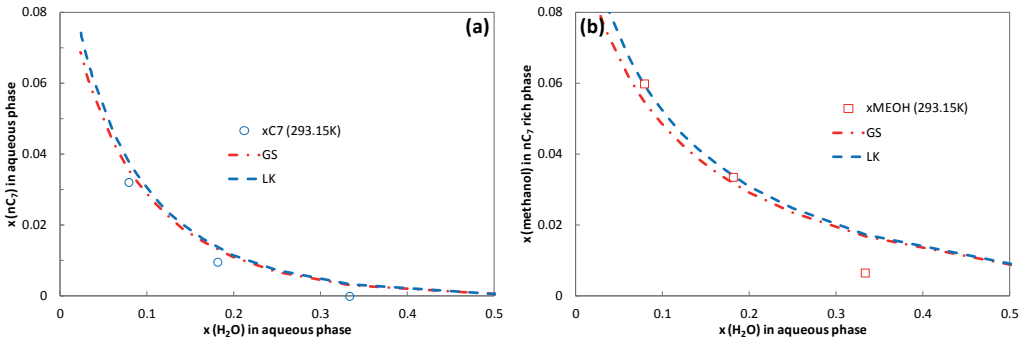

Figure 7.19 LLE of water + methanol + n-heptane, (a) the solubility of n-heptane in aqueous phase; (b) the solubility of methanol in n-heptane rich phase. The data are from Letcher et al. (1986) The model parameters of water and methanol are from Liang et al. (2012, 2014) GS and LK denote the universal constants from Gross and Sadowski (2001) and this work, respectively.

7.4.4 Polymer containing systems

The possibility is also evaluated for the polymer containing systems. The VLE of two polymer systems have been modeled by PC-SAFT with both universal constant sets. As seen from Figure 7.20, the two sets give quite similar pressure-composition curves with the same parameters. The two universal constant sets are further compared for their behavior on modeling the LLE of polypropylene (PP) + propane by assuming PP is monodisperse. The results are presented in Figure 7.21. It can be seen that the PC-SAFT (LK) predicts considerably different cloud points by using the k_{ij} from the PC-SAFT (GS), while it could give similar prediction with a slightly different k_{ij} as shown in Figure 21 (b).

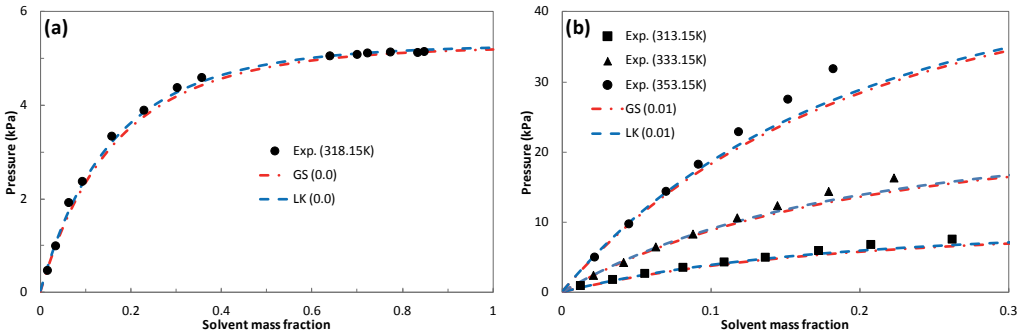

Figure 7.20 P-x diagrams of (a) PP + diisopropyl ketone at 318K. Data are from Brown et al. (1964) The model parameters of polypropylene and diisopropyl ketone are from Tumakaka et al. (2002) and Kouskoumvekaki et al. (2004), respectively; (b) poly(vinyl acetate) + propyl acetate at 313.15K, 333.15K and 353.15K. Data are from Wibawa et al. (2002) The model parameters of poly(vinyl acetate) and propyl acetate are from Tumakaka et al. (2002) and Gross and Sadowski (2001).

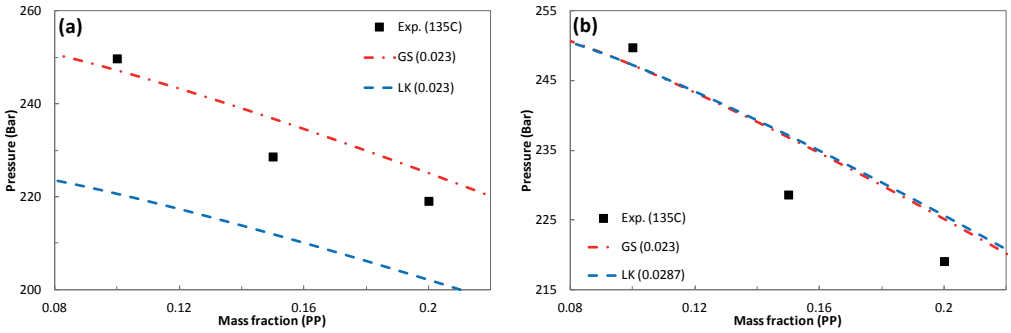

Figure 7.21 LLE of PP + propane, (a) same model parameters and kij, (b) same model parameters and different kij. The polypropylene parameters are from Tumakaka et al. (2002) The data are from Whaley et al. (1997) The k_{ij} values are shown in the parenthesis.

7.4.5 Natural gas systems

Since it is based on mean-field theory, the PC-SAFT EOS is believed to have difficulties in predicting the critical points when the model parameters are fitted to the vapor pressure and liquid density only. The critical points of 50 multicomponent systems are predicted from PC-SAFT with both universal constants using the model parameters from the PC-SAFT (GS), which are compared in Figure 7.22. It can be seen that the two models predict quite similar critical points.

The phase envelope of two natural gas systems are investigated with both universal constant sets by using the original model parameters in a predictive way, i.e. no binary interaction parameter is used. As shown in Figure 7.23, it can be seen that the shapes of the phase envelopes are quite similar.

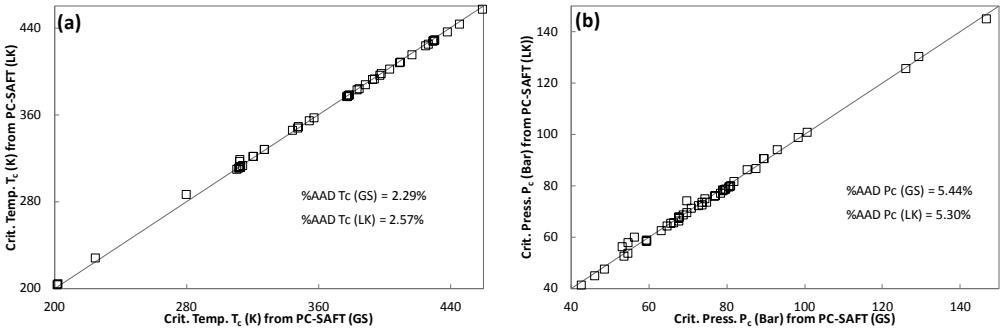

Figure 7.22 Critical temperature and pressure of 50 natural gas systems. The collections of the detailed data, including mixture composition, critical temperature and pressure, and literature can be found in Sørensen (2008). GS and LK denote the universal constants from Gross and Sadowski (2001) and this work, respectively.

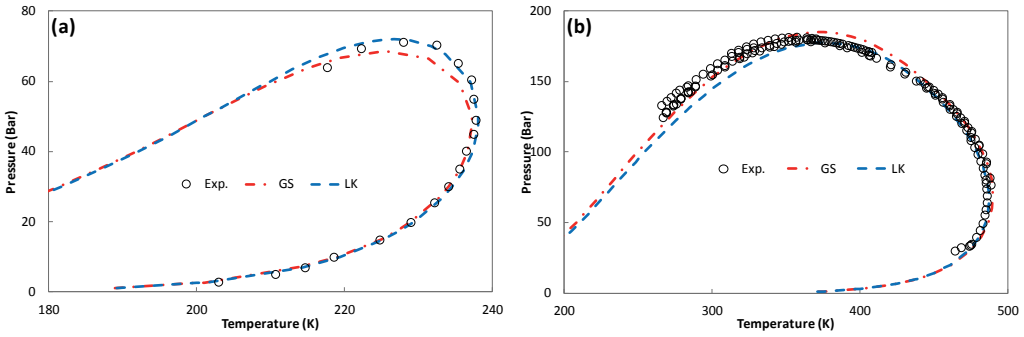

Figure 7.23 Phase envelope of (a) the Gas 2 from the work of Avila et al. (2002); (b) 60.0C1 + 31.0nC4 + 9.0nC10, from Urlic et al. (2003)

7.4.4 Petroleum fluid-water-MEG systems

It has been shown in Chapter 4 that the PC-SAFT EOS is able to successfully model the petroleum fluid-water-MEG systems by using the newly developed parameters of water and MEG, and petroleum fluid characterization procedures. These ternary mixtures are modelled with PC-SAFT (LK) by using the same characterization procedure CM7, i.e. directly replacing the universal constants with the new ones during calculations. The overall deviations from these two universal constant sets are compared in Table 7.2, and the modeling results of individual cases are compared in Figure 7.24.

It is readily seen from Table 7.2 that the overall deviations from the two universal constant sets are almost identical. The solubilities of water from the two models are almost identical, and the solubilities of MEG from PC-SAFT (LK) are almost identical to and slightly smaller than those from PC-SAFT (GS), respectively, for gas condensates (case 1 to case 12) and heavy oils (case 13 to case 19). PC-SAFT (LK) predicts larger solubilities of petroleum than PC-SAFT (GS), but the differences are lower than 5%.

Table 7.2 %AADs for the petroleum fluid-water-MEG systems from two universal constant sets

Model	Oil in polar phase	MEG in organic phase	H_2O in organic phase
PC-SAFT (LK)	26	25	26
PC-SAFT (GS)	27	25	26

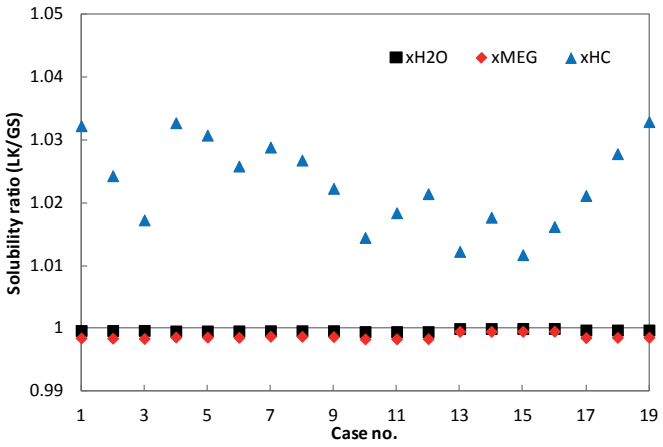

Figure 7.24 The ratios of solubility of petroleum fluid, water and MEG from PC-SAFT (LK) and PC-SAFT (GS) with the same characterization procedure.

7.5 Conclusions

Based on the total residual Helmholtz free energy calculated from well-established models, such as NIST reference models in this work, the temperature and volume dependences of the PC-SAFT EOS have been analyzed. The results reveal that the 6^{th} degree polynomials are sufficient for representing the volume dependence of the model, but the temperature dependence is only valid at low density region or in a narrow range of temperature. Moreover, this will lead to a deterministic procedure for obtaining the universal constants of the dispersion term if the framework and assumed pure component parameters could correctly represent the temperature dependences.

The behavior of isothermal curves, i.e. pressure versus reduced density at a given temperature, is investigated by screening the parameters and temperature over wide ranges. The results show that it is possible for the original universal constants to have more than three volume roots, or two stable liquid volume roots, and the discontinuity of volume roots can occur as the pressure increases, which will lead to unrealistic prediction of phase behavior. This investigation gives the limitation of the feasible parameter ranges, in which the PC-SAFT EOS will be free of numerical pitfalls.

Based on the step-wise procedure developed in the former work, a practical way is proposed to obtain the 42 universal constants by further assuming that propane has a fixed m=2. The same pure component parameters from the original PC-SAFT EOS are used. The new universal constants are compared with the original ones on the properties of n-alkanes from methane to decane. The results show that the new universal constants perform better on speed of sound and dP/dV, while the original ones have better description for the residual isochoric heat capacity of short chain n-alkanes and Joule-Thomson coefficients of long chain n-alkanes, and they show similar performance on vapor pressure, density and isobaric heat capacities. Different universal constants could give equally good correlations for vapor pressure and density, but it does not seem possible to obtain a unique set having the best description for all properties.

More importantly, the PC-SAFT EOS with the new universal constants is free of numerical pitfalls of the presence of more than three volume roots or the discontinuity of volume roots versus pressure in the real application conditions. The investigation on various types of mixtures reveals that it is feasible to use the original PC-SAFT model parameters with the new universal constants. It is even possible to use the original binary interaction parameter for the VLE modeling, while it might be necessary to tune the binary interaction parameter for some LLE systems.

From the author:

"*The possibility of using the original PC-SAFT parameters with the new universal constants has been shown for the hydrocarbon, water, chemical, polymer, petroleum fluid containing systems. It is also believed that the new universal constants have the correlation capability as good as the original ones, if not better. It is still recommended that the pure component parameters and binary interaction parameter are refitted to the new universal constants if the users have the expertise and the experimental data are available.* "

Chapter 8. Salt effects

Electrolyte solutions are believed to be more difficult to model than non-electrolyte mixtures. This is because the charged particles introduce much longer range interactions and more complex interaction schemes than neutral molecules, which in general results to more non-ideal mixtures than non-electrolyte solutions. In this chapter, the salt effects on the solubility of hydrocarbon in, speed of sound in and static permittivity of the aqueous phase are discussed. The relationship of the static permittivity and free site fraction from association theory is also briefly discussed, which is important for developing general electrolyte equation of state models within the primitive approach.

8.1 Introduction

In the oil and gas industry, the study of electrolyte solutions is significant in various aspects – oil recovery enhancement, gas hydrate inhibition enhancement and pipeline corrosion prevention. On on hand, the presence of salts will generally reduce the solubility of hydrocarbons in the aqueous phase from the viewpoint of phase equilibrium. On the other hand, the presence of salts will increase the speed of sound and decrease the static permittivity of fluids.

8.2 Salt effects

8.2.1 Phase equilibria

The salting out effects of the solubility of methane in aqueous phase are demonstrated in Figure 8.1, in which the temperature effects are also reported for one salt concentration. The experimental data are taken from O'Sullivan et al. (1970). It can be seen that the salt effects are significant, and much larger than the temperature effects on the solubility of methane, and that the salt effects get larger as the pressure increases.

Salt effects on the solubility of pentane and hexane in the aqueous phase are plotted in Figure 8.2. The data are taken from Shaw et al. (2006). Again, the salt shows significant impact on the solubility of hydrocarbons in the electrolyte solution, especially at the low salt concentration region.

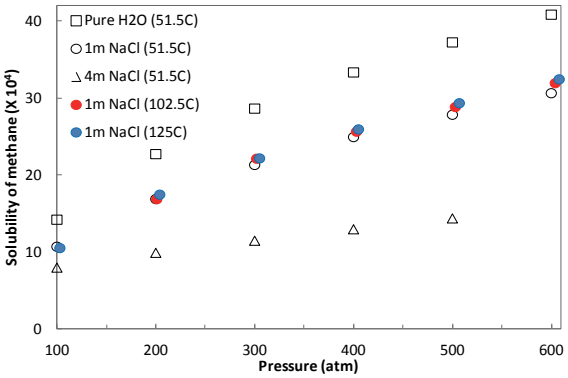

Figure 8.1 Salt effects on the solubility of methane in aqueous solution. Data are from O'Sullivan et al. (1970).

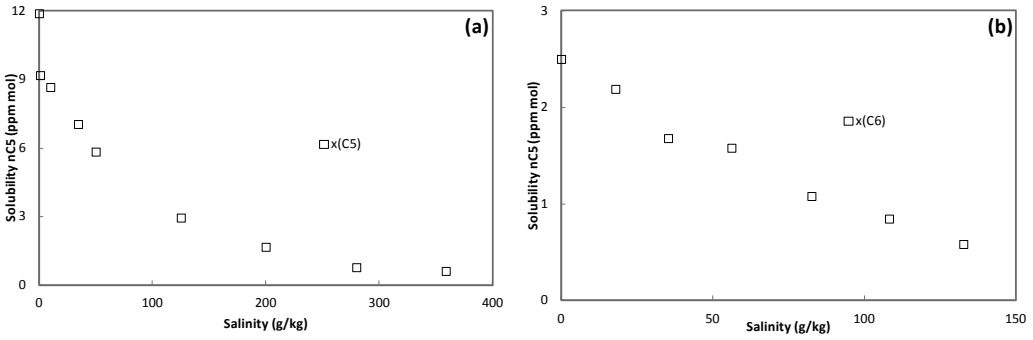

Figure 8.2 Salt effects on the solubility of hydrocarbons (a) n-pentane and (b) n-hexane in aqueous solution at 298.15K. Data are taken from Shaw et al. (2006).

8.2.2 Speed of sound

8.2.2.1 Water and seawater

The speed of sound in water has been extensively measured by many researchers [Wilson (1959), Del Grosso et al. (1972), Kroebel et al. (1976), Fujii et al. (1993), Bilaniuk et al. (1993), Plantier et al. (2002), Lampreia et al. (2005) and Benedetto et al. (2005)]. Figure 8.3 shows the speed of sound in saturated and compressed water. The speed of sound in saturated water reaches a mixmum around 350K. This can be observed also for the speed of sound in compressed water at 343.15K and 363.15K. The quantities of the speed of sound are very closeto each other at these two temperatures, and they intersect each other.

Speed of sound measurements for seawater have been of great interest to oceanographers for many years, and numerous experimental data has been published in the past 90 years. Among them, the most cited ones are those of Wilson (1960), Del Grosso et al. (1972) and Chen et al. (1977). As discussed in the previous chapters, none of the models can describe the speed of sound in water over wide temperature and pressure ranges. As an engineering solution, the speed of sound in water and seawater will be calculated by the sophisticated tool TEOS-10. TEOS-10 is an international standard package for calculating the thermodynamic properties of seawater [IOC, SCOR and IAPSO (2010)]. Experimental and calculated (with TEOS-10) speed of sound data of seawater are presented in Figure 8.4 for different salinity and temperature conditions, which a perfect match can be seen.

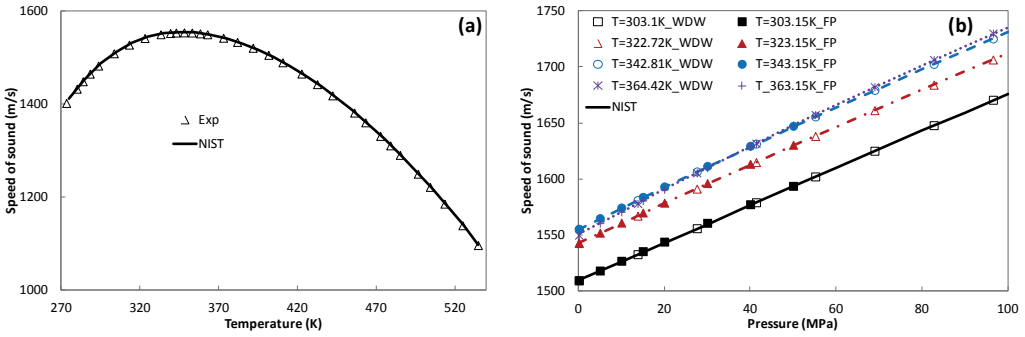

Figure 8.3 The speed of sound in (a) saturated water against temperature, and data are from Chávez et al. (1985); and (b) compressed water against pressure at constant temperature, and data are from Wilson (1959) and Plantier et al. (2002). Lines are data from NIST.

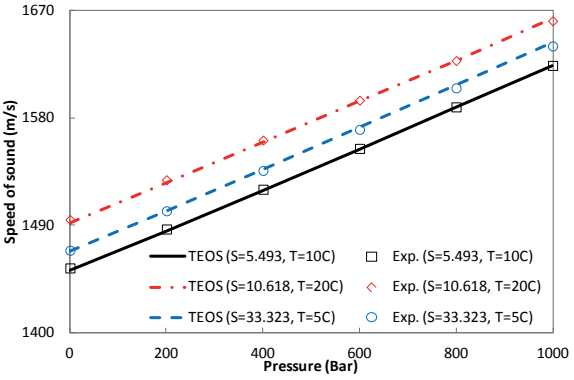

Figure 8.4 The speed of sound in seawater, comparison of experimental data and calculations from TEOS-10 [IOC, SCOR and IAPSO (2010)]. *S* denotes salinity (mol/kg).

8.2.2.2 Salt solutions

The speed of sound in electrolyte solutions could be very useful for fundamental research, for instance, it can be used a discriminate property to check the new electrolyte thermodynamic models. The speed of sound in various aqueous salt solutions has been measured by many researchers.

Millero and co-workers have made extensive and systematic studies on major sea salts solutions in wide ranges of temperature, pressure and composition. More than 99.98% of seawater by mass is composed of elements oxygen, hydrogen, chloride, sodium, magnesium, sulfur, calcium and potassium. Millero et al. (1977) measured the speed of sound in aqueous solutions containing compounds with different combinations of these elements in the molality range 0.01 to 1.0 mol/kg at 298.15K. Chen et al. (1978a) measured the speed of sound in four major sea salts NaCl, Na_2SO_4, $MgCl_2$, and $MgSO_4$ aqueous solutions over molality 0 to 1.0 mol/kg, temperature 273.15 to 328.15K, and pressure 0.1-100MPa. Later, Millero et al. (1982, 1987) reported the speed of sound in the aqueous solutions with the same four major sea salts from diluted to saturate solutions, from 273.15 to 318.15K and from 298.15 to 368.15K in two separate works. Besides single salt solutions, Millero et al. (1985a, 1985b) determined the speed of sound in possible combinations of the major sea salt ions (Na^+, Mg^{2+}, Cl^-, and SO_4^{2-}) at constant ionic strength (I=0.1, 0.5 or 3.0) and temperatures up to 298.15K, pressures up to 100MPa. They also proposed a method using the additivity principle to estimate the speed of sound from binary solutions.

It is commonly to use the relative concept to discuss the impact of salts on speed of sound in water solutions. The relative speed of sound is defined as the speed of sound in the salt solution minus that in the pure water at the same temperature and pressure conditions:

$$Ru = u_{sw} - u_{pw} \tag{8.1}$$

where the subscripts *sw* and *pw* denote the seawater (salt water) and pure water, respectively.

Figure 8.5 presents the relative speed of sound in NaCl solution up to molality 6 mol/kg at four temperatures and atmospheric pressure, which shows that the salt concentration has considerable impacts on speed of sound in the solution, and that, as expected, the speed of sound increases as the salt concentration. Figure 8.6 shows the relative speed of sound in seven electrolyte solutions versus concentrations at 298.15K and atmospheric pressure. The results show that the sodium and magnesium ions seem to have similar and slightly larger impact on the speed of sound than the potassium ion at the same concentration (mass fraction).

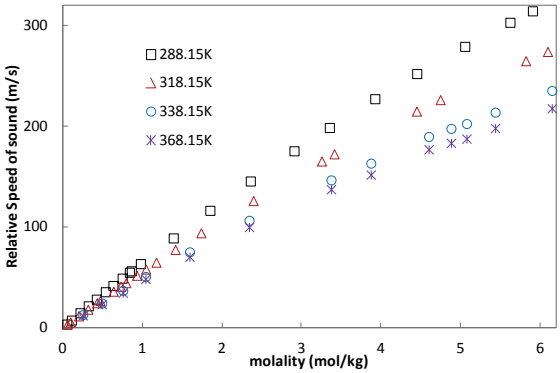

Figure 8.5 The relative speed of sound in NaCl solution up to high concentration at 288.15K, 318.15K, 338.15K and 368.15K and atmospheric pressure. Data are taken from Millero et al. (1987).

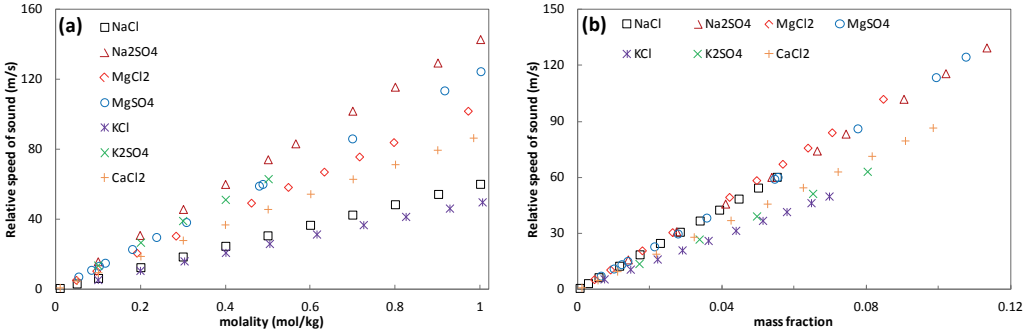

Figure 8.6 The relative speed of sound in seven electrolyte solutions at 298.15K and atmospheric pressure. Figure (b) is translated from Figure (a), i.e. from molality to mass fraction. Data are taken from Millero et al. (1977).

Figure 8.7 presents the relative speed of sound in two major salts solutions against the molality of NaCl with fixed total ionic strength 3.0. In this case, one salt is NaCl, and the molality of the other salt can be calculated from the total ionic strength. The difference of the speed of sound data between NaCl and Na_2SO_4 solutiosn are smaller than those between NaCl and MgCl.

In order to discuss the impact of temperature and pressure on the speed of sound in salt solutions, a new variable is introduced based on the relative speed of sound:

$$\Delta Ru = Ru(T, P) - Ru(T_0, P_0) \tag{8.2}$$

where T_0 and P_0 are set to T and P depending on the temperature or pressure impact is discussed.

Figure 8.8 shows the temperature and pressure dependence of relative speed of sound in NaCl solution at different concentrations. It reveals that pressure and temperature, respectively, have minor and moderate impacts on speed of sound.

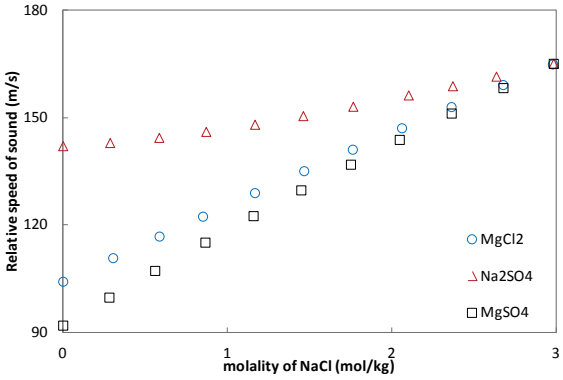

Figure 8.7 The relative speed of sound in two major salts solutions against the molality of NaCl with fixed the total ionic strength 3.0. Data are taken from Millero et al. (1985b).

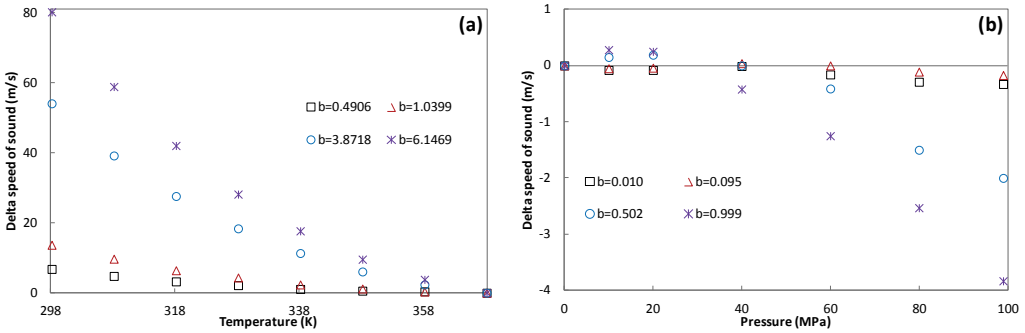

Figure 8.8 Temperature dependence of the speed of sound in NaCl solution (a) at molality 0.4906, 1.0399, 3.8718 and 6.1469 mol/kg at atmospheric pressure, minus that at 368.15K; (b) pressure dependence of the speed of sound at molality 0.010, 0.095, 0.502 and 0.999 mol/kg at 298.15K, minus that at atmospheric pressure. Data are from Chen et al (1978a) and Millero et al. (1987).

8.2.3 Static permittivity

Static permittivity plays a very important role in modeling the electrolyte solutions when the primitive approach is used, and it depends on the temperature, molar density, electric dipole moment and optical polarizability. Figure 8.9 (a) and (b) present the static permittivity of saturated water and the binary mixtures of water with methanol and ethanol. It can be seen from Figure 8.9 (a)

that, as expected, the static permittivity of saturated water decreases as the temperature increases. It is known from Figure 8.9 (b) that the static permittivity of water is higher than that of methanol, which is larger than that of ethanol. The static permittivity of these binary mixtures shows quite linear dependence on mass fraction in a relative large concentration range, i.e. from 20% to 100%.

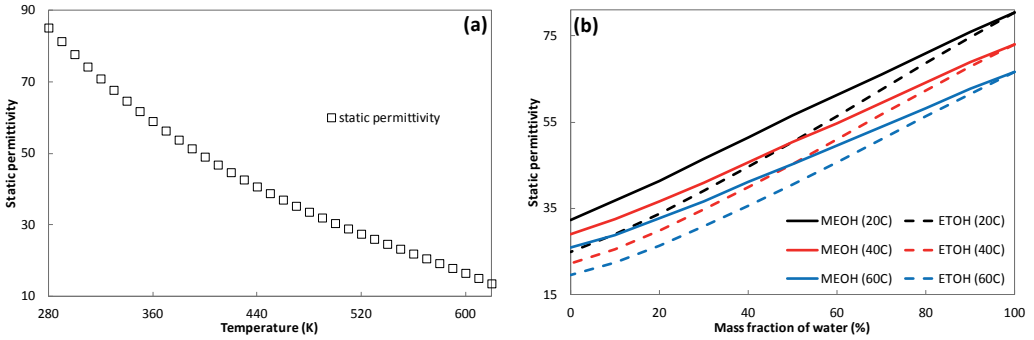

Figure 8.9 (a) Static permittivity of saturated water and (b) static permittivity of binary mixtures of water with methanol or ethanol. The experimental data are taken from NIST [REFPROP (2010)] and Åkerlöf (1932).

Figure 8.10 presents the static permittivity of NaCl solution at different temperatures. The static permittivity decreases as the solution gets concentrated at constant temperature, but the temperature dependence of the static permittivity at constant concentration is a bit more complex. The static permittivity decreases as the temperature increases if the concentration is smaller than 3mol/L, and temperature has very small impact on the static permittivity when the temperature is higher than 20C and the concentration is larger than 3.5mol/L.

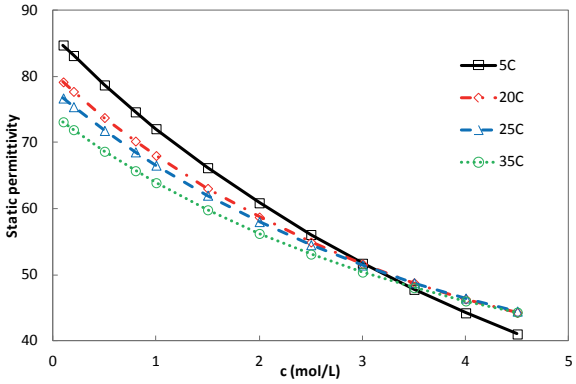

Figure 8.10 Static permittivity of NaCl solution at different temperatures. The experimental data are taken from Buchner et al. (1999).

8.3 Static permittivity and association models

Very recently, Maribo-Mogensen et al. (2013a, 2013b) developed a method to model the static permittivity with the association theory based equations of state. The key equation to connect the static permittivity and the association theory is the following one:

$$\frac{(2\varepsilon_r+\varepsilon_\infty)(\varepsilon_r-\varepsilon_\infty)}{\varepsilon_r(\varepsilon_\infty+2)^2}=\frac{N_A}{9\varepsilon_0 k_B T v}\sum_i x_i g_i \mu_{i,0}^2 \tag{8.3}$$

where the variable g_i is the Kirkwood g-factor, which is given by:

$$g_i=1+\sum_j \frac{z_{ij}P_{ij}cos(\gamma_{ij})}{P_i cos(\theta_{ij})+1}\frac{\mu_{0,j}}{\mu_{0,i}} \tag{8.4}$$

where P_{ij} is the possibility of two molecules to be bonded, and is given by definition:

$$P_{ij}=1-X^{A_i} \tag{8.5}$$

X^{A_i} is the non-bonded site fraction, which can be directly calculated from association theory-based equations of state.

The details can be found in the original articles of Maribo-Mogensen et al. (2013a, 2013b).

As discussed in the previous chapters, it is still an open question how to estimate the pure component parameters for associating fluids using pure properties only. Here we are interested at how to employ the static permittivity data in the parameter estimation by directly calculating the free site fraction with this newly developed theory.

For pure component system, equation (8.3) could be rewritten as below:

$$\frac{(2\varepsilon_r+\varepsilon_\infty)(\varepsilon_r-\varepsilon_\infty)}{\varepsilon_r(\varepsilon_\infty+2)^2}=\frac{N_A}{9\varepsilon_0 k_B T v} g\mu_0^2 \tag{8.6}$$

where ε_∞can be calculated from the following equation:

$$\frac{\varepsilon_\infty-1}{\varepsilon_\infty+2}=\frac{1}{3\varepsilon_0}\frac{N_A}{v}\alpha_0 \tag{8.7}$$

Equation (8.6) can be further arranged to be:

$$g = \frac{1}{\mu_0^2}\frac{(2\varepsilon_r + \varepsilon_\infty)(\varepsilon_r - \varepsilon_\infty)}{\varepsilon_r(\varepsilon_\infty + 2)^2}\frac{9\varepsilon_0 k_B T v}{N_A} \tag{8.8}$$

While from the definition of Kirkwood g-factor, i.e. equation (8.4) and (8.5), we can get:

$$g = 1 + \frac{z \times (1 - X^A) \times cos(\gamma)}{(1 - X^A) \times cos(\theta) + 1} \tag{8.9}$$

It can be reformulated as:

$$(1 - X^A) = \frac{g - 1}{zcos(\gamma) - (g - 1)cos(\theta)} \tag{8.10}$$

This means that it is possible to calculate the free site fraction from experimental static permittivity data, from equation (8.8) to (8.10), if the molecular structure information is known.

Let's take water as an example, the component specific parameters are:

$$\mu_0 = 1.855D, \theta = 109.47^\circ, \gamma = 69.4^\circ, \alpha_0 = 1.613 \times 10^{-40} \tag{8.11}$$

The calculated free site fractions are compared in Figure 8.11 with the experimental data [Luck (1980, 1991)] and the PC-SAFT results using the newly developed parameters from Chapter 2. The experimental density and static permittivity data are taken from NIST [REFPROP (2010)]. It can be seen that the two calculated results are in good agreement with each other and both lower than the experimental data.

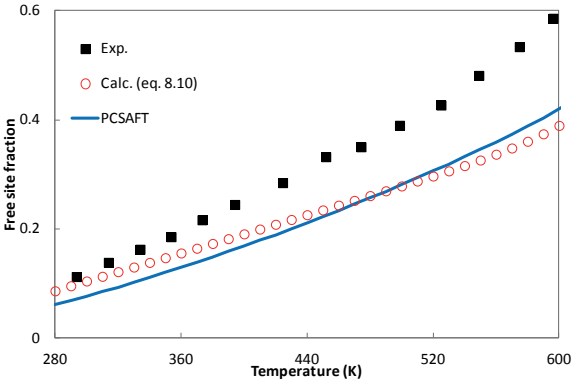

Figure 8.11 The free site fractions of saturated water from experimental work of Luck (1980, 1991), equation (8.10), and the PC-SAFT EOS with the newly developed parameters from Chapter 2.

When the free site fraction is known, it is possible to calculate the association strength for the pure component with a given association scheme. As discussed in Chapter 2, 4C is possibly the best association scheme option for water, and the association strength can be calculated as:

$$X^A = \frac{-1+\sqrt{1+8\rho\Delta}}{4\rho\Delta} \Longrightarrow \Delta = \frac{1-X^A}{2\rho(X^A)^2} \tag{8.12}$$

The calculated association strengths from static permittivity and experimental free site fraction data [Luck (1980, 1991)] are compared in Figure 8.12 versus temperature. It is readily seen that the association strengths calculated in this way show very good linear functions against reciprocal temperature below certain temperature, i.e. 450K, and they show quite different qualitative behavior above this temperature.

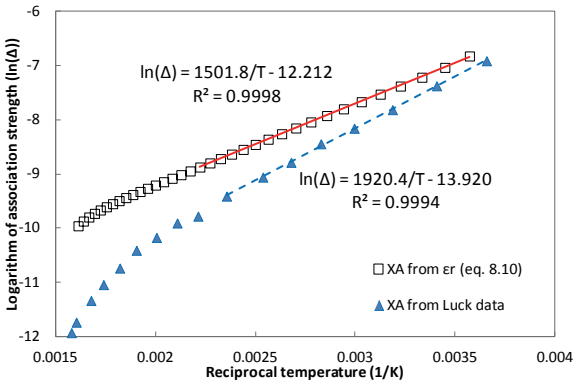

Figure 8.12 Association strength calculated from static permittivity of saturated water. Experimental data are from Luck (1980, 1991).

There are three ways to employ equation (8.12) in parameter estimation of associating fluids. The first way is to assume the temperature dependence of the radial distribution function is weak enough and $exp(\varepsilon^{HB}/kT) - 1 \approx exp(\varepsilon^{HB}/kT)$. As seen from the definition of the association strength (equation 2.19), the association energy could be read from the correlations 1500.4K from equation (8.10) or 1971.8K from experimental data. It is known from Kontogeorgis et al (2010a) that the experimental association energy is 1813K, so the association energy values from different sources varies over a large range.

$$1502K\ (\varepsilon_r) < 1704K\ (PCSAFT) < 1813K\ (exp.) < 1920K\ (eq.8.12) < 2003K\ (CPA)$$

For the given pure component parameters m, σ, ε, the association volume parameter κ can be directly calculated from the truncation values, so, in this way, there will only be three parameters left for fitting.

The second way is to combine the radial distribution function into the association strength and to assume $exp(\varepsilon^{HB}/kT) - 1 \approx exp(\varepsilon^{HB}/kT)$, as follows:

$$ln\left(\frac{\Delta}{g}\right) = lnK^{HB} + \frac{\varepsilon^{HB}}{kT} \tag{8.13}$$

where K^{HB} contains the contants and temperature-independent parameters.

During parameter estimation, the parameters ε^{HB} and K^{HB} could be directly calculated by linear regression as the other parameters are given, so there are also only three adjustable parameters left for fitting in this way.

The third way does not introduce any assumptions, but employ equation (8.12) as an additional constraint in the parameter estimation by using the experimental free site fraction data or calculating the free site fraction from the experimental static permittivity data.

8.4 Conclusions

The salt effects on the solubility of hydrocarbons and the speed of sound in water have been briefly discussed. The salts will decrease the solubility of hydrocarbons and increase the speed of sound in water. The effects of salts are larger than the effects of temperature on the solubility of hydrocarbons in water. The temperature and pressure have, respectively, moderate and minor effects on the speed of sound in salt solutions.

Based on the newly developed theory of Maribo-Mogensen et al. (2013a, 2013b), the feasibility of its usage in the parameter estimation has been discussed. With two simple approximations, there are three adjustable parameters left for fitting, and the two association parameters could be directly calculated before or during the parameter estimation. It has to be pointed out that the structure information angle(s) is/are used as adjustable parameters in the works of Maribo-Mogensen et al. (2013a, 2013b), and it is a question if the structure is stable over wide ranges of temperature and pressure, so more systematic experimental investigations are needed, and quantum chemistry computations would also provide valuable information on the aspects of molecular structure.

Chapter 9. Conclusions and future work

9.1 Conclusions

This PhD project belongs to a broader project which was initiated because of the oil spill in the Gulf of Mexico. The main purpose of the broader project is to integrate thermodynamic models into sophisticated mathematic modelings, from which a self-learning loop is constructed together with the-state-of-the-art sonar products. This advanced self-learning technology can be used to detect subsea targets. The most important properties from the thermodynamic models are speed of sound, solubility and density of oil-seawater systems.

From the viewpoint of knowledge exploration, this thesis is about the capabilities and limitations of the PC-SAFT framework, from the studies on phase behavior, speed of sound and fundamentals.

9.1.1 Phase behavior

Firstly, we have answered the question of which association scheme is a better choice for water within the PC-SAFT framework, and have developed an interactive step-wise optimization procedure, having a global character via a rather manual way, to estimate the model parameters for associating fluids by taking the liquid-liquid equilibrium data into account. The same procedure has been used for methanol and mono-ethylene-glycol (MEG). These newly estimated parameters have been applied to the phase equilibrium modeling of systems containing water, hydrocarbons and/or chemicals. Satisfactory results have been obtained when compared to calculations using other parameters or models. It has also been found that the parameters of methanol estimated with speed of sound data in consideration show equally good performance as the parameters obtained by the abovementioned procedure. These parameters and the corresponding binary interaction parameters (schemes) provide solid basis for modeling oil-water-chemical systems.

Secondly, in order to apply PC-SAFT into petroleum fluids, we have performed a comprehensive analysis on developing simple and reliable parameter estimation methods for ill-defined systems. The results show that the general characterization procedures and the number of pseudo-components give quite similar influence as for the traditional cubic EOS. The paraffinic-naphthenic-aromatic (PNA) estimation methods show quite different performance, so care should

be excercised when the PNA estimation is directly used in producing the PC-SAFT parameters. The binary interaction parameters between C_1 and C_2 to C_6, in general, have small impacts on predicting the saturation pressure, while the binary interaction parameter between C_1 and C_{7+} shows quite significant influence on individual cases. From an overall point of view, however, different binary interaction schemes between C_1 and C_{7+} give similar deviations for an oil databank considered in this project, so a compromise method has been proposed to combine the best results of each case, by using linear correlations for m and mε/k, and fitting the remaining parameter σ to specific gravity. Two candidate methods, including the compromise one, have been used to model the oil-water-chemical systems.

Finally, the overall modeling results of oil-water-chemical systems, with the estimated parameters of water and chemicals and proposed characterization methods, are quite satisfactory, if compared to the results using the avialble parameters and/or models in the literature, The two characterization methods give similar prediction from the quantitative point of view, but they produce different parameters, which lead to some systematic differences. The results reveal that the approach used in the compromise method is more attractive.

9.1.2 Speed of sound

Firstly, we have collected and reviewed the experimental speed of sound data of pure compounds (hydrocarbons and 1-alcohols), binary systems (hydrocarbon + hydrocarbon, hydrocarbon + 1-alcohol, and 1-alcohol + 1-alcohol), ternary hydrocarbons with or without 1-alcohol, and petroleum fluids. The conclusions are that speed of sound could be measured with very high accuracy, though small inconsistencies have been seen for some systems. The NIST reference models represent the speed of sound in most pure fluids, i.e. hydrocarbons and 1-alcohols available in the database, quite satisfactorily, but some deviations are seen for normal hexane and cyclo-hexane, depending on the temperature and pressure ranges. The correlations of speed of sound in different systems are also reviewed, and a single expression has been used to correlate the speed of sound in pure hydrocarbons and pure 1-alcohols.

Secondly, two approaches were proposed to improve the speed of sound description within the PC-SAFT framework. The first approach is to use the speed of sound data in the pure component parameter estimation, and the second approach is to firstly readjust the universal constants using the speed of sound data of saturated methane to decane, and then fit the pure component parameters

with vapor pressure, liquid density and speed of sound. These two approaches have been evaluated for the previously reviewed systems. The results show that the first approach works only for small associating fluids, due to the two extra association parameters, where the association term plays a very important role, while the second approach significantly improves the description of the speed of sound from both qualitative and quantitative points of view. Further investigations show that the second approach could give equally good phase equilibria for the considered systems, but it would deteriorate the density, especially for the systems containing long-chain molecules.

9.1.3 Fundamentals

The investigations of the temperature and density dependences of PC-SAFT reveal that the sixth polynomials are sufficient to represent the reduced density dependence, while the temperature dependence of the model is only valid at low density region or in a narrow range of temperature, with the given pure component parameters.

Following a similar procedure as that with the modeling of speed of sound, a new variant of the 42 universal constants has been developed with focus on vapor pressure and density. The results show that the new variant performs better than the original one for the vapor pressure, speed of sound and dP/dV, similar on density and heat capacities, but worse for the Joule-Thomson coefficients. The new universal constants give only three volume roots where the original ones show four or five volume roots, and more surprisingly, the new universal constants have almost completely avoided the most criticized issue, i.e. presence of more than three volume roots, in the real application range. Further investigations reveal that it is possible to directly apply the new universal constants into the systems considered in this PhD thesis without changing the model parameters and even the binary interaction parameter.

9.2 Future work

There is a clear degeneracy of the five pure component parameters for associating fluids during the parameter estimation. The approach of considering the liquid-liquid equilibrium data with inert compound in the parameter estimation works well for the phase behavior of the investigated water and/or mono-ethylene glycol systems, but its performance must be further investigated for other systems or properties. Putting speed of sound data in the parameter estimation of short-chain 1-alcohols improved the overall description, but does not work for long-chain 1-alcohols. It is still an open question how to develop a general parameter estimation procedure for all 1-alochols. In

Chapter 8, it is pointed out that, by applying the newly developed theory of calculating static permittivity from association theory based EOS, it is possible to fit only three or four pure component parameters for associating fluids with the given molecular structure, and to calculate the remaining parameters by using the experimental static permittivity data as input. But more systematic experimental investigations and/or quantum chemistry computations are needed to provide valuable information on the molecular structure, of which the monomer fractions or free site fractions of systems under consideration are extremely important.

Comprehensive analysis has been conducted on developing general oil characterization approaches for PC-SAFT. It is recommended to evaluate these approaches for routine PVT simulations over wide ranges of temperature, pressure and composition, phase equilibrium of oil and water, gas injections and asphaltene modeling. This could help developing even simpler and more robust characterization procedures, and then facilitate the acceptance of PC-SAFT in the upstream oil industry.

A new variant of the 42 universal constants has been developed with focus on vapor pressure and density. It has been shown that the new universal constants have practically avoided the most criticized numerical pitfalls, i.e. existence of more than three volume roots. In the meantime, equally good performance of phase behavior modeling has been obtained. It is recommended to extensively evaluate the new universal constants for various systems over wide ranges of temperature and pressure.

It would be very interesting to investigate what kind of fundamental changes could make the PC-SAFT framework sufficient enough to represent the temperature dependence of the Helmholtz free energy, e.g. residual isochoric heat capacity, speed of sound and Joule-Thomson coefficients simultaneously. An even more challenging problem is how to model the special properties of water, e.g. maximum points for density, speed of sound and isothermal compressibility versus temperature.

Reference

[1]. Abida, A.; Nain, A.K.; Hyder, S. ***J. Sol. Chem.*** 32 (**2003**) 865-877.

[2]. Al-Ajmi, M.F.; Tybjerg, P.; Rasmussen, C.P.; Azeem, J. SPE Middle East Oil and Gas Show and Conference, Manama, Bahrain, Sep. 25-28, **2011**, (SPE 141241).

[3]. Albo, P.A.G.; Lago, S.; Romeo, R.; Lorefice, S. ***J. Chem. Thermodyn.*** 58 (**2013**) 95-100.

[4]. Aparicio-Martínez, S.; Hall, K.R. ***Fluid Phase Equilib.*** 254 (**2007**) 112-125.

[5]. Automatic Leak Detection Sonar, Sonardyne. *http://www.sonardyne.com/* (accessed June 2012).

[6]. Avila, S.; Blanco, S.T.; Velasco, I.; Rauzy, E.; Otín, S. ***Energy & Fuels***, 16 (**2002**) 928-934.

[7]. Avlund, A.S. Extension of Association Models to Complex Chemicals. PhD Dissertation, Technical University of Denmark, Kgs. Lyngby, Denmark, **2011**.

[8]. Badalyan, A.L.; Otpuschennikov, N.F. ***Izv. Akad. Nauk. SSSR, Fiz. Zemli.*** 6 (**1971**) 207.

[9]. Baidakov, V.G.; Kaverin, A.M.; Skripov, V.P. ***J. Chem. Thermodyn.*** 14 (**1982**) 1003-1010.

[10]. Ball, S.J.; Trusler, J.P.M. ***Int. J. Thermophys.*** 22 (**2001**) 427-443.

[11]. Ball, S.J.; Goodwin, A.R.H.; Trusler, J.P.M. ***J. Petro. Sci. Eng.*** 34 (**2002**) 1-11.

[12]. Barker, J.A.; Henderson, D. ***J. Chem. Phys.*** 47 (**1967**) 2856-2861.

[13]. Barreau, A.; Gaillard, K.; Behar, E.; Daridon, J.L.; Lagourette, B.; Xans. P. ***Fluid Phase Equilib.*** 127 (**1997**) 155-171.

[14]. Batzle, M.; Wang, Z.J. ***Geophysics*** 57 (**1992**) 1396-1408.

[15]. Benedetto, G.; Gavioso, R.M; Albo, P.A.G.; Lago, S.; Ripa, D.M.; Spagnolo, R. ***Int. J. Thermophys.*** 26 (**2005**) 1667-1680.

[16]. Benson, G.C.; Handa, Y.P. ***J. Chem. Thermodyn.*** 13 (**1981**) 887-896.

[17]. Beregovykh, V.V.; Timofeev, V.S.; Lukyanova, R.N. ***Uch. Zap. Mosk. Inst. Tonkoi Khim. Tekhol.*** 1 (**1971**) 31-38.

[18]. Bessieres, D.; Saint-Guirons, H.; Daridon, J.L. ***High Press. Res.*** 18 (**2000a**), 279.

[19]. Bessieres, D.; Saint-Guirons, H.; Daridon, J.L. ***J. Therm. Anal. Calorim.*** 62 (**2000b**) 621.

[20]. Bilaniuk, N.; Wong, G.S.K. ***J. Acoust. Soc. Am.*** 93 (**1993**) 1609-1612.

[21]. Blandamer, M.J.; Davis, M.I.; Douhéret, G.; Reis, J.C.R. ***Chem. Soc. Rev.*** 30 (**2001**) 8-15.

[22]. Blas, F.J.; Vega, L.F. ***Mol. Phys.*** 92 (**1997**) 135.

[23]. Blas, F.J.; Vega, L.F. ***Ind. Eng. Chem. Res.*** 37 (**1998**) 660.

[24]. Bobik, M. ***J. Chem. Thermodyn.*** 10 (**1978**) 1137-1146.

[25]. Boelhouwer, J.W.M. ***Physica.*** 34 (**1967**) 484-492.

[26]. Bolotnikov, M.F.; Verveyko, V.N.; Verveyko, M.V. ***J. Chem. Eng. Data***, 49 (**2004**) 631-634.

[27]. Bolotnikov, M.F.; Neruchev, Y.A.; Melikhov, Y.F.; Verveyko, V.N.; Verveyko, M.V. ***J. Chem. Eng. Data***, 50 (**2005**) 1095-1098.

[28]. Boublik, T. ***Collect. Czech. Chem. Commun.*** 25 (**1960**) 285-287.

[29]. Brown W.B.; Gee, G.; Taylor, W.D. ***Polymer***, 5 (**1964**) 362-367.

[30]. Buchner, R.; Hefter, G.T.; May, P.M. ***J. Phys. Chem. A***, 103 (**1999**) 1-9.

[31]. Butler, J. A.V.; Thomson, D.W.; Maclennan, W.H. ***J. Chem. Soc.*** **1933**, 674-686.

[32]. Calvar, N.; González, B.; Gómez, E.; Canosa, J. ***J. Chem. Eng. Data***, 54 (**2009a**) 1334-1339.

[33]. Calvar, N.; Gómez, E.; González, B.; Domínguezm, Á. ***J. Chem. Thermodyn.*** 41 (**2009b**) 939-944.

[34]. Cameretti, L.F.; Sadowski, G.; Mollerup, J.M. ***Ind. Eng. Chem. Res.*** 44 (**2005**) 3355-3362.

[35]. Cameretti, L.F.; Sadowski, G. ***Chem. Eng. Process.*** 47 (**2008**) 1018-1025.

[36]. CERE Internal Databank, Technical University of Denmark, **2013**.

[37]. Chapman, W.G.; Jackson, G.; Gubbins, K.E. ***Mol. Phys.*** 65 (**1988**) 1057-1079.

[38]. Chapman, W.G.; Gubbins, K.E.; Jackson, G.; Radosz, M. ***Ind. Eng. Chem. Res.*** 29 (**1990)** 1709-1721.

[39]. Chapoy, A.; Mohammadi, A.H.; Richon, D.; Tohidi, B. ***Fluid Phase Equilib.*** 220 (**2004**) 113-121.

[40]. Chapoy, A.; Coquelet, C.; Richon, D. ***Fluid Phase Equilib.*** 230 (**2005a**) 210-214.

[41]. Chapoy, A.; Mohammadi, A.H.; Tohidi, B.; Richon, D. ***J. Chem. Eng. Data***, 50 (**2005b**) 1157-1161.

[42]. Chávez, M.; Palaclos, J.M.; Tsumura, E. ***J. Chem. Eng. Data***, 27 (**1982**) 350-351.

[43]. Chávez, M.; Sosa, V.; Tsumura, R. ***J. Acoust. Soc. Am.*** 77 (**1985**) 420-423.

[44]. Chen, C.T.; Millero, F.J. ***J. Acoust. Soc. Am.*** 62 (**1977**) 1129-1135.

[45]. Chen, C.T.; Chen, L.S.; Millero, F.J. ***J. Acoust. Soc. Am.*** 63 (**1978a**) 1795-1800.

[46]. Chen, C.T.; Millero, F.J.; ***J. Marine. Res.*** 36 (**1978b**) 657-691.

[47]. Chorazewski, M.; Dzida, M.; Zorebski, E.; Zorebski, M. ***J. Chem. Thermodyn.*** 58 (**2013**) 389-397.

[48]. Chiavone-Filho, O.; Proust, P.; Rasmussen, P. ***J. Chem. Eng. Data***, 38 (**1993**) 128-131.

[49]. Clark, G.N.I.; Haslam, A.J.; Galindo, A.; Jackson, G. ***Mol. Phys.*** 104 (**2006**) 3561-3581.

[50]. Coan, C.R.; King, A.D. ***J. Am. Chem. Soc.*** 93 (**1971**) 1857-1862.

[51]. Culberson, O.L.; Mcketta, J.J. ***Trans. AMIE.*** 189 (**1950**) 319-322.

[52]. Culberson, O.L.; Mcketta, J.J. ***Trans. AMIE.*** 192 (**1951**) 223-226.

[53]. Daridon, J.L.; Lagourette, B.; Xans, P. ***Fluid Phase Equilib.*** 100 (**1994**) 269-282.

[54]. Daridon, J.L.; Lagourette, B.; Labes, P. ***Int. J. Thermophys.*** 17 (**1996a**) 851-871.

[55]. Daridon, J.L.; Lagourette, B.; Gaubert, J.F.; Xans, P.; Montel, F. ***Ultrasonics***, 34 (**1996b**) 447-449.

[56]. Daridon, J.L.; Lagourette, B.; Grolier, J.P.E. ***Int. J. Thermophys.*** 19 (**1998a**) 145-160.

[57]. Daridon, J.L.; Lagrabette, A.; Lagourette, B. ***J. Chem. Thermodyn.*** 30 (**1998b**) 607-623.

[58]. Daridon, J.L.; Lagourette, B.; Xans, P.; Montel, F. ***J. Petroleum Sci. Eng.*** 19 (**1998c**) 281-293.

[59]. Daridon, J.L.; Lagourette, B.; Lagrabette, A. ***Phys. Chem. Liq.*** 37 (**1999**) 137-160.

[60]. Daridon, J.L.; Lagourette, B. ***High Temp. - High Pressures.*** 32 (**2000**) 83-87.

[61]. Daridon, J.L.; Pauly, J.; Coutinho, J.A.P.; Montel, F. ***Energy & Fuels***, 15 (**2001**) 730-735.

[62]. Daridon, J.L.; Carrier, H.; Lagourette, B. ***Int. J. Thermophys.*** 23 (**2002**) 697-708.

[63]. Davies, L.A.; Gil-Villegas, A.; Jackson, G. ***Int. J. Thermophys.*** 19 (**1998**), 675-686.

[64]. Davis, L.A.; Gordon, R.B. ***J. Chem. Phys.*** 46 (**1967**) 2650-2660.

[65]. de Hemptinne, J. C.; Ledanois, J. M.; Mougin, P.; Barreau, A. Select Thermodynamic Models for Process Simulation. Editions Technip: Paris, France, **2012**.

[66]. de Villiers, A. J. Evaluation and improvement of the sPC-SAFT equation of state for complex mixtures. PhD Dissertation, Stellenbosch University, Stellenbosch, South Africa, **2011**.

[67]. de Villiers, A.J.; Schwarz, C.E.; Burger A.J.; Kontogeorgis, G.M. ***Fluid Phase Equilib.*** 338 (**2013**) 1-15.

[68]. Deak, A.; Victorov, A.I.; de Loos, Th.W. ***Fluid Phase Equilib.*** 107 (**1995**) 277-301.

[69]. Deepwater Horizon oil spill, *http://en.wikipedia.org/wiki/Deepwater_Horizon_oil_spill*, (accessed June 2014).

[70]. Del Grosso, V.A.; Mader, C.W. ***J. Acoust. Soc. Am.*** 52 (**1972a**) 961-974.

[71]. Del Grosso, V.A.; Mader, C.W. ***J. Acoust. Soc. Am.*** 52 (**1972b**) 1442-1446.

[72]. Derawi, S.O.; Kontogeorgis, G.M.; Stenby, E.H.; Haugum, T.; Fredheim, A.O. ***J. Chem. Eng. Data***, 47 (**2002**) 169-173.

[73]. Dhima, A.; de Hemptinne, J.C.; Moracchini, G. ***Fluid Phase Equilib.*** 145 (**1998**) 129-150.

[74]. Diamantonis, N. I.; Economou, I. G. ***Energy & Fuels***, 25 (**2010**) 3334.

[75]. Ding, Z.S.; Alliez, J.; Boned, C.; Xans, P. ***Meas. Sci. Technol.*** 8 (**1997**) 154-161.

[76]. DIPPR Database, Design Institute for Physical Property Data; DIADEM, Information and Data Evaluation Manager, version 6.0.1, **2012**.

[77]. Douhéret, G.; Davis, M.I.; Reis, J.C.R. "The measurements, interpretation and prediction of speeds of sound in liquids and liquid mixtures" Focus on Lasers and Electro-Optics Research (Ed by W.T. Akin), Nova Science, Hauppauge, NY, 2004.

[78]. Dovnar, D.V.; Lebedinskii, Y.A.; Khasanshin, T.S.; Shchemelev, A.P. ***High Temperature***, 39 (**2001**) 835-839.

[79]. Dubey, G.P.; Sharma, M. ***Int. J. Thermophys.*** 29 (**2008a**) 1361-1375.

[80]. Dubey, G.P.; Sharma, M. ***J. Chem. Eng. Data***, 53 (**2008b**) 1032-1038.

[81]. Dubey, G.P.; Sharma, M.; Dubey, N. ***J. Chem. Thermodyn.*** 40 (**2008c**) 309-320.

[82]. Dubey, G.P.; Sharma, M. ***J. Chem. Thermodyn.*** 40 (**2008d**) 991-1000.

[83]. Dubey, G.P.; Sharma, M. ***J. Mol. Liq.*** 142 (**2008e**) 124-129.

[84]. Dubey, G.P.; Sharma, M. ***J. Mol. Liq.*** 143 (**2008f**) 109-114.

[85]. Durackova, S., Apostolo, M.; Canegallo, S.; Morbidelli, M. ***J. Appl. Polym. Sci.*** 57 (**1995**) 639-644.

[86]. Dutour, S.; Daridon, J.L.; Lagourette, B. ***Int. J. Thermophys.*** 21 (**2000**) 173-184.

[87]. Dutour, S.; Daridon, J.L.; Lagourette, B. ***High Temp. - High Pressures.*** 33 (**2001a**) 371-378.

[88]. Dutour, S.; Lagourette, B.; Daridon, J.L. ***J. Chem. Thermodyn.*** 33 (**2001b**) 765-774.

[89]. Dutour, S.; Lagourette, B.; Daridon, J.L. ***J. Chem. Thermodyn.*** 34 (**2002**) 475-484.

[90]. Dzida, M.; Ernst, S. ***J. Chem. Eng. Data***, 48 (**2003**) 1453-1457.

[91]. Dzida, M.; Zak, A.; Ernst, S. ***J. Chem. Thermodyn.*** 37 (**2005**) 405-414.

[92]. Dzida, M. ***J. Chem. Eng. Data***, 52 (**2007**) 521-531.

[93]. Dzida, M.; Cempa, M. ***J. Chem. Thermodyn.*** 40 (**2008**) 1531-1541.

[94]. Dzida, M. ***J. Chem. Eng. Data***, 54 (**2009a**) 1034-1040.

[95]. Dzida, M. ***J. Phys. Chem. B*** 113 (**2009b**) 11649-11661.

[96]. Elsharkawy, A.M. ***J. Petro. Sci. Eng.*** 38 (**2003**) 57-77.

[97]. Ekiner, O.; Thodos, G. ***J. Chem. Eng. Data***, 11 (**1966**) 457-460.

[98]. Ekiner, O.; Thodos, G. ***J. Chem. Eng. Data***, 13 (**1968**) 304-306.

[99]. Estrada-Alexanders, A.F.; Trusler, J.P.M.; Zarari, M.P. ***Int. J. Thermophys.*** 16 (**1995**) 663-667.

[100]. Estrada-Alexanders, A.F.; Trusler, J.P.M. ***J. Chem. Thermodyn.*** 29 (**1997**) 991-1015.

[101]. Etter, D.O.; Kay, W.B. ***J. Chem. Eng. Data***, 6 (**1961**) 409-414.

[102]. Faradonbeh, M. R.; Abede, J.; Harding, T. G. ***Can. J. Chem. Eng.*** 91 (**2013**) 101-110.

[103]. Folas, G.K.; Gabrielsen, J.; Michelsen, M.L.; Stenby, E.H.; Kontogeorgis, G.M. ***Ind. Eng. Chem. Res.*** 44 (**2005**) 3823-3833.

[104]. Folas, G.K.; Berg, O.J.; Solbraa, E.; Fredheim, A.O.; Kontogeorgis, G.M.; Michelsen, M.L.; Stenby, E.H. ***Fluid Phase Equilib.*** 251 (**2007**) 52-58.

[105]. Formann, J.C.; Thodos, F. ***AIChE J.*** 8 (**1962**) 209-213.

[106]. Frost, M.; Karakatsani, E.; von Solms, N.; Richon, D.; Kontogeorgios, G.M. ***J. Chem. Eng. Data***, 59 (**2014**) 961-967.

[107]. Frost, M.; Kontogeorgis, G.M.; Stenby, E.H.; Yussuf, M.A.; Haugum, T.; Christensen, K.O.; Solbraa, E.; Løkken, T.V. ***Fluid Phase Equilib.*** 340 (**2013**) 1-6.

[108]. Fujii, K.I.; Masui, R. ***J. Acoust. Soc. Am.*** 93 (**1993**) 276-282.

[109]. Galindo, A.; Davies, L. A.; Gil-Villegas, A.; Jackson, G. ***Mol. Phys.*** 93 (**1998**) 241-252.

[110]. Galivel-Solastiouk, F.; Laugier, S.; Richon, D. ***Fluid Phase Equilib.*** 28 (**1986**) 73-85.

[111]. Gammon, B.E.; Douslin, D.R. ***J. Chem. Phys.*** 64 (**1976**) 203-218.

[112]. Gapta, R. B.; Johnston, K. P. ***Fluid Phase Equilib.*** 99 (**1994**) 135-151.

[113]. Gayol, A.; Iglesias, M.; Goenaga, J.M.; Concha, R.G.; Resa, J.M. ***J. Mol. Liq.*** 135 (**2007**) 105-114.

[114]. Gepert, M.; Ernst, S. ***J. Sol. Chem.*** 32 (**2003**) 831-852.

[115]. Gepert, M.; Stachowska, B. ***J. Sol. Chem.*** 35 (**2006**) 425-454.

[116]. Ghasemi, M.; Alavian, S.A.; Whitson, C.H. SPE Heavy Oil Conference and Exhibition held in Kuwait City, Kuwait, Dec. 12-14, **2011** (SPE 148906)

[117]. Gil-Villegas, A.; Galinda, A.; Whitehead, P.J.; Mills, S.J.; Jackson, G.; Burgess, A.N. ***J. Chem. Phys.*** 106 (**1997**) 4168-4186.

[118]. Glanville, J.W.; Sage, B.H.; Lacey, W.N. ***Ind. Eng. Chem.*** 42 (**1950)** 508-513.

[119]. Gonzalez, M.H.; Lee, A.L. ***J. Chem. Eng. Data***, 13 (**1968**) 172-176.

[120]. Gonzaléz, D.L. Modeling of Asphaltene Precipitation and Deposition Tendency using the PC-SAFT Equation of State. PhD Thesis, Rice University, **2008**.

[121]. Goodwin, A. R. H. Method and apparatus for measuring fluid density downhole. ***U.S. Patent*** 6640625, **2003**.

[122]. Góral, M.; Oracz, P.; Skrzecz, A.; Bok, A.; Maczyński, A. ***J. Phys. Chem. Ref. Data***, 31 (**2002**) 701-748.

[123]. Gracia, M.; Sánchez, F.; Pérez, P.; Valero, J.; Losa, C.G. ***J. Chem. Thermodyn.*** 24 (**1992**) 843-849.

[124]. Gregorowicz, J.; O'Conell, J.P.; Peters, C.J. ***Fluid Phase Equilib.*** 116 (**1996**) 94-101.

[125]. Grenner, A.; Schmelzer, J.; von Solms, N.; Kontogeorgis, G.M. ***Ind. Eng. Chem. Res.*** 45 (**2006**) 8170-8179.

[126]. Grenner, A.; Kontogeorgis, G.M.; von Solms, N.; Michelsen, M.L. ***Fluid Phase Equilib.*** 258 (**2007a**) 83-94.

[127]. Grenner, A.; Kontogeorgis, G.M.; Michelsen, M.L.; Folas, G.K. ***Mol. Phys.*** 105 (**2007b**) 1797-1801.

[128]. Grenner, A.; Tsivintzelis, I.; Economou, I.G.; Panayiotou, C.; Kontogeorgis, G.M. ***Ind. Eng. Chem. Res.*** 47 (**2008**) 5636-5650.

[129]. Griswold, J.; Wong, S. Y. ***Chem. Eng. Prog. Symp. Ser.*** 48 (**1952**) 18-34.

[130]. Gross, J.; Sadowski, G. ***Ind. Eng. Chem. Res.*** 40 (**2001**) 1244-1260.

[131]. Gross, J.; Sadowski, G. ***Ind. Eng. Chem. Res.*** 41 (**2002**) 5510-5515.

[132]. Guedes, H.J.R.; Zollweg, J.A. ***Int. J. Refrigeration***, 15 (**1992**) 381-385.

[133]. Handa, Y.P.; Halpin, C.J.; Benson, G.C. ***J. Chem. Thermodyn.*** 13 (**1981**) 875-886.

[134]. Hasanov, V.H. ***High Temperatures***, 50 (**2012**) 44-51.

[135]. Hauptamann, P.; Hoppe, N.; Püttmer, A. ***Meas. Sci. Technol.*** 13 (**2002**) 73-83.

[136]. Hawley, S.; Allegra, J.; Holton, G. ***J. Acoust. Soc. Am.*** 47 (**1970**) 137-142.

[137]. He, C.C.; Li, J.L.; Peng, C.J.; Liu, H.L.; Hu, Y. ***Fluid Phase Equilib.*** 302 (**2011**) 139-152.

[138]. Heintz, A.; Dolch, E.; Lichtenthaler, R.N. ***Fluid Phase Equilib.*** 27 (**1986**) 61-79.

[139]. Held, C.; Neuhaus, T.; Sadowski, G. ***Biophys. Chem.*** 152 (**2010**) 28-39.

[140]. Held, C.; Cameretti, L. F.; Sadowski, G. ***Ind. Eng. Chem. Res.*** 50 (**2011**) 131-141.

[141]. Held, C.; Reschke, T.; Müller, R.; Kunz, W.; Sadowski, G. ***J. Chem. Thermodyn.*** 68 (**2014**) 1-12.

[142]. Held, C.; Sadowski, G.; Carneiro, A.; Rodríguez, O.; Macedo E.A. ***AIChE J.*** 59 (**2013**) 4794-4805.

[143]. Hong, J.H.; Malone, P.V.; Jett, M.D.; Kobayashi, R. ***Fluid Phase Equilib.*** 38 (**1987**) 83-96.

[144]. Huang, S. H.; Radosz, M. ***Ind. Eng. Chem. Res.*** 29 (**1990**) 2284-2294.

[145]. Huang, S. H.; Radosz, M. ***Ind. Eng. Chem. Res.*** 30 (**1991**) 1994-2005.

[146]. Hustad, O.S.; Jia, N.J.; Pedersen, K.S.; Memon, A.; Leekumjorn, S. SPE Annual Technical Conference and Exhibition, New Orleans, Louisiana, USA. Sep. 30 – Oct. 2, **2013** (SPE 166097).

[147]. IOC, SCOR and IAPSO, **2010**: The international thermodynamic equation of seawater – 2010: Calculation and use of thermodynamic properties. Intergovernmental Oceanographic Commission, Manuals and Guides No.56, UNESCO.

[148]. Ixtoc I oil spill, *http://en.wikipedia.org/wiki/Ixtoc_I_oil_spill* (accessed June 2014).

[149]. Jackson, G.; Chapman, W.G.; Gubbins, K.E. ***Mol. Phys.*** 65 (**1988**) 1-31.

[150]. Jaubert, J.N.; Avaullee, L.; Souvay, J.F. ***J. Petro. Sci. Eng.*** 34 (**2002**) 65-107.

[151]. Junquera, E.; Tardajos, G.; Aicart. E. ***J. Chem. Thermodyn.*** 20 (**1988**) 1461-1467.

[152]. Kesler, M.G.; Lee, B.I. ***Hydrocarbon Processing***, 55 (**1976**) 153-158.

[153]. Khammar, M.; Shaw, J.M. ***Fluid Phase Equilib.*** 288 (**2010**) 145-154.

[154]. Khasanshin, T.S. ***High Temperature***, 29 (**1992**) 554-559.

[155]. Khasanshin, T.S.; Shchemelev, A.P. ***High Temp. – Hihg Pressures***, 32 (**2000**) 663-668.

[156]. Khasanshin, T.S.; Shchemelev, A.P. ***High Temperature***, 39 (**2001**) 60-67.

[157]. Khasanshin, T.S.; Shchemelev, A.P. ***High Temperature***, 40 (**2002**) 207-211.

[158]. Khasanshin, T.S.; Shchamialiou, A.P.; Poddubskij, O.G. ***Int. J. Thermophys.*** 24 (**2003**) 1277-1289.

[159]. Khasanshin, T.S.; Shchamialiou, O.G.A.P.; Samuilov, V.S. ***Fluid Phase Equilib.*** 245 (**2006**) 26-31.

[160]. Khasanshin, T.S.; Samuilov, V.S.; Shchemelev, A.P. ***J. Eng. Phys. Thermophys.*** 82 (**2009**) 149-156.

[161]. Kiyohara, O.; Benson, G.C. ***J. Chem. Thermodyn.*** 11 (**1979**) 861-873.

[162]. Kleiner, M. Thermodynamic Modeling of Complex Systems: Polar and Associating Fluids and Mixtures. PhD Dissertation, Technical University of Dortmund, Dortmund, Germany, **2008**.

[163]. Kontogeorgis, G.M.; Voutsas, E.C.; Yakoumis, I.V.; Tassios, D.P. ***Ind. Eng. Chem. Res.*** 35 (**1996**) 4310-4318.

[164]. Kontogeorgis, G.M.; Yakoumis, I.V.; Meijer H.; Hendriks, E.; Moorwood, T. ***Fluid Phase Equilib.*** 158-160 (**1999**) 201-209.

[165]. Kontogeorgis, G.M.; Michelsen, M.L.; Folas, G.K.; Derawi, S.; Von Solms, N.; Stenby, E.H. ***Ind. Eng. Chem. Res.*** 45 (**2006a**) 4855-4868.

[166]. Kontogeorgis, G.M.; Michelsen, M.L.; Folas, G.K.; Derawi, S.; Von Solms, N.; Stenby, E.H. ***Ind. Eng. Chem. Res.*** 45 (**2006b**) 4869-4878.

[167]. Kontogeorgis, G.M; Folas, G. K. Thermodynamic models for industrial applications – from classical and advanced mixing rules to association theories. John Wiley and Sons: New York, (**2010a)**.

[168]. Kontogeorgis, G.M.; Tsivintzelis, I.; von Solms, N.; Grenner, A.; Bøgn, D.; Frost, M.; Knage-Rasmussen, A.; Economou, I.G. ***Fluid Phase Equilib.*** 296 (**2010b**) 219-229.

[169]. Kontogeorgis, G.M.; Tsivintzelis, I.; Michelsen, M.L.; Stenby, E.H. ***Fluid Phase Equilib.*** 301 (**2011**) 244-256.

[170]. Kortbeek, P.J.; Schouten, J.A. ***Int. J. Thermophys.*** 11 (**1990**) 455-466.

[171]. Kouskoumvekaki, I.A.; von Solms, N.; Michelsen, M.L.; Kontogeorgis, G.M. ***Fluid Phase Equilib.*** 215 (2004) 71-78.

[172]. Kroebel, W.; Mahrt, K.H. ***Acustica***, 35 (**1976**) 154-164.

[173]. Kumar, A. ***J. Chem. Eng. Data***, 48 (**2003**) 388-391.

[174]. Kurihara, K.; Minoura, T.; Takeda, K.; Kojima, K. ***J. Chem. Eng. Data***, 40 (**1995**) 679-684.

[175]. Kurihara, K.; Midorikawa, T.; Hashimoto, T.; Kojima, K.; Ochi, K. ***J. Chem. Eng.*** (*of Japan*), 35 (**2002**) 360-364.

[176]. Kushare, S.K.; Kolhapurkar, R.R.; Dagade, D.H.; Patil, K.J. ***J. Chem. Eng. Data***, 51 (**2006**) 1617-1623.

[177]. Labes, P.; Daridon, J.L.; Lagourette, B.; Saint-Guirons, H. ***Int. J. Thermophys.*** 15 (**1994**) 803-819.

[178]. Lafitte, T.; Bessieres, D.; Pineiro, M. M.; Daridon, J. L. ***J. Chem. Phys.*** 124 (**2006**) 024509 (1-16).

[179]. Lafitte, T.; Pineiro, M.M.; Daridon, J.L.; Bessieres, D.A. ***J. Phys. Chem. B.*** 111 (**2007**) 3447-3461.

[180]. Lafitte, T.; Apostolakou, A.; Avendaño, C.; Galindo, A.; Adjiman, C.S.; Müller, E.A.; Jackson, G. ***J. Chem. Phys.*** 139 (**2013**) 154504-154537.

[181]. Lago, S.; Albo, P.A.G; Ripa, D.M. ***Int. J. Thermophys.*** 27 (**2006**) 1083-1094.

[182]. Lagourette, B.; Daridon, J.L.; Gaubert, J.F.; Xans, P. **J. Chem. Thermodyn.** 26 (**1994**) 1051-1061.

[183]. Lagourette, B.; Daridon, J.L.; Gaubert, J.F.; Saint-Guiron, H. ***J. Chem. Thermodyn.*** 27 (**1995**) 259-266.

[184]. Lagourette, B.; Daridon, J.L. ***J. Chem. Thermodyn.*** 31 (**1999**) 987-1000.

[185]. Lainez, A.; Gopal, P.; Zollweg, J.A.; Streett, W.B. ***J. Chem. Thermody.*** 21 (**1989**) 773-777.

[186]. Lainez, A.; Zollweg, J.A.; Streett, W.B. ***J. Chem. Thermodyn.*** 22 (**1990**) 937-948.

[187]. Lampreia, I.M.S.; Mendonca, A.F.S.S. ***Meas. Sci. Technol.*** 16 (**2005**) 2391-2395.

[188]. Lee, B.I.; Kesler, M.G. ***AIChE J.*** 21 (**1975**) 510-527.

[189]. Lee, L.L.; Scheller, W.A. ***J. Chem. Eng. Data***, 12 (**1967**) 497-499.

[190]. Leekumjorn, S.; Krejbjerg, K. ***Fluid Phase Equilib.*** 359 (**2013**) 17-23.

[191]. Lekvam, K.; Bishnoi, P.R. ***Fluid Phase Equilib.*** 131 (**1997**) 297-309.

[192]. Letcher, T.M.; Wootton, S.; Shuttleworth, B.; Heyward, C. ***J. Chem. Thermodyn.*** 18 (**1986**) 1037-1042.

[193]. Lev, A.D.; Robinson, D.B.; Chung, S.Y.K.; Chen, C.J. ***Can. J. Chem. Eng.*** 70 (**1992**) 330-334.

[194]. Li, J.L.; He, H.H.; Peng, C.J.; Liu, H.L.; Hu, Y. ***Fluid Phase Equilib.*** 276 (**2009**) 57-68.

[195]. Liang, X.D.; Thomsen, K.; Yan, W.; Kontogeorgis, G.M. ***Fluid Phase Equilib.*** 360 (**2013**) 222-232.

[196]. Liang, X.D.; Maribo-Mogensen, B.; Thomsen, K.; Yan, W.; Kontogeorgis, G.M. ***Ind. Eng. Chem. Res.*** 51 (**2012**) 14903-14914.

[197]. Liang, X.D.; Tsivintzelis, I.; Kontogeorgis, G.M. ***Ind. Eng. Chem. Res.*** *53* (**2014**) 14493-14503.

[198]. Liu, H.L.; Hu, Y. ***Fluid Phase Equilib.*** 122 (**1996**) 75-97.

[199]. Llovell, F.; Pamies, J.C.; Vega, L.F. ***J. Chem. Phys.*** 121 (**2004**) 10715-10724.

[200]. Llovell, F.; Peters, C.J.; Vega, L.F. ***Fluid Phase Equilib.*** 248 (**2006a**) 115-122.

[201]. Llovell, F.; Vega, L.F. ***J. Phys. Chem. B.*** 110 (**2006b**) 11427-11437.

[202]. Luck, W.A.P. ***Angew. Chem. Int. Ed. Engl.*** 19 (**1980**) 28-41.

[203]. Luck, W.A.P.; Zeegers-Huyskens, T. Intermolecular forces: an introduction to modern methods and results. Chapter IX, Water – The Most Anomalous Liquid. Springer-Verlag: Berlin, Germany, **1991**.

[204]. Lundstrøm, C.; Michelsen, M.L.; Kontogeorgis, G.M.; Pedersen, K.S.; Sørensen, H. ***Fluid Phase Equilib.*** 247 (**2006**)149-157.

[205]. Machefer, S.; Schnitzlein, K. ***Chem. Eng. Technol.*** 30 (**2007**) 1381-1390.

[206]. Mączyński, A.; Wiśniewska-Gocłowska, B.; Góral, M. ***J. Phys. Chem. Ref. Data***, 33 (**2004**) 549-577.

[207]. Marczak, W.; Dzida, M.; Ernst, S. ***High Temp. - High Pressures***, 32 (**2000**) 283-292.

[208]. Maribo-Mogensen, B.; Kontogeorgis, G.M.; Thomsen, K. ***J. Phys. Chem. B***, 117 (**2013**a) 3389-3397.

[209]. Maribo-Mogensen, B.; Kontogeorgis, G.M.; Thomsen, K. ***J. Phys. Chem. B***, 117 (**2013**b) 10523-10533.

[210]. Matsuda, H.; Kurihara, K.; Ochi, K.; Kojima, K. ***Fluid Phase Equilib.*** 203 (**2002**) 269-284.

[211]. Matsuda, H.; Ochi, K. ***Fluid Phase Equilib.*** 224 (**2004**) 31-37.

[212]. Mehra V.S.; Thodos, G. ***J. Chem. Eng. Data***, 8 (**1963**) 1-8.

[213]. Meier, K.; Kabelac, S. ***J. Chem. Eng. Data***, 58 (**2013**) 1398-1406.

[214]. Meng, G.T.; Jaworski, A.J.; Dyakowski, T.; Hale J.M.; White, N.M. ***Meas. Sci. Technol.*** 16 (**2005**) 942-954.

[215]. Meng, G.T.; Jaworski, A.J.; White, N.M. ***Chem. Eng. Process, Proc. Intens.*** 45 (**2006**) 383-391.

[216]. Michelsen, M.L.; Hendriks, E.M. ***Fluid Phase Equilib.*** 180 (**2001**) 165-174.

[217]. Michelsen, M.L. ***Ind. Eng. Chem. Res.*** 45 (**2006**) 8449-8453.

[218]. Michelsen, M.L.; Mollerup, J.M. Thermodynamic Models: Fundamentals & Computational Aspects; Tie-Line Technology: Holte, Denmark, **2007**. ISBN-89-989961-3-4.

[219]. Millero, F.J.; Ward, G.K.; Chetirkin, P.V. ***J. Acoust. Soc. Am.*** 61 (**1977**) 1492-1498.

[220]. Millero, F.J.; Ricco, J.; Schreiber, D.R. ***J. Sol. Chem.*** 11 (**1982**) 671-686.

[221]. Millero, F.J.; Chen, C.A. ***J. Sol. Chem.*** 14 (**1985a**) 301-310.

[222]. Millero, F.J.; Lampreia, M.I.; ***J. Sol. Chem.*** 14 (**1985b**) 853-864.

[223]. Millero, F.J.; Vinokurova, F.; Fernandez, M.; Hershey, J.P. ***J. Sol. Chem.*** 16 (**1987**) 269-284.

[224]. Mohammadi, A.H.; Chapoy, A.; Richon, D.; Tohidi, B. ***Ind. Eng. Chem. Res.*** 43 (**2004**) 7148-7162.

[225]. More, J.J. Levenberg-Marquardt algorithm: implementation and theory. Technical Report, CONF-770636-1, Contract W-31-109-ENG-38; Argonne National Lab., IL, **1977**.

[226]. Morrison, G.; Kincaid, J.M. ***AIChE J.*** 30 (**1984**) 257-262.

[227]. Muringer, M.J.P.; Trappeniers, N.J.; Biswas, S.N. ***Phys. Chem. Liq.*** 14 (**1985**) 273-296.

[228]. Mørch, Ø.; Nasrifar, K.; Bolland, O.; Solbraa, E.; Fredheim, A.O.; Gjertsen, L.H. ***Fluid Phase Equilib.*** 239 (**2006**) 138-145.

[229]. Nath, J. ***J. Chem. Thermodyn.*** 29 (**1997**) 853-863.

[230]. Nath, J. ***J. Chem. Thermodyn.*** 30 (**1998a**) 1385-1392.

[231]. Nath, J. ***J. Chem. Thermodyn.*** 30 (**1998b**) 885-895.

[232]. Nath, J. ***Fluid Phase Equilib.*** 175 (**2000**) 63-73.

[233]. Nath, J. ***Fluid Phase Equilib.*** 203 (**2002a**) 261-268.

[234]. Nath, J. ***J. Chem. Thermodyn.*** 34 (**2002b**) 1857-1872.

[235]. Nezbeda, I.; Kolafa, J. ***Mol. Phys.*** 97 (**1999**) 1105-1116.

[236]. Niepmann, R. ***J. Chem. Thermodyn.*** 16 (**1984**) 851-860.

[237]. Niepmann, R.; Esper, G.J.; Riemann, K.A. ***J. Chem. Thermodyn.*** 19 (**1987**) 741-749.

[238]. Oakley, B.A; Hanna, D.; Shillor, M.; Barber, G. ***J. Phys. Chem. Ref. Data***, 32 (**1991**) 1535-1544.

[239]. Oakley, B.A.; Barber, G.; Worden, T.; Hanna, D. ***J. Phys. Chem. Ref. Data***, 32 (**2003**) 1501-1534.

[240]. Olds, R.H.; Sage, B.H.; Lacey, W.N. ***Ind. Eng. Chem.*** 34 (**1942**) 1223-1227.

[241]. Orge, B.; Iglesias, M.; Tojo, J. ***J. Chem. Eng. Data***, 40 (**1995**) 260-263.

[242]. Orge, B.; Iglesias, M.; Rodriguez, A.; Canosa, J.M.; Tojo, J. ***Fluid Phase Equilib.*** 133 (**1997**) 213-227.

[243]. Orge, B.; Rodriguez, A.; Canosa, J.M.; Marino, G.; Iglesias, M.; Tojo, J. ***J. Chem. Eng. Data***, 44 (**1999**) 1041-1047.

[244]. Oswal, S.L.; Prajapati, K.D. ***J. Chem. Eng. Data***, 43 (**1998**) 367-372.

[245]. Oswal, S.L.; Maisuria, M.M. ***J. Mol. Liq.*** 109 (**2002**) 91-112.

[246]. Oswal, S.L.; Maisuria, M.M.; Gardas, R.L. ***J. Mol. Liq.*** 109 (**2004**) 155-166.

[247]. Outcalt, S.; Laesecke, A.; Fortin, T.J. ***J. Chem. Thermodyn.*** 42 (**2010**) 700-706.

[248]. O'Sullivan, T.D.; Smith, N.O. ***J. Phys. Chem.*** 74 (**1970**) 1460-1466.

[249]. Padilla-Victoria, H.; Iglesias-Silva, G.A.; Ramos-Estrada, M.; Hall, K.R. ***Fluid Phase Equilib.*** 338 (**2013**) 119-127.

[250]. Pandey, J.D.; Vyas, V.; Jain, P.; Dubey, G.P.; Tripathi, N.; Dey, R. ***J. Mol. Liq.*** 81 (**1999**) 123-133.

[251]. Panuganti, S.R.; Vargas, F.M.; Gonzalez, D.L.; Kurup, A.S.; Chapman, W.G. ***Fuel***, 93 (**2012**) 658-669.

[252]. Panuganti, S.R.; Tavakkoli, M.; Vargas, F.M.; Gonzalez, D.L.; Chapman, W.G. ***Fluid Phase Equilib.*** 359 (**2013**) 2-16.

[253]. Parikh, J.S.; Bukacek, R.F.; Graham, L.; Leipziger, S. ***J. Chem. Eng. Data***, 29 (**1984**) 301-303.

[254]. Parke, S.A.; Birch, G.G. ***Food Chemistry*** 67 (**1999**) 241-246.

[255]. Pedersen, K.S.; Thomassen, P.; Fredenslund, A. ***Fluid Phase Equilib.*** 14 (**1983**) 209-218.

[256]. Pedersen, K.S.; Thomassen, P.; Fredenslund, A. ***Ind. Eng. Chem. Process Des. Dev.*** 23 (**1984**) 163-170.

[257]. Pedersen, K.S.; Blilie, A.L.; Meisingset, K.K. ***Ind. Eng. Chem. Res.*** 31 (**1992**) 1378-1384.

[258]. Pedersen, K.S.; Christensen, P.L. Phase Behavior of Petroleum Reservoir Fluids, Second Edition: CRC Press, Taylor & Francis, Boca Raton, Florida, USA, **2007a**. ISBN 0-8247-0694-3.

[259]. Pedersen, K.S.; Sørensen, C.H. SPE Annual Technical Conference and Exhibition, **2007b**, Anaheim, California, U.S.A.

[260]. Pedersen, K.S.; Leekumjorn, S.; Krejbjerg, K.; Azeem, J. Abu Dhabi International Petroleum Exhibition & Conference, Abu Dhabi, UAE, Nov. 11-14, **2012** (SPE 162346).

[261]. Pemberton, R.C.; Mash, C.J. ***J. Chem. Thermodyn.*** 10 (**1978**) 867-888.

[262]. Peng, D.Y.; Robinson, D.B. ***Ind. Eng. Chem. Fundam.*** 15 (**1976**) 59-65.

[263]. Peng, D.Y.; Robinson, D.B. ***AIChE J.*** 23 (**1977**) 127-144.

[264]. Pfohl, O.; Budich, M. ***Fluid Phase Equilib.*** 189 (**2001**) 179-185.

[265]. Phutela, R.C.; Kooner, Z.S.; Fenby, D.V. ***Austra. J. Chem.*** 32 (**1979**) 2353-2359.

[266]. Plantier, F.; Daridon, J.L.; Lagourette, B. ***J. Acoust. Soc. Am.*** 111 (**2002a**) 707-715.

[267]. Plantier, F.; Daridon, J.L.; Lagourette, B. ***J. Phys. D: Appl. Phys.*** 35 (**2002b**) 1063-1067.

[268]. Plantier, F.; Daridon, J.L.; Lagourette, B. ***High Temp.– High Pressures***, 35/36 (**2003/2004**) 109-116.

[269]. Plantier, F.; Bessieres, D.; Daridon, J.L.; Montel, F. ***Fuel***, 87 (**2008**) 196-201.

[270]. Plesnar, Z.; Gierycz, P.; Bylicki, A. ***Thermochim. Acta*** 128 (**1988**) 93-98.

[271]. Plesnar, Z.; Gierycz, P.; Gregorowicz, J.; Bylicki, A. ***Thermochim. Acta*** 150 (**1989**) 101-109.

[272]. Privat, R.; Gani, R.; Jaubert, J.N. ***Fluid Phase Equilib.*** 295 (**2010**) 76-92.

[273]. Privat, R.; Conte, E.; Jaubert, J.N.; Gani, R. ***Fluid Phase Equilib.*** 318 (**2012**) 61-76.

[274]. Polishuk, I.; Katz, M.; Levi Y.; Lubarsky, H. ***Fluid Phase Equilib.*** 316 (**2011a**) 66-73.

[275]. Polishuk, I. ***Ind. Eng. Chem. Res.*** 50 (**2011b**) 4183-4198.

[276]. Polishuk, I. ***Ind. Eng. Chem. Res.*** 50 (**2011c**) 11422-11431.

[277]. Polishuk, I. ***J. Supercrit. Fluids.*** 58 (**2011d**) 204-215.

[278]. Polishuk, I.; Privat, R.; Jaubert, J.N. ***Ind. Eng. Chem. Res.*** 52 (**2013**) 13875-13885.

[279]. Polishuk, I. ***Ind. Eng. Chem. Res.*** 53 (**2014**) 14127-14141.

[280]. Punnapala, S.; Vargas, F.M. ***Fuel***, 108 (**2013**) 417-429.

[281]. Rai, R.D.; Shukla, R.K.; Shukla, A.K.; Pandey, J.D. ***J. Chem. Thermodyn.*** 21 (**1989**) 125-129.

[282]. Randzio, S.L.; Grolier, J.P.E.; Quint, J.R.; Eatough, D.J.; Lewis, E.A.; Hansen, L.D. ***Int. J. Thermophys.*** 15 (**1994**) 415-441.

[283]. Razzouk, A.; Naccoul, R.A.; Mokbel, I.; Duchet-Suchaux, P.; Jose, J.; Rauzy, E.; Berro, C. ***J. Chem. Eng. Data***, 55 (**2010**) 1468-1472.

[284]. Reamer, H.H.; Sage, B.H. ***J. Chem. Eng. Data***, 7 (**1962)** 161-168.

[285]. REFPROP, NIST Standard Reference Database 23, Version 9.0, **2010**.

[286]. Riaz, M.; Kontogeorgis, G.M.; Stenby, E.H.; Yan, W.; Haugum, T.; Christensen, K.O.; Solbraa, E.; Løkken, T.V. ***Fluid Phase Equilib.*** 300 (**2011a**) 172-181.

[287]. Riaz, M.; Kontogeorgis, G.M.; Stenby, E.H.; Yan, W.; Haugum, T.; Christensen, K.O.; Løkken, T.V.; Solbraa, E. ***J. Chem. Eng. Data***, 56 (**2011b**) 4342-4351.

[288]. Riaz, M.; Yussuf, M.A.; Kontogeorgis, G.M.; Stenby, E.H.; Yan, W.; Solbraa, E. ***Fluid Phase Equilib.*** 337 (**2013**) 298-310.

[289]. Riaz, M.; Yussuf, M.A.; Frost, M.; Kontogeorgis, G.M.; Stenby, E.H.; Yan, W.; Solbraa, E. ***Energy & Fuels.*** 28 (**2014**) 3530-3538.

[290]. Riazi, M.R.; Daubert, T.E. ***Ind. Eng. Chem. Process Des. Dev.*** 25 (**1986**) 1009-1015

[291]. Riazi, M.R. Characterization and Properties of Petroleum Fractions, First Edition: ASTM stock number: MNL50, **2005**. ISBN 0-8031-3361-8.

[292]. Rodriguez, V.; Pardo, J.; López, M.C.; Royo, F.M.; Urieta, J.S. ***J. Chem. Eng. Data***, 38 (**1993**) 350-352.

[293]. Ruether, F.; Sadowski, G. ***J. Pharm. Sci.*** 98 (**2009**) 4205-4215.

[294]. Sastry, N.V.; Raj, M.M. ***J. Chem. Eng. Data***, 41 (**1996a**) 612-618.

[295]. Sastry, N.V.; Valand, M.K. ***J. Chem. Eng. Data***, 41 (**1996b**) 1421-1425.

[296]. Sastry, N.V.; Valand, M.K. ***J. Chem. Eng. Data***, 41 (**1996c**) 1428-1428.

[297]. Sehgal, C.M.; Porter, B.R.; Greenleaf, J.F. ***J. Acoust. Soc. Am.*** 79 (**1986**) 566-570.

[298]. Shaw, D.G.; Maczynski, A.; Hefter, G.T.; Kleinschmidt, M.; Mackay, D.; Meyers, P.A.; Miyamoto, H.; Shiu, W.Y. ***J. Phys. Chem. Ref. Data***, 35 (**2006**) 785-837.

[299]. Soave, G. ***Chem. Eng. Sci.*** 27 (**1972**) 1197-1203.

[300]. Søreide, I. Improved Phase Behavior Prediction of Petroleum Reservoir Fluids from a Cubic Equation of State. PhD Thesis, Norwegian Inst. of Technology, Trondheim, Norway, **1989**.

[301]. Sørensen, C.H. Thermodynamic Modeling of Hydrocarbon Mixtures with the PC-SAFT Model. Msc Thesis, Technical University of Denmark, Kgs. Lyngby, Denmark, **2008**.

[302]. Sørensen, J.M.; Arlt, W. Liquid-liquid equilibrium data collection (Binary Systems); DECHEMA Chemistry Data Series: Frankfurt/Main, Germany, **1995**, Vol. V, Part 1.

[303]. Straty, G.C. ***Cryogenics***, 14 (**1974**) 367-370.

[304]. Sun, T.F.; Kortbeek, P.J.; Trappeniers, N.J.; Biswas, S.N. ***Phys. Chem. Liq.*** 16 (**1987**) 163-178.

[305]. Sun, T.F.; Biswas, S.N.; Trappeniers, N.J.; Ten Seldam, C.A. ***J. Chem. Eng. Data***, 33 (**1988a**) 395-398.

[306]. Sun, T.F.; Ten Seldam, C.A.; Kortbeek, P.J.; Trappeniers, N.J.; Biswas, S.N. ***Phys. Chem. Liq.*** 18 (**1988b**) 107-116.

[307]. Sun, T.F.; Schouten, J.A.; Biswas, S.N. ***Int. J. Thermophys.*** 12 (**1991**) 381-395.

[308]. Takagi, T. ***J. Chem. Thermodyn.*** 12 (**1980**) 1183-1190.

[309]. Takagi, T.; Teranishi, H. ***J. Soc. Mater. Sci.*** (*in Japanese*) 33 (**1984**) 134-139.

[310]. Takagi, T.; Teranishi, H. ***Fluid Phase Equilib.*** 20 (**1985**) 315-320.

[311]. Takagi, T.; Teranishi, H. ***J. Chem. Thermodyn.*** 19 (**1987**) 1299-1304.

[312]. Takagi, T.; Kusunokl, M.; Hongo, M. ***J. Chem. Eng. Data***, 37 (**1992**) 39-41.

[313]. Takagi, T. ***J. Chem. Eng. Data***, 42 (**1997**) 1129-1132.

[314]. Takagi, T.; Sakura, T.; Guedes, H.J.R. ***J. Chem. Thermodyn.*** 34 (**2002**) 1943-1957.

[315]. Takagi, T.; Sawada, K.; Urakawa, H.; Ueda, M.; Cibulka, I. ***J. Chem. Eng. Data***, 49 (**2004a**) 1652-1656.

[316]. Takagi, T.; Sawada, K.; Urakawa, H.; Tsuji, T.; Cibulka, I. ***J. Chem. Eng. Data***, 49 (**2004b**) 1657-1660.

[317]. Takagi, T.; Sawada, K.; Urakawa, H.; Ueda, M.; Cibulka, I. ***J. Chem. Thermodyn.*** 36 (**2004c**) 659-664.

[318]. Tamura, K.; Ohomuro, K.; Murakami, S. ***J. Chem. Thermodyn.*** 15 (**1983**) 859-868.

[319]. Tamura, K.; Murakami, S. ***J. Chem. Thermodyn.*** 16 (**1984**) 33-38.

[320]. Tihić, A.; Kontogeorgis, G.M.; von Solms, N.; Michelsen, M.L. ***Fluid Phase Equilib.*** 248 (**2006**) 29-43.

[321]. Tihić, A.; Group Contribution sPC-SAFT Equation of State. PhD Thesis, Technical University of Denmark, **2008**.

[322]. Ting, P.D.; Joyce, P.C.; Jog, P.K.; Chapman, W.G.; Thies, M.C. ***Fluid Phase Equilib.*** 206 (**2003**) 267-286.

[323]. Ting, P.D. Thermodynamic Stability and Phase Behavior of Asphaltenes in Oil and of Other Highly Asymmetric Mixtures. PhD Thesis, Rice University, **2003b**.

[324]. Tourino, A.; Hervello, M.; Moreno, V.; Iglesias, M.; Marino, G. ***Phys. Chem. Liq.*** 42 (**2004**) 37-51.

[325]. Tsivintzelis, I.; Grenner, A.; Economou, I. G.; Kontogeorgis, G.M. ***Ind. Eng. Chem. Res.*** 47 (**2008**) 5651-5659.

[326]. Tsivintzelis, I.; Bøgh, D.; Karakatsani, E.; Kontogeorgis, G.M. ***Fluid Phase Equilib.*** 365 (**2014**) 11-122.

[327]. Tsonopoulos, C.; Wilson, G.M. ***AIChE J.*** 29 (**1983**), 990-999.

[328]. Tsonopoulos, C.; Wilson, G.M. ***AIChE J.*** 31 (**1985**), 376-384.

[329]. Tsumura, R.; Straty, G.C. ***Cryogenics***, 17 (**1977**) 195-200.

[330]. Tumakaka, F.; Gross, J.; Sadowski, G. ***Fluid Phase Equilib.*** 194-197 (**2002**) 541-551.

[331]. Twu, C.H. ***Fluid Phase Equilib.*** 16 (**1984**) 137-150.

[332]. Udovenko, V.V.; Mazanko, T.F.; Ya Plyngeu, V. Liquid-vapor equilibrium in normal propyl alcohol-water and normal propyl alcohol benzene systems. ***Zh. Fiz. Khim.*** **1972**, Vol. 46, 218.

[333]. Urlic, L.E.; Florusse, L.J.; Straver, E.J.M.; Degrange, S.; Peters, C.J. ***Transport in Porous Media***, 52 (**2003**) 141-157.

[334]. van Itterbeek, A.; Thoen, J.; Cops, A.; van Dael, W. ***Physica***, 35 (**1967**) 162-166.

[335]. van Nes, K.; van Western, H.A. Aspects of the Constitution of Mineral Oils. Elsevier. New York, **1951**.

[336]. van Poolen, L.J.; Holcomb, C.D. ***Fluid Phase Equilib.*** 165 (**1999**) 157-168.

[337]. Vargas, F.M. Modeling of Asphaltene Precipitation and Arterial Deposition. PhD Thesis, Rice University, **2010**.

[338]. von Solms, N.; Michelsen, M.L.; Kontogeorgis, G.M. ***Ind. Eng. Chem. Res.*** 42 (**2003**) 1098-1105.

[339]. von Solms, N.; Kouskoumvekaki, I.A.; Michelsen,M.L.; Kontogeorgis, G.M. ***Fluid Phase Equilib.*** 241 (**2006a**) 344-353.

[340]. von Solms, N.; Michelsen, M.L.; Passos, C.P.; Derawi, S.O. Kontogeorgis, G.M. ***Ind. Eng. Chem. Res.*** 45 (**2006b**) 5368-5374.

[341]. Wang, L.K.; Chen, G.J.; Han, G.H.; Guo, X.Q.; Guo, T.M. ***Fluid Phase Equilib.*** 207 (**2003**) 143-154.

[342]. Wang, Z.J.; Nur, A. ***Geophysics***, 55 (**1990a**) 723-733.

[343]. Wang, Z.J.; Nur, A.M.; Batzle, M.L. ***J. Pet. Tech.*** 42 (**1990b**) 192-200.

[344]. Wang, Z.J.; Nur, A. ***J. Acoust. Soc. Am.*** 89 (**1991**) 2725-2730.

[345]. Wertheim, M. S. ***J. Stat. Phys.*** 35 (**1984a**) 19-34.

[346]. Wertheim, M. S. ***J. Stat. Phys.*** 35 (**1984b**) 35-47.

[347]. Wertheim, M. S. ***J. Stat. Phys.*** 42 (**1986a**) 459-476.

[348]. Wertheim, M. S. ***J. Stat. Phys.*** 42 (**1986b**) 477-492.

[349]. Whaley, P.D.; Winter, H.H.; Ehrlich, P. ***Macromolecules***, 30 (**1997**) 4882-4886.

[350]. Whitson, C.H. ***SPE J.*** 23 (**1983**) 683-694.

[351]. Whitson, C.H.; Andersen, T.F.; Søreide, I. C7+ Characterization of Related Equilibrium Fluids Using the Gamma Distribution. C7+ Fraction Characterization, Advances in Thermodynamics, Taylor & Francis, New York, **1989**.

[352]. Whitson, C.H.; Brulé, M.R. Phase Behavior, Monograph Volume 20, Society of Petroleum Engineers Inc., Richardson, Texas, **2000**. ISBN 1-55563-087-1.

[353]. Wibawa, G.; Hatano, R.; Sato, Y.; Takishima, S.; Masuoka, H. ***J. Chem. Eng. Data***, 47 (**2002**) 1022-1029.

[354]. Wiese, H.C.; Jacob, J.; Sage, B.H. ***J. Chem. Eng. Data***, 15 (1970) 82-91.

[355]. Wilsak, R.A.; Campbell, S.W.; Thodos, G. ***Fluid Phase Equilib.*** 33 (**1987**) 157-171.

[356]. Wilson, W.D. ***J. Acoust. Soc. Am.*** 31 (**1959**) 1067-1072.

[357]. Wilson, W.D. ***J. Acoust. Soc. Am.*** 32 (**1960**) 641-644.

[358]. Wilson, W.D.; Bradley, D. ***J. Acoust. Soc. Am.*** 36 (**1964**) 333-337.

[359]. Wolf, B.A.; Enders, S. Polymer Thermodynamics – Liquid Polymer-Containing Mixtures. Spinger-Verlag Berlin Heidelberg, **2011**.

[360]. Wu, R.; Rosenegger, L. ***J. Can. Petro. Technol.*** 38 (**1999**) 1-10 (97-05).

[361]. Yakoumis, I.V.; Kontogeorgis, G.M.; Voutsas, E.C.; Hendriks, E.M.; Tassios, D.P. ***Ind. Eng. Chem. Res.*** 37 (**1998**) 4175-4182.

[362]. Yan, W.; Stenby, E.H. Presented at International conference on Properties and Phase Equilibria for Product and Process Design (PPEPPD), Suzhou, Jiangsu, China, May 16-21, **2010**.

[363]. Yan, W.; Liang, X.D. Heptane plus characterization, Private communication, **2013**.

[364]. Yarborough, L.; Smith, L.R. ***Soc. Petro. Eng. J.*** 10 (**1970**) 298-310.

[365]. Ye, S.; Alliez, J.; Lagourette, B.; Saint-Guirons, H.; Arman, J.; Xans, P. ***Revue. Phys. Appl.*** 25 (**1990**) 555-565.

[366]. Ye, S.; Lagourette, B.; Alliez, J.; Saint-Guirons, H.; Xans, P. ***Fluid Phase Equilib.*** 74 (**1992a**) 157-175.

[367]. Ye, S.; Lagourette, B.; Alliez, J.; Saint-Guirons, H.; Xans, P. ***Fluid Phase Equilib.*** 74 (**1992b**) 177-202.

[368]. Yelash, L.; Müller, M.; Paul, W.; Binder, K. ***J. Chem. Phys.*** 123 (**2005**) 14908 (1-15).

[369]. Yelash, L.; Müller, M.; Paul, W.; Binder, K. ***Phys. Chem. Chem. Phys.*** 7 (**2005**) 3728-3732.

[370]. Zuo, J.Y.; Zhang, D. Presented at the SPE Asia Pacific Oil and Gas Conference in Brisbane, Australia, Oct. 16-18, **2000** (SPE 64520-MS).

[371]. Åkerlöf, G. ***J. Am. Chem. Soc.*** 54 (**1932**) 4125-4139.

[372]. Żak, A.; Dzida, M.; Zorbski, M.; Ernst, S. ***Rev. Sci. Instrum.*** 71 (**2000**) 1756-1765.

List of Symbols

Physical constants

N_{av} = Avogadro's number

k_B = Boltzmann constant

R = Gas Constant

ε_0 = Vacuum permittivity

Physical properties

T = Temperature

P = Pressure

V = Total volume

ρ = Molar density

Z = Compressibility factor

u = Speed of Sound

C_V = Isochoric heat capacity

C_P = Isobaric heat capacity

Equation of state

EoS = Equation(s) of State

CPA = Cubic Plus Association

SAFT = Statistical Associating Fluid Theory

PC-SAFT = Perturbed-Chain Statistical Associating Fluid Theory

sPC-SAFT = Simplified-Perturbed-Chain Statistical Associating Fluid Theory

A^r = Residual Helmholtz free energy

a^r = Molar residual Helmholtz free energy

hs (seg) = Hard sphere (segment) term of reduced residual Helmholtz free energy

hc = Chain term of reduced residual Helmholtz free energy

disp = Dispersion term of reduced residual Helmholtz free energy

assoc = Association term of reduced residual Helmholtz free energy

OrgUC = sPC-SAFT with the original universal constants and parameters

OrgSS = sPC-SAFT with the original universal constants and new parameters fitted to the speed of sound containing data

NewUC = sPC-SAFT with the new universal constants and parameters readjusted to the the speed of sound containing data

PC-SAFT (GS)= sPC-SAFT with the original universal constants

PC-SAFT (LK)= sPC-SAFT with the new universal constants with fitting focus on vapor pressure and density

N = molar numbers

x_i = Molar fraction

m = Segment number

σ = Segment diameter

ε = Segment energy

$\varepsilon^{A_iB_i}$ or ε^{HB} = Association energy

$\kappa^{A_iB_i}$ or κ^{HB} = Association volume

d_i = Temperature-dependent segment diameter

η = Packing fraction (reduced density)

g_{ij}^{hs} = Radial distribution function of hard sphere fluid

$\Delta^{A_iB_j}$ = Association strength between site A_i and site B_j

X^{A_i} = Non-bonded site fraction of association site A of component *i*

k_{ij} = Binary interaction parameter

GS = Gross and Sadowski

DE = Diamantonis and Economou

XL = Xiaodong Liang

AG = Andreas Grenner

NVS = Nicolas von Solms

W2B = Water parameters with 2B association scheme

W3B = Water parameters with 3B association scheme

W3B_C = Water parameters with 3B association scheme, rescaled to critical points

W4C = Water parameters with 4C association scheme

Others

%AAD = Percentage average absolute deviation

%ARD = Percentage average relative deviation

%AD = Percentage absolute deviation

%RD = Percentage relative deviation

VLE = Vapor-Liquid Equilibria

LLE = Liquid-Liquid Equilibria

VLLE = Vapor-Liquid-Liquid Equilibria

MEG = Mono-Ethylene Glycol

SCN = Single Carbon Number

PNA = Paraffins, Naphthenes, Aromatics

CM = Candidate Method

List of Figures

List of Tables

APPENDICES

Appendix A. Petroleum fluid database

Table A.1 An overview of the petroleum fluid database

Fluid	% N2	% CO2	% H2S	% C1	N+	% C(+)	Mw(+)	SG(+)	Type	T range (K)
F01	0.13	0.18	0	61.92	7	6.85	143	0.795	GC	358.71
F02	0.84	2.77	0	77.74	11	1.02	203.2	0.797	GC	363.15~393.15
F03	0.49	0.97	0	71.12	11	3.96	233.55	0.827	GC	313.15~414.15
F04	0.60	3.34	0	74.16	20	0.47	362	0.877	GC	428.15
F05	0.64	3.53	0	70.78	20	0.62	381	0.880	GC	423.65
F06	0.35	2.53	0	65.43	20	3.86	280	0.885	GC	303.15~399.15
F07	0.16	0.91	0	36.47	7	33.29	218	0.852	OIL	377.6
F08	0.52	6.47	0	39.58	7	23.67	178	0.858	OIL	427.55
F09	0.03	8.39	0	47.43	7	18.61	180	0.83	OIL	419.25
F10	0.38	7.03	0	48.73	7	20.26	181	0.805	OIL	427.05
F11	0.34	7.10	0	48.43	7	19.17	183	0.805	OIL	429.85
F12	0.88	1.34	0	5.63	7	67.03	224	0.855	OIL	326.45
F13	0.33	0.35	0	6.72	7	71.06	225	0.858	OIL	332.05
F14	0.41	0.26	0	6.14	7	69.51	225	0.860	OIL	329.85
F15	0.68	0.16	0	22.84	7	47.9	226	0.864	OIL	342.05
F16	0.21	0.75	0.51	6.05	7	64.81	231	0.857	OIL	337.55
F17	0.30	0.01	0	7.14	7	67.15	233	0.86	OIL	333.15
F18	0.54	0.18	0	21.62	7	47.54	236	0.863	OIL	342.05
F19	0.31	0.28	0.02	6.80	7	66.76	237	0.858	OIL	335.35
F20	0.60	0.12	0	23.71	7	44.81	238	0.868	OIL	342.05
F21	0.53	0.12	0	22.80	7	46.04	242	0.864	OIL	342.05
F22	0.37	0.02	0	17.28	7	54.80	242	0.851	OIL	342.05
F23	1.39	0.28	0	21.32	7	47.03	257	0.870	OIL	342.05
F24	0.35	0.56	1.41	9.99	7	71.03	258	0.872	OIL	337.55
F25	0.29	0.46	0.49	10.75	7	72.86	261	0.861	OIL	335.95
F26	0.11	0.02	0	13.66	11	83.83	232.93	0.857	OIL	311.15
F27	5.50	33.54	0	18.58	11	20.18	244.84	0.866	OIL	409.15
F28	0.05	2.25	0	23.21	11	67.15	245.65	0.931	OIL	329.75
F29	0.24	2.10	0	26.12	11	69.4	265.81	0.894	OIL	318.35
F30	1.64	1.95	0	44.40	11	15.31	269.41	0.883	OIL	377.95
F31	0	0.45	0	48.76	11	16.00	271.19	0.890	OIL	358.15
F32	0.12	2.08	0	28.46	11	68.07	275.49	0.903	OIL	317.95
F33	0	0.20	0	36.33	11	23.59	275.78	0.895	OIL	347.15
F34	0.09	2.28	0	30.08	11	65.77	282.57	0.911	OIL	318.15
F35	0	0.14	0	50.21	11	21.38	286.91	0.887	OIL	344.35
F36	0.09	3.76	0	45.66	11	31.32	290.35	0.906	OIL	330.85
F37	0	1.81	0	49.83	11	19.28	292.93	0.891	OIL	337.25
F38	0.07	3.81	0	40.23	11	48.03	295.48	0.916	OIL	331.15
F39	3.57	20.78	0.55	21.99	11	23.52	298.54	0.914	OIL	401.05
F40	0.07	3.85	0	45.46	11	32.47	299.43	0.908	OIL	331.55

F41	0.17	0.08	0	44.72	11	24.78	299.83	0.905	OIL	335.25
F42	0.1	3.84	0	46.77	11	30.24	301.41	0.912	OIL	331.15
F43	0.16	0.23	0	39.45	11	36.02	305.16	0.949	OIL	346.15
F44	0.08	0.27	0	49.71	11	28.61	305.28	0.910	OIL	337.85
F45	0.23	0.05	0	37.62	11	38.27	314.09	0.930	OIL	342.15
F46	0	4.70	0	38.64	11	43.17	314.99	0.946	OIL	318.15
F47	0.24	2.54	0	40.82	11	41.27	317.89	0.916	OIL	323.35
F48	0	2.65	0	41.99	11	45.64	318.03	0.934	OIL	319.55
F49	0.07	3.59	0	35.53	11	40.33	319.42	0.943	OIL	339.85
F50	0	2.25	0	44.66	11	42.68	321.5	0.932	OIL	322.65
F51	0.66	0.11	0	19.54	11	50.82	322.87	0.908	OIL	351.65
F52	0.38	0.14	0	18.79	11	32.09	324.25	0.876	OIL	362.25
F53	0.13	0.09	0	41.32	11	41.53	343.32	0.943	OIL	344.95
F54	0.23	0.16	0	35.13	11	41.73	344.49	0.876	OIL	318.75
F55	0.5	0.04	0.88	21.50	11	49.53	345.5	0.929	OIL	331.15
F56	0.81	0.08	0	42.14	11	43.14	347.49	0.946	OIL	346.05
F57	0.32	0.97	0	30.17	11	53.69	371.28	0.987	OIL	329.15
F58	0.15	0.82	0	32.81	11	59.41	375.01	0.984	OIL	329.15
F59	0.12	1.94	0.96	13.15	11	45.85	380.92	0.913	OIL	312.15
F60	0	2.25	0	18.38	11	76.78	400.21	1.001	OIL	323.15
F61	0.12	0.02	0	3.90	11	70.45	427.41	0.958	OIL	332.15
F62	0.37	0.751	0	56.31	11	13.92	286.32	0.865	OIL	408.15~418.15
F63	0.39	0.30	0	40.20	20	6.64	453	0.918	OIL	370.65
F64	0.59	0.36	0	40.81	20	6.25	458	0.926	OIL	370.95
F65	0.25	3.60	2.32	47.64	20	6.02	411	0.881	OIL	303.25~417.85
F66	0.35	3.14	0	54.26	20	4.08	418	0.905	OIL	388.15
F67	0.40	2.55	0.36	47.24	20	6.01	434	0.917	OIL	394.25
F68	0	0.77	0	36.20	20	8.15	442	0.938	OIL	383.15
F69	0.45	2.07	0.38	26.58	20	12.96	450	0.956	OIL	394.25
F70	0.67	0.86	0	46.63	20	6.55	450	0.927	OIL	373.75
F71	0	2.13	0	31.28	20	6.33	455	0.915	OIL	393.15
F72	0.083	1.82	0	32.17	20	6.70	455	0.915	OIL	393.15
F73	0.32	2.80	1.49	45.29	20	6.04	460	0.939	OIL	299.85~394.25
F74	0.45	1.64	0	45.85	20	6.18	474	0.925	OIL	387.35
F75	0.20	1.34	0	23.64	20	12.03	530	0.949	OIL	372.05
F76	0.18	0.82	0	22.92	20	11.44	560	0.951	OIL	374.85
F77	1.25	0.90	0	37.54	20	13.17	678	0.900	OIL	377.55
F78	0.49	0.31	0	44.01	30	9.96	449	0.989	OIL	347.15
F79	0.29	0.22	0	21.66	36	6.66	291	0.895	OIL	350.4
F80	0.27	0.32	0	36.08	36	3.48	262	0.880	OIL	335.7
min	0	0.01	0	3.90	7	0.47	143	0.795		299.85
max	5.5	33.54	2.32	77.74	36	83.83	678	1.001		429.85

Appendix B. Detailed results for Chapter. 4

Table B.1 Characterization results of Live Oil 1

Comp.	z	Mw	CM5 (R)			CM7		
			m	σ (Å)	ε/k (K)	m	σ (Å)	ε/k (K)
P1	0.02499	94.70	3.10526	3.77873	248.40	3.15682	3.75318	244.34
P2	0.00732	114.20	3.56668	3.85154	253.61	3.61308	3.83129	250.35
P3	0.00637	128.30	3.87375	3.87700	258.37	3.94300	3.84923	253.83
P4	0.01563	148.70	4.27839	3.86920	266.51	4.42038	3.81850	257.95
P5	0.00732	184.51	5.07438	3.85849	272.91	5.25827	3.80351	263.37
P6	0.00778	218.70	5.73639	3.87103	282.13	6.05825	3.78685	267.14
P7	0.00640	266.57	6.74654	3.85876	288.36	7.17833	3.76341	271.01
P8	0.00534	338.31	8.30894	3.82789	293.12	8.85694	3.73022	274.98
P9	0.00323	495.03	11.84171	3.75204	296.08	12.52390	3.66736	279.95

Table B.2 Characterization of Live Oil 2

Comp.	z	Mw	CM5 (R)			CM7		
			m	σ (Å)	ε/k (K)	m	σ (Å)	ε/k (K)
P1	0.02824	106.42	3.43905	3.84784	247.56	3.43100	3.85158	248.14
P2	0.01694	148.42	4.34333	3.91174	262.08	4.41372	3.88639	257.90
P3	0.01016	190.42	5.34204	3.91121	266.79	5.39645	3.89523	264.10
P4	0.00874	243.29	6.64231	3.88982	268.94	6.63356	3.89189	269.29
P5	0.00651	365.37	9.24731	3.90470	283.36	9.49007	3.86383	276.11

Table B.3 Characterization results of the five dead oils

Pseudo Comp.	z	Mw	CM5 (R)			CM7		
			m	σ (Å)	ε/k (K)	m	σ (Å)	ε/k (K)
				Cond-1				
P1	0.16046	91.40	3.02720	3.76347	247.35	3.07960	3.73690	243.14
P2	0.16632	103.60	3.26702	3.79478	254.70	3.36506	3.74917	247.28
P3	0.08903	118.50	3.61186	3.83754	258.57	3.71369	3.79440	251.48
P4	0.05038	136.00	4.01464	3.87201	262.40	4.12316	3.83042	255.50
P5	0.03992	150.00	4.33481	3.88937	265.08	4.45074	3.84811	258.18
P6	0.03162	164.00	4.65829	3.90188	267.21	4.77831	3.86201	260.50
P7	0.02506	178.00	4.98502	3.91064	268.88	5.10589	3.87303	262.51
P8	0.01985	192.00	5.31486	3.91652	270.19	5.43346	3.88180	264.29
P9	0.02819	212.19	5.95940	3.87717	264.11	5.90584	3.89134	266.50
P10	0.01769	240.19	6.60332	3.89027	267.32	6.56099	3.90040	269.04
P11	0.01808	278.99	7.48585	3.90365	271.21	7.46879	3.90726	271.83
P12	0.01176	371.40	9.58049	3.91728	277.80	9.63102	3.90890	276.34
				Cond-2				
P1	0.20837	91.00	3.00568	3.75710	248.22	3.07031	3.72424	243.00
P2	0.18433	104.33	3.29076	3.80001	254.37	3.38202	3.75773	247.51
P3	0.08558	119.32	3.65308	3.84986	257.17	3.73276	3.81622	251.68
P4	0.02695	136.00	4.04361	3.88732	260.52	4.12316	3.85676	255.50
P5	0.02210	150.00	4.36993	3.91006	262.95	4.45074	3.88120	258.18
P6	0.03297	170.31	4.84627	3.93465	265.73	4.92589	3.90884	261.44
P7	0.01218	192.00	5.35813	3.95353	268.00	5.43346	3.93131	264.29
P8	0.00999	206.00	5.92732	3.89768	258.40	5.76104	3.94283	265.86
P9	0.01490	226.31	6.42081	3.90994	260.15	6.23619	3.95639	267.85
P10	0.01372	260.16	7.24020	3.92551	262.65	7.02826	3.97305	270.56
P11	0.00924	307.56	8.38755	3.93937	265.33	8.13745	3.98806	273.48
P12	0.00762	409.74	10.85822	3.95141	269.23	10.52814	4.00142	277.67
				Cond-3				
P1	0.26650	90.18	2.97766	3.75008	248.67	3.05106	3.71257	242.69
P2	0.21810	103.79	3.28496	3.80086	253.71	3.36951	3.76155	247.34
P3	0.06690	117.24	3.57143	3.82935	259.09	3.68421	3.78125	251.15
P4	0.02005	136.00	4.01814	3.87385	262.17	4.12316	3.83359	255.50
P5	0.01419	150.00	4.34902	3.89772	264.22	4.45074	3.86146	258.18
P6	0.01004	164.00	4.68106	3.91692	265.91	4.77831	3.88453	260.50
P7	0.00711	178.00	5.01418	3.93250	267.31	5.10589	3.90384	262.51
P8	0.00503	192.00	5.34829	3.94526	268.50	5.43346	3.92019	264.29
P9	0.00356	206.00	5.91248	3.89304	259.05	5.76104	3.93413	265.86
P10	0.00252	220.00	6.25596	3.90305	260.11	6.08861	3.94612	267.26
P11	0.00178	234.00	6.59974	3.91157	261.06	6.41618	3.95649	268.52
P12	0.00432	281.90	7.77067	3.93305	263.82	7.53681	3.98210	272.01

				Light-1				
P1	0.04920	92.14	3.04376	3.76662	247.67	3.09692	3.73981	243.42
P2	0.06210	107.14	3.39291	3.82489	252.38	3.44789	3.79983	248.36
P3	0.06090	123.24	3.78280	3.87846	255.44	3.82460	3.86117	252.65
P4	0.19315	155.74	4.50680	3.91639	263.67	4.58505	3.88923	259.17
P5	0.14476	211.74	5.93998	3.89957	264.45	5.89535	3.91148	266.46
P6	0.08423	261.33	7.12028	3.90135	268.19	7.05560	3.91578	270.65
P7	0.08740	309.74	8.20072	3.91116	273.18	8.18837	3.91355	273.59
P8	0.07913	371.99	9.57300	3.91844	278.44	9.64481	3.90656	276.37
P9	0.05518	441.99	11.11420	3.92029	282.85	11.28268	3.89635	278.63
P10	0.05039	523.98	12.96963	3.91133	285.57	13.20120	3.88317	280.56
P11	0.04203	644.01	15.61781	3.90333	289.65	16.00974	3.86389	282.56
P12	0.03012	865.23	20.37698	3.89292	296.16	21.18581	3.83106	284.86
				Light-2				
P1	0.1369	91.82	3.03797	3.76578	247.42	3.08943	3.73977	243.30
P2	0.1427	104.45	3.30540	3.80521	253.50	3.38495	3.76837	247.55
P3	0.0838	118.10	3.60110	3.83586	258.58	3.70433	3.79204	251.38
P4	0.08781	142.49	4.17363	3.88650	263.03	4.27497	3.84896	256.79
P5	0.03515	164.00	4.67793	3.91485	266.08	4.77831	3.88144	260.50
P6	0.05658	184.49	5.16247	3.93335	268.22	5.25770	3.90444	263.36
P7	0.04221	212.49	6.04881	3.89176	260.54	5.91285	3.92772	266.53
P8	0.03149	240.49	6.72452	3.90700	262.80	6.56800	3.94442	269.07
P9	0.03289	274.64	7.54476	3.92071	265.15	7.36703	3.95876	271.55
P10	0.02119	316.64	8.55596	3.93141	267.35	8.34975	3.97053	273.95
P11	0.02246	375.10	9.96249	3.93981	269.69	9.71756	3.97990	276.48
P12	0.01593	518.27	13.39703	3.94484	273.55	13.06756	3.98519	280.45

Table B.4 Mutual solubility of petroleum fluids and MEG*

T (K)	Case no.	Solubility of oil in polar phase					Solubility of MEG in organic phase				
		Exp.	AG		XL		Exp.	AG		XL	
			CM5 (R)	CM7	CM5 (R)	CM7		CM5 (R)	CM7	CM5 (R)	CM7
Cond-1 [Riaz, et al. (2011a)]											
275.15	1	None	3306	3277	3198	3172	53	70	70	57	57
283.15	2	None	3510	3477	3436	3407	74	113	113	92	92
303.15	3	4590	4083	4039	4097	4060	250	336	335	269	268
308.15	4	None	4242	4195	4279	4240	335	431	430	344	343
313.15	5	4524	4408	4358	4468	4426	431	549	548	436	436
318.15	6	5170	4582	4529	4665	4620	None	694	692	549	549
323.15	7	4937	4764	4707	4870	4823	722	871	869	687	686
326.55	8	None	4892	4832	5015	4965	711	1012	1009	797	796
Cond-2 [Riaz, et al. (2011b)]											
275.15	9	None	2483	2463	2420	2406	51	64	64	53	53
283.15	10	None	2672	2649	2635	2620	87	104	104	85	85
303.15	11	4879	3210	3178	3243	3221	290	310	310	249	249
308.15	12	None	3360	3326	3412	3389	355	399	398	319	319
313.15	13	5325	3518	3481	3588	3563	470	509	508	405	406
318.15	14	5860	3683	3643	3772	3746	None	643	643	511	512
323.15	15	6084	3856	3813	3965	3936	581	808	807	640	641
Cond-3 [Riaz, et al. (2014)]											
303.15	16	3485	4452	4400	4497	4455	196	273	272	222	221
313.15	17	3906	4826	4766	4925	4877	337	449	447	362	361
323.15	18	4239	5235	5165	5389	5334	654	714	711	574	572
Light-1 [Frost et al. (2013)]											
303.15	19	973	1081	1065	1088	1073	1931	638	643	478	482
313.15	20	1106	1153	1135	1172	1155	2630	1036	1044	769	776
323.15	21	1210	1234	1215	1265	1248	3488	1631	1643	1203	1213
Light-2 [Frost et al. (2013)]											
303.15	22	3433	3786	3765	3790	3773	385	390	390	307	308
313.15	23	3477	4062	4037	4106	4087	612	636	637	498	498
323.15	24	3738	4363	4334	4449	4427	916	1006	1007	782	783

* No decimal is used for the values.

Table B.5 Solubility of petroleum fluids, MEG and water from PC-SAFT with different parameters

Char. Method	Case no.	Oil in polar phase			MEG in organic phase			H_2O in organic phase		
		Exp	AG	XL	Exp	AG	XL	Exp	AG	XL
Cond-1 (323.15K) [Riaz, et al. (2011a)]										
CM5 (R)	1*	69	155	73	61	127	108	1218	855	1079
CM7			154	73		127	108		865	1092
CM5 (R)	2*	417	616	443	172	357	289	946	586	747
CM7			611	441		356	289		593	757
CM5 (R)	3	1793	2194	2029	381	634	504	402	277	356
CM7			2173	2013		633	504		280	361
Cond-2 (303.15K) [Riaz, et al. (2011b)]										
CM5 (R)	4	67	60	28	36	44	38	806	358	471
CM7			60	28		44	38		361	474
CM5 (R)	5	189	163	100	73	93	77	635	287	380
CM7			163	100		92	77		289	383
CM5 (R)	6	508	603	486	103	169	138	394	187	250
CM7			599	484		169	138		188	252
Cond-2 (323.15K) [Riaz, et al. (2011b)]										
CM5 (R)	7	91	82	42	82	118	101	1309	860	1082
CM7			82	42		118	101		867	1091
CM5 (R)	8	311	219	145	158	245	202	1119	695	880
CM7			218	144		245	202		701	887
CM5 (R)	9	1181	776	656	328	442	356	784	457	584
CM7			770	653		442	356		461	589
Cond-3 (313.15K) [Riaz, et al. (2014)]										
CM5 (R)	10	711	960	777	178	232	191	480	309	409
CM7			952	772		231	190		312	413
CM5 (R)	11	180	334	212	91	132	111	673	449	588
CM7			332	210		131	110		454	595
CM5 (R)	12	62	147	72	53	65	56	796	550	717
CM7			146	71		65	56		556	725
Light-1 (313.15K) [Frost et al. (2013)]										
CM5 (R)	13	230	272	226	493	545	410	722	367	431
CM7			268	223		549	413		374	438
CM5 (R)	14	117	96	61	270	268	207	908	571	662
CM7			94	60		270	209		581	675

Light-1 (323.15K) [Frost et al. (2013)]										
CM5 (R)	15	239	259	215	568	806	603	1023	605	694
CM7			256	213		812	608		615	706
CM5 (R)	16	129	118	80	363	475	362	1443	842	958
CM7			116	79		478	365		857	976
Light-2 (323.15K) [Frost et al. (2013)]										
CM5 (R)	17*	686	1092	897	549	548	432	917	473	594
CM7			1088	895		548	433		475	596
CM5 (R)	18+	270	379	240	529	301	243	1351	719	894
CM7			378	240		301	243		722	898
CM5 (R)	19+	125	173	84	238	147	123	1744	886	1095
CM7			172	84		148	123		889	1099

The calculation pressure is 1.01325bar, except (*) 1.21325bar and (+) 1.31325bar.

Appendix C. Speed of sound database

Table C.1 Temperature and pressure ranges of speed of sound measurements in pure n-alkane fluids

Comp.	T (K)	P (MPa)	Ref.	Comp.	T (K)	P (MPa)	Ref.
C1	113.15-323.15	0.11-25	1	nC11	271.15-394.15	0.101325	16
	91-186	saturated	2		278-318	1-100	[2]5
	100-300	1.6-35	2	nC12	273.15-473.15	0.1-140	14
	111.33 – 190	0.11-20	3		277.15-392.15	0.101325	16
	150-183	1.6-4.0	4		303.15-433.15	0.1-49	18
	148.15-295.15	0.1-1000	5		293.15-433.15	0.1-140	26
C2	91-303	saturated	6	nC13	303.15-433.15	0.1-49	18
	100-323.15	4.1-37	6		293.15-373.15	0.1-150	27
	220-450	0.014-10.5	7	nC14	283.15-393.15	0.101325	16
C3	200-340	0.02-60	8		303.15-433.15	0.1-49	18
nC4	200-375	0.002-60	8		293.15-373.15	0.1-150	27
nC5	205.67-308.4	saturated	9		293.15-433.15	0.1-140	28
	185.65-310.65	0.1-263	10	nC15	287.15-394.15	0.101325	16
	263.15-433.24	0.22-210	11		303.15-433.15	0.1-49	18
	293.15-373.15	5-100	[1]2		303.15-433.15	0.1-140	29
	293.15-313.15	0.1-600	[1]3		293.15-383.15	0.1-150	30
nC6	253.15-333.15	0.1-140	14	nC16	293.15-473.15	0.1-140	14
	303	0.1-392	15		303.15-393.15	0.1-70	24
	263.15-341.15	0.101325	16		296.15-392.15	0.101325	16
	293.15-373.15	0.1-150	17		303.15-433.15	0.1-49	18
	298.15-433.15	0.1-49	18		298.3-373.15	0.1-100	19
	298.3-373.15	0.1-100	19		293.15-333.15	0.101325	31
	293.15-333.15	0.101325	20		298.15-433.15	0.1-140	32
nC7	253.15-453.15	0.1-140	14		209.65-343.15	0.083	[3]3
	265.15-368.15	0.101325	16	nC17	303.15-383.15	0.1-150	30
	293.15-373.15	0.1-150	21	nC18	301.15-395.15	0.101325	16
	298.15-523.15	0.1-59	22		313.15-383.15	0.1-150	34
nC8	253.15-393.15	0.1-140	14	nC19	313.15-383.15	0.1-150	34
	265.15-392.15	0.101325	16	nC20	323.15-393.15	0.1-150	35
	293.15-363.15	5-90	12	nC22	323.15-393.15	0.1-150	35
	303.15-433.15	0.1-49	18		317.15-393.15	0.101325	16
	298.15-523.15	0.1-59	22	nC23	333.15-393.15	0.1-150	36
nC9	253.15-413.15	0.1-140	14	nC24	333.15-393.15	0.1-150	36
	293.15-393.15	0.1-100	[2]3	nC28	334.15-393.15	0.101325	16
nC10	300.15-413.15	0.1-60	[2]4		353.15-403.15	0.1-150	37
	268.15-391.15	0.101325	16	nC36	347.15-405.15	0.101325	16
	298.15-433.15	0.1-49	18		363.16-403.15	0.1-151	37

Reference for Table C.1: (1) Itterbeek et al. 81967), (2) Straty (1974), (3) Gammon et al. (1976), (4) Baidakov et al. (1982), (5) Kortbeek et al. (1990), (6) Tsumura et al. (1977), (7) Estrada-Alexanders et al. (1997), (8) Niepmann (1984), (9) Chávez et al. (1982), (10) Muringer et al. (1985), (11) Lainez et al. (1990), (12) Ding et al. (1997), (13) Bolotnikov et al. (2004), (14) Boelhouwer et al. (1967), (15) Hawley et al. (1970), (16) Wang et al. (1991), (17) Daridon et al. (1998a), (18) Khasanshin et al. (2001), (19) Ball et al. (2001), (20) Bolotnikov et al. (2005), (21) Daridon et al. (1999), (22) Hasanov (2012), (23) Lago et al. (2006), (24) Ye et al. (1990), (25) Giuliano Albo et al. (2013), (26) Khasanshin et al. (2003), (27) Daridon et al. (2000), (28) Khasanshin et al. (2002), (29) Dovnar et al. (2001), (30) Daridon et al. (2002), (31) Bolotnikov et al. (2005), (32) Khasanshin et al. (2009), (33) Outcalt et al. (2010), (34) Dutour et al. (2000), (35) Dutour et al. (2001a), (36) Dutour et al. (2001b), (37) Dutour et al. (2002).

Table C.2 The speed of sound database for binary hydrocarbon systems *

System	T (K)	P (MPa)	Ref.	System	T (K)	P (MPa)	Ref.
C1 + C3	262.75-413.45	10-70 (a)	1	nC6 + cC6	303.15	0.101325	9
C1 + nC8	293.15-373.15	25-100 (b)	1	nC6 + C6H6	313.15	0.101325	10
C1 + nC16	292.15-413.15	6.3-66 (c)	2	nC6 + C7H8	313.15	0.101325	10
nC6 + nC7	298.15	0.101325	3	nC7 + cC6	303.15	0.101325	9
nC6 + nC8	298.15	0.101325	3	nC7+ C6H6	298.15	0.101325	[1]1
nC6 + nC9	298.15	0.101325	3	nC7 + C6H6	313.15	0.101325	10
	293.16-313.73	0.101325	4	nC7 + C7H8	313.15	0.101325	10
nC6 + nC10	298.15	0.1-100	[5]	nC8 + cC6	303.15	0.101325	9
	298.15	0.101325	3	nC8 + C6H6	313.15	0.101325	10
nC6 + nC11	298.15	0.101325	3	nC8 + C7H8	313.15	0.101325	10
nC6 + nC12	298.15	0.101325	3	nC9 + C6H6	313.15	0.101325	10
nC6 + nC16	298.15-373.15	0.1-70 (d)	2	nC9 + C7H8	313.15	0.101325	10
	293.15-373.15	0.101325	6	cC6+ C6H6	293.15-303.15	0.1-200	[1]2
nC7 + nC8	298.15-523.15	0.1-59	7		298.15	0.101325	11
nC7 + nC12	293-318	0.1-101	8		293.15-303.15	0.101325	[1]3
nC10 + nC12	298.15	0.1-100	5		298.15	0.101325	[1]4
nC10 + nC14	298.15	0.1-100	5		303.15	0.101325	[1]5
					313.15	0.101325	16
				cC6+ C7H8	313.15	0.101325	16

* The composition range is mole fraction from 0 to 1 by default, except (a) x1 = 0.8998; (b) x1 = 0.98; (c) x1 = 0.323, 0.51, 0.679; (d) x1 = 0.2, 0.4, 0.6, 0.8

Reference of Table C.2: (1) Lagourette et al. (1994), (2) Ye et al. (1992), (3) Tourino et al. (2004), (4) Gepert et al. (2003), (5) [Takagi] et al. (1985), (6) Bolotnikov et al. (2005), (7) Hasanov et al. (2012), (8) Dzida et al. (2008), (9) Oswal et al. (2002), (10) Calvar et al. (2009b), (11) Tamura et al. (1983), (12) Takagi et al. (1980), (13) Tamura et al. (1984), (14) Junquera et al. (1988), (15) Oswal et al. (2004), (16) Calvar et al. (2009a).

Table C.3 The speed of sound database for ternary systems at 298.15K and atmospheric pressure

Comp. 1	Comp. 2	Comp. 3	Mole Fraction Range	%ARD	Points	Ref.
n-hexane	n-heptane	n-decane	x1=[0.1735-0.4500] x2=[0.2759-0.5179]	-3.17	15	1
n-hexane	n-heptane	cyclo-hexane	x1=[0.1533-0.6988] x2=[0.1823-0.4103]	-0.61	15	1
n-hexane	n-heptane	toluene	x1=[0.1522-0.6952] x2=[0.1838-0.4045]	-0.97	15	1
n-pentane	n-hexane	benzene	x1=[0.0966-0.4082] x2=[0.2877-0.4665]	-4.19	10	2
n-hexane	cyclo-hexane	benzene	x1=[0.0771-0.3448] x2=[0.3342-0.4851]	-2.62	10	2
n-heptane	cyclo-hexane	toluene	x1=[0.2837-0.4393] x2=[0.1124-0.4525]	-6.78	10	2
cyclo-hexane	benzene	1-pentanol	x1=[0.0401-0.7091] x2=[0.0572-0.8998]	2.36	41	3

Reference of Table C.3: (1) Pandey et al. (1999), (2) Rai et al. (1989), (3) Orge et al. (1995).

Table C.4 The speed of sound database for oils

System	Temp. range (K)	Press. range (MPa)	API or C1 composition	C11+ composition	ref.
Oil A	297.15-378.15	0.1-44	5° (API)		1
Oil B	296.15-375.15	0.1-44	7° (API)		1
Oil C	303.15-385.15	0.1-44	10° (API)		1
Oil D	294.15-387.15	0.1-44	10.5° (API)		1
Oil E	296.15-390.15	0.1-44	12° (API)		1
Oil F	298.15-380.15	0.1-44	34° (API)		1
Oil G	297.15-359.15	0.1-44	43° (API)		1
Oil H	296.15-363.15	0.1-44	57° (API)		1
Oil I	317.15-382.15	0.1-44	62° (API)		1
Oil J	296.15-345.15	0.8-44	23° (API)		1
Oil K	296.15-345.15	8.8-44	live oil		1
Oil L	262.40-354.00	12-70	x~88.4%		2
Oil M	272.90-413.60	20-70	x~89.6%		2
Oil N	313.15-453.15	40-120	x=68.4%	4.88%	3
Oil O	293.15-373.15	40-100	x=76.6%	1.73%	4
Oil P	273.05-373.45	40-70	x=61.9%	7.30%	5
Oil Q	313.15-453.15	40-120	x=69.1%	4.30%	5
Oil R	273.75-413.45	10-70	x=30.0%	31.1%	5
Oil S	293.15-373.15	0.1-150	synthetic system	100%	6
Oil T	293.15-373.15	0.1-150	distillation cut	100%	6
Oil U	335.10-402.10	12.6-70	x=34.3%	20.8%	7
Oil V	283.15-373.15	0.1-20	None	93.7%	8
Oil W	283.15-373.15	0.1-20	None	96.3%	8

Reference of Table C.4: (1) Wang et al. (1990b), (2) Labes et al. (1994), (3) Daridon et al. (1996b), (4) Barreau et al. (1997), (5) Daridon et al. (1998c), (6) Lagourette et al. (1999), (7) Ball et al. (2002), (8) Plantier et al. (2008).

Table C.5 Coefficients of correlation for the speed of sound in pure hydrocarbons and 1-alcohols with equation (5.8)

Comp.	Coefficient for temperature				
	a0	a1	a2	a3	c
nC5	0.212068	7.57345e-3	1.347817	-2.058622	-1.912743
nC6	0.327610	-2.074676	10.71832	-12.91560	-2.112133
nC7	0.343941	-2.045490	9.842795	-11.13332	-2.009931
nC8	0.655236	-4.637980	16.67994	-16.52105	-1.887652
nC9	1.503543	-12.46010	40.81211	-40.87069	-1.732812
nC10	0.568900	-3.765328	13.79155	-13.90872	-1.805046
nC11	0.192076	-0.500779	4.346802	-4.808256	-1.748128
nC12	0.299330	-1.502390	7.371681	-7.810305	-1.708618
nC13	0.165173	-0.303609	3.861754	-5.014875	-1.749733
nC14	0.147974	-0.122435	3.183280	-4.329440	-1.741384
nC15	0.270360	-1.204313	6.262105	-6.770369	-1.652112
nC16	0.250287	-1.034741	5.738589	-6.132522	-1.614573
nC17	0.0293568	0.935828	-0.119980	-0.908207	-1.681083
nC18	0.0132357	1.083803	-0.625768	-0.473679	-1.689141
nC19	0.190218	-0.493966	4.035938	-4.998633	-1.661775
nC20	-1.256293	11.90259	-31.28656	28.28115	-1.675184
nC22	-0.022899	1.341533	-1.289403	0.139508	-1.624181
nC23	-0.167505	2.531357	-4.594079	3.051720	-1.642080
nC24	0.112948	0.200237	1.832853	-2.861589	-1.636320
nC28	-0.469255	5.205791	-12.49757	10.59317	-1.628044
nC32	1.221912	-8.509352	24.48875	-22.55682	-1.602115
nC36	-1.772879	14.88992	-36.33291	30.30698	-1.518427
cC6	-0.876113	9.263434	-26.13995	24.15456	-2.288684
Benzene	0.438767	-3.047202	11.68608	-11.67896	-1.880101
Toluene	0.227227	-1.080297	6.216340	-7.852064	-1.931299
C1OH	-2.085638	22.16740	-68.11488	70.77175	-1.953617
C2OH	0.488784	-3.780596	18.27565	-23.46797	-1.755921
C3OH	-5.598469	56.90094	-183.3801	206.2862	-0.759965
C4OH	0.212071	7.54197e-3	1.347913	-2.058722	-1.912743
C5OH	1.104831	-9.590740	35.34638	-39.42883	-1.488062
C6OH	-0.131744	2.655069	-5.297635	4.468302	-1.605447
C7OH	1.499865	-13.22723	46.44495	-48.40760	-0.981517
C8OH	0.047158	1.035350	-1.142850	-1.053466	-1.976260
C9OH	0.862893	-6.991803	25.68677	-26.88268	-1.174164
C10OH	-0.464308	5.754787	-15.73310	14.53866	-1.833814

Comp.	Coefficients for pressure			
	b1	b2	b3	d
nC5	0.150526	-0.164302	0.157367	0.587264
nC6	0.232235	-0.0972733	0.0248121	0.857459
nC7	0.250922	-0.103857	0.0249824	0.886224
nC8	0.333414	-0.202573	0.0939259	0.992887
nC9	0.266674	-0.168712	0.0715825	0.922512
nC10	0.236484	-0.0573302	-0.0323692	0.871618
nC11	0.237099	-0.103164	0.0291584	0.863294
nC12	0.229912	-0.0914951	0.0221359	0.855233
nC13	0.161167	-0.0554454	0.0126638	0.719217
nC14	0.145632	-0.0470097	0.0101635	0.685614
nC15	0.189874	-0.0689852	0.0156544	0.782491
nC16	0.206872	-0.0798097	0.0196817	0.813228
nC17	0.142272	-0.0452343	9.65593e-3	0.677207
nC18	0.128265	-0.0392626	8.45507e-3	0.643371
nC19	0.129197	-0.0393608	8.32487e-3	0.647980
nC20	0.118483	-0.0351406	7.66272e-3	0.618130
nC22	0.129621	-0.0395939	8.34839e-3	0.646879
nC23	0.111381	-0.0300290	5.70816e-3	0.606004
nC24	0.111395	-0.0318087	6.74247e-3	0.602092
nC28	0.084579	-0.0176640	2.89094e-3	0.548891
nC32	0.093346	-0.0208488	3.45463e-3	0.563780
nC36	0.111325	-0.0322675	6.91334e-3	0.610190
cC6	-3.30997e-3	0.0397137	-0.0182198	0.317615
Benzene	0.195281	-0.0273543	-0.0169796	0.690872
Toluene	0.0928646	-0.0111089	-0 2.77118e-3	0.508280
C1OH	0.143815	-0.0312255	3.98001e-3	0.646859
C2OH	0.178722	-0.0435911	6.05255e-3	0.775934
C3OH	0.696505	-0.312281	0.0824123	1.863796
C4OH	0.150526	-0.164302	0.157367	0.587263
C5OH	0.237466	-0.0851677	0.0203957	0.887607
C6OH	0.153811	-0.0390488	5.24194e-3	0.708279
C7OH	0.384709	-0.152258	0.0395031	1.276415
C8OH	0.0261175	0.0150605	-8.12289e-3	0.365628
C9OH	0.251068	-0.0857784	0.0197680	0.976948
C10OH	0.0412392	0.0122681	-0.0114725	0.414458

Table C.6 Conditions and statistics of the data correlations

Comp.	max (du, m/s)	min (du, m/s)	%AAD	Tmin (K)	Tmax (K)	Pmin (MPa)	Pmax (MPa)
nC5	0.07	-0.08	0.0024	293.15	373.15	5	100
nC6	2.77	-9.02	0.0724	293.15	373.15	0.1	150
nC7	1.71	-2.59	0.0401	293.15	373.15	0.1	150
nC8	1.14	-2.97	0.0507	303.15	433.15	0.1	50
nC9	6.35	-5.80	0.1796	293.15	393.15	0.1	100
nC10	1.84	-2.82	0.0629	298.15	433.15	0.1	50
nC11	3.14	-22.30	0.0726	303.15	413.15	0.1	120
nC12	2.45	-2.40	0.0486	293.15	433.15	0.1	140
nC13	1.76	-1.18	0.0176	293.15	373.15	0.1	150
nC14	1.08	-1.11	0.0173	293.15	373.15	0.1	150
nC15	2.80	-1.92	0.0412	293.15	433.15	0.1	150
nC16	1.74	-2.99	0.0459	298.15	433.15	0.1	140
nC17	0.95	-1.53	0.0206	303.15	383.15	0.1	150
nC18	1.00	-1.21	0.0211	313.15	383.15	0.1	150
nC19	0.92	-1.19	0.0210	313.15	383.15	0.1	150
nC20	1.61	-7.82	0.0397	323.15	393.15	0.1	150
nC22	1.33	-1.48	0.0243	323.15	393.15	0.1	150
nC23	1.51	-2.12	0.0240	333.15	393.15	0.1	150
nC24	0.99	-0.97	0.0182	333.15	393.15	0.1	150
nC28	1.18	-2.25	0.0301	353.15	403.15	0.1	150
nC32	1.11	-1.72	0.0256	353.15	403.15	0.1	150
nC36	2.29	-1.26	0.0252	363.15	403.15	0.1	150
cC6	2.32	-3.29	0.0873	283.15	333.15	0.1	85
Benzene	4.48	-11.55	0.1371	283.15	461.65	0.1	60
Toluene	3.47	-5.96	0.0448	240	380	0.1	100
C1OH	3.00	-3.24	0.0565	274.74	373.15	0.1	276
C2OH	4.82	-6.90	0.1120	193.4	318.15	0.1	276
C3OH	1.28	-1.38	0.0318	293.15	318.15	0.1	120
C4OH	0.07	-0.08	0.0024	303.15	373.15	0.1	50
C5OH	0.28	-0.58	0.0100	293	318	0.1	100
C6OH	0.89	-0.70	0.0169	293	318	0.1	100
C7OH	0.40	-0.65	0.0135	293	318	0.1	100
C8OH	1.48	-1.33	0.0345	293	373.15	0.1	100
C9OH	0.53	-0.56	0.0151	293	318	0.1	100
C10OH	0.53	-0.77	0.0136	293	318	0.1	76

Appendix D. Detailed results for Chapter. 7

Table D.1 The model parameters of n-alkanes*

Alkanes	PC-SAFT (GS)+			PC-SAFT (LK)#		
	m	*σ (Å)*	*ε/k (K)*	*m*	*σ (Å)*	*ε/k (K)*
C1	1.0	3.6997	150.18	1.0	3.7075	149.85
C2	1.60640	3.5258	191.41	1.62319	3.5055	189.90
C3	1.98464	3.6270	209.21	2.00185	3.6098	207.87
C4	2.30312	3.7218	224.55	2.32014	3.7077	223.35
C5	2.67703	3.7650	232.04	2.69409	3.7544	231.00
C6	3.03141	3.8046	237.88	3.04588	3.7967	237.11
C7	3.45837	3.8066	239.48	3.47284	3.8006	238.86
C8	3.86157	3.8179	241.42	3.88157	3.8110	240.73
C9	4.21311	3.8422	244.39	4.23554	3.8348	243.73
C10	4.59397	3.8562	245.91	4.62638	3.8481	245.07
C11	5.04849	3.8445	245.40	5.07409	3.8428	244.87
C12	5.40389	3.8608	247.08	5.43101	3.8595	246.60
C13	5.82782	3.8635	247.01	5.85874	3.8621	246.54
C14	6.14811	3.8817	249.06	6.18361	3.8797	248.56
C15	6.46509	3.9023	250.74	6.50012	3.9009	250.33
C16	6.85832	3.9024	251.02	6.90210	3.8996	250.51
C17	7.22541	3.9099	251.81	7.26950	3.9076	251.38
C18	7.60403	3.9127	251.84	7.65229	3.9100	251.42
C19	8.05710	3.9008	251.09	8.11613	3.8967	250.59
C20	8.41319	3.9160	251.76	8.47251	3.9123	251.31

* For a fair comparison, the model parameters are estimated or re-estimated to the same data with the same procedure for the new and original universal constants. The experimental data are taken from NIST [REFPROP (2010)] for C1 to C10 and from DIPPR Database (2012) for C11 to C20. The data for pure component parameter estimation are from the saturated line only.

+ PC-SAFT (GS) denotes the PC-SAFT model with the original universal constants from Gross and Sadowski.

PC-SAFT (LK) denotes the PC-SAFT model with the new universal constants from this work, Liang and Kontogeorgis.

Table D.2 %AADs for vapor pressure (P), liquid density (ρ) and speed of sound (u) [*]

Comp.	PC-SAFT (GS)		PC-SAFT (LK)	
	P	ρ	P	ρ
C1	0.39	0.95	0.21	0.47
C2	0.10	0.28	0.13	0.31
C3	0.18	0.17	0.14	0.31
C4	0.33	0.24	0.28	0.29
C5	0.23	0.25	0.26	0.21
C6	0.46	0.37	0.54	0.34
C7	0.23	0.36	0.18	0.19
C8	0.46	0.43	0.13	0.19
C9	0.63	0.36	0.12	0.30
C10	0.66	0.36	0.08	0.21
C11	0.93	0.46	0.39	0.25
C12	0.83	0.46	0.25	0.23
C13	0.72	0.42	0.07	0.20
C14	0.91	0.41	0.06	0.20
C15	0.45	0.42	0.69	0.20
C16	1.14	0.32	0.08	0.20
C17	0.64	0.26	0.55	0.22
C18	0.62	0.23	0.72	0.27
C19	1.43	0.16	0.31	0.39
C20	1.57	0.14	0.74	0.42
Avg.[+]	0.65	0.35	0.30	0.27
Avg.[#]	0.90	0.31	0.34	0.28

[*] The data of C1 to C10 are from NIST [REFPROP (2010)], and the vapor pressure and liquid density data of C11 to C20 are from DIPPR Database (2012).

Avg. [+], and Avg. [#] denote the average %AAD from C1 to C20, and from C1 to C24, respectively.

Table D.3 %AADs for residual heat capacities, dP/dV and Joule-Thomson (JT) coefficients*

Comp.	PC-SAFT (GS)					PC-SAFT (LK)				
	u	C_V^r	C_P^r	dP/dV	JT	u	C_V^r	C_P^r	dP/dV	JT
C1	4.17	18.7	11.1	19.1	8.90	6.47	26.5	6.14	24.4	8.49
C2	8.26	33.6	3.92	9.01	5.04	8.08	39.9	3.14	8.08	3.97
C3	9.97	40.2	2.51	13.4	3.41	8.93	43.9	3.05	10.9	3.99
C4	9.58	49.3	3.22	14.4	7.02	8.13	51.0	4.05	11.0	3.62
C5	9.27	44.5	1.97	14.6	6.57	7.63	44.7	3.24	10.9	3.01
C6	8.89	45.2	3.80	14.6	6.93	6.76	45.9	4.92	9.54	5.52
C7	10.8	32.4	2.21	20.2	5.63	8.57	32.8	2.46	14.4	8.72
C8	10.2	23.6	2.29	20.3	9.14	7.74	24.4	2.74	13.6	53.8
C9	11.2	33.8	3.07	21.6	7.46	8.73	34.0	3.32	14.9	18.7
C10	10.7	33.8	2.71	19.8	7.47	8.32	34.4	3.36	13.7	12.6
Avg.	9.30	35.5	3.68	16.7	6.76	7.94	37.8	3.64	13.1	12.2

* The used data are only at ***saturated*** lines.

Table D.4 %AADs for density, speed of sound, residual heat capacities, dP/dV and Joule-Thomson (JT) coefficients *

Comp.	OrgUC						NewUC					
	ρ	u	C_V^r	C_P^r	dP/dV	JT	ρ	u	C_V^r	C_P^r	dP/dV	JT
C1	1.15	2.79	19.0	5.82	7.02	8.01	0.70	3.30	24.1	5.20	7.43	6.73
C2	1.33	6.02	30.9	4.62	5.53	10.1	1.26	5.83	34.4	4.55	4.67	10.2
C3	1.40	8.28	37.2	4.91	9.63	13.0	1.30	7.41	40.4	4.78	7.33	13.4
C4	1.41	7.96	46.1	5.92	9.73	8.55	1.34	6.99	47.3	5.50	7.52	8.78
C5	1.55	9.35	45.6	6.40	12.1	7.17	1.38	7.94	46.7	5.73	9.21	7.38
C6	1.49	8.14	42.5	7.78	10.5	7.95	1.41	6.87	42.8	7.37	7.91	8.83
C7	1.55	9.60	33.8	6.67	13.6	6.33	1.43	8.08	34.0	6.08	10.5	7.69
C8	1.34	8.65	24.2	6.52	12.9	6.98	1.29	7.25	24.3	6.25	10.0	14.0
C9	1.60	9.89	34.5	6.87	14.0	6.78	1.61	8.32	34.2	6.36	10.7	10.3
C10	1.66	10.2	33.0	8.08	15.6	6.70	1.60	8.66	33.2	7.48	11.6	8.77
Avg.	1.45	8.08	34.7	6.36	11.0	8.16	1.33	7.07	36.1	5.93	8.69	9.61

* The used data are over wide temperature and pressure ranges, which can be found in Chapter 6.

Table D.5 Critical points from both original and new universal constants *

Exp. data		Tc and Pc with %RD from PC-SAFT (GS)				Tc and PC with %RD from PC-SAFT (LK)				Ref.
Tc (K)	Pc (bar)	Tc (K)	Pc (bar)	%RD		Tc (K)	Pc (bar)	%RD		
				Tc	Pc			Tc	Pc	
345.37	70.12	356.99	67.59	3.36	-3.60	355.75	67.46	3.01	-3.79	1
336.48	73.43	354.14	70.79	5.25	-3.60	353.01	70.77	4.91	-3.63	1
327.59	77.08	347.19	74.27	5.98	-3.64	346.27	74.42	5.70	-3.45	1
380.37	68.40	388.11	64.56	2.04	-5.62	386.45	64.03	1.60	-6.38	1
362.04	83.98	378.35	73.53	4.51	-12.4	376.91	73.26	4.11	-12.8	1
318.71	117.20	343.93	98.25	7.91	-16.2	344.14	98.39	7.98	-16.1	1
377.59	82.53	383.06	81.73	1.45	-0.97	381.73	81.43	1.10	-1.33	2
344.26	100.53	347.47	100.54	0.93	0.01	347.66	100.50	0.99	-0.03	2
310.26	121.62	311.87	125.89	0.52	3.51	315.48	125.03	1.68	2.80	2
277.59	123.14	279.60	129.23	0.72	4.95	285.15	129.24	2.72	4.95	2
438.15	66.13	445.06	67.57	1.58	2.18	442.31	66.36	0.95	0.35	3
385.92	76.06	392.41	78.83	1.68	3.64	390.70	78.28	1.24	2.92	3
400.37	62.79	408.77	66.23	2.10	5.48	406.64	65.43	1.57	4.20	3
391.49	89.01	397.68	87.40	1.58	-1.80	395.96	86.81	1.14	-2.48	4
421.48	71.57	429.81	74.72	1.98	4.40	427.09	73.85	1.33	3.18	4
415.93	70.61	424.60	73.53	2.09	4.14	421.99	72.74	1.46	3.01	4
224.21	68.50	224.56	69.62	0.16	1.63	227.60	73.30	1.51	7.01	5
397.15	56.02	409.38	59.18	3.08	5.63	407.20	58.46	2.53	4.35	6
428.81	41.88	437.75	45.96	2.08	9.74	435.47	44.89	1.55	7.18	6
450.20	38.80	459.00	42.51	1.96	9.57	456.51	41.24	1.40	6.29	6
405.87	51.13	416.30	54.48	2.57	6.56	414.16	53.60	2.04	4.84	6
417.92	45.06	426.24	48.45	1.99	7.53	424.09	47.41	1.48	5.22	6
423.15	74.12	428.92	78.29	1.36	5.63	426.29	77.27	0.74	4.25	6
387.03	72.20	396.87	72.62	2.54	0.59	395.00	72.19	2.06	-0.01	6
385.42	56.24	393.56	59.30	2.11	5.44	391.67	58.62	1.62	4.24	6
366.44	67.20	378.00	69.63	3.16	3.61	376.21	69.29	2.67	3.12	7
366.44	66.20	377.46	68.71	3.01	3.80	375.69	68.38	2.53	3.29	7
366.44	63.80	377.10	67.54	2.91	5.87	375.38	67.21	2.44	5.34	7
366.44	61.20	376.89	65.50	2.85	7.02	375.18	65.09	2.39	6.36	7
394.22	61.00	402.81	63.05	2.18	3.35	400.70	62.39	1.64	2.28	7
421.99	60.70	430.12	59.33	1.93	-2.25	427.67	58.51	1.35	-3.62	7
421.99	51.90	429.46	53.49	1.77	3.06	427.17	52.51	1.23	1.18	7
310.53	137.48	312.09	146.58	0.50	6.62	316.62	144.52	1.96	5.12	8
376.42	65.36	384.32	67.53	2.10	3.32	382.61	67.08	1.64	2.63	8
322.03	86.75	326.97	85.12	1.53	-1.88	326.72	85.93	1.46	-0.95	9
322.03	92.05	326.89	89.50	1.51	-2.77	326.60	90.50	1.42	-1.69	9
313.70	92.32	320.20	89.34	2.07	-3.23	320.29	90.25	2.10	-2.24	9
313.70	97.98	320.10	92.87	2.04	-5.21	320.18	93.91	2.07	-4.16	9
303.60	72.56	312.03	78.92	2.78	8.77	308.00	77.00	1.45	6.11	10

303.90	72.51	311.37	79.62	2.46	9.80	307.67	77.94	1.24	7.49	10
303.20	72.63	310.23	79.36	2.32	9.27	306.74	77.87	1.17	7.22	10
302.00	69.37	312.38	76.74	3.44	10.6	307.76	74.47	1.91	7.35	10
306.10	72.12	312.40	76.92	2.06	6.66	307.83	74.67	0.56	3.54	10
309.10	72.31	312.41	76.93	1.07	6.39	307.84	74.67	-0.41	3.27	10
304.50	72.79	312.60	80.72	2.66	10.9	308.68	78.84	1.37	8.31	10
305.20	72.78	313.80	80.88	2.82	11.1	309.66	78.80	1.46	8.28	10
304.35	72.62	312.40	80.41	2.64	10.7	308.52	78.56	1.37	8.18	10
199.44	53.40	201.40	54.52	0.98	2.09	203.17	57.48	1.87	7.64	11
196.72	51.81	199.27	53.02	1.30	2.33	201.12	55.99	2.23	8.06	11
199.72	54.58	201.93	56.16	1.11	2.89	204.21	59.65	2.25	9.30	11
%AAD				2.29	5.44			1.96	4.83	

* The collection of the mixture composition can be found in Sørensen (2008).

Reference: (1) Formann et al. (1962); (2) Wiese et al. (1970); (3) Ekiner et al. (1966); (4) Ekiner et al. (1968); (5) Parikh et al. (1984); (6) Etter et al. (1961); (7) Mehra et al. (1963); (8) Peng et al. (1977); (9) Yarborough et al. (1970); (10) Morrison et al. (1984); (11) Gonzalez et al. (1968).

Appendix E. Academic activities

Peer reviewed journal articles

1. **Xiaodong Liang**; Bjørn Maribo-Mogensen; Kaj Thomsen; Wei Yan; Georgios M. Kontogeorgis. Approach to Improve Speed of Sound Calculation within PC-SAFT Framework. *Ind. Eng. Chem. Res.* 2012, Vol. 51(45), pp.14903-14914.

2. **Xiaodong Liang**; Kaj Thomsen; Wei Yan; Georgios M. Kontogeorgis. Prediction of the vapor-liquid equilibria and speed of sound in binary systems of 1-alkanols and n-alkanes with the simplified PC-SAFT equation of state. *Fluid Phase Equilib.* 2013, Vol. 360, pp.222-232.

3. **Xiaodong Liang**; Wei Yan; Kaj Thomsen; Georgios M. Kontogeorgis. On petroleum fluid characterization with PC-SAFT equation of state. *Fluid Phase Equilib.* 2014, Vol. 375, pp.254-268.

4. **Xiaodong Liang**; Ioannis Tsivintzelis; Georgios M. Kontogeorgis. Modeling water containing systems with the CPA and the simplified PC-SAFT equation of state. *Ind. Eng. Chem. Res.* 2012, Vol. 53 (45), pp.14493-14507.

5. **Xiaodong Liang**; Georgios M. Kontogeorgis. A New Variant of the Universal Constants in the Perturbed-Chain Statisical Association Fluid Theory Equation of State. Submitted to *Ind. Eng. Chem. Res.*

Conference presentations

1. **Xiaodong Liang**; Georgios M. Kontogeorgis. Speed of sound from SAFT-Family Equations of state (***Poster***), Study Trip, Houston TX, USA, March 17-23, 2012.

2. **Xiaodong Liang**; Georgios M. Kontogeorgis. Speed of Sound from Equations of State (***Oral***), CERE Annual Discussion Meeting, Hillerød, Denmark, June 13-15, 2012.

3. **Xiaodong Liang**; Georgios M. Kontogeorgis. What Can We Learn from Putting Speed of Sound Data into the Universal Constants Regression in PC-SAFT (***Poster***), 26th ESAT, Potsdam, Germany, Oct. 7-10, 2012.

4. **Xiaodong Liang**; Georgios M. Kontogeorgis. Investigation on pure component parameters of water with simplified PC-SAFT (***Oral***), CERE Annual Discussion Meeting, Snekkersten, Denmark, June 19-21, 2013.

5. **Xiaodong Liang**; Georgios M. Kontogeorgis. Phase equilibria and speed of sound from PC-SAFT approach (***Poster***), CERE Annual Discussion Meeting, Snekkersten, Denmark, June 19-21, 2013.

6. **Xiaodong Liang**; Georgios M. Kontogeorgis. Comparison of the pure component parameters of water with the simplified PC-SAFT EOS (***Poster***), Thermodynamics 2013, Manchester, UK, Sep. 3-6, 2013.

7. **Xiaodong Liang**; Kaj Thomsen; Wei Yan; Georgios M. Kontogeorgis. PC-SAFT in modeling speed of sound (***Oral***), SAFT 2014, Tróia, Portugal, April 22-24, 2014.

8. **Xiaodong Liang**; Ioannis Tsivintzelis; Georgios M. Kontogeorgis. Modeling water containing systems with the simplified PC-SAFT and the CPA equations of state (***Poster***), SAFT 2014, Tróia, Portugal, April 22-24, 2014.

9. **Xiaodong Liang**; Wei Yan; Kaj Thomsen; Georgios M. Kontogeorgis. Thermodynamic modeling of complex systems (***Oral***), CERE Annual Discussion Meeting, Snekkersten, Denmark, June 25-27, 2014.

10. **Xiaodong Liang**; Wei Yan; Kaj Thomsen; Georgios M. Kontogeorgis. Speed of sound modeling within PC-SAFT framework (***Poster***), CERE Annual Discussion Meeting, Snekkersten, Denmark, June 25-27, 2014.

11. **Xiaodong Liang**; Ioannis Tsivintzelis; Georgios M. Kontogeorgis. Water – a parameter study with the simplified PC-SAFT and the CPA equations of state (***Poster***), CERE Annual Discussion Meeting, Snekkersten, Denmark, June 25-27, 2014.

Teaching assistance

1. Assistant in Chemical Engineering Thermodynamics (2012, 2013).

2. Assistant in Thermodynamic Models – Fundamentals and Computational Aspects (2014).

Center for Energy Resources Engineering
Department of Chemical and
Biochemical Engineering
Technical University of Denmark
Søltofts Plads, Building 229
DK-2800 Kgs. Lyngby
Denmark

Phone: +45 4525 2800
Fax: +45 4525 4588
Web: www.cere.dtu.dk

ISBN : 978-87-93054-46-2